

เคมีและฤทธิ์ทางชีวภาพของสารผลิตภัณฑ์ธรรมชาติทางทะเล
จากฟองน้ำ *Acanthodendrilla* sp. และ *Xestospongia* sp.

นางสาวณัชนันท์ สิริมังคลกิตติ



จุฬาลงกรณ์มหาวิทยาลัย

CHULALONGKORN UNIVERSITY

บทคัดย่อและแฟ้มข้อมูลฉบับเต็มของวิทยานิพนธ์ตั้งแต่ปีการศึกษา 2554 ที่ให้บริการในคลังปัญญาจุฬาฯ (CUIR)
เป็นแฟ้มข้อมูลของนิสิตเจ้าของวิทยานิพนธ์ ที่ส่งผ่านทางบัณฑิตวิทยาลัย

The abstract and full text of theses from the academic year 2011 in Chulalongkorn University Intellectual Repository (CUIR)
are the thesis authors' files submitted through the University Graduate School.

วิทยานิพนธ์นี้เป็นส่วนหนึ่งของการศึกษาตามหลักสูตรปริญญาวิทยาศาสตรดุษฎีบัณฑิต

สาขาวิชาเภสัชเวช ภาควิชาเภสัชเวชและเภสัชพฤกษศาสตร์

คณะเภสัชศาสตร์ จุฬาลงกรณ์มหาวิทยาลัย

ปีการศึกษา 2558

ลิขสิทธิ์ของจุฬาลงกรณ์มหาวิทยาลัย

CHEMISTRY AND BIOACTIVITIES OF MARINE NATURAL PRODUCTS
FROM SPONGES *ACANTHODENDRILLA* SP. AND *XESTOSPONGIA* SP.

Miss Natchanun Sirimangkalakitti



A Dissertation Submitted in Partial Fulfillment of the Requirements
for the Degree of Doctor of Philosophy Program in Pharmacognosy

Department of Pharmacognosy and Pharmaceutical Botany

Faculty of Pharmaceutical Sciences

Chulalongkorn University

Academic Year 2015

Copyright of Chulalongkorn University

Thesis Title CHEMISTRY AND BIOACTIVITIES OF MARINE NATURAL PRODUCTS FROM SPONGES *ACANTHODENDRILLA SP.* AND *XESTOSPONGIA SP.*

By Miss Natchanun Sirimangkalakitti

Field of Study Pharmacognosy

Thesis Advisor Khanit Suwanborirux, Ph.D.

Thesis Co-Advisor Associate Professor Pithi Chanvorachote, Ph.D.
Supakarn Chamni, Ph.D.

Accepted by the Faculty of Pharmaceutical Sciences, Chulalongkorn University in
Partial Fulfillment of the Requirements for the Doctoral Degree

.....Dean of the Faculty of Pharmaceutical Sciences
(Assistant Professor Rungpetch Sakulbumrungsil, Ph.D.)

THESIS COMMITTEE

.....Chairman
(Professor Kittisak Likhitwitayawuid, Ph.D.)

.....Thesis Advisor
(Khanit Suwanborirux, Ph.D.)

.....Thesis Co-Advisor
(Associate Professor Pithi Chanvorachote, Ph.D.)

.....Thesis Co-Advisor
(Supakarn Chamni, Ph.D.)

.....Examiner
(Associate Professor Boonchoo Sritularak, Ph.D.)

.....Examiner
(Assistant Professor Taksina Chuanasa, Ph.D.)

.....External Examiner
(Associate Professor Anuchit Plubrukarn, Ph.D.)

.....External Examiner
(Associate Professor Kornkanok Ingkaninan, Ph.D.)

ณัชนันท์ สิริมังคลกิตติ : เคมีและฤทธิ์ทางชีวภาพของสารผลิตภัณฑ์ธรรมชาติทางทะเลจากฟองน้ำ *Acanthodendrilla* sp. และ *Xestospongia* sp. (CHEMISTRY AND BIOACTIVITIES OF MARINE NATURAL PRODUCTS FROM SPONGES *ACANTHODENDRILLA* SP. AND *XESTOSPONGIA* SP.) อ.ที่ปรึกษา วิทยาลัยพยาบาล: อ. ภก. ดร.คณิต สุวรรณปริวัณ, อ.ที่ปรึกษาวิทยาลัยพยาบาลร่วม: รศ. ภก. ดร.ปิติ จันทร์วโรชิต, อ. ดร.ศุภกาญจน์ ชำนิ, 253 หน้า.

ในการศึกษาทางเคมีของสารออกฤทธิ์ทางชีวภาพจากฟองน้ำทะเล *Acanthodendrilla* sp. ทำให้สามารถแยกสารในกลุ่ม bromotyrosine alkaloids ได้ทั้งหมด 21 ชนิด ซึ่งประกอบด้วยสารใหม่ 2 ชนิด ได้แก่ 13-oxosubereamolline D และ acanthodendrilline ในการวิจัยนี้ ได้ทำการพิสูจน์โครงสร้างทางเคมีของสารที่แยกได้ โดยใช้เทคนิค UV, IR, mass และ NMR spectroscopy ร่วมกับการเปรียบเทียบข้อมูลเหล่านี้กับข้อมูลที่มีการรายงานแล้ว จากนั้นได้กำหนด absolute configuration ของสาร 13-oxosubereamolline D โดยการเปรียบเทียบสเปกตรัม CD และค่า specific optical rotation กับสารที่มีโครงสร้างใกล้เคียงกัน และได้กำหนด absolute configuration ของสาร acanthodendrilline ที่ตำแหน่ง 11 เป็น S โดยการเปรียบเทียบค่า specific optical rotation กับคู่สาร enantiomers ที่สังเคราะห์ขึ้น เมื่อทำการประเมินฤทธิ์ยับยั้งเอนไซม์ acetylcholinesterase ของสารทั้งหมดที่แยกได้ พบว่าสารที่มีฤทธิ์แรงที่สุด คือ สาร homoerothionin (IC_{50} 4.5 μ M) ซึ่งยับยั้งการทำงานของเอนไซม์แบบแข่งขัน โดยที่โครงสร้างส่วน spirocyclohexadienylisoxazoline และความยาวที่จำเพาะของ alkyl diamine linkage เป็นส่วนสำคัญต่อความแรงของฤทธิ์ยับยั้งเอนไซม์ของสารชนิดนี้ นอกจากนี้ได้ทดสอบฤทธิ์เป็นพิษต่อเซลล์มะเร็งปอดชนิดเซลล์ไม่เล็ก ชนิด H292 ของคู่สาร enantiomers ของสาร acanthodendrilline ที่สังเคราะห์ขึ้น พบว่าสาร (S)-acanthodendrilline มีความแรงมากกว่า (R)-acanthodendrilline 3 เท่า ผลที่ได้แสดงให้เห็นว่า stereochemistry ตำแหน่ง 11 เป็นส่วนสำคัญต่อฤทธิ์เป็นพิษต่อเซลล์มะเร็ง

ในการศึกษาทางเคมีและฤทธิ์เป็นพิษต่อเซลล์มะเร็งของสารกลุ่ม bistetrahydroisoquinolinequinone alkaloids จากฟองน้ำทะเลสีน้ำเงิน *Xestospongia* sp. ได้ทำการเตรียมอนุพันธ์ 22-O-ester ของ jorunnamycin A (JA) จำนวน 18 ชนิด ได้แก่ อนุพันธ์ที่มีหมู่ benzoyl และ *trans*-cinnamoyl ต่อกับหมู่ดึง electron และอนุพันธ์ที่มีหมู่ nitrogen-heterocyclic rings โดยสารตั้งต้น JA เตรียมจากสาร renieramycin M (RM) ซึ่งเป็นสารประกอบหลักที่แยกได้จากฟองน้ำชนิดนี้ จากนั้นได้ทำการประเมินฤทธิ์เป็นพิษต่อเซลล์มะเร็งปอดชนิดเซลล์ไม่เล็ก ชนิด H292 และ H460 พบว่า nitrogen-heterocyclic esters ของสารอนุพันธ์ ช่วยเพิ่มฤทธิ์เป็นพิษต่อเซลล์มะเร็ง และสาร 22-O-(4-pyridinecarbonyl)jorunnamycin A แสดงฤทธิ์เป็นพิษต่อเซลล์มะเร็งแรงที่สุดในบรรดาอนุพันธ์ทั้งหมดที่สังเคราะห์ขึ้น โดยมีความแรงมากกว่า RM 20 และ 5 เท่า ต่อเซลล์มะเร็งปอดชนิด H292 และ H460 ตามลำดับ นอกจากนี้ได้ทำการศึกษาศักยภาพของสาร RM ในการยับยั้งการแพร่กระจายเซลล์มะเร็ง พบว่าที่ความเข้มข้นต่ำกว่าระดับความเป็นพิษ สาร RM สามารถเพิ่มความไวต่อกระบวนการ anoikis ของเซลล์มะเร็งปอดชนิด H460 ที่คือต่อกระบวนการ anoikis โดยผ่านกลไกการลดระดับโปรตีน p-ERK, p-AKT, BCL2 และ MCL1 และที่ความเข้มข้นนี้ สาร RM ยังสามารถทำลายเซลล์คล้ายเซลล์ต้นกำเนิดของเซลล์มะเร็งปอดชนิด H460 ได้

ภาควิชา	เภสัชเวชและเภสัชพฤกษศาสตร์	ลายมือชื่อนิสิต
สาขาวิชา	เภสัชเวช	ลายมือชื่อ อ.ที่ปรึกษาหลัก
ปีการศึกษา	2558	ลายมือชื่อ อ.ที่ปรึกษาร่วม
		ลายมือชื่อ อ.ที่ปรึกษาร่วม

5376967133 : MAJOR PHARMACOGNOSY

KEYWORDS: BROMOTYROSINE ALKALOIDS, ACETYLCHOLINESTERASE INHIBITORY ACTIVITY, ACANTHODENDRILLA SP., BISTETRAHYDROISOQUINOLINEQUINONE ALKALOIDS, 22-O-ESTER DERIVATIVES, JORUNNAMYCIN A, RENIERAMYCIN M, XESTOSPONGIA SP., NON-SMALL CELL LUNG CANCER, CYTOTOXICITY, ANOIKIS-SENSITIZING ACTIVITY, STEM CELL-LIKE CANCER CELL SUPPRESSING ACTIVITY

NATCHANUN SIRIMANGKALAKITTI: CHEMISTRY AND BIOACTIVITIES OF MARINE NATURAL PRODUCTS FROM SPONGES *ACANTHODENDRILLA* SP. AND *XESTOSPONGIA* SP.. ADVISOR: KHANIT SUWANBORIRUX, Ph.D., CO-ADVISOR: ASSOC. PROF. PITHI CHANVORACHOTE, Ph.D., SUPAKARN CHAMNI, Ph.D., 253 pp.

Investigation of chemical constituents from the sponge *Acanthodendrilla* sp. led to the isolation of twenty-one bromotyrosine alkaloids, including two new natural products, 13-oxosubereamolline D and acanthodendrilline. The chemical structures of these alkaloids were determined by means of spectroscopic analysis, including UV, IR, mass, and NMR spectroscopy, as well as comparison of those with previously reported data. The absolute configuration of 13-oxosubereamolline D was determined by comparing the CD spectrum and specific optical rotation value with those of the related compounds. The absolute configuration of acanthodendrilline was determined as 11-*S* by comparing the specific optical rotation value with that of the synthetic enantiomers. These isolated alkaloids were evaluated for acetylcholinesterase inhibitory activity, and the most active compound was identified as homoaerthionin (IC₅₀ 4.5 μM), which acted as a competitive enzyme inhibitor. The bispirocyclohexadienylisoxazoline moiety and the specific length of the alkyl diamine linkage were proposed as the crucial parts for its strong inhibitory activity. Moreover, both synthetic enantiomers of acanthodendrilline were evaluated for cytotoxicity against H292 non-small cell lung cancer (NSCLC) cell line. Interestingly, (*S*)-acanthodendrilline exhibited approximately 3-fold more potent than (*R*)-acanthodendrilline, suggesting that the stereochemistry at C-11 is a key feature related to the cytotoxicity.

Regarding the chemical and cytotoxicity studies of bistetrahydroisoquinolinequinone alkaloids from the blue sponge *Xestospongia* sp., eighteen 22-*O*-ester derivatives of jorunnamycin A (JA), having a benzoyl or *trans*-cinnamoyl moiety with electronegative and electron-withdrawing functional groups, together with nitrogen-heterocyclic rings, were prepared from JA. The starting material JA was prepared from renieramycin M (RM), which was isolated as a major component from the sponge. Their cytotoxicity was evaluated against H292 and H460 NSCLC cell lines. The finding suggested that the nitrogen-heterocyclic esters of the analogues elevated the cytotoxicity, and 22-*O*-(4-pyridinecarbonyl)jorunnamycin A was the most potent among all analogues, exhibiting 20-fold and 5-fold more cytotoxic than RM toward H292 and H460 cell lines, respectively. Further investigation revealed that RM at a subtoxic concentration was a potential anti-metastatic agent by sensitizing anoikis-resistant H460 cells to anoikis through the suppression of the levels of proteins p-ERK, p-AKT, BCL2 and MCL1. Moreover, RM at a subtoxic concentration also attenuates stem cell-like cancer cells in H460 cell line.

Department:	Pharmacognosy and Pharmaceutical	Student's Signature
	Botany	Advisor's Signature
Field of Study:	Pharmacognosy	Co-Advisor's Signature
Academic Year:	2015	Co-Advisor's Signature

ACKNOWLEDGEMENTS

I would like to express my sincere appreciation to my thesis advisor, Dr. Khanit Suwanborirux, Department of Pharmacognosy and Pharmaceutical Botany, Faculty of Pharmaceutical Sciences, Chulalongkorn University, for his invaluable support, kind advice, and unlimited encouragement throughout the course of my work.

I would like to deeply acknowledge my two co-advisors, Associate Professor Pithi Chanvorachote and Dr. Supakarn Chamni for the continued support of my Ph.D study and research. I am very thankful to my thesis committee members for their insightful comment, suggestion and discussion.

My gratitude and appreciation are expressed to Professor Dr. Naoki Saito and Assistant Professor Dr. Masashi Yokoya, Meiji Pharmaceutical University for providing chemical synthesis research opportunity and invaluable suggestion during my stay in Japan. I would also like to thank Associate Professor Dr. Anuchit Plubrukarn, Faculty of Pharmaceutical Sciences, Prince of Songkla University for helping and teaching me in his natural product chemistry laboratory and Associate Professor Dr. Kornkanok Ingkaninan, Faculty of Pharmaceutical Sciences, Naresuan University for her assistance in determination of acetylcholinesterase inhibitory activity.

I especially thank to the Thailand Research Fund for the Royal Golden Jubilee Ph.D. Program Grant No. PHD/0276/2552 and the Meiji Pharmaceutical University Asia/Africa Center for Drug Discovery (MPU-AACDD) for financial supports.

I would like to express my special gratitude to all teachers, staff, and graduate students in the Department of Pharmacognosy and Pharmaceutical Botany, Department of Pharmacology and Physiology, and Pharmaceutical Research Instrument Center, Faculty of Pharmaceutical Sciences, Chulalongkorn University; the Department of Pharmacognosy and Pharmaceutical Botany, Faculty of Pharmaceutical Sciences, Prince of Songkla University; the Department of Pharmaceutical Chemistry and Pharmacognosy, Faculty of Pharmaceutical Sciences, Naresuan University; and Meiji Pharmaceutical University for their help, hospitality, and friendship. This thesis work would not have been done without their assistance.

Finally, my highest gratitude to my family for their unconditional love, understanding, constant support and encouragement.

CONTENTS

	Page
THAI ABSTRACT	iv
ENGLISH ABSTRACT	v
ACKNOWLEDGEMENTS	vi
CONTENTS	vii
LIST OF FIGURES	xi
LIST OF TABLES	xxi
CHAPTER I GENERAL INTRODUCTION	1
CHAPTER II LITERATURE REVIEW	4
1. Sponge <i>Acanthodendrilla</i> sp.....	4
1.1. Taxa and description of the sponge <i>Acanthodendrilla</i> sp.....	4
1.2. Chemistry and biological activities of marine natural products from sponges of the genus <i>Acanthodendrilla</i>	4
1.3. Chemistry and biological activities of bromotyrosine alkaloids	7
1.4. Acetylcholinesterase inhibitory activity	16
2. Sponge <i>Xestospongia</i> sp.....	21
2.1. Taxa and description of the sponge <i>Xestospongia</i> sp.	21
2.2. Tetrahydroisoquinoline alkaloids	22
2.2.1. Biosynthesis of tetrahydroisoquinoline alkaloids	23
2.2.2. Marine tetrahydroisoquinoline alkaloids as anticancer drugs and potential drug candidates	24
2.3. Renieramycins	25
2.3.1. Chemistry of renieramycins.....	25
2.3.2. Bioactivities of renieramycins	28

	Page
2.3.3. Structure modification at C-22 of renieramycins.....	30
2.3.4. Other related anticancer activities of renieramycins	37
2.4. Targeted therapy for metastatic lung cancer	38
CHAPTER III EXPERIMENTAL PROCEDURES	41
1. Chromatography.....	41
2. Spectroscopy	43
3. Optical Activity	45
CHAPTER IV BROMOTYROSINE ALKALOIDS WITH ACETYLCHOLINESTERASE INHIBITORY ACTIVITY FROM THE THAI SPONGE <i>ACANTHODENDRILLA</i> SP.	47
1. Introduction	47
2. Experimental.....	48
3. Results and Discussion.....	51
4. Conclusion.....	59
5. References.....	59
CHAPTER V SYNTHESIS AND ABSOLUTE CONFIGURATION OF ACANTHODENDRILLINE, A NEW CYTOTOXIC BROMOTYROSINE ALKALOID, FROM THE THAI MARINE SPONGE <i>ACANTHODENDRILLA</i> SP.	64
1. Introduction	64
2. Experimental.....	66
3. Results and Discussion.....	69
4. Conclusion.....	74
5. References.....	74

CHAPTER VI CHEMISTRY OF RENIERAMYCINS. PART 15: SYNTHESIS OF 22-O-ESTER DERIVATIVES OF JORUNNAMYCIN A AND THEIR CYTOTOXICITY AGAINST NON-SMALL CELL LUNG CANCER CELLS.....	78
1. Introduction	78
2. Experimental.....	81
3. Results and Discussion.....	83
4. Conclusion.....	88
5. References.....	88
CHAPTER VII RENIERAMYCIN M SENSITIZES ANOIKIS-RESISTANT H460 LUNG CANCER CELLS TO ANOIKIS.....	95
1. Introduction	95
2. Experimental.....	96
3. Results.....	100
4. Discussion	106
5. Conclusion.....	108
6. References.....	108
CHAPTER VIII RENIERAMYCIN M ATTENUATES CANCER STEM CELL-LIKE PHENOTYPES IN H460 LUNG CANCER CELLS.....	112
1. Introduction	112
2. Experimental.....	113
3. Results.....	116
4. Discussion	119
5. References.....	121
CHAPTER IX CONCLUSION.....	126

	Page
REFERENCES	129
APPENDICES.....	150
APPENDIX A SPONGE MATERIALS, EXTRACTION, AND ISOLATION	151
APPENDIX B PHYSICAL AND SPECTROSCOPIC DATA OF BROMOTYROSINE ALKALOIDS.....	154
APPENDIX C PHYSICAL AND SPECTROSCOPIC DATA OF RENIARAMYCIN DERIVATIVES	199
APPENDIX D LETTERS OF PERMISSION.....	249
VITA.....	253



LIST OF FIGURES

Figure 1.1 Chemical structures of marine sponge-derived drugs approved by the U.S. FDA and marine natural products currently in phase I clinical trials	2
Figure 2.1 Examples of sesterterpenoids isolated from <i>Acanthodendrilla</i> sp.....	5
Figure 2.2 Examples of sterols isolated from <i>Acanthodendrilla</i> sp.....	6
Figure 2.3 Meroterpenoids isolated from <i>Acanthodendrilla</i> sp.....	7
Figure 2.4 Examples of simple bromotyrosine derivatives	8
Figure 2.5 Proposed biosynthetic pathway of verogiaquinol	9
Figure 2.6 Formation of spirocyclohexadienylisoxazoline.....	9
Figure 2.7 Examples of spirocyclohexadienylisoxazoline bromotyrosine derivatives .	10
Figure 2.8 Formation of spirooxepinisoxazoline.....	11
Figure 2.9 Examples of spirooxepinisoxazoline bromotyrosine derivatives	12
Figure 2.10 Examples of oxime bromotyrosine derivatives	13
Figure 2.11 Examples of bastadins.....	14
Figure 2.12 Examples of miscellaneous bromotyrosine derivatives	15
Figure 2.13 Schematic view of the active site gorge of <i>Torpedo californica</i> acetylcholinesterase	17
Figure 2.14 Chemical principle of the Ellman's method.....	18
Figure 2.15 Acetylcholinesterase inhibitors approved by the U.S. FDA for symptomatic treatment of Alzheimer's disease.....	19
Figure 2.16 Acetylcholinesterase inhibitors from marine origins	20
Figure 2.17 Bromotyrosine alkaloids acting as acetylcholinesterase inhibitors	20
Figure 2.18 Chemical structures of selected saframycin type compounds	23
Figure 2.19 Biosynthetic precursors of saframycin A.....	24

Figure 2.20 Marine tetrahydroisoquinoline alkaloids as anticancer drugs and potential drug candidates.....	25
Figure 2.21 Synthetic scheme of jorunnamycin A (JA) from renieramycin M (RM).....	30
Figure 2.22 Natural products reported to target anokis-resistant cancer cells and cancer stem cells	40
Figure 4.1 Structures of bromotyrosine alkaloids isolated from the Thai marine sponge <i>Acanthodendrilla</i> sp.....	52
Figure 4.2 Selected ^1H - ^1H COSY (—) and HMBC (→) correlations of 13-oxosubereamolline D (B5).	54
Figure 4.3 Binding study of homoaerotherionin (B7) on <i>hrAChE</i>	58
Figure 5.1 Structures of some bioactive bromotyrosine alkaloids	65
Figure 5.2 Structure of acanthodendrilline [(<i>S</i>)- B21].	69
Figure 5.3 Selected ^1H - ^1H COSY (—) and HMBC (→) correlations of acanthodendrilline [(<i>S</i>)- B21].	71
Figure 5.4 Synthetic scheme of (<i>S</i>)- and (<i>R</i>)-acanthodendrillines (B21)	72
Figure 6.1 Structures of representative tetrahydroisoquinoline marine-derived natural products	79
Figure 6.2 Synthetic scheme of 22- <i>O</i> -ester derivatives of jorunnamycin A from renieramycin M (RM)	84
Figure 6.3 A: Chemical structure of 22- <i>O</i> -[3-(4-pyridyl)acryloyl]jorunnamycin A (R18). B: Selected NOESY correlations (↔) for R18 and energy-minimized 3D structure using Discovery Studio 4.0 Visualizer.	85
Figure 7.1 Cell viability and cell morphology of H460 lung cancer cells in a detached condition.	100
Figure 7.2 Expression of survival and apoptotic proteins of H460 lung cancer cells in a detached condition.....	101

Figure 7.3 A: Cytotoxic effect of renieramycin M (RM) on H460 lung cancer and normal dermal papilla (DP) cells under attached conditions. B: Cytotoxic effect of RM on AR_H460 cells in a detached condition.....	103
Figure 7.4 Cell morphology of AR_H460 lung cancer cells in a detached condition treated with renieramycin M (RM) at subtoxic concentrations	104
Figure 7.5 Expression of survival and apoptotic proteins of AR_H460 lung cancer cells treated with renieramycin M (RM) at subtoxic concentrations	105
Figure 7.6 The scheme represents the effect of renieramycin M (RM) on anoikis-resistant lung cancer cells.	107
Figure 8.1 Cytotoxic effect of renieramycin M (RM) on H460 lung cancer and normal dermal papilla (DP) cells under normal culturing conditions.....	116
Figure 8.2 Colony formation of anoikis-resistant H460 cells treated with RM at subtoxic concentrations	117
Figure 8.3 Spheroid formation of H460 lung cancer cells treated with RM at subtoxic concentrations	118
Figure 8.4 Expression of the lung cancer stem cell markers of anoikis-resistant H460 lung cancer cells treated with RM at subtoxic concentrations	119
Figure 9.1 Bromotyrosine alkaloids isolated from the sponge <i>Acanthodendrilla</i> sp... 127	
Figure 9.2 22-O-ester derivatives of jorunnamycin A prepared from renieramycin M (RM), isolated from the blue sponge <i>Xestospongia</i> sp.....	128
Figure A1 Underwater (left) and surface (right) photographs of the sponge <i>Acanthodendrilla</i> sp. collected from Ha Island, Krabi, Thailand	151
Figure A2 Underwater (left) and surface (right) photographs of the blue sponge <i>Xestospongia</i> sp. collected from Si Chang Island, Chonburi, Thailand.....	151
Figure A3 Extraction and isolation scheme of bromotyrosine alkaloids from the sponge <i>Acanthodendrilla</i> sp.....	152

Figure A4 Extraction and isolation scheme of renieramycin M (RM) from the blue sponge <i>Xestospongia</i> sp.	153
Figure B1 ^1H NMR spectrum (300 MHz) of subereamolline C (B1) in CDCl_3	155
Figure B2 ^{13}C NMR spectrum (75 MHz) of subereamolline C (B1) in CDCl_3	155
Figure B3 ^1H NMR spectrum (300 MHz) of subereamolline D (B2) in CDCl_3	157
Figure B4 ^{13}C NMR spectrum (75 MHz) of subereamolline D (B2) in CDCl_3	157
Figure B5 ^1H NMR spectrum (500 MHz) of B3 in acetone- d_6	159
Figure B6 ^{13}C NMR spectrum (125 MHz) of B3 in acetone- d_6	159
Figure B7 ^1H NMR spectrum (500 MHz) of B4 in acetone- d_6	161
Figure B8 ^{13}C NMR spectrum (125 MHz) of B4 in acetone- d_6	161
Figure B9 ^1H NMR spectrum (500 MHz) of 13-oxosubereamolline D (B5) in acetone- d_6	162
Figure B10 ^{13}C NMR spectrum (125 MHz) of 13-oxosubereamolline D (B5) in acetone- d_6	162
Figure B11 ^1H - ^1H COSY spectrum (300 MHz) of 13-oxosubereamolline D (B5) in acetone- d_6	163
Figure B12 HSQC spectrum (300 MHz) of 13-oxosubereamolline D (B5) in acetone- d_6	164
Figure B13 HMBC spectrum (500 MHz) of 13-oxosubereamolline D (B5) in acetone- d_6	165
Figure B14 NOESY spectrum (300 MHz) of 13-oxosubereamolline D (B5) in acetone- d_6	166
Figure B15 HRESIMS spectrum of 13-oxosubereamolline D (B5)	167
Figure B16 CD spectrum of 13-oxosubereamolline D (B5)	168
Figure B17 ^1H NMR spectrum (300 MHz) of aerothionin (B6) in acetone- d_6	170
Figure B18 ^{13}C NMR spectrum (75 MHz) of aerothionin (B6) in acetone- d_6	170

Figure B19	^1H NMR spectrum (300 MHz) of homoaerothionin (B7) in CDCl_3	172
Figure B20	^{13}C NMR spectrum (75 MHz) of homoaerothionin (B7) in CDCl_3	172
Figure B21	^1H NMR spectrum (500 MHz) of 11-oxoaerothionin (B8) in acetone- d_6 ...	174
Figure B22	^{13}C NMR spectrum (125 MHz) of 11-oxoaerothionin (B8) in acetone- d_6 ..	174
Figure B23	^1H NMR spectrum (500 MHz) of oxohomoaerothionin (B9) in acetone- d_6 .	176
Figure B24	^{13}C NMR spectrum (125 MHz) of oxohomoaerothionin (B9) in acetone- d_6	176
Figure B25	^1H NMR spectrum (500 MHz) of fistularin 1 (B10) in $\text{DMSO}-d_6$	178
Figure B26	^{13}C NMR spectrum (125 MHz) of fistularin 1 (B10) in $\text{DMSO}-d_6$	178
Figure B27	^1H NMR spectrum (300 MHz) of 11,19-dideoxyfistularin 3 (B11) in acetone- d_6	180
Figure B28	^{13}C NMR spectrum (75 MHz) of 11,19-dideoxyfistularin 3 (B11) in acetone- d_6	180
Figure B29	^1H NMR spectrum (300 MHz) of 19-deoxyfistularin 3 (B12) in acetone- d_6 .	182
Figure B30	^{13}C NMR spectrum (75 MHz) of 19-deoxyfistularin 3 (B12) in acetone- d_6	182
Figure B31	^1H NMR spectrum (300 MHz) of 3,5-dibromo-1-hydroxy-4,4-dimethoxy-2,5-cyclohexadiene-1-acetamide (B13) in $\text{DMSO}-d_6$	184
Figure B32	^{13}C NMR spectrum (75 MHz) of 3,5-dibromo-1-hydroxy-4,4-dimethoxy-2,5-cyclohexadiene-1-acetamide (B13) in $\text{DMSO}-d_6$	184
Figure B33	^1H NMR spectrum (500 MHz) of verongiaquinol (B14) in $\text{DMSO}-d_6$	186
Figure B34	^{13}C NMR spectrum (125 MHz) of verongiaquinol (B14) in $\text{DMSO}-d_6$	186
Figure B35	^1H NMR spectrum (300 MHz) of cavernicolins-1 and -2 (B15 and B16) mixture in acetone- d_6	188
Figure B36	^{13}C NMR spectrum (75 MHz) of cavernicolins-1 and -2 (B15 and B16) mixture in acetone- d_6	188

Figure B37 ^1H NMR spectrum (500 MHz) of 7β - and 7α -bromo-5-chlorocavernicolins (B17 and B18) mixture in $\text{DMSO}-d_6$	190
Figure B38 ^{13}C NMR spectrum (125 MHz) of 7β - and 7α -bromo-5-chlorocavernicolins (B17 and B18) mixture in $\text{DMSO}-d_6$	190
Figure B39 ^1H NMR spectrum (500 MHz) of $5,7\beta$ - and $5,7\alpha$ -dichlorocavernicolins (B19 and B20) mixture in $\text{acetone}-d_6$	191
Figure B40 ^{13}C NMR spectrum (125 MHz) of $5,7\beta$ - and $5,7\alpha$ -dichlorocavernicolins (B19 and B20) mixture in $\text{acetone}-d_6$	191
Figure B41 HRESIMS spectrum of $5,7\beta$ - and $5,7\alpha$ -dichlorocavernicolins (B19 and B20) mixture	192
Figure B42 ^1H NMR spectrum (300 MHz) of 11 <i>S</i> -acanthodendrilline [(<i>S</i>)- B21] in CDCl_3	193
Figure B43 ^{13}C NMR spectrum (75 MHz) of 11 <i>S</i> -acanthodendrilline [(<i>S</i>)- B21] in CDCl_3	193
Figure B44 $^1\text{H}-^1\text{H}$ COSY spectrum (300 MHz) of 11 <i>S</i> -acanthodendrilline [(<i>S</i>)- B21] in CDCl_3	194
Figure B45 HSQC spectrum (300 MHz) of 11 <i>S</i> -acanthodendrilline [(<i>S</i>)- B21] in CDCl_3	195
Figure B46 HMBC spectrum (300 MHz) of 11 <i>S</i> -acanthodendrilline [(<i>S</i>)- B21] in CDCl_3	196
Figure B47 HRFABMS spectrum of 11 <i>S</i> -acanthodendrilline [(<i>S</i>)- B21]	197
Figure B48 ^1H NMR spectrum (400 MHz) of synthetic acanthodendrilline [(<i>S</i>)- B21] in CDCl_3	198
Figure B49 ^1H NMR spectrum (400 MHz) of synthetic acanthodendrilline [(<i>R</i>)- B21] in CDCl_3	198
Figure C1 ^1H NMR spectrum (300 MHz) of renieramycin M (RM)	199
Figure C2 ^1H NMR spectrum (500 MHz) of jorunnamycin A (JA)	200

Figure C3 ^1H NMR spectrum (500 MHz) of 22- <i>O</i> -(3,3,3-trifluoropropionyl) jorunnamycin A (R1) in CDCl_3	202
Figure C4 ^{13}C NMR spectrum (125 MHz) of 22- <i>O</i> -(3,3,3-trifluoropropionyl) jorunnamycin A (R1) in CDCl_3	202
Figure C5 ^1H - ^1H COSY spectrum (500 MHz) of 22- <i>O</i> -(3,3,3-trifluoropropionyl) jorunnamycin A (R1) in CDCl_3	203
Figure C6 HMQC spectrum (500 MHz) of 22- <i>O</i> -(3,3,3-trifluoropropionyl) jorunnamycin A (R1) in CDCl_3	204
Figure C7 HMBC spectrum (500 MHz) of 22- <i>O</i> -(3,3,3-trifluoropropionyl) jorunnamycin A (R1) in CDCl_3	205
Figure C8 NOESY spectrum (500 MHz) of 22- <i>O</i> -(3,3,3-trifluoropropionyl) jorunnamycin A (R1) in CDCl_3	206
Figure C9 ^1H NMR spectrum (500 MHz) of 22- <i>O</i> -(4-fluorobenzoyl)jorunnamycin A (R2) in CDCl_3	208
Figure C10 ^{13}C NMR spectrum (125 MHz) of 22- <i>O</i> -(4-fluorobenzoyl)jorunnamycin A (R2) in CDCl_3	208
Figure C11 ^1H - ^1H COSY spectrum (500 MHz) of 22- <i>O</i> -(4-fluorobenzoyl) jorunnamycin A (R2) in CDCl_3	209
Figure C12 HMQC spectrum (500 MHz) of 22- <i>O</i> -(4-fluorobenzoyl) jorunnamycin A (R2) in CDCl_3	210
Figure C13 HMBC spectrum (500 MHz) of 22- <i>O</i> -(4-fluorobenzoyl) jorunnamycin A (R2) in CDCl_3	211
Figure C14 NOESY spectrum (500 MHz) of 22- <i>O</i> -(4-fluorobenzoyl) jorunnamycin A (R2) in CDCl_3	212
Figure C15 ^1H NMR spectrum (500 MHz) of 22- <i>O</i> -(3-fluorobenzoyl)jorunnamycin A (R3) in CDCl_3	214

Figure C16 ^{13}C NMR spectrum (125 MHz) of 22- <i>O</i> -(3-fluorobenzoyl)jorunnamycin A (R3) in CDCl_3	214
Figure C17 ^1H NMR spectrum (500 MHz) of 22- <i>O</i> -(2-fluorobenzoyl)jorunnamycin A (R4) in CDCl_3	216
Figure C18 ^{13}C NMR spectrum (125 MHz) of 22- <i>O</i> -(2-fluorobenzoyl)jorunnamycin A (R4) in CDCl_3	216
Figure C19 ^1H NMR spectrum (500 MHz) of 22- <i>O</i> -(4-trifluoromethyl benzoyl) jorunnamycin A (R5) in CDCl_3	218
Figure C20 ^{13}C NMR spectrum (125 MHz) of 22- <i>O</i> -(4-trifluoromethyl benzoyl) jorunnamycin A (R5) in CDCl_3	218
Figure C21 ^1H NMR spectrum (500 MHz) of 22- <i>O</i> -(3-trifluoromethyl benzoyl) jorunnamycin A (R6) in CDCl_3	220
Figure C22 ^{13}C NMR spectrum (125 MHz) of 22- <i>O</i> -(3-trifluoromethyl benzoyl) jorunnamycin A (R6) in CDCl_3	220
Figure C23 ^1H NMR spectrum (500 MHz) of 22- <i>O</i> -(2-trifluoromethyl benzoyl) jorunnamycin A (R7) in CDCl_3	222
Figure C24 ^{13}C NMR spectrum (125 MHz) of 22- <i>O</i> -(2-trifluoromethyl benzoyl) jorunnamycin A (R7) in CDCl_3	222
Figure C25 ^1H NMR spectrum (500 MHz) of 22- <i>O</i> -cinnamoyl jorunnamycin A (R8) in CDCl_3	224
Figure C26 ^{13}C NMR spectrum (125 MHz) of 22- <i>O</i> -cinnamoyl jorunnamycin A (R8) in CDCl_3	224
Figure C27 ^1H - ^1H COSY spectrum (500 MHz) of 22- <i>O</i> -cinnamoyl jorunnamycin A (R8) in CDCl_3	225
Figure C28 HMQC spectrum (500 MHz) of 22- <i>O</i> -cinnamoyl jorunnamycin A (R8) in CDCl_3	226

Figure C29 HMBC spectrum (500 MHz) of 22- <i>O</i> -cinnamoyl jorunnamycin A (R8) in CDCl ₃	227
Figure C30 NOESY spectrum (500 MHz) of 22- <i>O</i> -cinnamoyl jorunnamycin A (R8) in CDCl ₃	228
Figure C31 ¹ H NMR spectrum (500 MHz) of 22- <i>O</i> -(4-fluorocinnamoyl)jorunnamycin A (R9) in CDCl ₃	230
Figure C32 ¹³ C NMR spectrum (125 MHz) of 22- <i>O</i> -(4-fluorocinnamoyl) jorunnamycin A (R9) in CDCl ₃	230
Figure C33 ¹ H NMR spectrum (500 MHz) of 22- <i>O</i> -(3-fluorocinnamoyl) jorunnamycin A (R10) in CDCl ₃	232
Figure C34 ¹³ C NMR spectrum (125 MHz) of 22- <i>O</i> -(3-fluorocinnamoyl) jorunnamycin A (R10) in CDCl ₃	232
Figure C35 ¹ H NMR spectrum (500 MHz) of 22- <i>O</i> -pentafluorocinnamoyl jorunnamycin A (R11) in CDCl ₃	234
Figure C36 ¹³ C NMR spectrum (125 MHz) of 22- <i>O</i> -pentafluorocinnamoyl jorunnamycin A (R11) in CDCl ₃	234
Figure C37 ¹ H NMR spectrum (500 MHz) of 22- <i>O</i> -(2-chlorocinnamoyl) jorunnamycin A (R12) in CDCl ₃	236
Figure C38 ¹³ C NMR spectrum (125 MHz) of 22- <i>O</i> -(2-chlorocinnamoyl) jorunnamycin A (R12) in CDCl ₃	236
Figure C39 ¹ H NMR spectrum (500 MHz) of 22- <i>O</i> -(4-nitrocinnamoyl) jorunnamycin A (R13) in CDCl ₃	238
Figure C40 ¹³ C NMR spectrum (125 MHz) of 22- <i>O</i> -(4-nitrocinnamoyl) jorunnamycin A (R13) in CDCl ₃	238
Figure C41 ¹ H NMR spectrum (500 MHz) of 22- <i>O</i> -[3-(4-pyridyl)acryloyl] jorunnamycin A (R17) in CDCl ₃	240

Figure C42 ^{13}C NMR spectrum (125 MHz) of 22-O-[3-(4-pyridyl)acryloyl] jorunnamycin A (R17) in CDCl_3	240
Figure C43 ^1H NMR spectrum (500 MHz) of 22-O-[3-(3-pyridyl)acryloyl] jorunnamycin A (R18) in CDCl_3	242
Figure C44 ^{13}C NMR spectrum (125 MHz) of 22-O-[3-(3-pyridyl)acryloyl] jorunnamycin A (R18) in CDCl_3	242
Figure C45 ^1H - ^1H COSY spectrum (500 MHz) of 22-O-[3-(3-pyridyl)acryloyl] jorunnamycin A (R18) in CDCl_3	243
Figure C46 HMQC spectrum (500 MHz) of 22-O-[3-(3-pyridyl)acryloyl] jorunnamycin A (R18) in CDCl_3	244
Figure C47 HMBC spectrum (500 MHz) of 22-O-[3-(3-pyridyl)acryloyl] jorunnamycin A (R18) in CDCl_3	245
Figure C48 NOESY spectrum (500 MHz) of 22-O-[3-(3-pyridyl)acryloyl] jorunnamycin A (R18) in CDCl_3	246
Figure C49 HRFABMS spectrum of 22-O-[3-(3-pyridyl)acryloyl]jorunnamycin A (R18)	247
Figure C50 IR spectrum of 22-O-[3-(3-pyridyl)acryloyl]jorunnamycin A (R18).....	248
Figure C51 CD spectrum of 22-O-[3-(3-pyridyl)acryloyl]jorunnamycin A (R18) in MeOH	248

LIST OF TABLES

Table 2.1 Cytotoxicity of renieramycins with different C-21 functional groups against human cancer cell lines.....	28
Table 2.2 Cytotoxicity of renieramycins with different C-14 and C-22 functional groups against human cancer cell lines.....	29
Table 2.3 Cytotoxicity of renieramycins M and T against human cancer cell lines....	29
Table 2.4 Cytotoxicity of the 22- <i>O</i> -ester derivatives of jorunnamycin A.....	31
Table 2.5 Cytotoxicity of the 22- <i>O</i> -ester derivatives of jorumycin	33
Table 2.6 Cytotoxicity of the 22- <i>O</i> -ester derivatives of renieramycin G (RG)	35
Table 3.1 Reversed-phase high-performance liquid chromatography (RP-HPLC) columns.....	43
Table 4.1 ¹ H and ¹³ C NMR data for 13-oxosubereamolline D (B5) in acetone- <i>d</i> ₆	55
Table 4.2 The <i>Ee</i> AChE inhibitory activity of all isolated bromotyrosine alkaloids at 100 μM.....	57
Table 4.3 IC ₅₀ s for cholinesterase inhibitory activity of subereamolline C (B1), subereamolline D (B2), arothionin (B6), homoaerothionin (B7), and fistularin-1 (B10)	57
Table 4.4 The <i>hr</i> AChE inhibition kinetics of homoaerothionin (B7).....	58
Table 5.1 ¹ H- and ¹³ C-NMR data of acanthodendrilline [(<i>S</i>)- B21] in CDCl ₃	71
Table 5.2 Cytotoxicity of synthetic acanthodendrillines [(<i>S</i>)- and (<i>R</i>)- B21] against the cancer (H292) and normal (HaCaT) cells.....	73
Table 6.1 Cytotoxicity of renieramycin M (RM), jorunnamycin A (JA), and 22- <i>O</i> -ester derivatives of JA against non-small cell lung cancer H292 and H460 cell lines.....	87

CHAPTER I

GENERAL INTRODUCTION

More than 70% of the Earth's surface is covered by the oceans, which are the habitat of a wide variety of marine lives. Marine animals, particularly invertebrates such as sponges, tunicates, cnidarians, mollusks, bryozoans, and echinoderms, are mostly sessile, slow moving, and lack physical defense structures to protect themselves from predators and competitors as well as infectious microorganisms. To compensate for these deficiencies, they have developed potent chemical defensive mechanisms known as secondary metabolites [1]. Marine secondary metabolites possess unique structures that are different from those of terrestrial counterparts, and some of which display interesting bioactivity, such as anticancer, anti-infectious, anti-inflammatory, and anti-Alzheimer's activities [2-3]. Discovery of marine natural products was started in the 1950s with the isolation of the unusual nucleosides from the Caribbean sponge *Tectitethya crypta* [4]. These nucleosides served as leads for development of anticancer cytarabine (ara-C) and antiviral drugs, such as vidarabine (ara-A) and acyclovir [5-6]. Moreover, the discovery of prostaglandin derivatives, important mediators involved in inflammatory diseases, fever, and pain, from the Caribbean Gorgonian *Plexaura homomalla* in 1969 [7] is usually considered as the starting point for any serious search for "drugs from the sea" [5].

Among all invertebrates, marine sponges have shown the largest number and the greatest chemical diversity of bioactive compounds, contributing to almost 30% of all marine natural products. Nearly 5,000 different natural products have been discovered [3, 6], and more than 200 new compounds are reported each year over the last decade [8]. To date, there are three US FDA-approved marine sponge-derived drugs (Figure 1.1), namely cytarabine (ara-C, Cytosar-U[®]), vidarabine (ara-A, Vira-A[®]), and eribulin mesylate (Halaven[®]). Cytarabine is a synthetic pyrimidine nucleoside, which was developed from spongothymidine, a nucleoside originally isolated from the Caribbean sponge *Tethya crypta* [4]. It was approved in 1969 for treatment of cancers

of white blood cells such as acute myeloid leukemia and non-Hodgkin lymphoma [9]. Vidarabine is a synthetic purine nucleoside whose synthesis was inspired by spongouridine, which was reported together with spongothymidine from the sponge *T. crypta* [4]. It was received approval in 1976 as an antiviral drug, which is active against herpes simplex and varicella zoster viruses [9]. Eribulin mesylate approved in 2010 for treatment of metastatic breast cancer [10] is a synthetic analogue of halichondrin B, a polyether macrolide first isolated from the marine sponge *Halichondria okadai* [11]. In addition, the marine sponge-derived polyketide, namely PM060184, is currently in phase I clinical trials. PM060184 is a tubulin-binding agent, originally isolated from the marine sponge *Lithoplocamia lithistoides* [12]. Consequently, marine sponges are considered as a potential source for development of new drug candidates that can lead to clinically useful treatments.

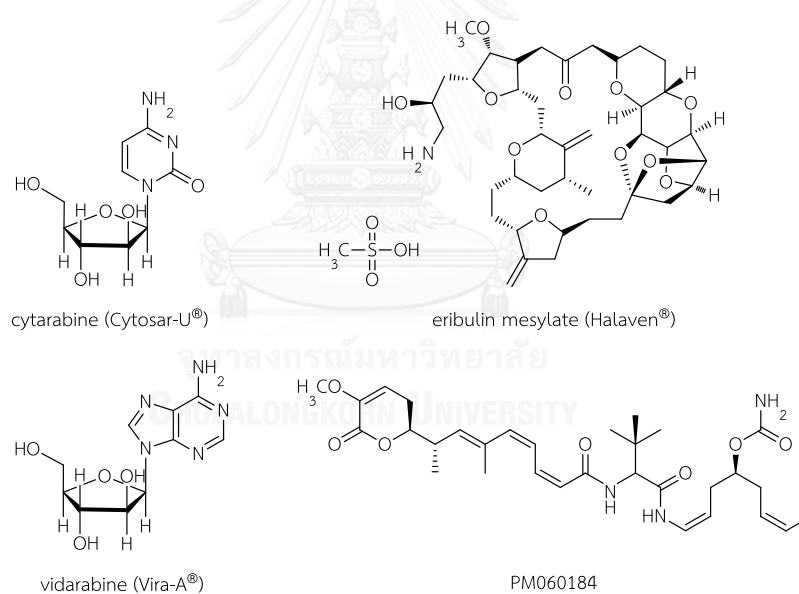


Figure 1.1 Chemical structures of marine sponge-derived drugs approved by the U.S. FDA and marine natural products currently in phase I clinical trials

In this dissertation, chemistry and bioactivities of marine natural products from two sponges *Acanthodendrilla* sp. (**chapters IV and V**) and *Xestospongia* sp. (**chapters VI-VIII**) were investigated.

According to our preliminary study, the MeOH crude extract of the sponge *Acanthodendrilla* sp. showed a strong acetylcholinesterase (AChE) inhibitory activity (80% inhibition of electric eel AChE at 100 µg/mL). The isolation and bioactive chemical constituents of the extract were therefore investigated.

Regarding our continuing investigation, the blue sponge *Xestospongia* sp. is an important source of potent cytotoxic bistetrahydroisoquinoline alkaloids, namely renieramycins. Due to the unique structures together with their potent cytotoxicity to several human cancer cell lines, renieramycins are extremely attractive from organic chemists worldwide and expected to be one of the candidates for new effective anticancer drugs. 22-*O*-Ester derivatives of jorunnamycin A (JA) were prepared from renieramycin M (RM), a major component from this blue sponge pretreated with KCN. The structure-cytotoxicity relationship of the derivatives against H292 and H460 non-small cell lung cancer cell lines were evaluated. In addition, the effects of RM on new therapeutic targets related to antimetastatic activity, including anoikis-resistant lung cancer cells and lung cancer stem-like cells, were explored. These studies will be useful for drug development in both lung cancer and lung metastatic cancer treatments.

The overall objectives of the dissertation are

1. To study chemical constituents and evaluate AChE inhibitory activity of the isolated pure compounds from the marine sponge *Acanthodendrilla* sp.
2. To prepare new 22-*O*-ester derivatives of jorunnamycin A from renieramycin M and evaluate their cytotoxicity against lung cancer cell lines.
3. To study the effects of renieramycin M on new therapeutic targets related to antimetastatic activity, including anoikis-resistant lung cancer cells and lung cancer stem-like cells.

Three publications (**chapters IV** [13], **V** [14], and **VII** [15]) and two manuscripts (**chapters VI** and **VIII**) are presented as parts of my dissertation and appear as individual chapter.

CHAPTER II

LITERATURE REVIEW

1. Sponge *Acanthodendrilla* sp.

1.1. Taxa and description of the sponge *Acanthodendrilla* sp.

Kingdom: Animalia

Phylum: Porifera

Class: Demospongiae

Subclass: Keratosa

Order: Dendroceratida

Family: Dictyodendrillidae

Genus: *Acanthodendrilla* Bergquist, 1995

A nonspicule-forming sponge *Acanthodendrilla* has an irregular mesh arrangement with all elements cored with detritus of the reticulate fibrous skeleton. Reticulation is more pronounced superficially, and ascending primary fibers project markedly above the sponge surface. Family Dictyodendrillidae contains 4 valid genera: *Dictyodendrilla*, *Acanthodendrilla*, *Spongionella*, and *Igernella*. The irregular reticulum and strongly cored fibers distinguish *Acanthodendrilla* from *Dictyodendrilla* and *Spongionella*, and the absence of spongin spicules distinguishes it from *Igernella* [16-18].

1.2. Chemistry and biological activities of marine natural products from sponges of the genus *Acanthodendrilla*

During the last two decades, the sponges of the genus *Acanthodendrilla* have attracted scientific interests to study their chemical constituents and biological activities. These sponges were found to be rich sources of novel bioactive terpenoids [19-24].

1.2.1. Sesterterpenoids

Luffariellolide is a linear sesterterpene first isolated from the Palauan sponge *Luffariella* sp. and possessed anti-inflammatory activity through reversible inhibition of phospholipase-A₂ [25]. Then, five luffariellolide-related sesterterpenes, acantholides A-E, together with luffariellolide and its 25-O-methyl and 25-O-ethyl derivatives, were isolated from the Indonesian sponge *Acanthodendrilla* sp. Acantholide B, luffariellolide and its 25-O-methyl congener (Figure 2.1) were active against bacteria *Staphylococcus aureus*, *Bacillus subtilis*, and *Escherichia coli*, yeast *Candida albicans*, and plant pathogenic fungus *Cladosporium herbarum*. In addition, acantholide E, luffariellolide and its 25-O-methyl congener (Figure 2.1) were cytotoxic to mouse lymphoma L5187Y cell line [20].

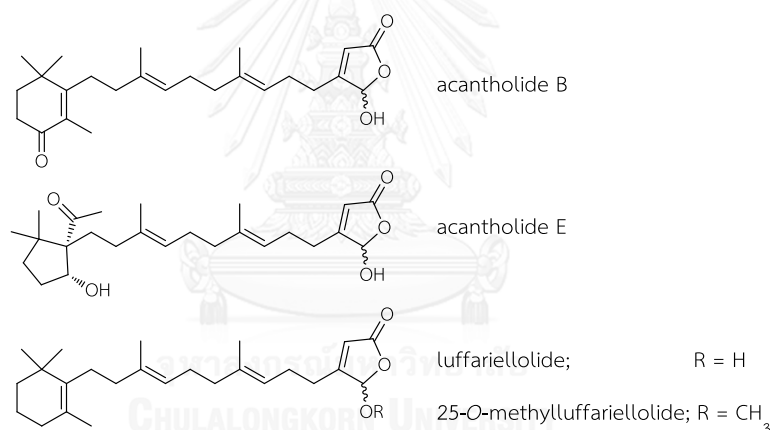


Figure 2.1 Examples of sesterterpenoids isolated from *Acanthodendrilla* sp.

1.2.2. Sterols

Steroidal sulfates commonly found in marine sponges showed a variety of biological activities, such as antimicrobial, antithrombin, HIV-inhibitory, and tyrosine kinase inhibitory activities. Ten steroidal sulfates, acanthosterol sulfates A-J, were isolated from the Japanese sponge *Acanthodendrilla* sp. Among them, acanthosterol sulfates I and J (Figure 2.2) showed antifungal activity against the yeast *Saccharomyces cerevisiae* A364A and its mutants at 0.1 mg/disk [19].

Agosterols, polyhydroxylated sterols, were initially isolated from a marine sponge *Spongia* sp. and found to reverse multidrug resistance in tumor cells [26-27]. Then, seven polyhydroxylated sterols were isolated from the Japanese sponge *Acanthodendrilla* sp. as proteasome inhibitors. Agosterol C (Figure 2.2) most strongly inhibited chymotrypsin-like activity of the proteasome with an IC_{50} value of 10 $\mu\text{g/mL}$ [22].

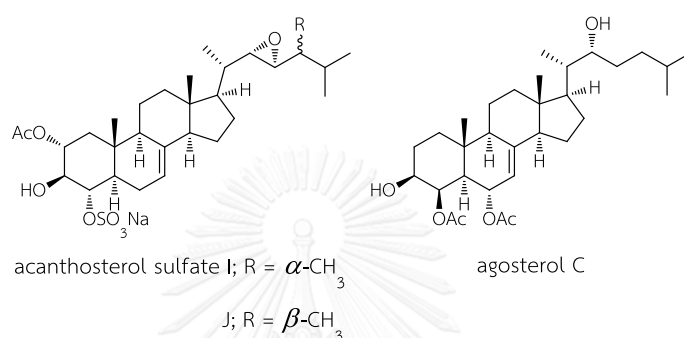


Figure 2.2 Examples of sterols isolated from *Acanthodendrilla* sp.

1.2.3. Meroterpenoids

Acanthosulfate (Figure 2.3), a disulfated merosesterterpene having a scalarane-type skeleton, was isolated from the Philippines sponge *Acanthodendrilla* sp. and showed an IC_{50} value of 4.5 μM for inhibition of the proteasome function, the enzyme is responsible for the degradation of endogenous proteins [23].

Two meroterpenoids, (+)-makassaric acid and (+)-subersic acid (Figure 2.3), were isolated from the Indonesian sponge *Acanthodendrilla* sp. and showed IC_{50} values of 20 and 9.6 μM , respectively, for inhibition of the protein kinase MAPKAP [24]. MAPKAP kinase inhibitors represent potential therapeutic agents to treat various inflammatory diseases, such as rheumatoid arthritis, where $\text{TNF-}\alpha$ plays a key role.

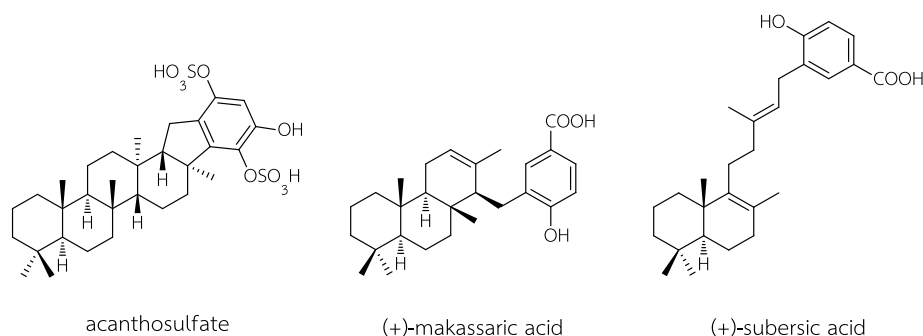


Figure 2.3 Meroterpenoids isolated from *Acanthodendrilla* sp.

1.3. Chemistry and biological activities of bromotyrosine alkaloids

Bromide is the second most abundant halide ion in sea water [28]. It is believed that marine organisms are constantly exposed to these ions and have developed to incorporate halogens into the biosynthesis of marine compounds. These brominated marine natural products might be used as chemical defenses against their pathogens and predators [29-30]. Bromotyrosine alkaloids, a specific class of brominated secondary metabolites, are very common occurrence within marine sponges belonging to the order Verongiida [31]. However, these alkaloids have been also isolated from other sponges belonging to distinct taxa and other marine organisms, such as the sponges *Oceanapia* sp. (order Haplosclerida) [32], *Jaspis wondoensis* and *Poecillastra wondoensis* (order Tetractinellida) [33], and *Cymbastela* sp. and *Axinella* sp. (order Axinellida) [34-35], the ascidian *Polycitor africanus* [36], and the crinoid *Himerometra magnipinna* [37].

Since the first bromotyrosine derivative, verongiaquinol, was discovered in 1967 [38], knowledge of the chemistry of these compounds driven by the diverse bioactivities has grown tremendously. To date, more than 300 different bromotyrosine alkaloids have been identified and mainly categorized into 6 classes according to their chemical structures [39]:

1. Simple bromotyrosine derivatives

One bromotyrosine unit undergoes alkylation, degradation, esterification, hydroxylation, or reduction with simple functional groups, such as verongiaquinol and its dimethoxyketal (3,5-dibromo-1-hydroxy-4,4-dimethoxy-2,5-cyclohexadiene-1-acetamide); aeroplysinins-1 and -2; cavernicolins-1 and -2; and LL-PPA216 (Figure 2.4).

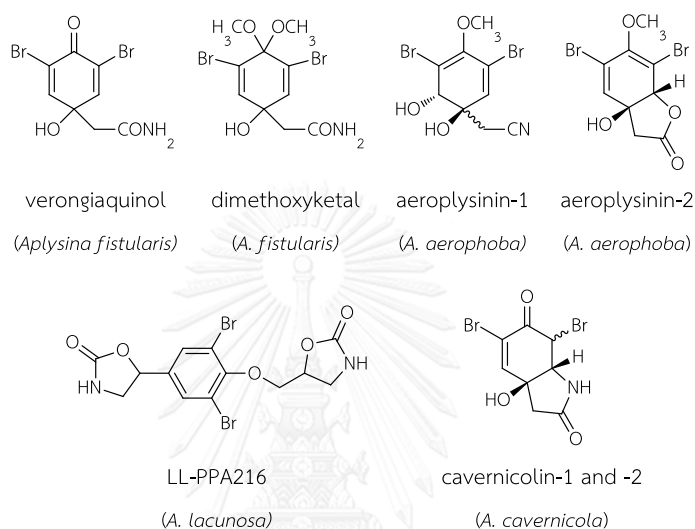


Figure 2.4 Examples of simple bromotyrosine derivatives

The proposed biosynthetic scheme of verongiaquinol shown in Figure 2.5 was involved in enzymatic bromination of tyrosine, oxidation to oxime, decarboxylation to nitrile, hydration to amide, and then conversion into the dienone [40]. The dimethoxyketal was considered as artifacts generated during the MeOH extraction process [41]. Verongiaquinol exhibited antimicrobial activity against *S. aureus*, *Enterococcus faecium*, *B. subtilis* and *E. coli* with MIC 1.56, 50.0, 1.56, 12.5 $\mu\text{g/ml}$, respectively [42]; cytotoxic activity against Ehrlich ascites tumor and HeLa tumor cells with IC_{50} s 26.1 and 15.6 μM , respectively [43]; and Na^+/K^+ -ATPase inhibitory activity [44]. In contrast, bioactivity of the dimethoxyketal has not yet been reported.

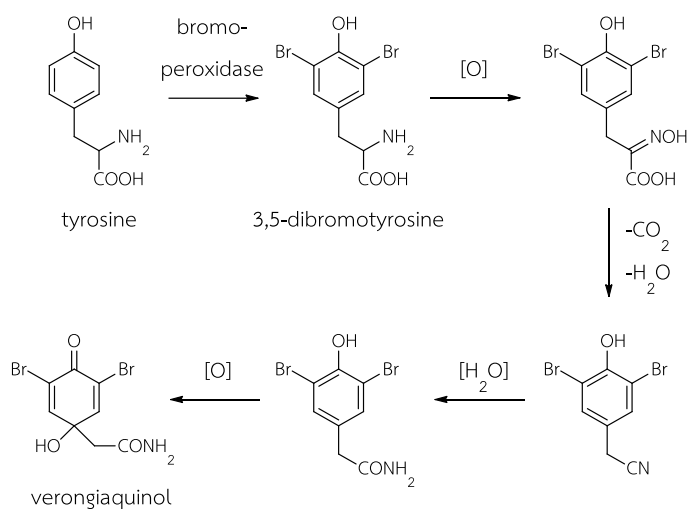


Figure 2.5 Proposed biosynthetic pathway of verogiaquinol

2. Spirocyclohexadienylisoxazoline bromotyrosine derivatives

One or two bromotyrosine units are transformed into spirocyclohexadienylisoxazoline (SHI) *via* arene oxide biosynthetic pathway (Figure 2.6) [39]. Nucleophilic epoxide opening by oxime moiety furnishes the SHI core. Based on this mechanism, the *trans* relative configuration between the hydroxyl (C-1) and oxygen (C-6) in the SHI moiety is conserved.

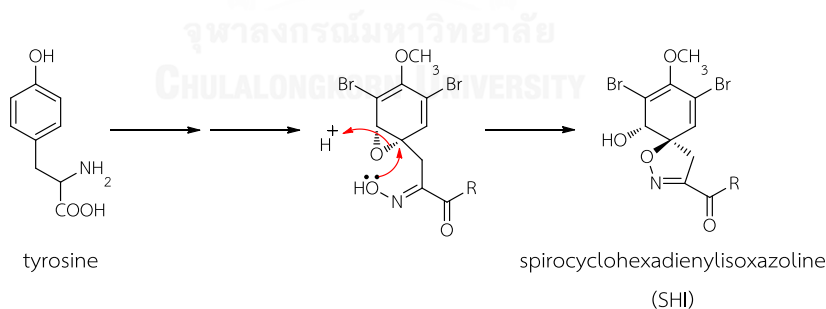


Figure 2.6 Formation of spirocyclohexadienylisoxazoline

This group generally consists of one to three bromotyrosine-derived units (e.g., arothionin, homoaerthionin, and fistularin-1) and other functional groups, such as histamine (e.g., pseudoceratinine A), and linear hydrocarbon side chain (e.g., subereamolline D) as shown Figure 2.7. Arothionin and homoaerthionin are the first bromotyrosine derivatives of this class [45]. The SHI moieties are derived from

bromotyrosine units, while the C₄ and C₅ side chains of aerothionin and homoaerothionin are probable derived from ornithine and lysine, respectively. The absolute configuration of the SHI moiety of aerothionin was determined as 1*R*, 1'*R*, 6*S*, and 6'*S* by X-ray crystallographic analysis and the positive optical rotation and positive Cotton effects near 250 and 290 nm in CD spectrum [46]. On the other hand, the absolute configuration of pseudoceratinine A was deduced as 1*S*, 6*R* by the negative optical rotation and negative Cotton effects near 250 and 290 nm [47]. Aerothionin and homoaerothionin inhibited the growth of *S. aureus* at 100 µg/disk, *B. subtilis* at 50 µg/disk and *C. albicans* at 50 µg/disk [48]. Moreover, aerothionin exhibited antimycobacterial activity against *Mycobacterium kansasii* (MIC 50 µg/ml), *M. scrofulaceum* (MIC 100 µg/ml), and *M. avium* (MIC 100 µg/ml) [49] and cytotoxicity against HeLa cells (EC₅₀ 42 µM) [50].

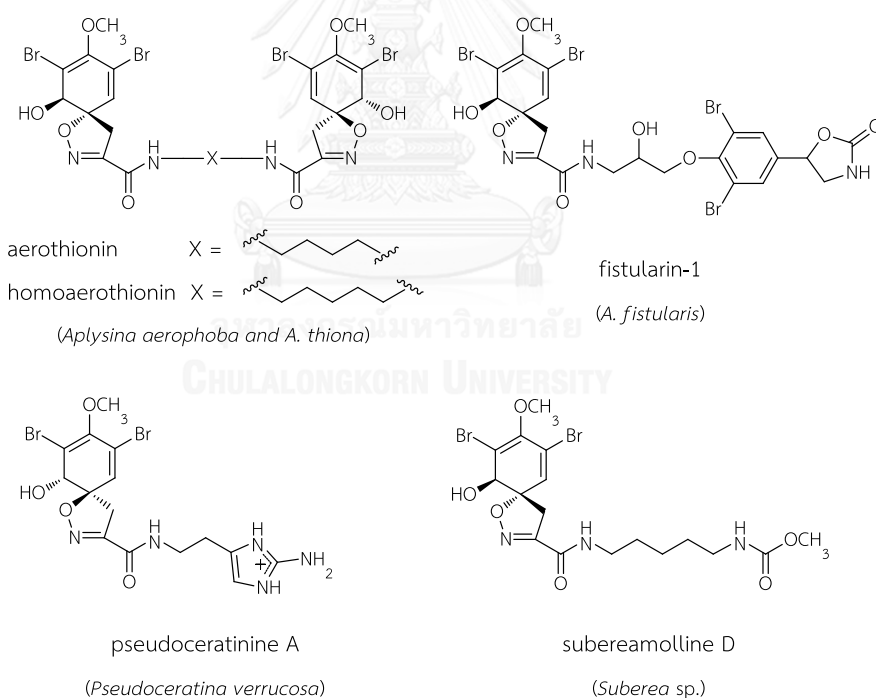


Figure 2.7 Examples of spirocyclohexadienylisoxazoline bromotyrosine derivatives

3. Spirooxepinisoxazoline bromotyrosine derivatives

One bromotyrosine unit is transferred into spirooxepinisoxazoline (SOI) as shown in Figure 2.8. Tyrosine precursor is oxidized by epoxidase, and then undergoes rearrangement to the oxepin, which subsequently reacts with oxime to give the SOI moiety [51].

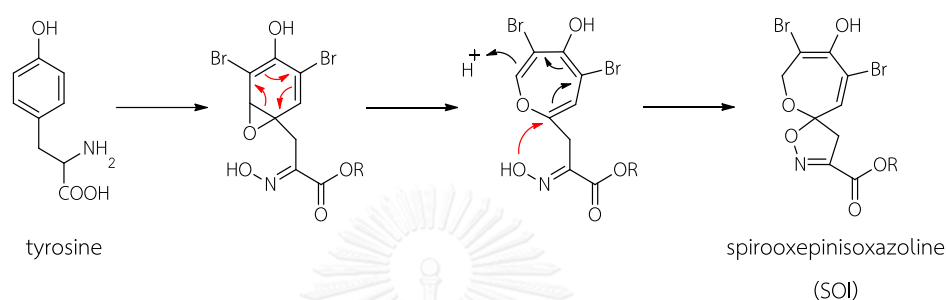


Figure 2.8 Formation of spirooxepinisoxazoline

To date, twelve compounds have been reported in this class, including psammaplysins A-J and ceratinamides A and B (Figure 2.9), which were isolated from *Aplysinella* sp. [52], *Hyattella* sp. (order Dictyoceratida) [53], *Pseudoceratina* sp. [54-56], *Rhaphoxya* sp. (order Bubarida) and *Suberea* sp. [57]. Psammaplysins A, B, and C exhibited moderate cytotoxicity (IC_{50} s 6, 6, and 3 $\mu\text{g}/\text{ml}$, respectively) against HCT116 colon tumor cells [54]. Psammaplysins F, G, and H displayed antimalarial activity (IC_{50} s 1.9, 5.2, and 0.4 μM , respectively) against chloroquine-sensitive (3D7) *Plasmodium falciparum* [56].

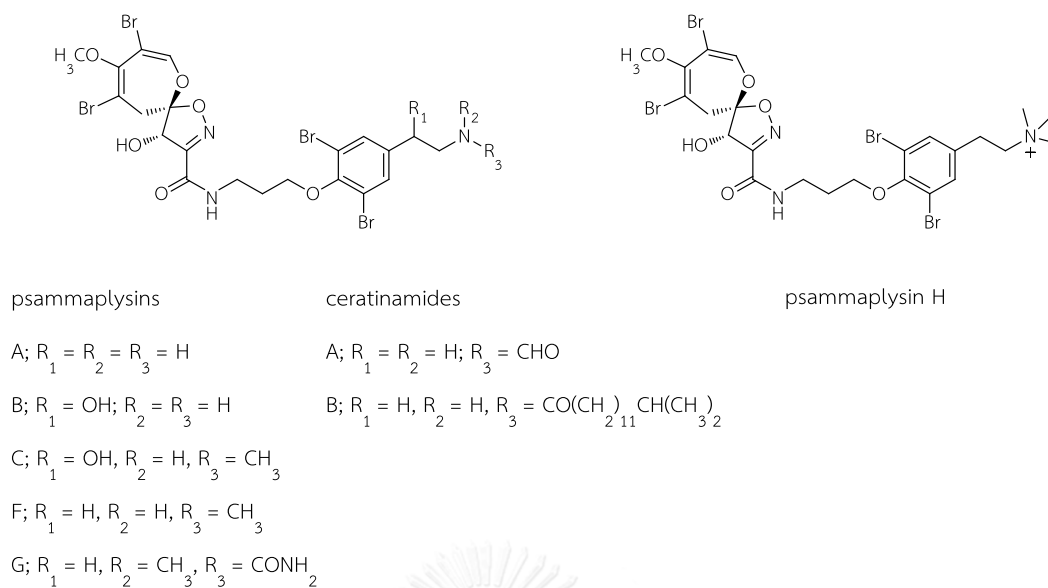


Figure 2.9 Examples of spirooxepinisoxazoline bromotyrosine derivatives

4. Oxime bromotyrosine derivatives

The amine functionality of bromotyrosine is oxidized into the oxime. The majority of these compounds have been shown to have a (*E*)-2-(hydroxyimino)-*N*-alkylamide functional motif. (*E,Z*)-Psammaplin A is the first bromotyrosine derivative possessing the *Z*-isomeric motif. The geometry was determined by the chemical shifts of the C-7, which are about 27 and 36 ppm for the *E*-geometry and *Z*-geometry, respectively [58]. This class are categorized into 3 groups based on their structures (Figure 2.10): oxime-tyramine (e.g., purealidin C, aplysamin-2), oxime-histamine (e.g., verongamine), and oxime-disulfide (e.g., psammaplin A).

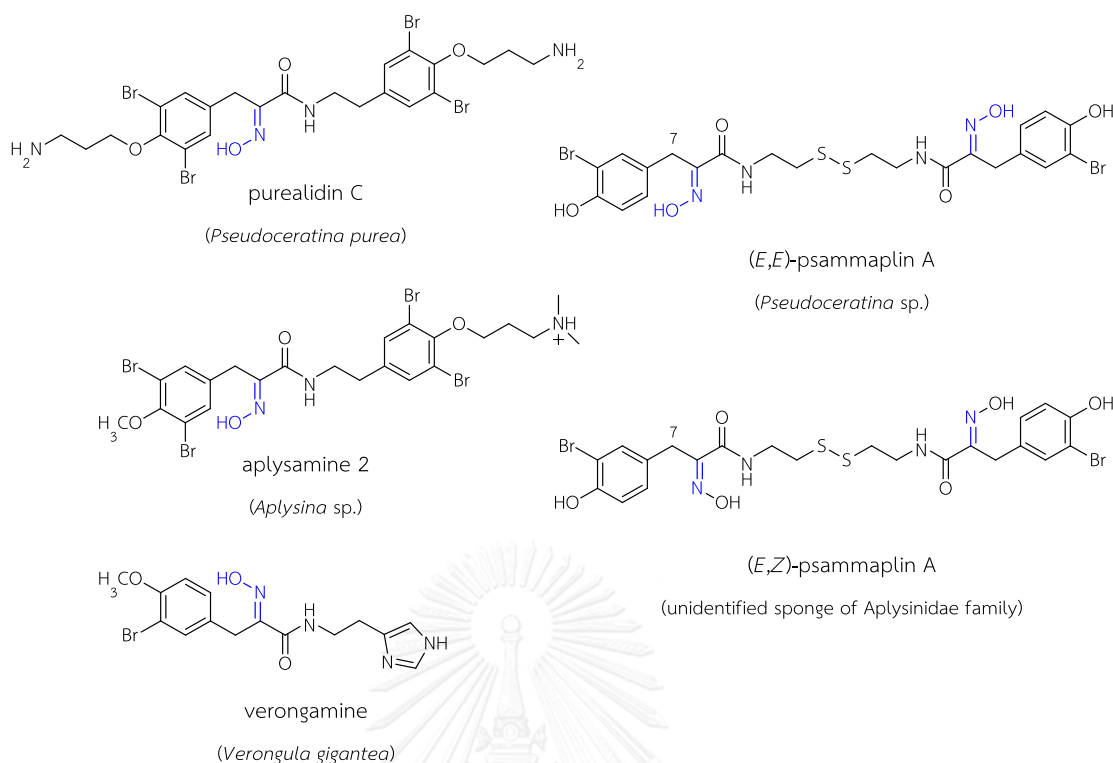


Figure 2.10 Examples of oxime bromotyrosine derivatives

Purealidin C showed modest antibacterial activity against *S. aureus*, *Sarcina lutea*, and *B. subtilis*; antifungal activity against *C. albicans*, *Cryptococcus neoformans*, and *Paecilomyces variotii*; and cytotoxicity against KB epidermoid carcinoma and L1210 murine lymphoma cells with IC_{50} s 3.2 and 2.4 $\mu\text{g/ml}$ [59]. Alypsamine 2 showed acetylcholinesterase inhibitory activity with IC_{50} 1.3 μM [60]. Verongamine gave specific histamine- H_3 receptor binding with IC_{50} 0.5 μM [61]. (*E,E*)-Psammaplin A has a significant cytotoxicity to several cancer cell lines, such as lung A549, ovarian SK-OV-3, skin SK-MEL-2, CNS XF498, and colon HCT15 [33] and potent human topoisomerase II and histone deacetylase inhibitory activities with IC_{50} s 18.8 and 0.003 μM , respectively [62-63]. In addition, it inhibited mycothiol-S-conjugate amidase from *Mycobacterium tuberculosis* with IC_{50} 2.8 μM [64].

5. Bastadins

Bastadins are a class of acyclic and macrocyclic bromotyrosine alkaloids, which are derived from four bromotyrosines. The majority of bastadins were isolated from marine sponges of the genera *Ianthella* and *Pseudoceratina*. Bastadins-4, -8, and -9 (Figure 2.11) isolated from *I. basta* exhibited cytotoxicity against L-1210 mouse lymphocytic leukemia with ED_{50} 5 $\mu\text{g/ml}$ [65].

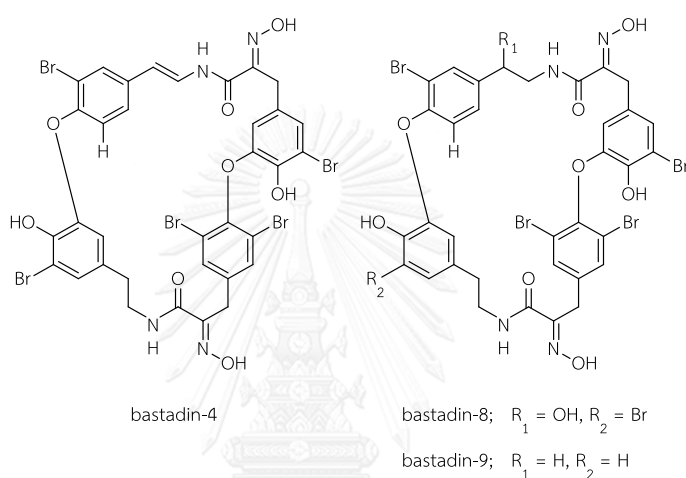


Figure 2.11 Examples of bastadins

6. Miscellaneous

A number of bromotyrosine-derived compounds are not classified to any above classes, such as, aplysillin A, ma'edamine A, polyandrocarpamide A, and geodiamolide J (Figure 2.12). The common feature of this class is biogenetic bromotyrosine precursor.

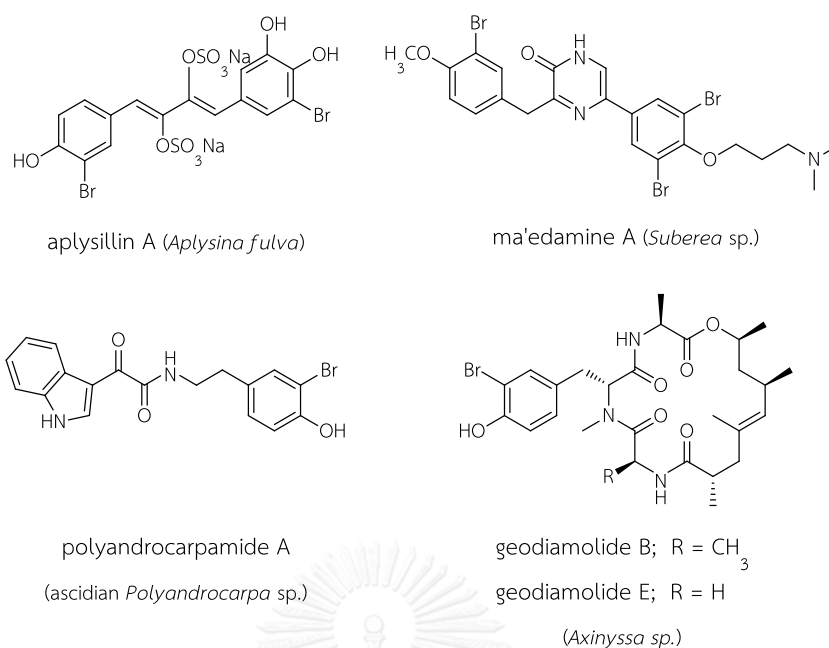


Figure 2.12 Examples of miscellaneous bromotyrosine derivatives

Aplysillin A is a weak thrombin receptor antagonist isolated from *Aplysina fulva*, which is typically known for its production of bromotyrosine derivatives [66]. Ma'edamine A is probably derived from 11,12-dehydro form of aplysamine 2 through the cyclization of six-membered ring and dihydroxylation. It exhibited cytotoxicity against murine leukemia L1210 and KB cells with IC₅₀s 4.3 and 5.2 µg/ml, respectively [67]. Polyandropamidines are derived from tyrosine and tryptophan units [68]. Geodiamolides are cyclic desipeptides that vary in type and position of amino acids and polyketide fragments [34, 69-72]. Geodiamolides A-F originally isolated from *Geodia* sp. (order Tetractinellida) and *Axinyssa* sp. (order Suberitida) showed potent cytotoxicity against L1210 with IC₅₀ values in the range of 2.5-14.0 ng/ml [70].

Most of these alkaloids possess a wide range of bioactivities, including antimicrobial [42, 48-49, 59, 73-75], antiviral [76], antifungal [48, 59], antimalarial [56, 77], cytotoxic [33, 43, 50, 54, 59, 65, 67, 70, 73-74, 78-81], anti-inflammatory [82], histamine H₃ antagonism [61], thrombin receptor antagonism [66] and enzyme inhibitory activities, such as Na⁺-K⁺-ATPase [44], protein tyrosine phosphatase [83], mycothiol S-conjugate amidase [64], topoisomerase II [62], histone deacetylase [63],

and acetylcholinesterase [60]. Among the diverse bioactivities of these alkaloids, the antimicrobial and cytotoxic activities have been most frequently reported.

1.4. Acetylcholinesterase inhibitory activity

Alzheimer's disease (AD) is a neurodegenerative disorder and the leading cause of dementia, mainly affects people over the age of sixty. Approximately 46.8 million people worldwide are living with dementia according to the 2015 estimation and this number will increase dramatically in the future, escalating up to 131.5 million cases by 2050 [84]. AD is characterized by loss of neurons and synapses in the cerebral cortex and subcortical regions, collapse of cognitive functions, and formation of amyloid plaques and neurofibrillary tangles. The causes of AD are not well understood so several competing hypotheses exist trying to explain the cause of the disease, such as cholinergic, glutamatergic, amyloid, and tau hypotheses [85]. However, most currently available drug therapies are based on the cholinergic hypothesis involving in the reduction of acetylcholine (ACh). The reduction of ACh synthesis in AD patients leads to loss of ACh receptor stimulation that appears to relevant to cognitive process and memory [85-88]. Acetylcholinesterase (AChE) is a serine hydrolase that hydrolyzes acetylcholine (ACh) into inactive choline and acetic acid, which terminates the neurotransmission process. AChE is mainly expressed in nervous tissues, neuromuscular junctions and red blood cells [85]. Inhibition of AChE results in a prolongation of the existence and the activity of ACh [88]. Another type of cholinesterase is butyrylcholinesterase (BChE) that hydrolyses many different choline-based esters. BChE is made in liver and found mainly in blood plasma and neuroglia. BChE is less substrate specific towards ACh and hydrolyses ACh slower than AChE. The physiological role in the cholinergic transmission has not been fully understood, but the possibility to use selective BChE inhibitors or dual action AChE/BChE inhibitors was suggested for symptomatic improvement in AD [89].

Structural insights on AChE and most *in vitro* work on AChE inhibitors have been carried out using the AChEs of electric eel *Electrophorus electricus* (EeAChE) and

electric ray *Torpedo californica* (TcAChE), which are structurally similar to that of mammalian. As shown in Figure 2.13, the active site of AChE (the catalytic anionic site, CAS) located in the bottom of a deep and narrow gorge is divided into 4 main subsites: esteratic subsite (ES), anionic subsite (AS), oxyanion hole (OX), and acyl pocket (AP). The ES contains the catalytic triad of serine200-histidine440-glutamate327 responsible for nucleophilic attack to the carbonyl ester of ACh. The AS mainly comprising of aromatic residues is responsible for the interaction with quaternary ammonium group of ACh. The OX stabilizes the tetrahedral intermediate of ACh formed during the catalytic process. The AP is believed to play a role in substrate selectivity. The major differences between AChE and BChE involve this subsite [88]. Another important subunit known as the peripheral anionic site (PAS) is located at the active center gorge entry. Binding at the PAS could lead to changes in the allosteric conformation of the active catalytic center [90]. The CAS is highly conserved in AChEs from different species, while the PAS varies among them [88, 91].

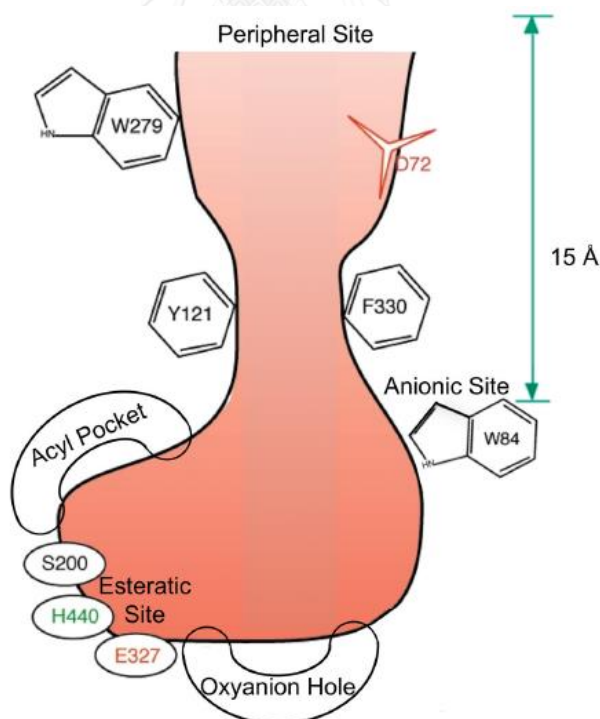


Figure 2.13 Schematic view of the active site gorge of *Torpedo californica* acetylcholinesterase. The bottom of the gorge consists of the esteratic site, anionic site, oxyanion hole, and acyl pocket, and the peripheral anionic subsite is located close to the entry of the gorge [92].

The AChE inhibitory activity is measured according to the *in vitro* modified Ellman's method [93-94]. The chemical principle of the enzymatic reaction is depicted in Figure 2.14. Acetylthiocholine iodide (ATCI) and 5,5'-dithiobis(2-nitrobenzoic acid) (DTNB, Ellman's reagent) are used as substrates. AChE hydrolyzes ATCI to thiocholine iodide and acetic acid. Then, thiol of thiocholine iodide cleaves the disulfide bond of DTNB to produce 5-thio-2-nitrobenzoate that has yellow color. The color intensity of the product is measured at 405 nm. The BChE inhibitory assay is carried out under the same protocol as described above, except the substrate and enzyme were replaced with butyrylthiocholine chloride and BChE, respectively.

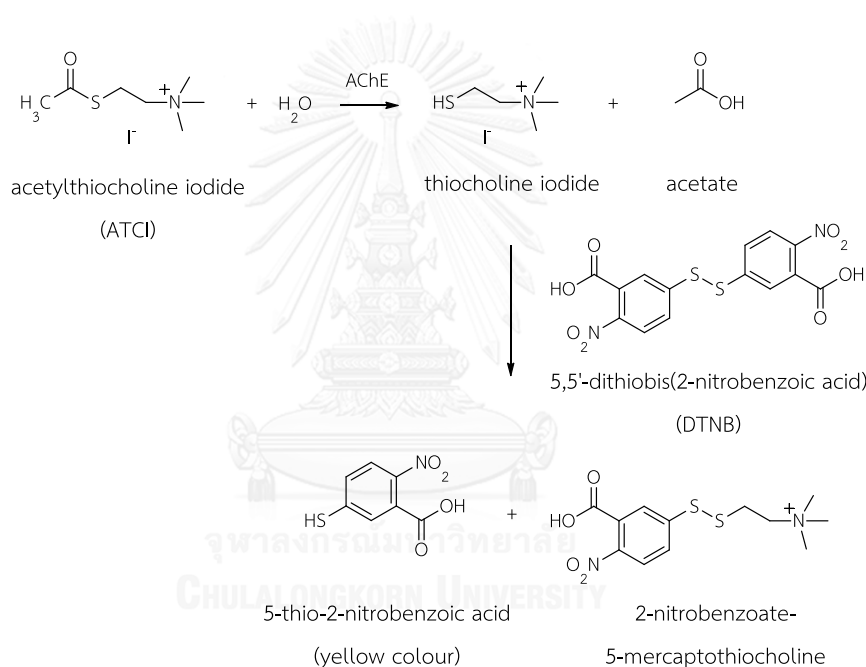


Figure 2.14 Chemical principle of the Ellman's method

To date, three prescription drugs acting as AChE inhibitors have been approved by the U.S. Food and Drug Administration (FDA) for symptomatic treatment of AD, including donepezil (Aricept[®]), a selective, non-competitive, reversible AChE inhibitor; rivastigmine (Exelon[®]), a dual AChE/BChE, non-competitive, slow-reversible carbamate inhibitor; and galantamine (Razadyne[®]), a selective, competitive, rapidly-reversible AChE inhibitor (Figure 2.15). Two of them are derived from natural sources, including rivastigmine, a synthetic analog of physostigmine isolated from the seeds of

Physostigma venenosum [88, 95], and galantamine, a natural product isolated from *Galanthus woronowii* and several other plants within the order Amaryllidaceae [96]. Consequently, extensive research has been focused on the discovery of naturally derived AChE inhibitors.

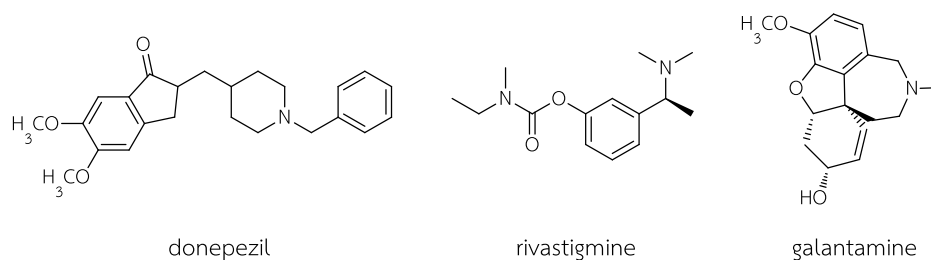


Figure 2.15 Acetylcholinesterase inhibitors approved by the U.S. FDA for symptomatic treatment of Alzheimer's disease

The majority of the naturally occurring AChE inhibitors are primarily reported from plants, with a comparatively few molecules from marine origins [88, 95]. However, those reported marine natural products have exhibited strong inhibitory activity against AChE compared to standard drugs, tacrine and galantamine (IC_{50} s 0.06 and 0.6 μ M, respectively). These include 4-acetoxy-plakinamine B (IC_{50} 3.8 μ M), a steroidal alkaloid isolated from the sponge *Corticium* sp. [97]; petrosamine (IC_{50} 0.09 μ M), a pyridoacridine alkaloid isolated from the sponge *Petrosia* n. sp. [98]; phlorofucofuroeckol A (IC_{50} 4.9 μ M), a phlorotannin isolated from the brown algae *Ecklonia stolonifera* [99]; and marinoquinoline A (IC_{50} 4.9 μ M), a pyrrole alkaloids isolated from the marine gliding bacterium *Rapidithrix thailandica* [100] (Figure 2.16).

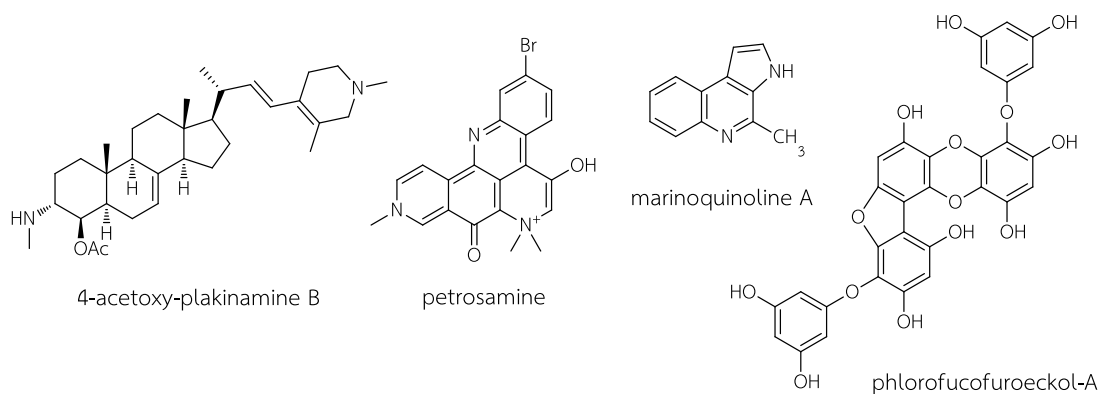


Figure 2.16 Acetylcholinesterase inhibitors from marine origins

Recently, non-competitive inhibition of AChE by four bromotyrosine alkaloids, including purealidin Q, isoanomoian A, aplyzanzine A, and aplysamine 2 (IC_{50} s 1.2, 70, 104, and 1.3 μ M, respectively), from the sponge *Pseudoceratina cf. purpurea* has been reported (Figure 2.17). The *N,N*-dimethylaminopropoxydibromotyramine moiety of these compounds were proposed as an important subunit for AChE inhibitory activity [60].

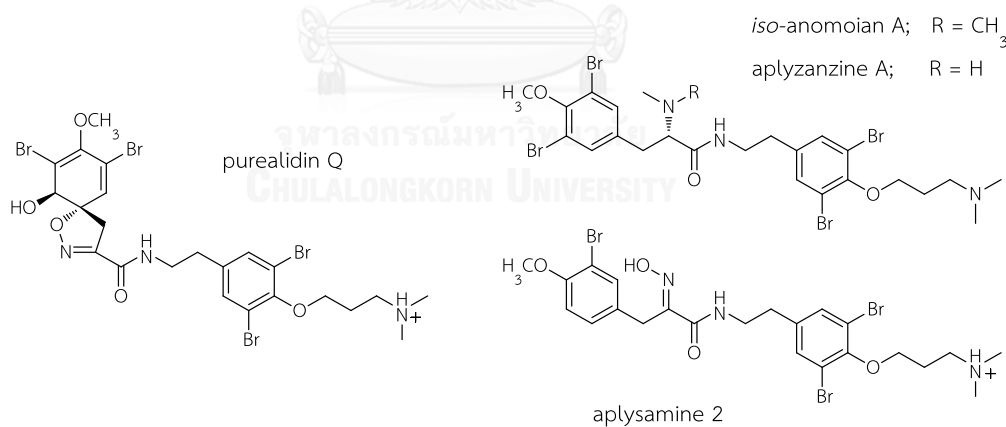


Figure 2.17 Bromotyrosine alkaloids acting as acetylcholinesterase inhibitors from *Pseudoceratina cf. purpurea*

2. Sponge *Xestospongia* sp.

2.1. Taxa and description of the sponge *Xestospongia* sp.

Kingdom: Animalia

Phylum: Porifera

Class: Demospongiae

Subclass: Heteroscleromorpha

Order: Haplosclerida

Family: Petrosiidae

Genus: *Xestospongia* de Laubenfels, 1932

Family Petrosiidae contains 4 valid genera: *Petrosia*, *Neopetrosia*, *Xestospongia*, and *Acanthostrongylophora*. Spicule forms and sizes are considered as an important taxonomic characters among different genera. Desqueyroux-Faúndez and Valentine (2002) provide key to this genus as follows [101]:

“Ectosomal skeleton undifferentiated from choanosomal skeleton, consisting of a very dense disordered network of free spicules, with a single type of spicule of a single size class larger than 200 μm long. Choanosomal skeleton consisting of short longitudinal, undivided, pauci- to multispicular tracts connected by few oxeas, causing irregular meshes”

The blue sponge sample was collected from Sichang Island, the Gulf of Thailand and identified as *Xestospongia* sp. #2133 (family Petrosiidae) by Dr. John N. A. Hooper. The voucher specimen was deposited at the Queensland Museum, South Brisbane, Australia (sample code QMG306998) and the Department of Pharmacognosy and Pharmaceutical Botany, Faculty of Pharmaceutical Sciences, Chulalongkorn University, Bangkok, Thailand. This sponge exhibits thick, encrusted, lobate growth. Its texture is hard, brittle and easily crumbled. Its color is light grayish-blue when alive and turns to pinkish in ethanol. Oscula are numerous and of moderate size, and are found, on apexes of surface lobes, with slightly raised lips. Its surface has prominent bulbous surface lobes with some that are nearly digitate in size. The surface is

translucent, membranous, optically smooth, macroscopically bulbous, and microscopically even, with choanosomal drainage canals that are slightly visible below the surface. Ectosomal skeleton membranes have no specialized speculation or structure. The choanosomal skeleton with isotropic reticulation of paucispicular tracts of oxeas forms tight oval meshes. Many free oxeas are scattered between tracts. Small to moderately sized subdermal cavities are observed throughout skeleton. There are no visible fibers and only small amounts of collagen in the mesophyll. The oxeas are robust, straight or slightly curved at the center, sharply pointed, and hastate (190-210 × 12-18 m) [102].

2.2. Tetrahydroisoquinoline alkaloids

A study of tetrahydroisoquinoline family started from the isolation of an antibiotic naphthyridinomycin from *Streptomyces lusitanus* in 1974 [103]. These alkaloids are chemically classified into saframycin, naphthyridinomycin, quinocarcin, and tetrazomine families. Saframycin family is bistetrahydroisoquinolines divided into 4 groups, including saframycins, safracins, renieramycins, and ecteinascidins (Figure 2.18). These tetrahydroisoquinoline alkaloids have been isolated from bacteria, sponges, tunicates, and nudibranchs. Most of them display antimicrobial and anticancer activities [104]. The main difference among 4 groups is the C-22 side chain: saframycins contain a pyruvamide, safracins contain an alanyl amide, renieramycins contain an angelate ester, whereas ecteinascidins contain a ten membered sulfide-containing lactone ring attached with a tetrahydroisoquinoline or a tetrahydro- β -carboline or a chain of carbon units [105].

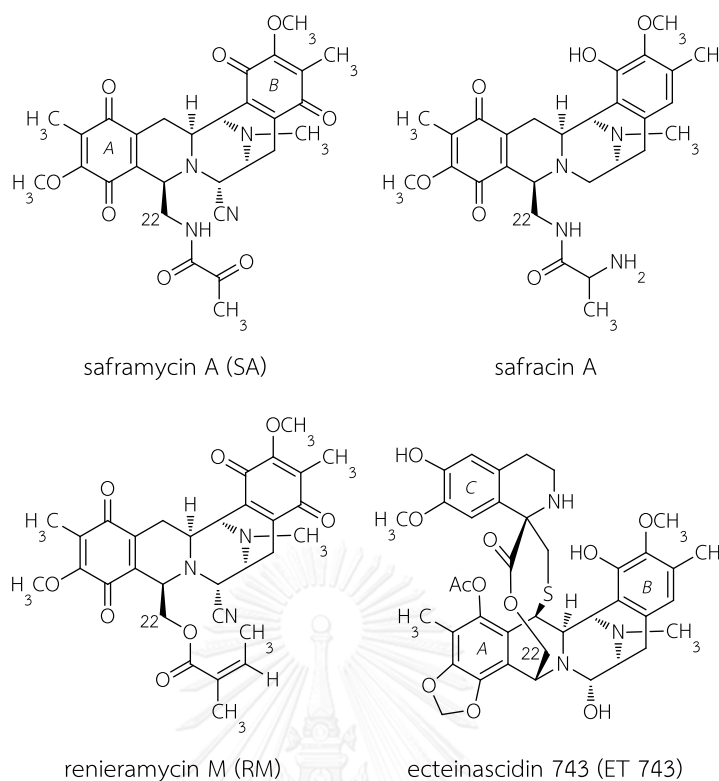


Figure 2.18 Chemical structures of selected saframycin type compounds

2.2.1. Biosynthesis of tetrahydroisoquinoline alkaloids

The chemical structures of saframycins, safracins, renieramycins, and ecteinascidins are formed by a two-fused tetrahydroisoquinoline ring (units A and B) linked to different C-22 side chains. The similarity of the conserved A and B subunits suggested that they might share biosynthetic pathway and precursors. The biosynthesis of saframycins A (SA), which was isolated from *Streptomyces lavendulae* [106] have been elucidated by feeding experiments of the carbon-labeled precursors. It was proposed that SA is biosynthesized by the condensation of two tyrosine molecules to generate the quinone ring system. A dipeptide of glycine and alanine were incorporated as the precursors for pyruvamide side chain, and the five methyl groups arose directly from methionine (Figure 2.19) [107-108]. Moreover, biosynthetic study of saframycin Mx1 (SMx1), which was isolated from *Myxococcus xanthus* [109], revealed that enzymes involved in its biosynthesis were two multifunctional nonribosomal peptide synthetases (NRPS) and one *O*-methyltransferase [110].

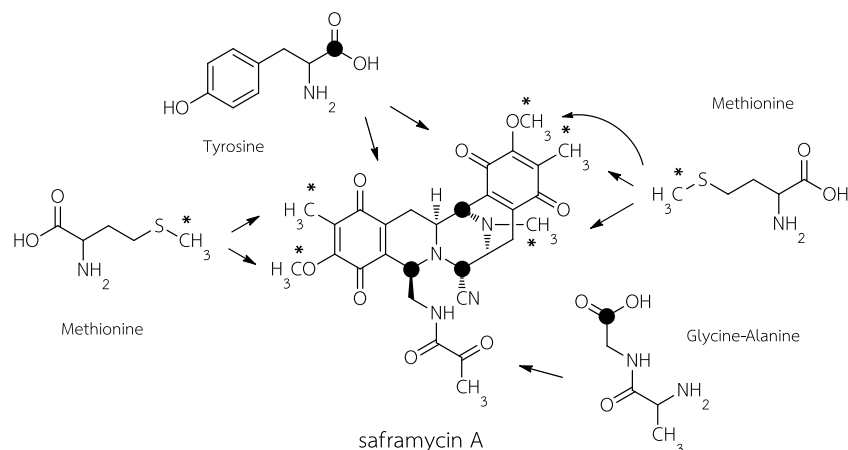


Figure 2.19 Biosynthetic precursors of saframycin A

Biosynthesis of renieramycins has not yet been defined; however, Cheun-arom (2012) proposed that RM may be derived from two molecules of tyrosine and one molecule of glycine through the same NRPS biosynthetic pathway with saframycins [111].

2.2.2. Marine tetrahydroisoquinoline alkaloids as anticancer drugs and potential drug candidates

Ecteinascidin 743 (ET 743) is a tristetrahydroisoquinoline alkaloid that was initially isolated from the Caribbean tunicate *Ecteinascidia turbinata* in 2002 [112]. ET 743 or trabectedin is a marine anticancer drug under the trade name Yondelis approved by the European Commission in 2007 and the U.S. Food and Drug Administration in 2015 for the treatment of patients with advanced liposarcoma and leiomyosarcoma after failure of standard treatments [113-114]. Its mechanism of action is unique from that of the other alkylating agents used in chemotherapy, such as cisplatin and ifosfamide. Traditional alkylating agents mostly bind to the N7 position of guanine nucleotides in DNA major groove, while ET 743 binds to the exocyclic N2 amino group of guanine nucleotides in DNA minor groove through an iminium intermediate of the carbinolamine moiety presenting in unit A. This binding is additionally stabilized through hydrogen bonding and van der Waals interactions between units A and B with neighboring nucleotides in the DNA double helix. In

addition, the formation of DNA adducts of ET 743 in the minor groove results in bending the helix toward the major groove. The units A and B are responsible for covalent interaction and hydrogen bonding with the target DNA, whereas C subunit protrudes from the DNA duplex, allowing an interaction with DNA binding proteins, such as DNA repair proteins and transcription factors [115-116].

Lurbinectedin (PM01183) and Zalypsis[®] (PM00104), synthetic tetrahydroisoquinoline alkaloids related to trabectedin, have been progressed in phase II clinical trials. Trabectedin, lurbinectedin and Zalypsis[®] contain the same units A and B, but differ in unit C (Figure 2.20). The tetrahydroisoquinoline presenting in unit C of trabectedin was replaced by the tetrahydro- β -carboline in lurbinectedin, while Zalypsis[®] lack of 10-membered lactone ring, and replaced the tetrahydroisoquinoline of trabectedin by trifluorocinnamic acid moiety. All compounds showed antiproliferative activity against several cancer cell lines at concentrations in the nM range. However, antitumor activity in several tumor models *in vivo* and clinical pharmacokinetic properties were different [117].

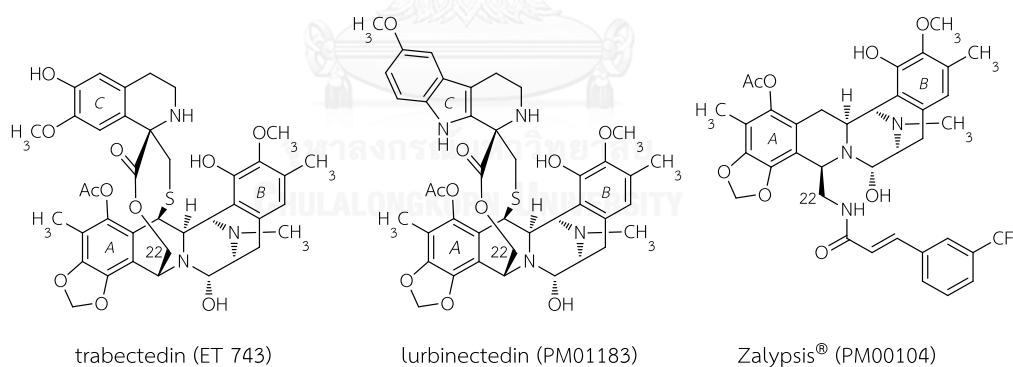


Figure 2.20 Marine tetrahydroisoquinoline alkaloids as anticancer drugs and potential drug candidates

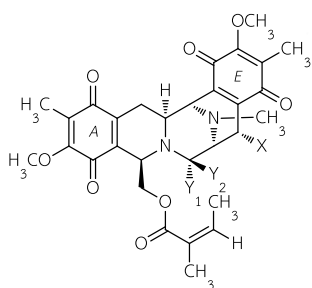
2.3. Renieramycins

2.3.1. Chemistry of renieramycins

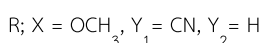
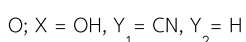
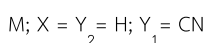
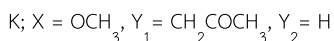
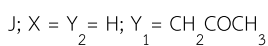
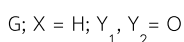
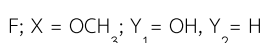
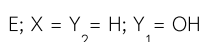
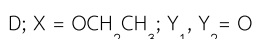
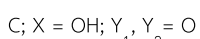
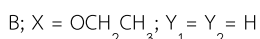
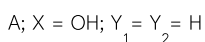
Renieramycins are a group of bistetrahydroisoquinoline alkaloids mainly comprising an angelate ester side chain at C-22. To date, twenty-five renieramycins

isolated from marine sponges of the genera *Reniera* [118-119], *Xestospongia* [102, 120-124], *Haliclona* [125], *Cribrochalina* [126], and *Neopetrosia* [127] have been reported. Eight other renieramycin-related alkaloids, including jorumycin [128], jorunnamycins A-C [129], and fennebricins A-D [130-131], isolated from the sponge-eating nudibranch *Jorunna funebris* have been also reported. They could be divided into 4 groups based on rings A and E.

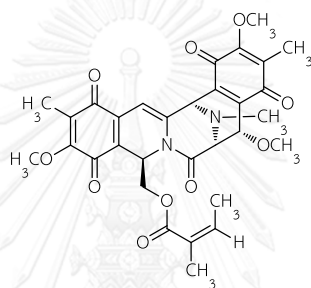
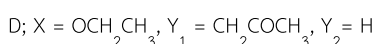
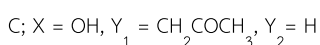
1. Renieramycins with two quinones (rings A and E) comprise renieramycins A-G, I-K, M, O, R, S, V, and W [102, 118-121, 123, 125]; jorumycin [128]; jorunnamycins A and C [129]; and fennebricin A, C, and D [130-131].



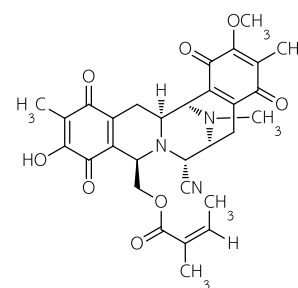
renieramycins



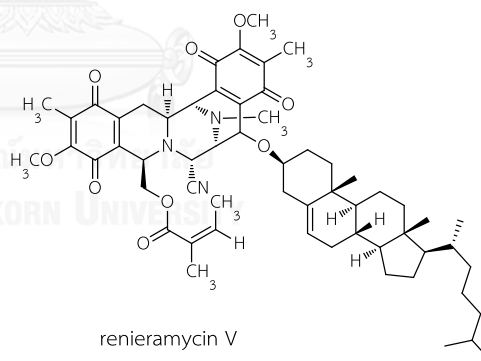
fennebricins



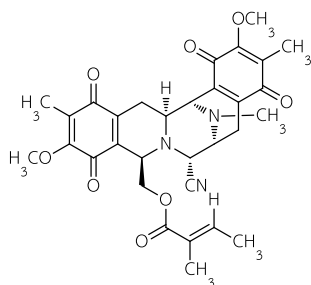
renieramycin I



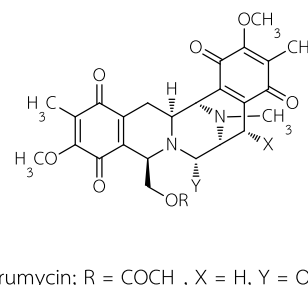
renieramycin S



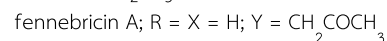
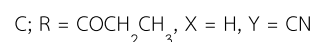
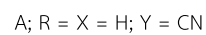
renieramycin V



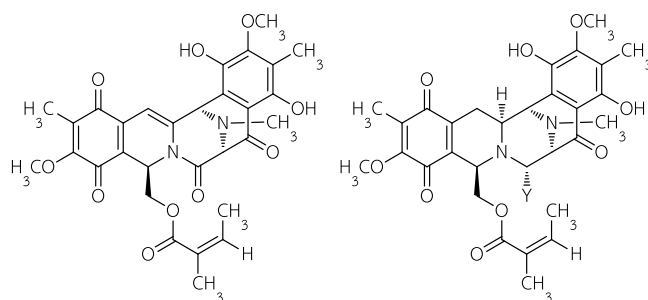
renieramycin W

jorumycin; R = $COCH_3$, X = H, Y = OH

jorunnamycins



2. Renieramycins with one quinone (ring A) and one dihydroquinone (ring E) comprise renieramycins H (cribrostatin 4), L, N, P, and Q [102, 121, 126-127]; and jorunnamycins B [129].

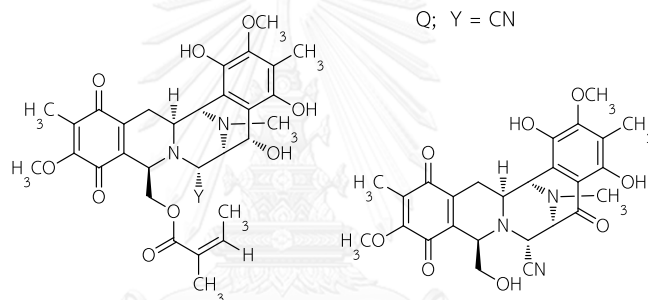


renieramycin H
(cribrostatin 4)

renieramycins

L; Y = CH_2COCH_3

Q; Y = CN



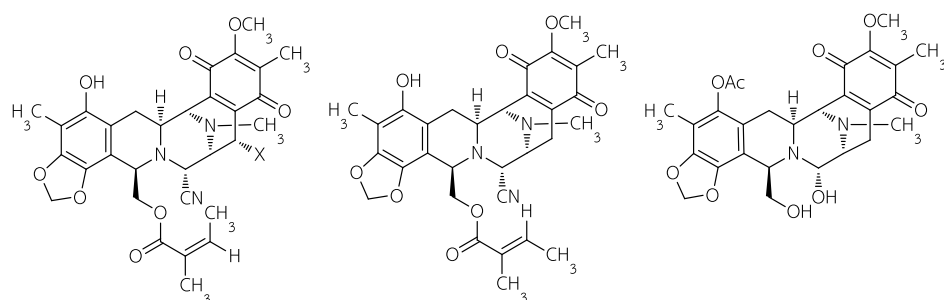
renieramycins

jorunnamycin B

N; Y = CN

P; Y = OH

3. Renieramycins with a methylenedioxy functionality on ring A and a quinone (ring E) comprise renieramycins T, U and X [122]; and fennebricin B [130].



renieramycins

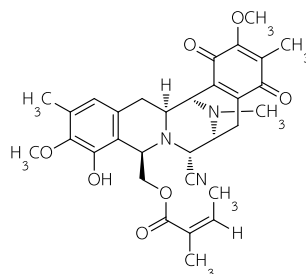
renieramycin X

fennebricin B

T; X = H

U; X = OH

4. Renieramycins with a penta-substituted phenol ring (ring A) and a quinone (ring E) comprise renieramycin Y [124].



renieramycin Y

2.3.2. Bioactivities of renieramycins

Renieramycins A-D showed moderate antimicrobial activity against *S. aureus*, *B. subtilis*, and *Vibrio anguillarum* [118]. Renieramycin G exhibited moderate active against KB and LoVo cell lines with MIC 0.5 and 1.0 $\mu\text{g/mL}$, respectively [120]. Renieramycin P displayed cytotoxicity against 3Y1, HeLa, and P388 cell lines with IC_{50} s 5.3, 12.3, and 0.53 nM, respectively [127].

Table 2.1 Cytotoxicity of renieramycins with different C-21 functional groups against human cancer cell lines [132]

	R	IC_{50} (nM)		
		C-21	HCT116	QG56
renieramycin E (RE)	OH	<0.4	1.0	<0.4
renieramycin J (RJ)	CH_2COCH_3	730.0	510.0	370.0
renieramycin M (RM)	CN	7.9	11.0	NT

HCT116: human colon carcinoma

QG56: human lung carcinoma

DU145: human prostate cancer

NT: not tested

The cytotoxic profile in Table 2.1 showed that RJ without the reactive leaving group at C-21 was dramatically less active than RE and RM. Thus, the leaving group (OH or CN) at C-21 was apparently essential for cytotoxicity.

Table 2.2 Cytotoxicity of renieramycins with different C-14 and C-22 functional groups against human cancer cell lines [102, 121, 129]

	R			IC ₅₀ (nM)				
	C-14	C-21	C-22	HCT116	DLD1	QG56	H460	DU145
renieramycin M (RM) ^{a,b,c}	H	CN	angelate ester	7.9	9.6	19.0	5.9	NT
renieramycin O (RO) ^{a,b}	OH	CN	angelate ester	28.0	NT	40.0	NT	NT
renieramycin R (RR) ^b	OCH ₃	CN	angelate ester	23.0	NT	29.0	NT	NT
saframycin A (SA) ^a	H	CN	pyruvamide	0.4	0.6	5.5	2.1	NT
gorunnamycin A (JA) ^c	H	CN	hydroxy	13.0	NT	59.0	NT	29.0
gorunnamycin B (JB) ^c	=O	CN	hydroxy	455.0	NT	618.0	NT	448.0
gorunnamycin C (JC) ^c	H	CN	propionate ester	1.5	NT	2.8	NT	0.3

HCT116 and DLD1: human colon carcinoma

QG56 and H460: human lung carcinoma

DU145: human prostate carcinoma

NT: not tested

^asee ref. [102]; ^bsee ref. [121]; ^csee ref. [129]

As shown in Table 2.2, renieramycins with the presence of the oxygenated substituent at C-14 (RO and RR) were much less active than RM. In the same way, JB with the carbonyl group at C-14 was also less cytotoxic than JA. Moreover, the difference of the C-22 side chain among RM, SA, JA and JC apparently affect their cytotoxic potency.

Table 2.3 Cytotoxicity of renieramycins M and T against human cancer cell lines [122]

	IC ₅₀ (nM)			
	HCT116	QG56	T47D	AsPC1
renieramycin M (RM)	8.7	14.0	0.8	20.0
renieramycin T (RT)	39.0	77.0	4.7	98.0

HCT116: human colon carcinoma

QG56: human lung carcinoma

T47D: human ductal breast epithelial tumor

AsPC1: human pancreatic adenocarcinoma

The cytotoxic profile in Table 2.3 suggested that the methylenedioxy functionality on ring A of RT decreased the cytotoxicity against all 4 cancer cell lines compared to the quinone of renieramycin RM.

2.3.3. Structure modification at C-22 of renieramycins

Charupant et al. (2009) prepared twenty-four 22-*O*-ester derivatives of jorunnamycin A and evaluated their cytotoxicity against HCT116 human colon carcinoma and MDA-MB-435 human breast carcinoma. The results are summarized in Table 2.4. The starting material jorunnamycin A was prepared from renieramycin M that was isolated from the Thai blue sponge *Xestospongia* sp., via three-step transformation, including hydrogenation, hydride reduction and air oxidation, as shown in Figure 2.21 [132].

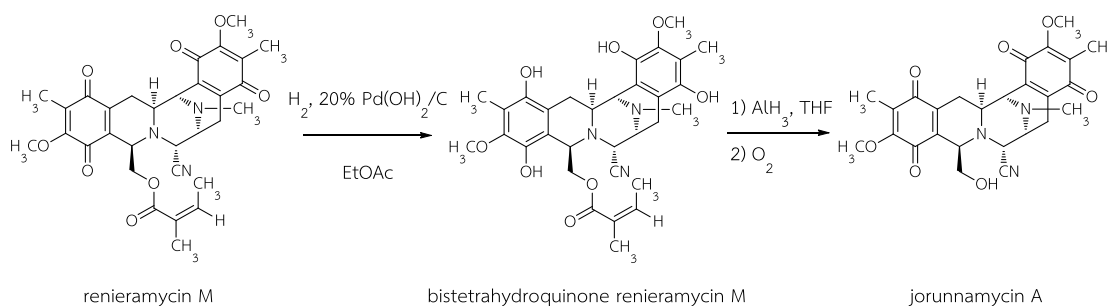
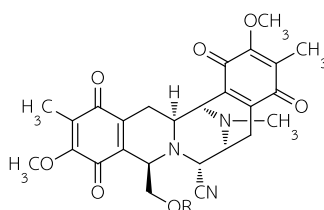
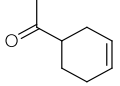
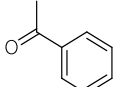
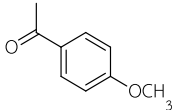
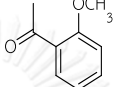
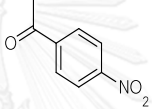
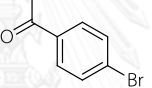
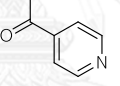
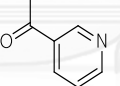
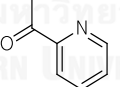
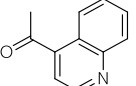
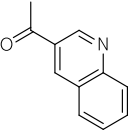
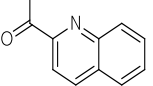
**Figure 2.21** Synthetic scheme of jorunnamycin A (JA) from renieramycin M (RM)

Table 2.4 Cytotoxicity of the 22-O-ester derivatives of jorunnamycin A

derivative	R		IC ₅₀ (nM)	
	chemical name	chemical structure	HCT116	MDA-MB-435
	renieramycin M		9.4	3.8
	jorunnamycin A	H	130.0	290.0
1	tiglic acid ester derivative		34.0	11.0
2	3,3-dimethylacryloyl ester derivative		27.0	11.0
3	formic acid ester derivative		38.0	38.0
4	butyric acid ester derivative		34.0	12.0
5	2'-methylpropanoic acid ester derivative		22.0	10.0
6	2'-(R/S)-methylbutanoic acid ester derivative		33.0	12.0
7	hexanoic acid ester derivative		100.0	40.0
8	3'-chloropropanoic acid ester derivative		16.0	12.0
9	cyclopentanecarboxylic acid ester derivative		93.0	30.0
10	1'-cyclopentenecarboxylic acid ester derivative		33.0	13.0
11	3'-cyclopentenecarboxylic acid ester derivative		33.0	13.0
12	1'-cyclohexenecarboxylic acid ester derivative		49.0	29.0

Table 2.4 (continued).

derivative	R		IC ₅₀ (nM)	
	chemical name	chemical structure	HCT116	MDA-MB-435
13	3'-cyclohexenecarboxylic acid ester derivative		49.0	29.0
14	benzenecarboxylic acid ester derivative		25.0	8.6
15	4'-methoxybenzenecarboxylic acid ester derivative		26.0	8.9
16	2'-methoxybenzenecarboxylic acid ester derivative		34.0	11.0
17	4'-nitrobenzenecarboxylic acid ester derivative		26.0	9.4
18	4'-bromobenzenecarboxylic acid ester derivative		38.0	13.0
19	4'-pyridinecarboxylic acid ester derivative		10.0	4.4
20	3'-pyridinecarboxylic acid ester derivative		7.9	3.5
21	2'-pyridinecarboxylic acid ester derivative		3.3	1.4
22	4'-quinolinecarboxylic acid ester derivative		10.0	4.1
23	3'-quinolinecarboxylic acid ester derivative		10.0	3.8
24	2'-quinolinecarboxylic acid ester derivative		11.0	4.2

HCT116: human colon carcinoma; MDA-MB-435: human breast carcinoma

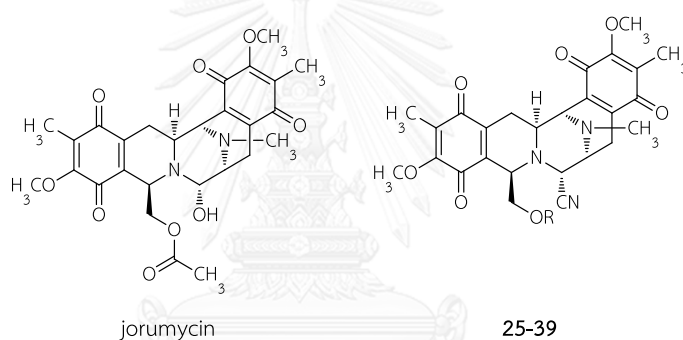
Boldface refers to IC₅₀ less than that of RM

Among 22-O-ester derivatives, nitrogen-containing heterocyclic ester derivatives, including pyridinecarboxylic acid ester (**19-21**) and quinolinecarboxylic acid ester

derivatives (**22-24**) had similar cytotoxicity to RM. 2'-pyridinecarboxylic acid ester derivative **21** was the most active, approximately 3-fold more cytotoxic than RM. In contrast, the derivatives possessing isomeric esters (**1-2**), formyl ester (**3**), long aliphatic alkyl esters (**4-7**), aliphatic cyclic esters (**9-12**), aryl ester (**14**), and monosubstituted aryl esters (**15-18**) showed decreased cytotoxicity [133].

Later, Liu et al. (2012) synthesized jorumycin and its 22-*O*-ester derivatives and evaluated their cytotoxicity against 10 cancer cell lines. The results are summarized in Table 2.5.

Table 2.5 Cytotoxicity of the 22-*O*-ester derivatives of jorumycin



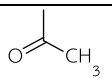
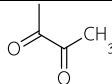
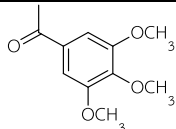
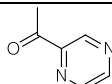
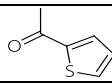
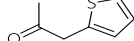
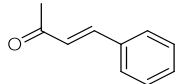
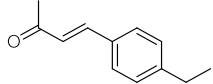
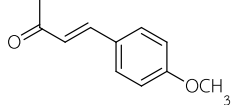
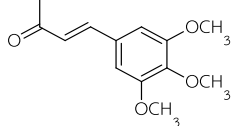
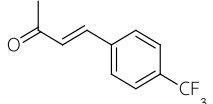
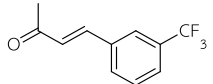
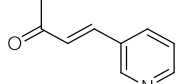
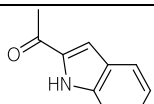
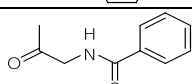
derivative	R	IC ₅₀ (nM)									
		MCF-7	Hela	HCT-8	BGC-823	BEL-7402	HEL-F	A549	KB	A2780	Ketr3
	jorumycin	18.6	2.1	12.8	3.3	1.2	3.6	1.1	2.6	3.8	5.7
25		3.4	0.8	7.6	0.9	2.1	1.4	7.1	1.5	7.7	7.7
26		NT	43.4	NT	NT	NT	95.7	NT	88.6	NT	NT
27		0.3	0.3	25.9	1.5	NT	5.3	3.3	2.0	31.5	4.5
28		1.7	0.8	9.6	3.4	28.2	1.8	1.2	7.0	7.4	1.0
29		2.8	2.5	18.0	3.5	1.8	3.0	1.6	8.0	8.9	11.8
30		16.1	3.5	26.5	20.1	46.2	9.0	30.7	6.6	9.0	23.1

Table 2.5 (Continued)

derivative	R	IC ₅₀ (nM)									
		MCF-7	Hela	HCT-8	BGC-823	BEL-7402	HEL-F	A549	KB	A2780	Ketr3
31		11.6	1.8	82.0	33.7	28.2	18.7	16.1	10.9	45.4	17.8
32		NT	12.2	NT	32.2	NT	NT	23.2	5.9	100.0	85.9
33		9.5	2.9	82.5	4.6	46.2	37.7	9.4	4.4	88.5	27.6
34		1.0	0.3	28.2	3.5	1.8	12.0	2.2	2.2	75.0	26.1
35		19.5	77.9	NT	51.1	NT	NT	15.2	41.3	86.3	79.9
36		NT	52.0	NT	22.7	NT	NT	NT	7.7	NT	89.2
37		42.7	3.2	NT	13.8	20.1	20.3	21.5	22.4	50.1	52.3
38		5.6	0.9	20.5	1.3	NT	3.3	2.1	3.3	7.2	7.6
39		1.7	0.2	8.6	0.7	2.1	1.7	1.5	1.4	1.6	1.9

MCF-7: human breast cancer;

Hela: human cervical cancer;

HCT-8: human colon cancer;

BGC-823: human gastric adenocarcinoma;

BEL-7402: human hepatic carcinoma;

HEL-F: human embryonic lung fibroblast carcinoma;

A549: human lung cancer;

KB: human oral epidermoid carcinoma;

A2780: human ovarian cancer;

Ketr3: human renal cell carcinoma.

NT: not tested

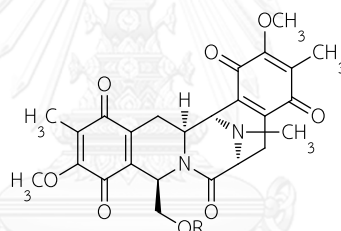
Boldface refers to IC₅₀ less than that of jorumycin

Compound **26** with pyruvic acid side chain that existed in saframycin A showed dramatically decreased cytotoxicity. The aryl ester derivatives (**27-29**) showed similar potency to jorumycin. The one carbon insertion in the side chain of **30** might cause

less potent cytotoxicity than that of **29**. The aryl acryloyl ester derivatives (**31-37**) showed generally decreased cytotoxicity that might be affected by the two-carbon elongation between the aryl and carboxylic groups. Moreover, **33** and **34** with electron-donating groups on the aromatic ring seemed to exhibit stronger cytotoxicity than those of **35** and **36** with electron-withdrawing groups. Noticeably, the hippuric acid ester derivative **39** was the most potent cytotoxicity among all of the compounds [134].

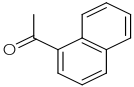
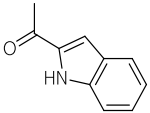
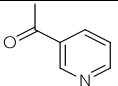
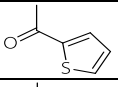
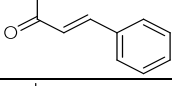
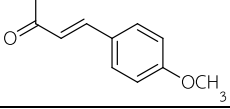
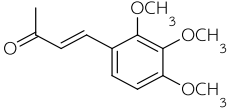
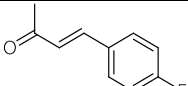
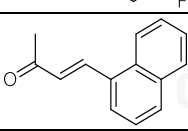
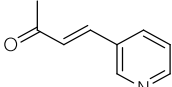
Moreover, renieramycin G and its 22-O-ester derivatives were totally synthesized and evaluated their cytotoxicity against 9 cancer cell lines by Liu et al. (2011). The IC_{50} values of most derivatives (Table 2.6) were at the level of μM .

Table 2.6 Cytotoxicity of the 22-O-ester derivatives of renieramycin G (RG)



derivative	R	IC_{50} (μM)								
		MCF-7	Hela	HCT-8	BGC-823	BEL-7402	A549	KB	A2780	Ketr3
RG		3.8	2.9	8.8	3.4	9.1	5.0	3.3	4.2	3.4
40		4.9	2.7	5.7	4.3	4.0	4.5	2.3	3.3	4.6
41		23.8	12.7	24.7	10.7	23.9	7.4	5.3	25.3	17.2
42		2.5	2.4	3.5	3.5	2.1	3.2	2.0	2.4	3.9
43		17.5	3.4	19.4	3.4	6.5	5.9	3.2	12.2	4.6
44		2.0	1.3	2.7	1.2	2.3	2.2	1.8	2.2	2.2

Table 2.6 (Continued)

derivative	R	IC ₅₀ (μM)								
		MCF-7	Hela	HCT-8	BGC-823	BEL-7402	A549	KB	A2780	Ketr3
45		14.1	7.6	28.0	17.5	10.9	12.5	5.4	15.0	13.8
46		3.9	2.7	7.9	2.6	4.6	4.1	3.4	3.8	4.4
47		4.9	3.1	6.1	8.4	3.8	3.9	2.8	3.1	8.8
48		1.9	0.5	1.5	0.5	1.6	0.7	0.02	1.4	1.7
49		3.6	4.4	5.0	3.3	2.3	5.0	3.0	5.0	7.8
50		3.7	2.8	8.9	3.8	7.3	8.3	3.7	4.2	3.1
51		10.6	5.1	12.4	9.3	14.0	10.6	8.2	16.8	9.3
52		9.7	10.0	9.2	7.4	14.2	8.3	4.0	15.8	10.4
53		3.9	7.4	9.3	11.7	9.8	5.0	8.7	9.1	7.9
54		2.2	1.2	2.1	1.3	2.3	2.1	0.4	2.2	1.4

MCF-7: human breast cancer;

Hela: human cervical cancer;

HCT-8: human colon cancer;

BGC-823: human gastric adenocarcinoma;

BEL-7402: human hepatic carcinoma;

A549: human lung cancer;

KB: human oral epidermoid carcinoma;

A2780: human ovarian cancer;

Ketr3: human renal cell carcinoma.

Boldface refers to IC₅₀ less than that of RG

Among the non-aromatic acid ester (**40-42**), the crotonic acid ester derivative **41** was the least cytotoxic, while **40** with acetyl group and **42** with elongated conjugate

system exhibited similar potency to RG. Among the aryl esters (43-48), 45 with a bulky 1-naphthyl group was the least cytotoxic. Noticeably, 2-thiophene carboxylic acid ester derivative 48 was the most potent among all of the compounds. It exhibited potent cytotoxicity against several cancer cell lines, especially KB cell line with IC_{50} 20 nM. Among the aromatic acrylic acid ester (49-54), 51 and 52 with three methoxy groups and a fluoro group, respectively, on the benzene ring showed decreased cytotoxic potency, while 54 with *trans*-3-(3-pyridyl)acrylic acid ester was more potent than RG [135].

2.3.4. Other related anticancer activities of renieramycins

Halim et al. (2011) demonstrated promising anticancer and antimetastatic activities of renieramycin M (RM) against NSCLC cells. RM has been shown to possess potent cytotoxicity against several cancer cell lines, including H460 NSCLC cell line. This study indicated that apoptosis was the primary mode of cell death in response to RM and this apoptosis was induced through a *p53*-dependent mechanism, which subsequently down-regulated anti-apoptotic proteins BCL-2 and MCL-1, while the level of pro-apoptotic protein BAX was not changed. Moreover, RM at subtoxic concentrations can sensitize H460 cells to anoikis. Anoikis, an apoptosis induced by loss of cell adhesion or inappropriate cell adhesion, has been widely accepted to be one of the most important mechanisms for inhibition of cancer metastasis. RM inhibited anchorage-independent growth of H460 cells subjected to soft agar colony-formation assay. The abilities to survive and grow under anchorage-independent condition are a key characteristic of metastatic cancer cells. RM also inhibited cell migration and invasion, which are important abilities in determining aggressiveness of metastatic cancer. The results suggested that RM possessed a strong cytotoxic activity against H460 NSCLC cells and has potential antimetastatic properties [136].

2.4. Targeted therapy for metastatic lung cancer

Cancer is a group of diseases involving in the uncontrolled cell growth with the potential to invade and spread to other sites of the body. Cancer remains a serious health problem. In 2012, there were 8.2 million people die from cancer, accounting for 13% of all deaths worldwide. Lung cancer is the most common cause of cancer deaths, approximately 1.6 million deaths representing 19% of all cancer deaths [137]. There are two main types of lung cancer: about 17% of lung cancer cases are small-cell lung carcinoma (SCLC) and about 80% of lung cancer cases are non-small-cell lung carcinoma (NSCLC). Metastasis is the major cause of cancer deaths and more than 60% of patients with lung cancer are diagnosed with metastatic cancer [138-139]. The platinum-based doublet, including cisplatin or carboplatin and either paclitaxel, docetaxel, gemcitabine, vinorelbine, irinotecan or pemetrexed, is a standard regimen for metastatic NSCLC. These regimens are effective in terms of response rate, time to progress, and overall survival compared with cisplatin alone or older platinum-based combinations [140-142]. Despite new drugs and therapeutic regimens, the overall five-year survival rate for patients with NSCLC is less than 15% and after surgical resection in patients with early-stage cancer, 65% of cancer recurrence occur within the first 2 years [138]. Cancer metastasis, tumor relapse, and drug resistance are major causes of treatment failure. Understanding of the molecular mechanisms of these processes could improve clinical management of cancer.

Metastasis is a multistep process including detachment of cells from primary tissues, intravasation, transport through the circulatory system, extravasation, and subsequent formation of tumors in distant secondary organs. All of these steps are required for metastatic development, especially the survival of cells in the circulatory system [143-145]. The presence of a high number of circulating tumor cells (CTCs) in blood is associated with poor survival in patients with lung metastatic cancer [146]. Therefore, targeting CTCs represent a promising approach to reducing metastasis, thereby improving patient survival. Anoikis is a programmed cell death induced upon cell detachment from the extracellular matrix and neighboring cells [147]. Tumor cells

that acquire malignant potential can develop resistance to anoikis through multiple mechanisms, such as constitutive activation of pathways responsible for cell survival, integrin switch, epithelial-mesenchymal transition, and oxidative stress [143-145, 148-149]. Stimulation of prosurvival signals and suppression of death signals are proposed as primary mechanisms responsible for anoikis resistance and metastasis. In lung cancer, the up-regulation of proteins in the survival pathways, including activated extracellular signal-regulated kinase (ERK) and ATP-dependent tyrosine kinase (AKT), was shown to increase anoikis-resistant potential [150]. Moreover, the proteins of the B-cell lymphoma-2 family in the apoptotic pathways, such as anti-apoptotic proteins, B-cell lymphoma-2 (BCL2) and myeloid cell leukemia-1 (MCL1); and pro-apoptotic protein BCL2-associated X (BAX), have been found to associate with anoikis resistance in circulating tumor cells in several cancers [151-154]. To date, CTCs have been detected in several cancers, such as lung, colon, prostate, and breast cancers [155-158]. There are significant efforts to understand the biological properties and triggering mechanisms of CTCs; however, a few chemotherapeutic drugs are specifically active toward killing CTCs. This treatment failure may contribute to cancer recurrence and metastasis [159]. Recently, it was reported that alkaloid berberine (Figure 2.22) inhibited the growth of anoikis-resistant breast cancer cells by inducing cell cycle arrest [160].

Cancer stem cell (CSC) is believed to be one of the major cause of drug-resistance, cancer recurrence, and metastasis after chemotherapy [161-163]. CSCs are cancer cells that possess characteristics associated with normal stem cells, specifically the abilities of self-renewal and differentiation into multiple cell types. Cancer stem cells were first identified in human acute myeloid leukemia in 1997 [164]. Since the early 2000s CSCs have been reported in several solid cancers, such as breast, brain, prostate, pancreatic, colon, and lung cancers [165-170]. Based on CSC capabilities to undergo self-renewal and differentiate at the single cell level, colony- and sphere-formation assays has been widely used to identify them [167, 170-173]. Cell surface markers that are specific for normal stem cells are commonly used for isolating CSCs. Putative markers for lung CSCs have been reported including CD133, CD44, and ALDH [161, 170-175]. Targeting CSCs might prevent cancer recurrence and metastasis.

Salinomycin (Figure 2.22), a polyether antibiotic first isolated in 1972 from a culture of *Streptomyces albus*, have been found to selectively reduce the proportion of breast CSCs in mice by more than 100-fold relative to paclitaxel, a commonly used chemotherapeutic drug in breast cancer [176]. In addition, curcumin; piperine [177]; sulforaphane, a dietary component of broccoli/broccoli sprouts [178]; shogaol isolated from ginger (*Zingiber officinale*) [179]; and gigantol, a bibenzyl derivative isolated from orchid, *Dendrobium draconis* [180], have recently reported to target CSCs (Figure 2.22).

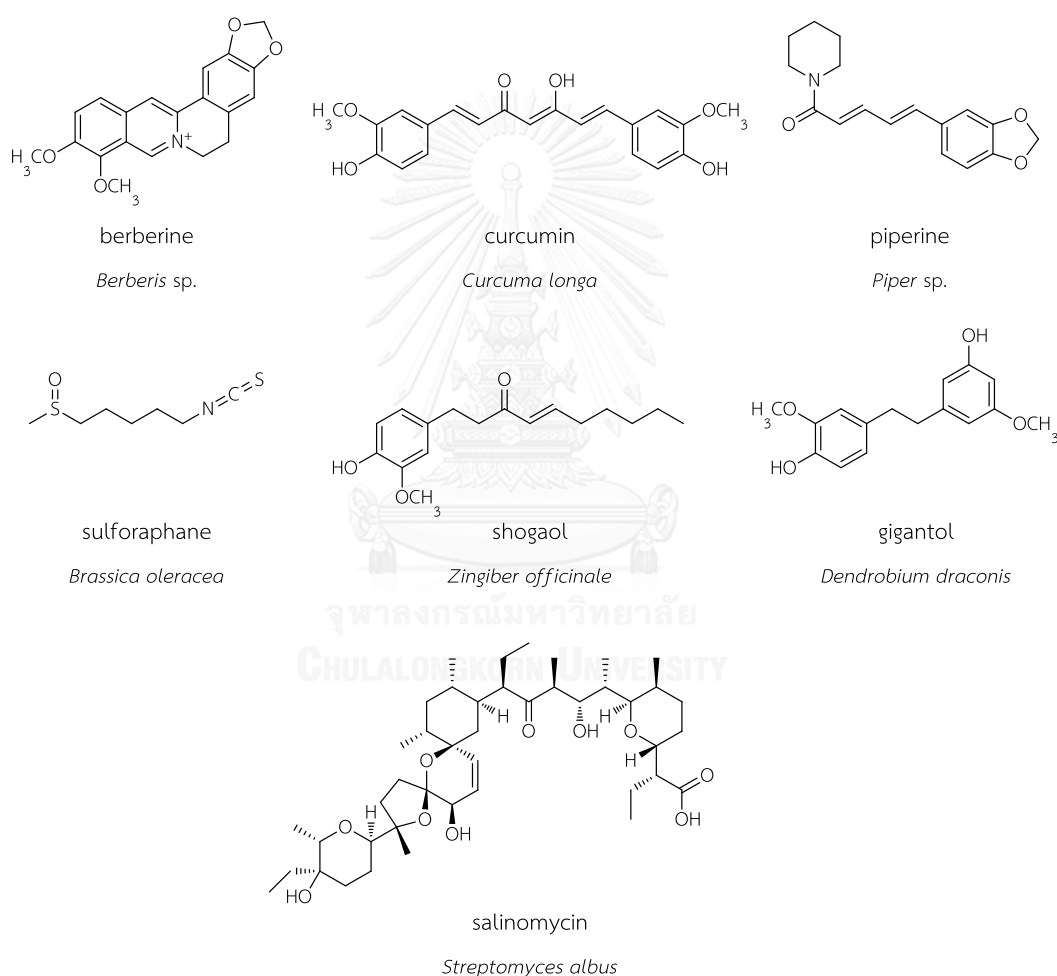


Figure 2.22 Natural products reported to target anokis-resistant cancer cells and cancer stem cells

CHAPTER III

EXPERIMENTAL PROCEDURES

1. Chromatography

1.1. Analytical thin-layer chromatography (TLC)

- Technique : One dimension, ascending direction
- Adsorbent : Silica gel 60 F₂₅₄ coated on an aluminium sheet (Merck)
- Layer thickness : 0.2 mm
- Distance : 5 cm
- Temperature : Room temperature (30-35 °C)
- Detection : 1. Visual detection under daylight.
2. Ultraviolet light at a wavelength of 254 nm.
3. Spraying with *p*-anisaldehyde-sulfuric acid reagent and heating until colors develop.

1.2. Gel filtration chromatography

- Adsorbent : Sephadex LH-20 (Pharmacia).
- Column size : diameter 2.3 cm, length 60-110 cm for sample size of 100-1000 mg
- Packing method : Wet-packing method was used to prepare a column. The adsorbent was kept in an eluent overnight for maximum swelling. The adsorbent was carefully poured into the column and allowed to equally settle.
- Sample loading : The sample was dissolved in a small amount of the eluent and then applied gently on top of the column.
- Detection : Each fraction was monitored by TLC technique as mentioned above.

1.3. Normal-phase vacuum liquid chromatography

- Adsorbent : Silica gel 60 particle size 0.063-0.200 mm, 70-230 mesh ASTM (Merck)

- Column size : diameter 7 cm, length 3 cm for sample size of ~700 mg (silica gel 65 g)
diameter 11 cm, length 4 cm for sample size of ~30 g (silica gel 120 g)
- Packing method : Wet-packing method was used to prepare a column. The adsorbent was suspended in an eluent, and the slurry was carefully poured into the sintered glass funnel used as the column. Reduced pressure (negative pressure) produced by a water aspirator allowed the eluent to drain and helped to equally settle the adsorbent.
- Sample loading : The sample was dissolved in a small amount of more volatile CH_2Cl_2 , mixed with kieselguhr, triturated, dried and then transferred to surface of the column. The eluent was sucked by reduced pressure.
- Detection : Each fraction was monitored by TLC technique as mentioned above.

1.4. Normal-phase flash column chromatography

- Adsorbent : Silica gel 60 particle size 0.040-0.063 mm, 230-400 mesh ASTM (Merck)
- Column size :
diameter ~1 cm, length ~30 cm for sample size of 25-150 mg (silica gel ~30 g)
diameter ~2 cm, length ~30 cm for sample size of 120-300 mg (silica gel ~50 g)
diameter ~3 cm, length ~30 cm for sample size of 0.3-0.8 g (silica gel ~130 g)
diameter ~4 cm, length ~30 cm for sample size of 0.8-1.2 g (silica gel ~170 g)
diameter ~5 cm, length ~30 cm for sample size of 2-5 g (silica gel ~230 g)
- Packing method : Wet-packing method was used to prepare a column. The adsorbent was suspended in an eluent, and the slurry was carefully poured into the column. Compressed air (positive pressure) allowed the eluent to drain and helped to equally settle the adsorbent. The flow rate was adjusted to 1-2 mL/min by compressed air and a stopcock.
- Sample loading : The sample was dissolved in a small amount of the eluent and then loaded gently on top of the column. The eluent was pushed through the column by compressed air.
- Detection : Each fraction was monitored by TLC technique as mentioned above.

1.5. Preparative reversed-phase high-performance liquid chromatography (RP-HPLC)

HPLC was performed on a Shimadzu apparatus equipped with a LC-20AB binary pump, a Rheodyne 7125 injector port, and a SPD-20A UV/Vis detector (Faculty of Pharmaceutical Sciences, Chulalongkorn University) and on a Waters apparatus equipped with a 1525 binary pump, a Rheodyne 7125 injector port, and a 2998 photodiode array (PDA) detector (Faculty of Pharmaceutical Sciences, Prince of Songkla University).

Table 3.1 Reversed-phase high-performance liquid chromatography (RP-HPLC) columns

adsorbent	particle size	column size		brand
		diameter	length	
C-18	5 μm	4 mm	250 mm	LiChrosphere [®] 100
C-18	5 μm	4.6 mm	150 mm	VertiSep [™]
C-18	5 μm	7 mm	150 mm	Apollo
C-18	10 μm	10 mm	250 mm	LiChrosphere [®] 100
C-18	10 μm	10 mm	250 mm	VertiSep [™]
C-8	5 μm	4 mm	250 mm	LiChrosphere [®] 100
C-8	5 μm	10 mm	250 mm	Ascentis [™]

C-18: octadecylsilane (ODS)
C-8: octylsilane

2. Spectroscopy

2.1. Ultraviolet (UV) and visible (Vis) spectroscopy

UV-Vis spectra were obtained on a Shimadzu UV-160A spectrophotometer (Faculty of Pharmaceutical Sciences, Chulalongkorn University) with cuvette cells SCC 282 1.000, 1-cm path length. Samples were dissolved in MeOH (analytical grade, Labscan, Thailand) and applied to measure the UV spectra plotted with the absorbance on the Y-axis and the wavelength on the X-axis. Molar absorptivity (ϵ) at a specified wavelength of a particular compound is a constant value that can be calculated using the following equation:

$$\varepsilon = \frac{A}{c \times l}$$

A is the absorbance

c is the molar concentration

l is the pathlength of cell (cm)

2.2. Infrared (IR) spectroscopy

IR spectra were obtained on a Shimadzu IRAffinity-1 FTIR spectrophotometer (Meiji Pharmaceutical University). Samples were either mixed with KBr powder and compressed as KBr disc or dissolved in CHCl₃ (specially prepared reagent grade, Nacalai Tesque, Kyoto, Japan).

2.3. Mass spectrometry (MS)

The high-resolution electron impact (EI) and fast atom bombardment (FAB) mass spectra were recorded on a JEOL JMS 700 mass spectrometer (Meiji Pharmaceutical University). The high-resolution electrospray ionization (ESI) mass spectrum was obtained on an Agilent 6200 ESI-TOF (Medicinal Plant Research Institute, Department of Medical Sciences, Ministry of Public Health). The exact molecular weight was calculated to confirm the molecular formula of the isolated compounds.

2.4. Nuclear magnetic resonance (NMR) spectroscopy

One-dimensional proton (¹H) and carbon (¹³C) NMR, and two-dimensional NMR, including ¹H-¹H correlation spectroscopy (COSY), heteronuclear single-quantum correlation (HSQC) spectroscopy, heteronuclear multiple-bond correlation (HMBC) spectroscopy, and nuclear Overhauser effect spectroscopy (NOESY) were obtained on a Bruker Avance DPX-300 (Faculty of Pharmaceutical Sciences, Chulalongkorn University), a JEOL JNM-AL 300, a JEOL JNM-AL 400 (Meiji Pharmaceutical University), and a Varian Inova-500 NMR spectrometers (Scientific and Technological Research Equipment Centre, Chulalongkorn University). Solvent signals themselves served as internal standards (CDCl₃: δ_{H} 7.26/ δ_{C} 77.0, acetone-d₆: δ_{H} 2.05/ δ_{C} 29.8 and 206.3, DMSO-d₆: δ_{H} 2.50/ δ_{C} 39.5).

3. Optical Activity

3.1.1. Optical rotation

Optical rotation measurements were obtained on a Perkin Elmer Polarimeter 341 (Faculty of Pharmaceutical Sciences, Chulalongkorn University) and a Horiba SEPA-200 polarimeter (Meiji Pharmaceutical University). Samples were dissolved in MeOH (analytical grade, Labscan, Thailand; spectro grade, Kanto Chemical Co., Inc., Tokyo, Japan). Specific optical rotation ($[\alpha]$) value can be calculated using the following equation:

$$[\alpha]_{\lambda}^T = \frac{100 \times \alpha}{c \times l}$$

α is the observed rotation in degrees

c is the concentration in g/100 ml

l is the pathlength of cell (dm)

T is the temperature (°C)

λ is the wavelength of the light (nm)

3.1.2. Circular dichroism (CD)

CD measurements were taken on a Jasco J-715 (Faculty of Pharmaceutical Sciences, Chulalongkorn University) and a Jasco J-820 spectropolarimeters (Meiji Pharmaceutical University). Samples were dissolved in MeOH (analytical grade, Labscan, Thailand; spectro grade, Kanto Chemical Co., Inc., Tokyo, Japan) and applied to measure the CD spectra plotted with the ellipticity (θ) or molecular circular dichroism (Mol.CD, $\Delta\epsilon$) on the Y-axis and the wavelength on the X-axis. CD values are expressed as either molar ellipticity ($[\theta]$) or molecular circular dichroism ($\Delta\epsilon$).

Molar ellipticity ($[\theta]$) can be calculated using the following equation:

$$[\theta] = \frac{\theta}{10 \times c \times l}$$

θ is the ellipticity (mdeg)

c is the molar concentration

l is the pathlength of cell (cm)



CHAPTER IV

BROMOTYROSINE ALKALOIDS WITH ACETYLCHOLINESTERASE INHIBITORY

ACTIVITY FROM THE THAI SPONGE *ACANTHODENDRILLA* SP.*

Natchanun Sirimangkalakitti,^a Opeyemi J. Olatunji,^b Kanokwan Changwichit,^c
Tongchai Saesong,^c Supakarn Chamni,^a Pithi Chanvorachote,^d Kornkanok Ingkaninan,^c
Anuchit Plubrukarn,^b and Khanit Suwanborirux^a

^aCenter for Bioactive Natural Products from Marine Organisms and Endophytic Fungi (BNPME),
Department of Pharmacognosy and Pharmaceutical Botany, Faculty of Pharmaceutical
Sciences, Chulalongkorn University, Bangkok 10330, Thailand; ^bDepartment of Pharmacognosy
and Pharmaceutical Botany, Faculty of Pharmaceutical Sciences, Prince of Songkla University,
Hat-Yai, Songkhla 90112, Thailand; ^cDepartment of Pharmaceutical Chemistry and
Pharmacognosy, Faculty of Pharmaceutical Sciences and Center of Excellence for Innovation in
Chemistry, Naresuan University, Phitsanulok 65000, Thailand; ^dCell-Based Drug and Health
Product Development Research Unit and Department of Pharmacology and Physiology, Faculty
of Pharmaceutical Sciences, Chulalongkorn University, Bangkok 10330, Thailand

1. Introduction

Acetylcholinesterase (AChE: E.C. 3.1.1.7) is a serine hydrolase enzyme that hydrolyzes acetylcholine (ACh), the cholinergic neurotransmitter, into inactive choline and acetic acid. The cholinergic hypothesis proposes that the causes of cognitive impairment in Alzheimer's disease (AD) patients are involved in the loss of cholinergic neurons in the brain and consequently, the reduction of ACh [1]. Thus, the inhibition of AChE is one of the therapeutic approaches in AD treatment. To date, there are four prescription drugs, donepezil, rivastigmine, galantamine, and memantine, approved by the U.S. Food and Drug Administration for symptomatic treatment of AD. The

* Reproduced by permission of Natural Product Communications, 10 (11), 1945-1949, 2015.

discoveries of rivastigmine and galantamine, AChE inhibitors derived from natural sources, have been a driving force for the search of new natural leads for AD drug development. The majority of the naturally occurring compounds with AChE inhibitory activity are primarily reported from plants, with a comparatively few molecules from marine sources [2-3]. However, those reported marine natural products have exhibited strong inhibitory activity against AChE. These include 4-acetoxy-plakinamine B from the sponge *Corticium* sp. [4], petrosamine from the sponge *Petrosia* n. sp. [5], purealidin Q and aplysamine 2 from the sponge *Pseudoceratina* cf. *purpurea* [6], phlorofucofuroeckol A from the brown algae *Ecklonia stolonifera* [7], and marinoquinoline A from the marine gliding bacterium *Rapidithrix thailandica* [8].

2. Experimental

General. ^1H and ^{13}C NMR spectra were obtained on either a Bruker Avance DPX-300 or a Varian Inova-500 NMR spectrometer. Solvent signals themselves served as internal standards (CDCl_3 : δ_{H} 7.26/ δ_{C} 77.0, acetone- d_6 : δ_{H} 2.05/ δ_{C} 29.8 and 206.3, DMSO- d_6 : δ_{H} 2.50/ δ_{C} 39.5). High-resolution mass spectra were acquired from either an Agilent 6200 ESI-TOF or a JEOL JMS 700 mass spectrometer. Optical rotation measurements were obtained on a Perkin Elmer Polarimeter 341. Circular dichroism measurements were taken on a Jasco J-715 spectropolarimeter. UV spectra were obtained from a Shimadzu UV-160A spectrophotometer, and IR spectra from a Shimadzu IRAffinity-1 FTIR spectrophotometer. HPLC was performed on a Shimadzu apparatus equipped with a LC-20AB binary pump, a Rheodyne 7125 injector port, and a SPD-20A UV/Vis detector or on a Waters apparatus equipped with a 1525 binary pump, a Rheodyne 7125 injector port, and a 2998 photodiode array (PDA) detector.

Animal material. *Acanthodendrilla* sp. was collected by scuba divers from Koh-Ha Islets, Krabi, Thailand at a depth of 15-20 m in December 2011 and frozen until used. The sponge sample was taxonomically identified as *Acanthodendrilla* sp., family Dictyodendrillidae, by Dr Sumaitt Putchakarn of the Institute of Marine Science, Burapha University, Chonburi, Thailand. This nonspicule-forming sponge has an irregular

shape and looks like an encrusting sheet. The texture consistency is soft and compressible. The outer surface is clean and smooth to the touch, slippery, conulose with irregularly disposed conules 1-4 mm high and 2-5 mm apart. The inner surface has several irregular hollows. The color of the specimen is creamy white underwater and becomes light brown on the surface. The voucher specimens have been deposited at the Department of Pharmacognosy and Pharmaceutical Botany, Faculty of Pharmaceutical Sciences, Chulalongkorn University and Prince of Songkla University, under the code number AP11-001-01.

Extraction and isolation. The sponge specimen (6.8 kg wet weight) was macerated with MeOH. The aqueous-methanolic extract was partitioned with EtOAc to give the EtOAc extract (67.81 g). This was chromatographed on a silica gel column with a gradient of *n*-hexane:EtOAc (40-100%) and EtOAc:MeOH (0-100%) to obtain 7 combined fractions. The major fraction (14.97 g) eluted with 70-100% EtOAc in *n*-hexane was crystallized from EtOAc-*n*-hexane to yield the major compound **B13** (8.12 g). The mother liquor (5.91 g) was further fractionated on a silica gel column eluted with 50% EtOAc in CH₂Cl₂ to afford 4 sub-fractions A (230.6 mg), B (94.5 mg), C (2.05 g), and D (1.51 g), which were separately subjected to Sephadex[®] LH-20 (MeOH), silica gel, and HPLC columns (LiChrospher 100 RP-18, 10 mm × 250 mm, 10 μm) to yield **B11** (4.9 mg) from sub-fraction A; **B12** (14.3 mg) from sub-fraction B; **B1** (30.6 mg), **B2** (2.8 mg), **B6** (121.7 mg), and **B7** (72.7 mg) from sub-fraction C; and **B3** (33.8 mg), **B4** (10.1 mg), **B5** (4.0 mg), **B8** (13.9 mg), **B9** (5.8 mg), **B10** (7.2 mg), **B14** (8.1 mg), **B15-16** (39.5 mg), **B17-18** (24.8 mg), and **B19-20** (5.6 mg) from sub-fraction D.

13-Oxosubereamolline D (B5): Colorless amorphous powder. $[\alpha]_D^{20}$: +143.1 (c 0.1, MeOH). IR (CHCl₃): 3422, 2938, 1715, 1676, 1533, 1233, 989 cm⁻¹. UV λ_{\max} (MeOH) nm (log ϵ): 231 (4.05), 283 (3.78). CD $[\theta]_i^{25}$: $[\theta]_{284}$ +51 745, $[\theta]_{248}$ +60 532 (c 0.001, MeOH). ¹H NMR (500 MHz, acetone-*d*₆): Table 4.1. ¹³C NMR (125 MHz, acetone-*d*₆): Table 4.1. HRESIMS: m/z [M+Na]⁺ calcd for C₁₇H₂₁Br₂N₃O₇Na: 559.9644; found: 559.9649.

5,7β-Dichlorocavernicolin (B19) and 5,7α-dichlorocavernicolin (B20): Colorless amorphous powder. $[\alpha]_D^{20}$: +14.0 (c 0.1, MeOH). UV λ_{\max} (MeOH) nm (log ϵ):

245 (3.88). ^1H NMR (500 MHz, acetone- d_6) of **B19**: δ 7.76 (1H, br, NH), 7.21 (1H, br s, H-4), 5.50 (1H, s, OH), 5.07 (1H, d, $J = 10.4$ Hz, H-7), 4.05 (1H, dd, $J = 10.4, 1.7$ Hz, H-7a), 2.90 and 2.44 (each 1H, each d, $J = 16.9$ Hz, H-3). ^1H NMR (500 MHz, acetone- d_6) of **B20**: δ 7.24 (1H, br, NH), 7.09 (1H, d, $J = 1.0$ Hz, H-4), 5.71 (1H, s, OH), 5.27 (1H, d, $J = 3.9$ Hz, H-7), 4.46 (1H, br d, $J = 3.9$ Hz, H-7a), 2.70 (2H, s, H-3). ^{13}C NMR (125 MHz, acetone- d_6) of **B19**: δ 184.1 (C-6), 173.8 (C-2), 145.9 (C-4), 130.1 (C-5), 75.4 (C-3a), 69.1 (C-7a), 66.8 (C-7), 42.9 (C-3). ^{13}C NMR (125 MHz, acetone- d_6) of **B20**: δ 184.0 (C-6), 173.1 (C-2), 144.9 (C-4), 129.9 (C-5), 74.6 (C-3a), 65.0 (C-7a), 61.9 (C-7), 45.8 (C-3). HRESIMS: m/z $[\text{M}+\text{H}]^+$ calcd for $\text{C}_8\text{H}_8\text{Cl}_2\text{NO}_3$; 235.9881; found: 235.9889.

Cholinesterase inhibitory activity. The AChE and butyrylcholinesterase (BChE) inhibitory activities were measured according to the modified Ellman's method [30-31]. Briefly, 25 μL of 1.5 mM ATCI, 125 μL of 3 mM DTNB, 50 μL of 50 mM Tris buffer (pH 8), and 25 μL of the test sample dissolved in the buffer containing not more than 10% MeOH were added to a 96-well microplate. Hydrolysis of the substrate was initiated with an addition of 25 μL of 0.28 U/mL of either electric eel AChE (*EeAChE*) or human recombinant AChE (*hrAChE*). To determine BChE inhibitory activity, in the same procedure, the substrate and enzyme were replaced with BTCC and 2.8 U/mL BChE, respectively. The developing yellow color of the product was measured at 405 nm every 5 s for 2 min using a BioStack microplate stacker (BioTek Instruments, Inc., Winooski, VT, USA). Every experiment was carried out in triplicate. Enzyme activity was calculated as a percentage of the velocity of the test sample compared with that of the non-treated control. Inhibitory activity was calculated by subtracting the percentage of enzyme activity from 100% enzyme activity. The IC_{50} of inhibitory activity was analyzed using GraphPad Prism (Graphpad software, USA). Galantamine was used as a positive control. To study the *hrAChE* inhibition kinetics of **B7**, the same methodology at the IC_{50} (4.5 μM) with various ATCI concentrations (0.05-10 mM) was used. The velocities of the reactions with or without the presence of **B7** were recorded and plotted in the graph according to the Michaelis-Menten and Lineweaver-Burk equations. The kinetic parameters including V_{max} and K_{m} values were calculated using GraphPad Prism.

Cytotoxicity assay. The effect of **B7** on the viability of normal human keratinocyte HaCaT cells (Cell Lines Service, Eppelheim, Germany) cultured in Dulbecco's modified Eagle's medium was investigated by MTT assay [33]. Cells were seeded into a 96-well plate at a density of 1×10^4 cells/well and allowed to adhere overnight. After that, the cells were treated with various concentrations of **B7** dissolved in the medium containing not more than 0.2% DMSO for 24 h and then incubated with 0.5 mg/mL MTT for 4 h. The absorbance of the formazan products solubilized by DMSO was measured at 570 nm using a VICTOR3 multilabel plate reader (PerkinElmer, Waltham, MA, USA). The percentage viability was calculated in respect to non-treated control cells. Every experiment was carried out in triplicate. Statistical analysis was performed using one-way ANOVA with Dunnett's T3 post hoc test at a significant level of p -values < 0.05 (IBM SPSS statistics version 20, USA).

3. Results and Discussion

In the course of this study for biologically active compounds from marine invertebrates, the MeOH crude extract of the sponge *Acanthodendrilla* sp. collected from Koh-Ha Islets, Krabi, Thailand, showed a strong AChE inhibitory activity (80% inhibition of *EeAChE* at 100 $\mu\text{g/mL}$). Extensive chemical purification of the extract by chromatographic combination of silica gel, Sephadex[®] LH-20, and RP-HPLC columns led to the isolation of 20 bromotyrosine-derived alkaloids (Figure 4.1), including a new compound 13-oxosubereamolline D (**B5**), together with 19 known compounds, subereamolline C (**B1**), subereamolline D (**B2**) [9], **B3**, **B4** [10], arothionin (**B6**) [11-12], homoarothionin (**B7**) [11], 11-oxoarothionin (**B8**) [13], oxohomoarothionin (**B9**) [14], fistularin 1 (**B10**) [15], 11,19-dideoxyfistularin 3 (**B11**) [12], 19-deoxyfistularin 3 (**B12**) [16], 3,5-dibromo-1-hydroxy-4,4-dimethoxy-2,5-cyclohexadiene-1-acetamide (**B13**) [17-18], verongiaquinol (**B14**) [19-20], cavernicolin-1 (**B15**), cavernicolin-2 (**B16**) [21], 7 β -bromo-5-chlorocavernicolin (**B17**), 7 α -bromo-5-chlorocavernicolin (**B18**) [22], 5,7 β -dichloro-cavernicolin (**B19**), and 5,7 α -dichloro-cavernicolin (**B20**) [23]. Bromotyrosine-derived alkaloids are a well-known group of marine secondary metabolites isolated from sponges, mostly belonging to the order Verongiida [24]. Therefore, this is the first

report of such derivatives from the sponge *Acanthodendrilla* sp. of the different order Dendroceratida. Bromotyrosine alkaloids were previously reported to possess various biological activities such as antimicrobial, antifungal, antiviral, cytotoxic, and enzyme inhibitory activities [25]. Recently, non-competitive inhibition was reported of AChE by bromotyrosine alkaloids from the sponge *Pseudoceratina* cf. *purpurea* [6]. Herein, we report the structure elucidation of the isolated bromotyrosine-derived alkaloids by careful analyses of UV, IR, NMR, high-resolution MS, and circular dichroism spectra, together with literature comparisons, and also their cholinesterase inhibitory activity.

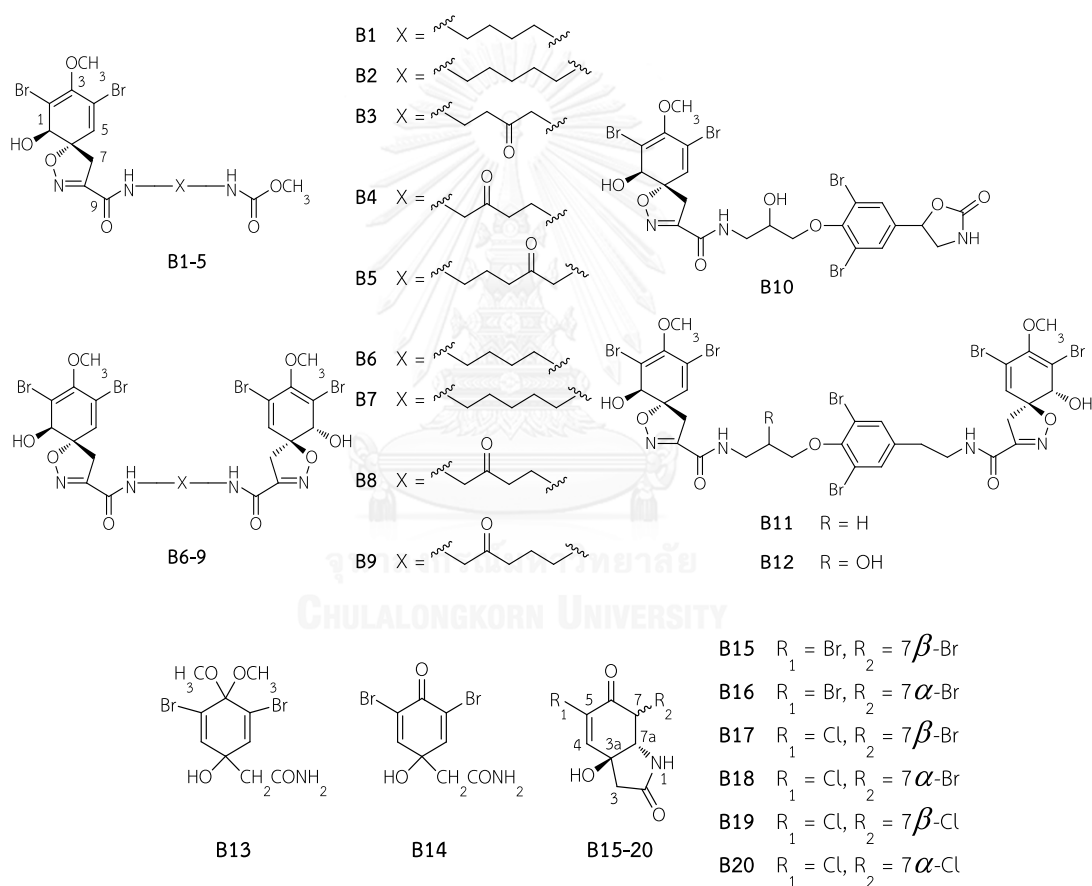


Figure 4.1 Structures of bromotyrosine alkaloids isolated from the Thai marine sponge *Acanthodendrilla* sp.

13-Oxosubereamolline D (**B5**) was isolated as a colorless amorphous powder. A pseudomolecular ion at m/z 559.9649 $[M+Na]^+$ (calcd for 559.9644) in the HRESIMS suggested the molecular formula $C_{17}H_{21}Br_2N_3O_7$ for **B5**, which required 8 degrees of

unsaturation. The UV absorptions at λ_{max} 283 and 231 nm were attributed to a cyclohexadienyl moiety [14], whereas the IR bands at 3422 and 1676 cm^{-1} showed the presence of a hydroxyl and α -iminoamide carbonyl function, respectively [14,26]. Careful interpretation of the ^1H , ^{13}C , ^1H - ^1H COSY, HSQC, and HMBC NMR data (Table 4.1) indicated that **B5** possessed a 1-hydroxy-2,4-dibromo-3-methoxy-8-carbamoyl spiro-cyclohexadienylisoxazoline (SHI) moiety due to the signals of an oxymethine [δ_{H} 4.16 (d, $J = 7.8$ Hz, H-1)/ δ_{C} 75.2 (C-1)], a hydroxy [δ_{H} 5.43 (d, $J = 7.8$ Hz, 1-OH)], two conjugated olefins [δ_{C} 113.8 (C-2), δ_{C} 149.0 (C-3), δ_{C} 122.0 (C-4), δ_{H} 6.51 (s, H-5)/ δ_{C} 132.4 (C-5)], a methoxy [δ_{H} 3.71 (s, 3-OCH₃)/ δ_{C} 60.2 (3-OCH₃)], a quaternary oxygenated carbon [δ_{C} 91.5 (C-6)], a methylene [δ_{H} 3.82 (d, $J = 18.0$ Hz, H-7b) and 3.16 (d, $J = 18.0$ Hz, H-7a)/ δ_{C} 40.2 (C-7)], and an iminoamide [δ_{H} 7.67 (br, 9-NH), δ_{C} 155.3 (C-8), δ_{C} 160.1 (C-9)]. The remaining acyclic part of the molecule consisted of four aliphatic methylenes [δ_{H} 3.30 (q, $J = 6.9$ Hz, H₂-10)/ δ_{C} 39.2 (C-10), δ_{H} 1.82 (quintet, $J = 6.9$ Hz, H₂-11)/ δ_{C} 24.1 (C-11), δ_{H} 2.54 (t, $J = 6.9$ Hz, H₂-12)/ δ_{C} 37.0 (C-12), δ_{H} 3.96 (d, $J = 5.5$ Hz, H₂-14)/ δ_{C} 50.9 (C-14)], a ketone carbonyl [δ_{C} 206.0 (C-13)], and a methylcarbamate [δ_{H} 6.33 (br, 15-NH), δ_{C} 158.0 (C-15), δ_{H} 3.59 (s, 15-OCH₃)/ δ_{C} 52.1 (15-OCH₃)]. The IR spectrum showed a strong broad band at 1700-1750 cm^{-1} , confirming the presence of a ketone and carbamate carbonyl function. The sequential arrangement of the methylene groups was assigned based on the ^1H - ^1H COSY correlations of H₂-10–H₂-11–H₂-12, and the location of the ketone carbonyl at C-13 was assured by the HMBC correlations from H₂-11, H₂-12 and H₂-14 to C-13 (Figure 4.2). Furthermore, the connectivity of the methylcarbamate to C-14 was supported by the ^1H - ^1H COSY correlation from H₂-14 to 15-NH and the HMBC correlation from H₂-14 to C-15 (Figure 4.2). This acyclic part was finally connected to the SHI moiety by the ^1H - ^1H COSY correlation from 9-NH to H₂-10 and the HMBC correlation from H₂-10 to C-9 (Figure 4.2). Comparison of the ^1H and ^{13}C NMR and mass spectra of **B5** with those of **B2** [9] revealed that one methylene group at C-13 in **B2** was replaced by the ketone carbonyl group. Therefore, the new compound **B5** was named as 13-oxosubereamolline D.

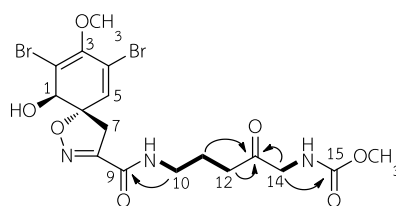


Figure 4.2 Selected ^1H - ^1H COSY (—) and HMBC (→) correlations of 13-oxosubereamolline D (**B5**).

The *trans*-geometry of the hydroxyl group at C-1 and the oxygen atom at C-6 of **B5**, commonly found in marine natural products consisting of the SHI moiety, was supported by the characteristic proton chemical shifts of, in particular, H-1 (δ_{H} 4.16), H-5 (δ_{H} 6.51), and H₂-7 (δ_{H} 3.16 and 3.82) [27]. In addition, the carbon chemical shifts of C-1 to C-8 of the SHI moiety of **B5** were almost identical to those of the other *trans*-SHI containing compounds [10,14,28]. The *trans*-geometry was finally ensured by the 2D NOESY correlation between 1-OH (δ_{H} 5.43) and H-7b (δ_{H} 3.82). The absolute configuration of the chiral centers C-1 and C-6 of **B5** was determined by comparing the CD spectrum with that of the related compounds **B3**, **B4** [10], and **B6** [29]. The analogous values of the positive Cotton effect ($[\theta]_{284} +51\ 745$, $[\theta]_{248} +60\ 532$) in the CD spectrum suggested the absolute configuration of **5** as 1*R*,6*S*.

Table 4.1 ^1H and ^{13}C NMR data for 13-oxosubereamolline D (**B5**) in acetone- d_6

Position	δ_{H} (multiplicity)	δ_{C} , type	HMBC correlations from H to C
1	4.16 (1H, d, $J = 7.8$)	75.2 (CH)	C-2, C-3, C-5, C-6
2		113.8 (C)	
3		149.0 (C)	
4		122.0 (C)	
5	6.51 (1H, s)	132.4 (CH)	C-1, C-2, C-3, C-4, C-6, C-7
6		91.5 (C)	
7a	3.16 (1H, d, $J = 18.0$)	40.2 (CH ₂)	C-1, C-5, C-6, C-8, C-9
7b	3.82 (1H, d, $J = 18.0$)		
8		155.3 (C)	
9		160.1 (C)	
10	3.30 (2H, q, $J = 6.9$)	39.2 (CH ₂)	C-9, C-11, C-12
11	1.82 (2H, quintet, $J = 6.9$)	24.1 (CH ₂)	C-10, C-12, C-13
12	2.54 (2H, t, $J = 6.9$)	37.0 (CH ₂)	C-10, C-11, C-13
13		206.0 (C)	
14	3.96 (2H, d, $J = 5.5$)	50.9 (CH ₂)	C-13, C-15
15		158.0 (C)	
1-OH	5.43 (1H, d, $J = 7.8$)		C-1, C-2, C-6
3-OCH ₃	3.71 (3H, s)	60.2 (CH ₃)	C-3
15-OCH ₃	3.59 (3H, s)	52.1 (CH ₃)	C-15
9-NH	7.67 (1H, br)		
15-NH	6.33 (1H, br)		

Chemical shifts (δ) are expressed in ppm, and J values are presented in Hz.

5,7 β -Dichlorocavernicolin (**B19**) and 5,7 α -dichlorocavernicolin (**B20**) were obtained from the sponge *Acanthodendrilla* sp. as an inseparable mixture with a ratio of 1:3, respectively, based on the ^1H and ^{13}C intensities in the NMR spectra. The mixture of the compounds was previously reported from the sponge *Aplysina fistularis* in 1985 without the NMR assignments [23]. In this study, the complete spectral data assignments of **B19** and **B20** are described for the first time. Compounds **B19** and **B20** are C-7 epimeric having a molecular formula $\text{C}_8\text{H}_7\text{Cl}_2\text{NO}_3$ determined by a pseudomolecular ion at m/z 235.9889 $[\text{M}+\text{H}]^+$ (calcd for 235.9881) in the HRESIMS. The complete ^1H and ^{13}C assignments were assured by the ^1H - ^1H COSY, HSQC and comparison with the reported data of **B15** and **B16** [21] and **B17** and **B18** [22]. The larger coupling constant (10.4 Hz) between H-7 and H-7a of **B19** revealed their trans diaxial relationship, while the smaller coupling constant (3.9 Hz) of **B20** revealed the *cis* relationship for H-7 and H-7a.

All isolated compounds were evaluated *in vitro* for their inhibition potency towards AChE and BChE by the modified Ellman's method [30-31], using galantamine as a positive control. The enzyme inhibitory activity of the isolated compounds at 100 μM was preliminarily screened using *EeAChE*. The primary results of the % inhibition (Table 4.2) showed that the mono- and bis-SHI containing compounds (**B1-12**) exhibited weak to strong *EeAChE* inhibitory activity (~9-97% inhibitions), while the simple bromotyrosine derivatives (**B13-20**) were relatively inactive (~3-11% inhibitions). Among them, **B7** showed the highest inhibitory potency (97.1% inhibition), while **B1**, **B2**, **B6**, and **B10** showed weak to moderate inhibitory activity (~32-66% inhibitions). These active compounds were further evaluated with IC_{50}s for *EeAChE*, *hrAChE*, and BChE inhibitory activities, as shown in Table 4.3. The results indicated that **B7** exhibited the strongest inhibitory activity with IC_{50}s of 2.9, 4.5, and 6.2 μM against *EeAChE*, *hrAChE*, and BChE, respectively, and **B1**, **B2**, and **B6** showed much lower potency (IC_{50}s >100 μM). Interestingly, **B10** was rather selectively active to *hrAChE* (IC_{50} 47.5 μM), while it was less active towards both *EeAChE* and BChE (IC_{50}s >100 μM). However, **B7** showed less inhibitory activity than galantamine. In addition, **B7** at 10 μM did not show cytotoxic activity against a normal human keratinocyte HaCaT cell line.

Table 4.2 The EeAChE inhibitory activity of all isolated bromotyrosine alkaloids at 100 μ M

Compound	%inhibition	Compound	%inhibition	Compound	%inhibition
B1	65.7 \pm 2.0	B7	97.1 \pm 0.3	B13	5.2 \pm 1.4
B2	31.7 \pm 2.9	B8	14.3 \pm 3.5	B14	11.0 \pm 8.9
B3	23.6 \pm 2.1	B9	12.1 \pm 3.8	B15-16	6.0 \pm 4.1
B4	18.6 \pm 0.6	B10	35.1 \pm 6.9	B17-18	4.3 \pm 1.0
B5	26.7 \pm 2.2	B11	8.7 \pm 6.0	B19-20	3.4 \pm 0.5
B6	31.9 \pm 4.5	B12	11.2 \pm 4.5	galantamine	98.4 \pm 0.6

Values are expressed as mean \pm standard deviation

Table 4.3 IC₅₀s for cholinesterase inhibitory activity of subreamolline C (**B1**), subreamolline D (**B2**), arothionin (**B6**), homoaerothionin (**B7**), and fistularin-1 (**B10**)

Compound	IC ₅₀ \pm S.D. (μ M)		
	<i>EeAChE</i>	<i>hrAChE</i>	BChE
B1	>100	>100	>100
B2	>100	>100	>100
B6	>100	>100	>100
B7	2.9 \pm 0.3	4.5 \pm 0.9	6.2 \pm 0.9
B10	>100	47.5 \pm 9.0	>100
Galantamine	1.5 \pm 0.2	0.6 \pm 0.1	7.8 \pm 1.1

Values are expressed as mean \pm standard deviation

To study the inhibition mode of **B7** against *hrAChE*, the enzyme activity was measured at its IC₅₀ concentration (4.5 μ M) using different concentrations of the substrate acetylthiocholine iodide (ATCI, 0.05-10 mM) and plotted in the graph according to the Michaelis-Menten and Lineweaver-Burk equations (Figure 4.3). The kinetic parameters including K_m and V_{max} values of the reaction with and without the presence of **B7** were calculated (Table 4.4). The increased K_m value and unchanged V_{max} value demonstrated that **B7** was a competitive inhibitor against AChE similar to galantamine [32]. A molecular docking study of **B7** is required for further investigation to explain and understand its binding mode in the active site of AChE.

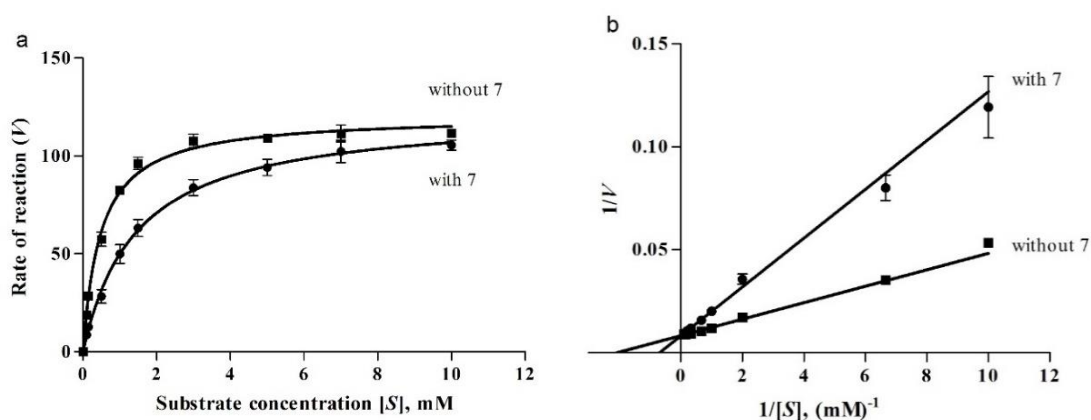


Figure 4.3 Binding study of homoaerthionin (**B7**) on *hrAChE*.

(a) Michaelis-Menten saturation curve of the rate of reaction (V) against substrate concentration ($[S]$) for the reaction with or without the presence of **B7**

(b) Lineweaver-Burk plot of the inverse rate of reaction ($1/V$) against the inverse substrate concentration ($1/[S]$) for the reaction with or without the presence of **B7**. The X-axis intercept is equal to $-1/K_m$, and the Y-axis intercept is equal to $1/V_{max}$

Table 4.4 The *hrAChE* inhibition kinetics of homoaerthionin (**B7**)

Treatment	<i>hrAChE</i> -inhibition kinetics	
	K_m (μM)	V_{max}
Without B7	482.6	120.7
With B7	1451.0	122.3

Although the number of the isolated bromotyrosine-derived alkaloids is limited, the chemical structural features associated with the AChE inhibitory activity are described for further investigation. Based on the % enzyme inhibition data (Table 4.2), the simple bromotyrosine derivatives (**B13-20**) became dramatically less active compared with the other alkaloids (**B1-12**); thus, it is clear that the presence of a SH1 moiety is essential for AChE inhibitory activity. This is in agreement with the previous report [6]. Among the alkaloids possessing an alkyl diamine chain (**B1-9**), the presence of a ketone group in the chain (**B3-5**, **B8**, and **B9**) diminished the inhibitory activity up to 2-8 fold. Although additional structure-related alkaloids are required for concrete evidence, among the four active compounds (**B1**, **B2**, **B6**, and **B7**), the specific length

of the alkyl diamine chain is important for the enzyme inhibitory potency. Compared with compounds **B10-12** containing an aminopropoxydibromotyramine unit, it is noted that the second SHI on the other end decreased the enzyme inhibition activity up to 3-4 fold. This information additionally supports the previously reported data [6].

4. Conclusion

In conclusion, 20 bromotyrosine-derived alkaloids, including a new compound, 13-oxosubereamolline D (**B5**), were isolated from the Thai sponge *Acanthodendrilla* sp., and this report is the first occurrence of bromotyrosine alkaloids from the sponge of the order Dendroceratida. The complete ^1H and ^{13}C NMR assignments of **B19** and **B20** are also described herein for the first time. The most active compound against AChE was identified as **B7**, which acted as a competitive inhibitor. It is likely that the SHI and specific length of the alkyl diamine chain affect the inhibitory activity. Therefore, **B7** could be considered as a promising new lead for the development of new AD drugs.

5. References

- [1] Francis, P. T., Palmer, A. M., Snape, M., and Wilcock, G. K. The cholinergic hypothesis of Alzheimer's disease: A review of progress. **Journal of Neurology, Neurosurgery & Psychiatry** 66 (1999): 137-147.
- [2] Houghton, P. J., Ren, Y., and Howes, M. J. Acetylcholinesterase inhibitors from plants and fungi. **Natural Product Reports** 23 (2006): 181-199.
- [3] Williams, P., Sorribas, A., and Howes, M. J. Natural products as a source of Alzheimer's drug leads. **Natural Product Reports** 28 (2011): 48-77.
- [4] Langjae, R., Bussarawit, S., Yuenyongsawad, S., Ingkaninan, K., and Plubrukarn, A. Acetylcholinesterase-inhibiting steroidal alkaloid from the sponge *Corticium* sp. **Steroids** 72 (2007): 682-685.
- [5] Nukoolkarn, V. S., Saen-oon, S., Rungrotmongkol, T., Hannongbua, S., Ingkaninan, K., and Suwanborirux, K. Petrosamine, a potent anticholinesterase pyridoacridine

- alkaloid from a Thai marine sponge *Petrosia* n. sp. **Bioorganic & Medicinal Chemistry** 16 (2008): 6560-6567.
- [6] Olatunji, O. J., Ogundajo, A. L., Oladosu, I. A., Changwichit, K., Ingkaninan, K., Yuenyongsawad, S., and Plubrukarn, A. Non-competitive inhibition of acetylcholinesterase by bromotyrosine alkaloids. **Natural Product Communications** 9 (2014): 1559-1561.
- [7] Yoon, N. Y., Chung, H. Y., Kim, H. R., and Choi, J. S. Acetyl- and butyrylcholinesterase inhibitory activities of sterols and phlorotannins from *Ecklonia stolonifera*. **Fisheries Science** 74 (2008): 200-207.
- [8] Sangnoi, Y., Sakulkeo, O., Yuenyongsawad, S., Kanjana-opas, A., Ingkaninan, K., Plubrukarn, A., and Suwanborirux, K. Acetylcholinesterase-inhibiting activity of pyrrole derivatives from a novel marine gliding bacterium, *Rapidithrix thailandica*. **Marine Drugs** 6 (2008): 578-586.
- [9] Shaala, L. A., Youssef, D. T., Badr, J. M., Sulaiman, M., and Khedr, A. Bioactive secondary metabolites from the Red Sea marine Verongid sponge *Suberea* species. **Marine Drugs** 13 (2015): 1621-1631.
- [10] Ciminiello, P., Dell'Aversano, C., Fattorusso, E., Magno, S., and Pansini, M. Chemistry of Verongida sponges. 9. Secondary metabolite composition of the Caribbean sponge *Aplysina cauliformis*. **Journal of Natural Products** 62 (1999): 590-593.
- [11] Moody, K., Thomson, R. H., Fattorusso, E., Minale, L., and Sodano, G. Aerothionin and homoaerothionin: Two tetrabromo spirocyclohexadienylisoxazoles from *Verongia* sponges. **Journal of the Chemical Society, Perkin Transactions 1** (1972): 18-24.
- [12] Kernan, M. R., Cambie, R. C., and Bergquist, P. R. Chemistry of sponges, VII. 11, 19-Dideoxyfistularin 3 and 11-hydroxyaerothionin, bromotyrosine derivatives from *Pseudoceratina durissima*. **Journal of Natural Products** 53 (1990): 615-622.
- [13] Acosta, A. L., and Rodríguez, A. D. 11-Oxo-aerothionin: A cytotoxic antitumor bromotyrosine-derived alkaloid from the Caribbean marine sponge *Aplysina lacunosa*. **Journal of Natural Products** 55 (1992): 1007-1012.
- [14] Ciminiello, P., Fattorusso, E., Forino, M., Magno, S., and Pansini, M. Chemistry of Verongida sponges VIII - Bromocompounds from the Mediterranean sponges

- Aplysina aerophoba* and *Aplysina cavernicola*. **Tetrahedron** 53 (1997): 6565-6572.
- [15] Gopichand, Y., and Schmitz, F. J. Marine natural products: Fistularin-1, -2 and -3 from the sponge *Aplysina fistularis* forma *fulva*. **Tetrahedron Letters** 20 (1979): 3921-3924.
- [16] Mancini, I., Guella, G., Laboute, P., Debitus, C., and Pietra, F. Hemifistularin 3: A degraded peptide or biogenetic precursor? Isolation from a sponge of the order Verongida from the Coral Sea or generation from base treatment of 11-oxofistularin 3. **Journal of the Chemical Society, Perkin Transactions 1** (1993): 3121-3125.
- [17] Sharma, G. M., Vig, B., and Burkholder, P. R. Studies on the antimicrobial substances of sponges. IV. Structure of a bromine-containing compound from a marine sponge. **The Journal of Organic Chemistry** 35 (1970): 2823-2826.
- [18] Qi, S. H., Wang, Y. F., and Zhang, S. Steroids and alkaloids from the South China Sea sponge *Axinella* sp. **Journal of Asian Natural Products Research** 11 (2009): 1040-1044.
- [19] Sharma, G. M., and Burkholder, P. R. Studies on the antimicrobial substances of sponges II. Structure and synthesis of a bromine-containing antibacterial compound from a marine sponge. **Tetrahedron Letters** 42 (1967): 4147-4150.
- [20] Capon, R. J., and Macleod, J. K. Two epimeric dibromo nitriles from the Australian sponge *Aplysina laevis*. **Australian Journal of Chemistry** 40 (1987): 341-346.
- [21] D'Ambrosio, M., Guerriero, A., Traldi, P., and Pietra, F. Cavernicolin-1 and cavernicolin-2, two epimeric dibromolactams from the Mediterranean sponge *Aplysina* (*Verongia*) *cavernicola*. **Tetrahedron Letters** 23 (1982): 4403-4406.
- [22] D'Ambrosio, M., Guerriero, A., and Pietra, F. Novel, racemic or nearly-racemic antibacterial bromo- and chloroquinols and γ -lactams of the verongiaquinol and the cavernicolin type from the marine sponge *Aplysina* (= *Verongia*) *cavernicola*. **Helvetica Chimica Acta** 67 (1984): 1484-1492.
- [23] Goo, Y. M. Antimicrobial and antineoplastic tyrosine metabolites from a marine sponge, *Aplysina fistularis*. **Archives of Pharmacal Research** 8 (1985): 21-30.

- [24] Nuñez, C. V., Almeida, E. V. R., Granato, A. C., Marques, S. O., Santos, K. O., Pereira, F. R., Macedo, M. L., Ferreira, A. G., Hajdu, E., Pinheiro, U. S., Muricy, G., Peixinho, S., Freeman, C. J., Gleason, D. F., and Berlinck, R. G. S. Chemical variability within the marine sponge *Aplysina fulva*. **Biochemical Systematics and Ecology** 36 (2008): 283-296.
- [25] Peng, J., Li, J., and Hamann, M. T. The marine bromotyrosine derivatives. **The Alkaloids: Chemistry and Biology** 61 (2005): 59-262.
- [26] Coates, J. Interpretation of infrared spectra, a practical approach. In R. A. Meyers (ed.) **Encyclopedia of Analytical Chemistry**, pp. 10815-10837. Chichester, UK: John Wiley & Sons, 2000.
- [27] Nishiyama, S., and Yamamura, S. Total syntheses of (±)-aerotionin, (±)-homoaerotionin, and (±)-aerophobin-1. **Bulletin of the Chemical Society of Japan** 58 (1985): 3453-3456.
- [28] Kalaitzis, J. A., Davis, R. A., and Quinn, R. J. Unequivocal ¹³C NMR assignment of cyclohexadienyl rings in bromotyrosine-derived metabolites from marine sponges. **Magnetic Resonance in Chemistry** 50 (2012): 749-754.
- [29] McMillan, J. A., Paul, I. C., Goo, Y. M., Rinehart Jr, K. L., Krueger, W. C., and Pschigoda, L. M. An X-ray study of aerotionin from *Aplysina fistularis* (pallas). **Tetrahedron Letters** 22 (1981): 39-42.
- [30] Ellman, G. L., Courtney, K. D., Andres jr, V., and Featherstone, R. M. A new and rapid colorimetric determination of acetylcholinesterase activity. **Biochemical Pharmacology** 7 (1961): 88-95.
- [31] Ingkaninan, K., Temkitthawon, P., Chuenchom, K., Yuyaem, T., and Thongnoi, W. Screening for acetylcholinesterase inhibitory activity in plants used in Thai traditional rejuvenating and neurotonic remedies. **Journal of Ethnopharmacology** 89 (2003): 261-264.
- [32] Nicola, C., Salvador, M., Gower, A. E., Moura, S., and Echeverrigaray, S. Chemical constituents antioxidant and anticholinesterasic activity of *Tabernaemontana catharinensis*. **The Scientific World Journal** 2013 (2013): 519858.
- [33] Riss, T. L., Moravec, R. A., Niles, A. L., Benink, H. A., Worzella, T. J., and Minor, L. Cell viability assays. In G. S. Sittampalam, N. P. Coussens, H. Nelson (eds), **Assay**

Guidance Manual [Internet], Bethesda, MD: Eli Lilly & Company and the National Center for Advancing Translational Sciences, 2004.



CHAPTER V

SYNTHESIS AND ABSOLUTE CONFIGURATION OF ACANTHODENDRILLINE, A NEW CYTOTOXIC BROMOTYROSINE ALKALOID, FROM THE THAI MARINE SPONGE *ACANTHODENDRILLA* SP.*

Nachanun Sirimangkalakitti,^a Masashi Yokoya,^b Supakarn Chamni,^a
Pithi Chanvorachote,^c Anuchit Plubrukarn,^d Naoki Saito,^b and Khanit Suwanborirux^a

^aCenter for Bioactive Natural Products from Marine Organisms and Endophytic Fungi (BNPME),
Department of Pharmacognosy and Pharmaceutical Botany, Faculty of Pharmaceutical
Sciences, Chulalongkorn University, Pathumwan, Bangkok 10330, Thailand; ^bGraduate School of
Pharmaceutical Sciences, Meiji Pharmaceutical University, 2-522-1 Noshio, Kiyose, Tokyo 204-
8588, Japan; ^cCell-Based Drug and Health Product Development Research Unit and Department
of Pharmacology and Physiology, Faculty of Pharmaceutical Sciences, Chulalongkorn University,
Pathumwan, Bangkok 10330, Thailand; ^dDepartment of Pharmacognosy and Pharmaceutical
Botany, Faculty of Pharmaceutical Sciences, Prince of Songkla University, Hat-Yai, Songkhla
90112, Thailand.

1. Introduction

Bromotyrosine alkaloids are a large group of secondary metabolites and commonly found in marine sponges [1]. The remarkable diversities of their chemical structures, together with the wide range of bioactivities, including antimicrobial [2-6], antiviral [7], antiprotozoal [8], cytotoxic [3, 4, 9-12], anti-inflammatory [13], and enzyme inhibitory activities [14-16], make them highly attractive to both natural product chemists and molecular biologists. In the course of our search for bioactive secondary metabolites from Thai marine organisms, we recently reported the isolation of a series

* Reproduced with permission from Chemical and Pharmaceutical Bulletin, 64 (3), 258-262, 2016.
Copyright 2016 The Pharmaceutical Society of Japan.

of bromotyrosine alkaloids from the Thai marine sponge *Acanthodendrilla* sp. along with homoaerotionin (**B7**) (Figure 5.1), a potent cholinesterase inhibitor [17]. In addition, several bromotyrosine alkaloids isolated from this sponge, including verongiaquinol (**B14**), aerotionin (**B6**), 11-oxoaerotionin (**B8**), and 11,19-dideoxyfistularin-3 (**B11**) (Figure 5.1), were previously reported by other research groups as cytotoxic agents against several cancer cell lines [3, 4, 12, 18].

Further investigation of the crude EtOAc extract from this sponge resulted in the isolation of a new bromotyrosine alkaloid, acanthodendriline (**B21**, Figure 5.2). In this work, we describe the structure elucidation of **B21** based on spectroscopic techniques and synthetic protocols. The enantiomers of **B21** were prepared from commercially available starting materials and used to determine the absolute configuration. We also report the cytotoxicity of the enantiomers to human non-small cell lung cancer H292 and normal human keratinocyte HaCaT cell lines.

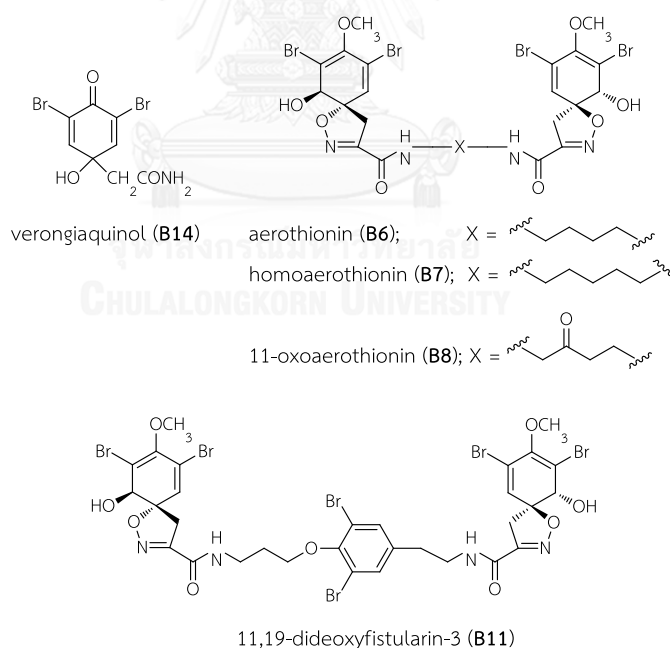


Figure 5.1 Structures of some bioactive bromotyrosine alkaloids

2. Experimental

General Experimental Procedures. ^1H - and ^{13}C -NMR spectra were measured on Bruker Avance DPX-300, JEOL JNM-AL 300, and JEOL JNM-AL 400 NMR spectrometers. The solvent signals served as the internal standard (CDCl_3 : δ_{H} 7.26/ δ_{C} 77.0). IR spectra were recorded on a Shimadzu IRAffinity-1 Fourier transform-infrared (FT-IR) spectrophotometer. HR-MS were acquired with a JEOL JMS 700 mass spectrometer. Optical rotation and circular dichroism measurements were carried out on a Horiba SEPA-200 polarimeter and a Jasco J-820 spectropolarimeter, respectively. HPLC was performed on a Shimadzu apparatus equipped with an LC-20AB binary pump, a Rheodyne 7125 injector port, and an SPD-20 A UV/Vis detector. Silica gel 60 F254 aluminum sheets were used for TLC. Spots on TLC chromatograms were detected under UV light (254 nm) and by spraying with *p*-anisaldehyde reagent. Silica gel 60 (230-400 and 70-230 mesh) and Sephadex[®] LH-20 were used for column chromatography.

Extraction and Isolation. The EtOAc extract (67.81 g) previously prepared from the Thai marine sponge *Acanthodendrilla* sp. [17] was fractionated with the following chromatographic steps: SiO_2 (70% EtOAc in *n*-hexane; then 100% EtOAc), SiO_2 (50% EtOAc in *n*-hexane), Sephadex LH-20 (MeOH), SiO_2 (4% MeOH in CH_2Cl_2), and C_{18} RP-HPLC (LiChrospher[®] 100 RP-18, 10 μm , 10 mm \times 250 mm, 65% MeOH in H_2O , flow rate 3.0 mL/min, UV detector 230 nm), to yield **B21** (43.1 mg, 0.0006% yield of sponge wet weight).

Acanthodendrilline (B21): Colorless amorphous powder. ^1H -NMR (300 MHz) and ^{13}C -NMR (75 MHz), see Table 5.1. IR (KBr) cm^{-1} : 3329, 2950, 1751, 1705, 1541, 1466, 1449, 1256, 1094, 739. UV λ_{max} (MeOH) nm (log ϵ): 214 (4.37). HR-FAB-MS m/z : 450.9512 $[\text{M}+\text{H}]^+$ (calcd for $\text{C}_{14}\text{H}_{17}\text{Br}_2\text{N}_2\text{O}_5$: 450.9504). $[\alpha]_{\text{D}}^{25}$ +25.8 ($c=0.1$, MeOH).

4-(2-Aminoethyl)-2,6-dibromophenol (B23): Tetrabutylammonium tri-bromide [$(n\text{-Bu})_4\text{NBr}_3$, 14.1 g, 29.9 mmol] was added to a solution of tyramine (**B22**, 2.0 g, 14.6 mmol) in CH_2Cl_2 (105 mL) and MeOH (70 mL). The reaction mixture was stirred

at room temperature for 30 min. After the solvent was removed *in vacuo*, the residue was suspended in EtOAc-CHCl₃ (1:1), and the precipitate was filtered off and washed with CH₂Cl₂. Compound **B23** was obtained as a pale yellow powder (2.71 g, 63%). ¹H-NMR (300 MHz, CD₃OD) δ : 7.43 (2H, s), 3.14 (2H, t, *J*=7.7 Hz), 2.86 (2H, t, *J*=7.7 Hz) [19]. HR-electron ionization (EI)-MS *m/z* 292.9045 [M]⁺ (calcd for C₈H₉Br₂NO: 292.9051).

Methyl-[2-(3,5-dibromo-4-hydroxyphenyl)ethyl]carbamate (B24): Methyl chloroformate (ClCO₂CH₃, 47.7 mL, 0.59 mmol) was added to a solution of **B23** (151 mg, 0.51 mmol) in tetrahydrofuran (THF) (2 mL), H₂O (2 mL), and NaHCO₃ (135 mg, 1.61 mmol) at 0°C. After stirring for 1.5 h, the reaction mixture was diluted with EtOAc (20 mL) and then extracted with 1 N NaOH aq. (2×10 mL). The combined alkaline solution was acidified with 1 N HCl aq. and then extracted with CHCl₃ (3×10 mL). The combined extract was washed with brine (10 mL), dried, and concentrated *in vacuo* to give a residue (103 mg). Chromatography on a silica gel column with *n*-hexane-EtOAc (2:1) as the eluent gave **B24** (100.3 mg, 56%) as a colorless powder. ¹H-NMR (400 MHz, CDCl₃) δ : 7.28 (2H, s), 4.87 (1H, br s), 3.67 (3H, s), 3.38 (2H, q, *J*=6.8 Hz), 2.71 (2H, t, *J*=6.8 Hz). ¹³C-NMR (100 MHz, CDCl₃) δ : 157.0 (s), 148.1 (s), 133.3 (s), 132.1 (d), 109.9 (s), 52.2 (q), 42.0 (t), 34.7 (t). HR-EI-MS *m/z* 350.9104 [M]⁺ (calcd for C₁₀H₁₁Br₂NO₃: 350.9106).

(5S)-5-(Chloromethyl)-1,3-oxazolidin-2-one [(S)-B26]: (*S*)-Epichlorohydrin [(*S*)-**B25**, 390 μ L, 4.99 mmol] and MgSO₄ (1.2 g, 10 mmol) were added to a solution of potassium cyanate (KOCN, 811 mg, 10 mmol) in H₂O (5 mL). After stirring at 100°C for 5 h, the reaction mixture was diluted with H₂O (5 mL) and then extracted with EtOAc (3×20 mL). The combined extract was washed with brine (20 mL), dried, and concentrated *in vacuo* to give a residue (304 mg). Chromatography on a silica gel column with *n*-hexane-EtOAc (1:2) as the eluent gave (*S*)-**B26** (275.7 mg, 41%) as a colorless powder. ¹H-NMR (300 MHz, CDCl₃) δ : 6.37 (1H, br s, NH), 4.92-4.81 (1H, m), 3.76 (1H, td, *J*=9.2, 0.7 Hz), 3.72-3.70 (2H, m), 3.54 (1H, ddd, *J*=9.2, 5.9, 0.9 Hz) [20]. HR-EI-MS *m/z* 135.0087 [M]⁺ (calcd for C₄H₆ClNO₂: 135.0087). [α]_D²⁵ +10.0 (*c*=1.0, CHCl₃).

(5R)-5-(Chloromethyl)-1,3-oxazolidin-2-one [(R)-B26]: (*R*)-Epichlorohydrin [(*R*)-**B25**, 390 μ L, 4.99 mmol] and MgSO₄ (1.2 g, 10 mmol) were added to a solution of

KOCN (811 mg, 10 mmol) in H₂O (5 mL). After stirring at 100°C for 5 h, the reaction mixture was diluted with H₂O (5 mL) and then extracted with EtOAc (3×20 mL). The combined extract was washed with brine (20 mL), dried, and concentrated *in vacuo* to give a residue (320 mg). Chromatography on a silica gel column with *n*-hexane-EtOAc (1:2) as the eluent gave (*R*)-**B26** (272.8 mg, 40%) as a colorless powder. ¹H-NMR (300 MHz, CDCl₃) δ : 6.37 (1H, br s, NH), 4.92-4.81 (1H, m), 3.76 (1H, td, *J*=9.2, 0.7 Hz), 3.72-3.70 (2H, m), 3.54 (1H, ddd, *J*=9.2, 5.9, 0.9 Hz) [20]. HR-EI-MS *m/z* 135.0086 [M]⁺ (calcd for C₄H₆ClNO₂: 135.0087). [α]_D²⁵ -9.9 (*c*=1.0, CHCl₃).

Methyl-(2-(3,5-dibromo-4-(((5*S*)-2-oxo-1,3-oxazolidin-5-yl)methoxy)

phenyl)ethyl)carbamate [(*S*)-B21]: (*S*)-**B26** (21.7 mg, 160 μ mol) in *N,N*-dimethylformamide (DMF, 4.0 mL) was added to a solution of **B24** (43.5 mg, 123 μ mol). K₂CO₃ (204 mg, 1.48 mmol) was added, and the reaction mixture was stirred at 140°C for 45 min. The mixture was filtered, and the filtrate was diluted with H₂O (5 mL) and then extracted with CHCl₃ (3×30 mL). The combined extract was washed with brine (20 mL), dried, and concentrated *in vacuo* to give a residue (60 mg). Chromatography on a silica gel column with *n*-hexane-EtOAc (1:2-1:1) as the eluent gave (*S*)-**B21** (26.8 mg, 48%) as a colorless powder. ¹H-NMR (400 MHz, CDCl₃) δ : 7.35 (2H, s), 5.79 (1H, br), 5.02 (1H, ddt, *J*=8.7, 6.2, 5.0 Hz), 4.82 (1H, br), 4.20 (2H, d, *J*=5.0 Hz), 3.91 (1H, dd, *J*=8.7, 6.2 Hz), 3.82 (1H, t, *J*=8.7 Hz), 3.67 (3H, s), 3.39 (2H, q, *J*=6.7 Hz), 2.74 (2H, t, *J*=6.7 Hz). HR-FAB-MS *m/z* 450.9498 [M+H]⁺ (calcd for C₁₄H₁₇Br₂N₂O₅: 450.9504). [α]_D²⁵ +21.4 (*c*=0.1, MeOH).

Methyl-(2-(3,5-dibromo-4-(((5*R*)-2-oxo-1,3-oxazolidin-5-yl)methoxy)

phenyl)ethyl)carbamate [(*R*)-B21]: (*R*)-**B26** (21.7 mg, 160 μ mol) in DMF (4.0 mL) was added to a solution of **B24** (43.5 mg, 123 μ mol). K₂CO₃ (204 mg, 1.48 mmol) was added, and the reaction mixture was stirred at 140°C for 1 h. The reaction mixture was filtered, and the filtrate was diluted with H₂O (5 mL) and then extracted with CHCl₃ (3×30 mL). The combined extract was washed with brine (20 mL), dried, and concentrated *in vacuo* to give a residue (60 mg). Chromatography on a silica gel column with *n*-hexane-EtOAc (1:1) as the eluent gave (*R*)-**B21** (20.5 mg, 37%) as a colorless solid. ¹H-NMR (400

MHz, CDCl₃) δ : 7.35 (2H, s), 5.75 (1H, br), 5.02 (1H, ddt, $J=8.7, 6.1, 5.1$ Hz), 4.81 (1H, br), 4.20 (2H, d, $J=5.1$ Hz), 3.91 (1H, dd, $J=8.7, 6.1$ Hz), 3.82 (1H, t, $J=8.7$ Hz), 3.67 (3H, s), 3.39 (2H, q, $J=6.6$ Hz), 2.74 (2H, t, $J=6.6$ Hz). HR-FAB-MS m/z 450.9507 [M+H]⁺ (calcd for C₁₄H₁₇Br₂N₂O₅: 450.9504). $[\alpha]_D^{25}$ -19.7 ($c=0.3$, MeOH).

Cytotoxicity. Cytotoxicity to the human non-small cell lung cancer NCI-H292 cell line (ATCC, Manassas, VA, USA) and the normal human keratinocyte HaCaT cell line (Cell Lines Service, Eppelheim, Germany) was investigated by performing the MTT assay [21]. H292 cells and HaCaT cells were seeded onto 96-well plates at the densities of 2.5×10^3 and 1×10^4 cells/well, respectively, and were treated with various concentrations of samples dissolved in the culture medium containing not more than 0.5% dimethyl sulfoxide (DMSO) for 72 h. The detailed experimental procedure was described in our previous study [17]. Cell viability was calculated with respect to non-treated control cells. IC₅₀ was determined using GraphPad Prism (GraphPad Software, USA).

Acetylcholinesterase Inhibitory Activity. Inhibitory activity toward acetylcholinesterase from electric eel (*Electrophorus electricus*) was determined by the modified Ellman's method [22-23]. Details of the experimental procedure were described in our previous report [17].

3. Results and Discussion

The EtOAc extract of the Thai marine sponge *Acanthodendrilla* sp. [17] was repeatedly subjected to silica gel column chromatography, Sephadex[®] LH-20 column chromatography, and preparative HPLC to afford B21 (Figure 5.2).

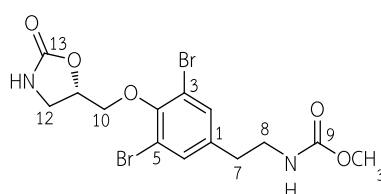


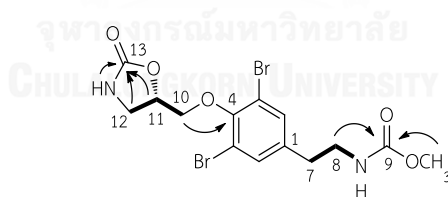
Figure 5.2 Structure of acanthodendrilline [(S)-B21].

Compound **B21**, obtained as a colorless amorphous powder, was optically active $[\alpha]_D^{25} +25.8$ ($c=0.1$, MeOH). The appearance of the protonated molecular parent ion at m/z 450.9512 $[M+H]^+$ (calcd for 450.9504) in the high resolution (HR)-FAB-MS of **B21** suggested that the molecular formula was $C_{14}H_{16}Br_2N_2O_5$. The 1H -NMR, ^{13}C -NMR, and heteronuclear multiple bond connectivity (HMBC) spectra of **B21** (Table 5.1) indicated that **B21** possessed a 3,5-dibromotyramine skeleton: signals assignable to two aromatic protons [δ_H 7.36 (s, H-2, 6)], six aromatic carbons [δ_C 138.3 (C-1), δ_C 133.1 (C-2, 6), δ_C 118.0 (C-3, 5), δ_C 150.6 (C-4)], and two methylenes [δ_H 2.75 (t, $J=6.8$ Hz, H₂-7)/ δ_C 34.9 (C-7), δ_H 3.40 (td, $J=6.8, 6.3$ Hz, H₂-8)/ δ_C 41.8 (C-8)] were observed. The presence of a methylcarbamate moiety was suggested by the typical chemical shifts of OCH₃ (δ_C 52.2) and C-9 (δ_C 157.0) in the ^{13}C -NMR spectrum and confirmed by the HMBC correlation from the methoxy protons [δ_H 3.69 (s, OCH₃)] to C-9. The connectivity of the dibromotyramine and carbamate moieties was confirmed by the 1H - 1H correlation spectroscopy (COSY) correlations of H₂-7/H₂-8/9-NH and the HMBC correlation from H₂-8 to C-9. In addition, a 5-methyl-2-oxazolidone moiety [δ_H 4.21 (d, $J=5.1$ Hz, H₂-10)/ δ_C 71.9 (C-10), δ_H 5.04 (ddt, $J=8.7, 5.9, 5.1$ Hz, H-11)/ δ_C 74.2 (C-11), δ_H 3.93 (dd, $J=8.7, 5.9$ Hz, H-12b) and δ_H 3.83 (t, $J=8.7$ Hz, H-12a)/ δ_C 42.6 (C-12), δ_H 5.64 (br, 13-NH)/ δ_C 159.3 (C-13)] was deduced from the 1H - 1H COSY correlations of H₂-10/H-11/H-12 and the HMBC correlations from H-11, H-12, and 13-NH to C-13. The HMBC correlation from H₂-10 to C-4 suggested the connectivity of the dibromotyramine and 2-oxazolidone moieties. Selected 1H - 1H COSY and HMBC correlations are illustrated in Figure 5.3. Thus, **B21** was elucidated as methyl-(2-(3,5-dibromo-4-((2-oxo-1,3-oxazolidin-5-yl)methoxy) phenyl)ethyl)carbamate and named acanthodendrilline. Our spectroscopic studies depicted that **B21** contained a stereogenic center at C-11. However, the absolute configuration of **B21** remained ambiguous. Therefore, we decided to access the *S* and *R* enantiomers of **B21** by chemical synthesis. Both synthetic enantiomers could serve as standards for the comparison of chemical and physical properties.

Table 5.1 ^1H - and ^{13}C -NMR data of acanthodendrilline [(*S*)-**B21**] in CDCl_3

position	δ_{H} (multiplicity)	δ_{C} , type	HMBC correlation from H to C
1		138.3 (C)	
2, 6	7.36 (2H, s)	133.1 (CH)	C-2,6/C-3,5/C-4/C-7
3, 5		118.0 (C)	
4		150.6 (C)	
7	2.75 (2H, t, $J=6.8$)	34.9 (CH_2)	C-1/C-2,6/C-8
8	3.40 (2H, td, $J=6.8, 6.3$)	41.8 (CH_2)	C-1/C-7/C-9
9		157.0 (C)	
10	4.21 (2H, d, $J=5.1$)	71.9 (CH_2)	C-4/C-11/C-12
11	5.04 (1H, ddt, $J=8.7, 5.9, 5.1$)	74.2 (CH)	C-13
12	a 3.83 (1H, t, $J=8.7$) b 3.93 (1H, dd, $J=8.7, 5.9$)	42.6 (CH_2)	C-10/C-11/C-13
13		159.3 (C)	
9-NH	4.82 (1H, br)		
13-NH	5.64 (1H, br)		C-11/C-12/C-13
OCH_3	3.69 (3H, s)	52.2 (CH_3)	C-9

Chemical shifts (δ) are expressed in ppm, and coupling constants (J) are presented in Hz.

**Figure 5.3** Selected ^1H - ^1H COSY (—) and HMBC (→) correlations of acanthodendrilline [(*S*)-**B21**].

The four-step synthesis of (*S*)-B21 and (*R*)-B21 is shown in Figure 5.4. Tyramine (**B22**) was used as the starting material to prepare methyl-[2-(3,5-dibromo-4-hydroxyphenyl) ethyl] carbamate (**B24**) in two steps. First, **B22** was brominated by tetrabutylammonium tribromide to give 3,5-dibromotyramine (**B23**) [19] in 63% yield. Subsequent acylation of **B23** with a stoichiometric amount of methyl chloroformate at 0°C provided **B24** in 56% yield. Commercially available (*S*)- and (*R*)-epichlorohydrins (**B25**) were separately transformed in one step into the respective enantiomers 5-chloromethyl-2-oxazolidinone [(*S*)-**B26** and (*R*)-**B26**, each *ca.* 40% yield] using potassium cyanate as the nucleophile to transform the oxirane ring into the oxazolidinone motif [20]. Both (*S*)-**B26** and (*R*)-**B26** were finally coupled with **B24** by base-mediated nucleophilic substitution to furnish (*S*)-**B21** (48% yield) and (*R*)-**B21** (37% yield), respectively.

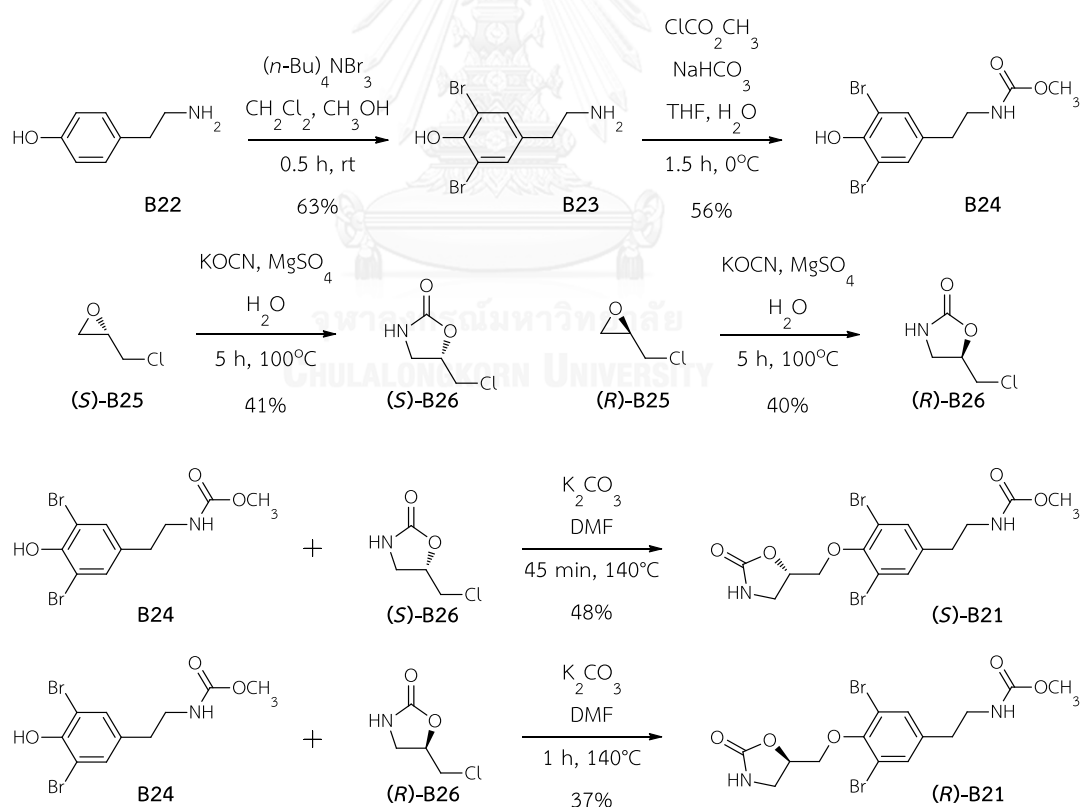


Figure 5.4 Synthetic scheme of (*S*)- and (*R*)-acanthodendrillines (**B21**)

The $^1\text{H-NMR}$ data of the synthetic enantiomers were identical to that of natural **B21**. Determination of the specific rotation of the enantiomers clarified that (*S*)-**B21** $\{[\alpha]_D^{25} +21.4 (c=0.1, \text{MeOH})\}$ and natural **B21** $\{[\alpha]_D^{25} +25.8 (c=0.1, \text{MeOH})\}$ possessed almost identical optical rotation values, whereas the optical rotation of (*R*)-**B21** was the opposite $\{[\alpha]_D^{25} -19.7 (c=0.3, \text{MeOH})\}$. Thus, the absolute configuration at C-11 of natural **B21** was unambiguously determined as *S*. Interestingly, measurement of the circular dichroism (CD) spectra of **B21** and the synthetic enantiomers yielded no characteristic absorptions.

The cytotoxicity of the synthetic enantiomers was evaluated by the 3-(4,5-dimethylthiazol-2-yl)-2,5-diphenyltetrazolium bromide (MTT) assay [21]. The results (Table 5.2) indicated that (*S*)-**B21** (IC_{50} 58.5 μM) was approximately threefold more potent than (*R*)-**B21** (IC_{50} 173.5 μM) against the H292 cell line. Interestingly, both enantiomers were not cytotoxic to normal HaCaT cell line (IC_{50} s >400 μM). Moreover, the acetylcholinesterase (AChE) inhibitory activity of the synthetic enantiomers was determined by the modified Ellman's method [22-23]. Both (*S*)-**B21** and (*R*)-**B21** showed weak inhibitory activity toward AChE (23% and 25% enzyme inhibition at 100 μM , respectively).

Table 5.2 Cytotoxicity of synthetic acanthodendrillines [(*S*)- and (*R*)-**B21**] against the cancer (H292) and normal (HaCaT) cells

Compound	$\text{IC}_{50} \pm \text{SD} (\mu\text{M})$	
	H292	HaCaT
(<i>S</i>)- B21	58.5 \pm 6.7	>400
(<i>R</i>)- B21	173.5 \pm 24.7	>400
cisplatin	7.5 \pm 0.6	4.6 \pm 0.9

4. Conclusion

(*S*)-Acanthodendrinine [(*S*)-**B21**], a new bromotyrosine alkaloid, was isolated from the Thai marine sponge *Acanthodendrilla* sp. It is the first example of a bromotyrosine alkaloid that is composed of dibromotyramine, methylcarbamate, and 2-oxazolidone moieties in the molecule. The concise synthesis of the enantiomers of **B21** was accomplished from commercial tyramine (**B22**) and (*S*)- and (*R*)-epichlorohydrins (**B25**). By comparing the specific rotation values of natural **B21** and the synthetic enantiomers, the stereocenter at C-11 of natural **B21** was assigned the *S* configuration. Both enantiomers exhibited weak AChE inhibitory activity. Interestingly, cytotoxicity evaluation revealed that (*S*)-**B21** was approximately threefold more cytotoxic to the human non-small cell lung cancer H292 cell line than (*R*)-**B21**. This biological information clearly emphasized the importance of the stereochemistry at C-11 of **B21** as a key feature related to the cytotoxicity.

5. References

- [1] Peng, J., Li, J., and Hamann, M. T. The marine bromotyrosine derivatives. **The Alkaloids: Chemistry and Biology** 61 (2005): 59-262.
- [2] Kernan, M. R., Cambie, R. C., and Bergquist, P. R. Chemistry of sponges, VII. 11, 19-Dideoxyfistularin 3 and 11-hydroxyaerothionin, bromotyrosine derivatives from *Pseudoceratina durissima*. **Journal of Natural Products** 53 (1990): 615-622.
- [3] Acosta, A. L., and Rodríguez, A. D. 11-Oxo-aerothionin: A cytotoxic antitumor bromotyrosine-derived alkaloid from the Caribbean marine sponge *Aplysina lacunosa*. **Journal of Natural Products** 55 (1992): 1007-1012.
- [4] Teeyapant, R., Woerdenbag, H. J., Kreis, P., Hacker, J., Wray, V., Witte, L., and Proksch, P. Antibiotic and cytotoxic activity of brominated compounds from the marine sponge *Verongia aerophoba*. **Zeitschrift für Naturforschung C** 48 (1993): 939-945.
- [5] Encarnación-Dimayuga, R., Ramírez, M. R., and Luna-Herrera, J. Aerothionin, a bromotyrosine derivative with antimycobacterial activity from the marine

- sponge *Aplysina gerardogreeni* (Demospongia). **Pharmaceutical Biology** 41 (2003): 384-387.
- [6] Ankudey, F. J., Kiprof, P., Stromquist, E. R., and Chang, L. C. New bioactive bromotyrosine-derived alkaloid from a marine sponge *Aplysinella* sp. **Planta Medica** 74 (2008): 555-559.
- [7] Ross, S. A., Weete, J. D., Schinazi, R. F., Wirtz, S. S., Tharnish, P., Scheuer, P. J., and Hamann, M. T. Mololipids, a new series of anti-HIV bromotyramine-derived compounds from a sponge of the order Verongida. **Journal of Natural Products** 63 (2000): 501-503.
- [8] Mani, L., Jullian, V., Mourkazel, B., Valentin, A., Dubois, J., Cresteil, T., Folcher, E., Hooper, J. N., Erpenbeck, D., Aalbersberg, W., and Debitus, C. New antiplasmodial bromotyrosine derivatives from *Suberea ianthelliformis* Lendenfeld, 1888. **Chemistry & Biodiversity** 9 (2012): 1436-1451.
- [9] Tsukamoto, S., Kato, H., Hirota, H., and Fusetani, N. Ceratinamine: An unprecedented antifouling cyanoformamide from the marine sponge *Pseudoceratina purpurea*. **The Journal of Organic Chemistry** 61 (1996): 2936-2937.
- [10] Tabudravu, J. N., and Jaspars, M. Puralidin S and purpuramine J, bromotyrosine alkaloids from the Fijian marine sponge *Druinella* sp. **Journal of Natural Products** 65 (2002): 1798-1801.
- [11] Tran, T. D., Pham, N. B., Fechner, G., Hooper, J. N., and Quinn, R. J. Bromotyrosine alkaloids from the Australian marine sponge *Pseudoceratina verrucosa*. **Journal of Natural Products** 76 (2013): 516-523.
- [12] Shaala, L. A., Youssef, D. T., Badr, J. M., Sulaiman, M., and Khedr, A. Bioactive secondary metabolites from the Red Sea marine Verongid sponge *Suberea* species. **Marine Drugs** 13 (2015): 1621-1631.
- [13] de Medeiros, A. I., Gandolfi, R. C., Secatto, A., Falcucci, R. M., Faccioli, L. H., Hajdu, E., Peixinho, S., and Berlinck, R. G. 11-Oxoerothionin isolated from the marine sponge *Aplysina fistularis* shows anti-inflammatory activity in LPS-stimulated macrophages. **Immunopharmacol Immunotoxicol** 34 (2012): 919-924.

- [14] Gorshkov, B. A., Gorshkova, I. A., Makarieva, T. N., and Stonik, V. A. Inhibiting effect of cytotoxic bromine-containing compounds from sponges (Aplysinidae) on Na⁺-K⁺-ATPase activity. **Toxicon** 20 (1982): 1092-1094.
- [15] Carr, G., Berrue, F., Klaiklay, S., Pelletier, I., Landry, M., and Kerr, R. G. Natural products with protein tyrosine phosphatase inhibitory activity. **Methods** 65 (2014): 229-238.
- [16] Olatunji, O. J., Ogundajo, A. L., Oladosu, I. A., Changwichit, K., Ingkaninan, K., Yuenyongsawad, S., and Plubrukarn, A. Non-competitive inhibition of acetylcholinesterase by bromotyrosine alkaloids. **Natural Product Communications** 9 (2014): 1559-1561.
- [17] Sirimangkalakitti, N., Olatunji, O., Changwichit, K., Saesong, T., Chamni, S., Chanvorachote, P., Ingkaninan, K., Plubrukarn, A., and Suwanborirux, K. Bromotyrosine marine alkaloids with acetylcholinesterase inhibitory activity from the Thai sponge *Acanthodendrilla* sp. **Natural Product Communications** 10 (2015): 1945-1949.
- [18] Kalaitzis, J. A., Leone Pde, A., Hooper, J. N., and Quinn, R. J. lanthesine E, a new bromotyrosine-derived metabolite from the Great Barrier Reef sponge *Pseudoceratina* sp. **Natural Product Research** 22 (2008): 1257-1263.
- [19] Garcia-Egido, E., Paz, J., Iglesias, B., and Munoz, L. Synthesis of cyanoformamides from primary amines and carbon dioxide under mild conditions. Synthesis of ceratinamine. **Organic & Biomolecular Chemistry** 7 (2009): 3991-3999.
- [20] Schierle-Arndt, K., Kolter, D., Danielmeier, K., and Steckhan, E. Electrogenerated chiral 4-methoxy-2-oxazolidinones as diastereoselective amidoalkylation reagents for the synthesis of β -amino alcohol precursors. **European Journal of Organic Chemistry** 2001 (2001): 2425-2433.
- [21] Riss, T. L., Moravec, R. A., Niles, A. L., Benink, H. A., Worzella, T. J., and Minor, L. Cell viability assays. In G. S. Sittampalam, N. P. Coussens, H. Nelson (eds), **Assay Guidance Manual [Internet]**, Bethesda, MD: Eli Lilly & Company and the National Center for Advancing Translational Sciences, 2004.

- [22] Ellman, G. L., Courtney, K. D., Andres jr, V., and Featherstone, R. M. A new and rapid colorimetric determination of acetylcholinesterase activity. **Biochemical Pharmacology** 7 (1961): 88-95.
- [23] Ingkaninan, K., Temkitthawon, P., Chuenchom, K., Yuyaem, T., and Thongnoi, W. Screening for acetylcholinesterase inhibitory activity in plants used in Thai traditional rejuvenating and neurotonic remedies. **Journal of Ethnopharmacology** 89 (2003): 261-264.



CHAPTER VI

CHEMISTRY OF RENIERAMYCINS. PART 15:

SYNTHESIS OF 22-O-ESTER DERIVATIVES OF JORUNNAMYCIN A AND THEIR CYTOTOXICITY AGAINST NON-SMALL CELL LUNG CANCER CELLS*

Natchanun Sirimangkalakitti,^a Supakarn Chamni,^a Kornvika Charupant,^b
Pithi Chanvorachote,^c Nanae Mori,^d Naoki Saito,^d and Khanit Suwanborirux^d

^aCenter for Bioactive Natural Products from Marine Organisms and Endophytic Fungi (BNPME), Department of Pharmacognosy and Pharmaceutical Botany, Faculty of Pharmaceutical Sciences, Chulalongkorn University; Pathumwan, Bangkok 10330, Thailand; ^bBureau of Drug and Narcotic, Department of Medical Sciences, Ministry of Public Health, Nonthaburi 11000, Thailand; ^cCell-Based Drug and Health Product Development Research Unit and Department of Pharmacology and Physiology, Faculty of Pharmaceutical Sciences, Chulalongkorn University; Pathumwan, Bangkok 10330, Thailand; ^dGraduate School of Pharmaceutical Sciences, Meiji Pharmaceutical University; 2-522-1 Noshio, Kiyose, Tokyo 204-8588, Japan.

1. Introduction

Renieramycins, such as renieramycins E, G, M (RM), H, and T, are bistetrahydroisoquinoline marine natural products mainly isolated from marine sponges of the genera *Reniera* [1, 2], *Xestospongia* [3-8], *Haliclona* [9], *Cribrochalina* [10], and *Neopetrosia* [11]. Other renieramycin-type alkaloids, such as jorumycin [12], jorunnamycin A (JA) [13], and fennebricin B [14-15], were isolated from the sponge-eating nudibranch *Jorunna funebris* (Figure 6.1). Renieramycins are structurally and biologically related to ecteinascidins 743 (ET 743) isolated from the tunicate *Ecteinascidia turbinata* [16-17]. ET 743 (trabectedin under the trade name Yondelis)

* This manuscript has been submitted for publication to Journal of Natural Products since 12th May 2016.

has been approved by the European Commission and U.S. Food and Drug Administration for the treatment of patients with advanced soft tissue sarcomas [18-19]. Renieramycins possess highly potent cytotoxicity toward a wide range of cancer cell lines, such as breast, colon, lung, pancreatic, and prostate cancer cells [4-6, 13, 20]. According to their unique structures together with their pronounced anticancer activity, renieramycins have been remarkable synthetic targets for medicinal chemists worldwide, and most synthetic approaches have been focused on total synthesis [21-34]. Despite their medicinal importance, there are very few structure-activity relationship (SAR) studies owing to the meager amount of available natural products.

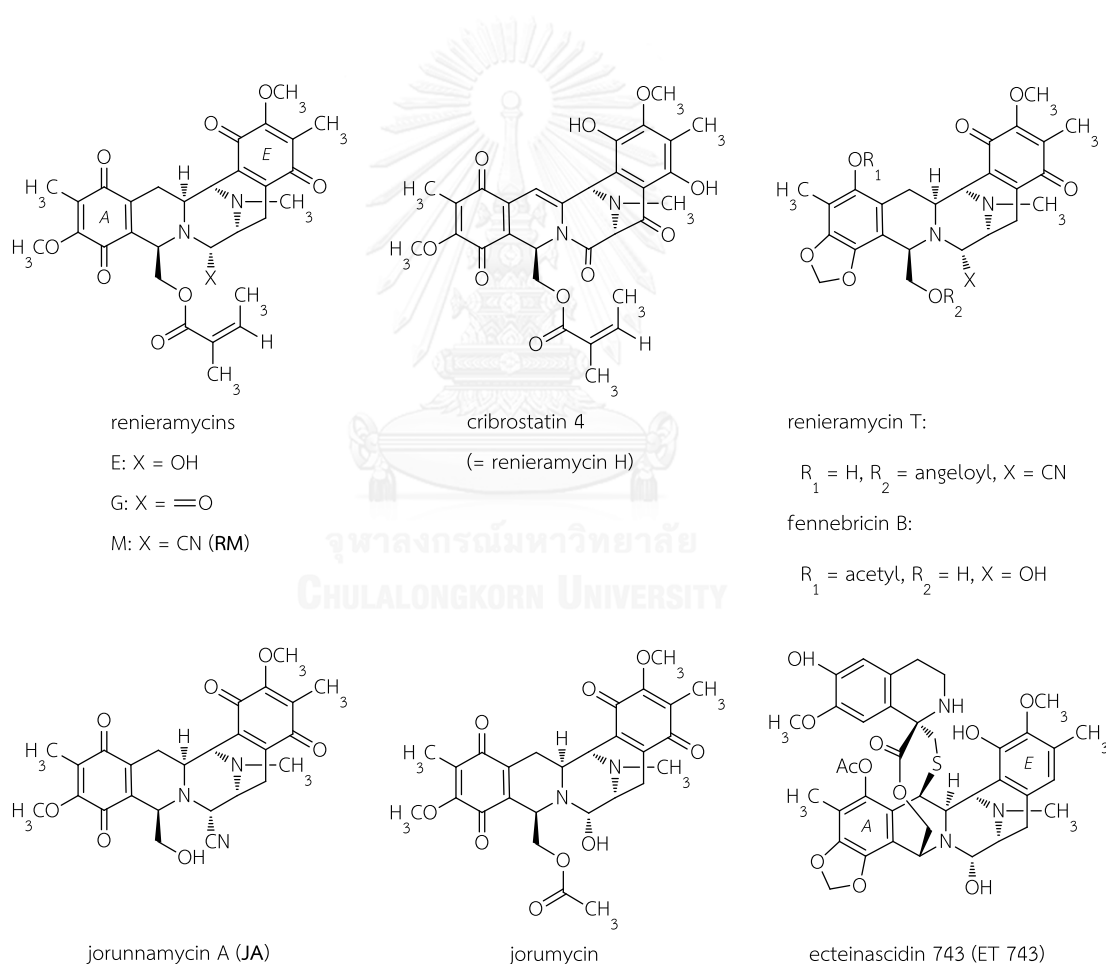


Figure 6.1 Structures of representative tetrahydroisoquinoline marine-derived natural products

As a result of untiring efforts to establish the medicinal chemistry of marine-derived antitumor renieramycins, this study was able to prepare several renieramycin derivatives with an eye to improving cytotoxicity profiles [35]. Of particular significance is renieramycin M (RM), which was isolated as a major component in high yield from the Thai blue sponge *Xestospongia* sp. pretreated with potassium cyanide [4]. RM exhibits potent cytotoxicity with an IC_{50} value in the nanomolar concentration range against several human cancer cell lines [4-6, 13, 20]. Recently, other related anticancer activities of RM have been discovered, including anoikis sensitization, inhibition of migration, invasion, and anchorage-independent growth of lung cancer cells [36-37]. Earlier, it was reported that the leaving group (OH and CN) at C-21 is essential for cytotoxicity, while the presence of either a lactam carbonyl at C-21 or an oxygenated substituent at C-14 leads to a dramatic decrease in cytotoxicity [20]. To extend the scope of SARs of these fascinating marine-derived natural products, this study has focused on the preparation of 22-O-ester analogues. A previous study's result suggested that the introduction of nitrogen-heterocyclic aromatic side chains such as pyridinecarbonyl moieties improves cytotoxic potency [35]. Recently, Liu and co-workers [38-40] studied the syntheses of the less cytotoxic (-)-renieramycin G and (-)-jorumycin along with their cytotoxicity profiles. The result of their research also indicated that C-22 ester side chains play an important role in the activity against several cancer cell lines.

Over the past decades, lung cancer has become a leading cause of cancer that has led to deaths of both men and women worldwide, approximately 1.6 million deaths in 2012, or as high as 19.4% of all cancer deaths [41]. Approximately 80% of all lung cancer cases are non-small cell lung cancers (NSCLC). Although many chemotherapeutic drugs, such as cisplatin, paclitaxel, docetaxel, and gemcitabine, have been used to treat NSCLC [42,43], the overall five-year survival rate for NSCLC patients is less than 15% [42-44]. Therefore, much research is now focusing on the discovery and development of the new series of more effective anticancer drugs to treat patients with lung cancer.

This report aims to extend previous research to gain additional information for the further development of renieramycins as new anticancer agents. For this reason, an additional series of 22-*O*-ester derivatives of jorunnamycin A (JA), having benzoyl and *trans*-cinnamoyl moieties with electronegative and electron-withdrawing functional groups together with nitrogen-heterocyclic rings, was prepared from RM *via* JA. The results of their cytotoxicity against H292 and H460 NSCLC cell lines are also discussed.

2. Experimental

General Experimental Procedures. Optical rotations were measured on a Horiba SEPA-200 polarimeter in a 1 decimeter cell (length); concentration (*c*) is reported in g/100 mL. Circular dichroism (CD) spectra were obtained on a Jasco J-820 spectropolarimeter. IR spectra were taken on a Shimadzu IRAffinity-1 FTIR spectrophotometer. ¹H and ¹³C NMR spectra were obtained on a JEOL JNM-ECA 500 FT NMR spectrometer. ¹H NMR chemical shifts (δ) and coupling constants (*J*) were given in ppm and Hz, respectively, with tetramethylsilane (TMS, 0.00 ppm) as an internal standard. Deuterated chloroform (CDCl₃, 77.0 ppm) served as an internal standard for the ¹³C NMR spectra. All proton and carbon signals were assigned by extensive 2D NMR measurements, including ¹H-¹H COSY, HMQC and HMBC techniques. Mass spectra were recorded on a JEOL JMS 700 mass spectrometer.

Sponge Material and Isolation of RM. The Thai blue sponge *Xestospongia* sp. (9 kg wet weight) was collected by SCUBA diving in the vicinity of Sichang Island, the Gulf of Thailand, at 4-5 m depth in June 2013. According to our published extraction and isolation procedure [4], RM as brightly orange prisms (1.2 g, 0.01% yield based on the sponge wet weight) was isolated from the ethyl acetate extract (18.8 g) of the sponge after pretreatment with KCN in pH 7 buffer. The chemical structure of RM was assured by comparing its NMR data with the authentic renieramycin M [4].

General synthetic procedure of R1-13 and R18. Fifteen equimolar quantities of the corresponding acid chloride were added to a stirred solution of JA (10.0 mg, 0.02 mmol) and DMAP (0.3 mg, 0.002 mmol) in pyridine (1.0 mL) at -17 °C. After that, the stirring was continued at -17 °C for 1 h. The reaction mixture was quenched by addition of 5% NaHCO₃ and then extracted with CHCl₃. The combined organic layer was washed with brine and evaporated to dryness under reduced pressure to produce a residue. The residue was purified by silica gel flash column chromatography using an appropriate ratio of *n*-hexane/EtOAc as an eluent to produce the corresponding 22-*O*-ester derivative of JA. The physical and spectroscopic data of **R1-13** and **R18** are provided in Appendix C.

Synthesis of R17. 3-(4-Pyridyl)acrylic acid (13.5 mg, 0.09 mmol) was added to a stirred solution of JA (15.0 mg, 0.03 mmol), DMAP (0.4 mg, 0.003 mmol), and 0.1 M DCC (0.9 mL, 0.09 mmol) in CH₂Cl₂ (1.5 mL) at 25 °C. The reaction mixture was continuously stirred overnight. The organic solvent was evaporated from the mixture under reduced pressure to give a residue (55.8 mg). The residue was repeatedly washed with EtOAc and filtered. The combined filtrates were dried and subjected to silica gel flash column chromatography with *n*-hexane/EtOAc (3:2) as an eluent to produce **R17**. The physical and spectroscopic data of **R17** are provided in Appendix C.

Cytotoxicity assay. The cytotoxic activity against two human H292 and H460 NSCLC cell lines (American Type Culture Collection) were investigated by MTT assay [46]. The cells were seeded into a 96-well plate at a density of 2×10³ cells/well and allowed to adhere overnight. After that, cells were treated with various concentrations of the analogues dissolved in RPMI medium containing not more than 0.2% DMSO for 72 h and then incubated with 0.5 mg/mL MTT for 4 h. The absorbance of the formazan products solubilized by DMSO was measured at 570 nm using a VICTOR3 multilabel plate reader (PerkinElmer). The percentage of viability was calculated with respect to non-treated control cells. The IC₅₀ of cell viability was analyzed using GraphPad Prism (Graphpad software, USA). Means±standard deviations (SD) were obtained from three independent experiments. Cisplatin was used as a positive control.

3. Results and Discussion

RM was isolated in gram quantity from the Thai blue sponge *Xestospongia* sp. after pretreatment with KCN as previously reported [4]. The starting material JA was prepared from RM *via* our published three-step transformation [20], including hydrogenation with 20% Pd(OH)₂/C in EtOAc, aluminium hydride reduction in tetrahydrofuran at -20°C, and air oxidation, in 44% overall yield (Figure 2.21). Acylation of JA with a corresponding acid chloride in the presence of pyridine as a solvent and 4-dimethylaminopyridine (DMAP) as a catalyst at -17 °C for 1 h gave an acyclic ester analogue (**R1**) and thirteen aromatic ester analogues (**R2-13** and **R18**) in 55-82% yields (Figure 6.2). Preparation of **R17** by the above method was unsuccessful; however, **R17** was subsequently obtained by coupling of JA with 3-(4-pyridyl)acrylic acid in the presence of *N,N'*-dicyclohexylcarbodiimide (DCC) and DMAP in CH₂Cl₂ at 25°C overnight. The yield of **R17** was surprisingly low (35%) because it was difficult to completely remove the DCC-urea by-product during purification of **R17**. Three 22-*O*-pyridinecarbonyl analogues (**R14-16**) were prepared from JA as reported in our previous publication [35].

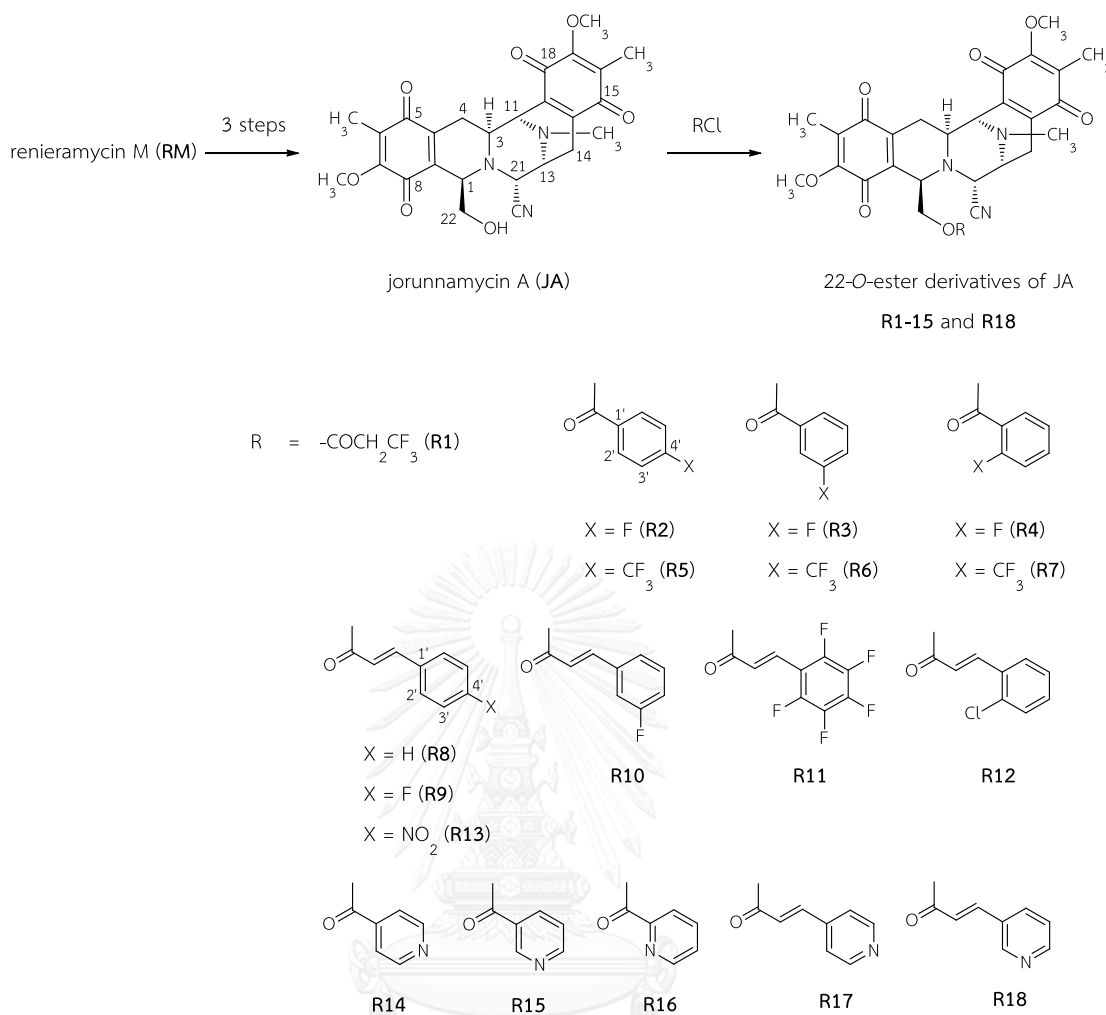


Figure 6.2 Synthetic scheme of 22-O-ester derivatives of jorunnamycin A from renieramycin M (RM)

All synthetic ester analogues were characterized by IR, MS, and ^1H and ^{13}C NMR measurements. The configurations of all analogues were in agreement with both JA and RM, which were confirmed by the 2D NOESY and ECD spectra, and the negative specific rotations [4, 20]. All proton and carbon signals were unambiguously assigned by COSY, HMQC and HMBC experiments, together with literature comparisons [4, 35, 45]. The ^1H and ^{13}C NMR spectral data of the ester analogues were almost identical to those of JA, except the deshielded protons [δ_{H} 3.93-4.39 (H-22a) and 4.40-5.03 (H-22b) ppm] adjacent to the ester carbonyl group compared to those of JA [δ_{H} 3.48 ($\Delta\delta_{\text{H-22a}}$ average = 0.60 ppm) and 3.71 ($\Delta\delta_{\text{H-22b}}$ average = 1.16 ppm) ppm, respectively]. The additional proton and carbon signals in the ^1H and ^{13}C NMR spectra of the ester side

chains at C-22 of the analogues were respectively assigned. The aromatic acyl esters of **R2-18** showed signals of aromatic protons in the range of δ_{H} 7.01-8.83 ppm and aromatic carbons in the range of δ_{C} 114.2-165.7 ppm. The *trans*-olefinic protons of the ester moieties of **R8-13**, **R17** and **R18** showed proton signals in the range of δ_{H} 6.00-6.40 (COCH=CH-) and 7.34-7.74 (COCH=CH-) ppm together with carbon signals in the range of δ_{C} 116.3-124.7 (COCH=CH-) and 129.2-144.5 (COCH=CH-) ppm. The connectivity of the ester moieties to C-22 was clearly confirmed by the HMBC correlations of H₂-22 to the ester carbonyl carbons in the range of δ_{C} 163.4-165.9 ppm. Interestingly, 16-CH₃ and 17-OCH₃ proton signals of **R2-18** were shielded to δ_{H} 1.60-1.79 and 3.69-3.94 ppm when compared to those of JA [δ_{H} 1.93 ($\Delta\delta_{\text{H}}$ average = 0.25 ppm) and 3.98 ($\Delta\delta_{\text{H}}$ average = 0.19 ppm) ppm, respectively]. This information revealed that the possible orientation of the aromatic ring of ester group might be placed above the quinone ring E. This estimation was also supported by distinct NOE correlations, for example, the 2D-NOESY spectrum of **R18** displayed correlations of 16-CH₃ to H-2', H-5', and H-6' of the aromatic ring and a correlation of H-4 β to H- β of the α,β -unsaturated carbonyl of the ester moiety as illustrated in Figure 6.3.

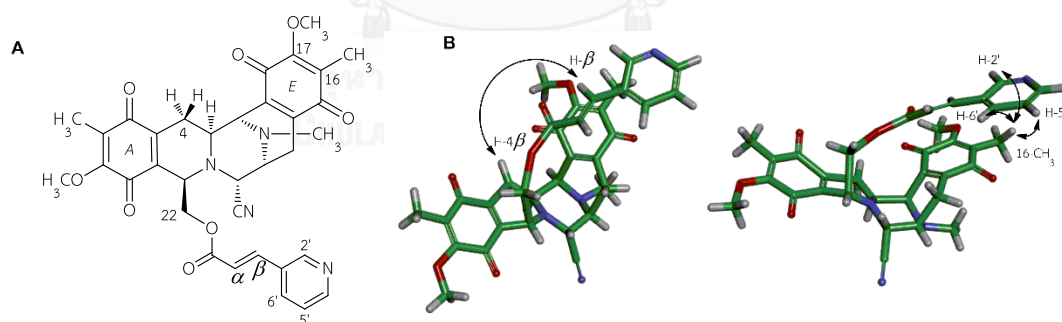


Figure 6.3 A: Chemical structure of 22-O-[3-(4-pyridyl)acryloyl]jorunnamycin A (**R18**). B: Selected NOESY correlations (\leftrightarrow) for **R18** and energy-minimized 3D structure using Discovery Studio 4.0 Visualizer.

All of the 22-*O*-ester analogues together with RM and JA were evaluated *in vitro* for their cytotoxicity by the 3-(4,5-dimethylthiazol-2-yl)-2,5-diphenyltetrazolium bromide (MTT) assay [46] against two representative human H292 and H460 NSCLC cell lines. These two cell lines have been widely used as models to study molecular mechanisms of metastatic process and drug resistance in NSCLC [47-50]. The IC₅₀ values of all ester analogues (Table 6.1) are less than cisplatin, a traditional chemotherapeutic drug for lung cancer treatment. Not surprisingly, the parent compound JA with a free OH and **R1** with a trifluoropropionyl side chain were dramatically less cytotoxic than RM. A previous report demonstrated that the monosubstituted benzoyl esters with electron-donating substituents, such as 4-methoxybenzoyl and 2-methoxybenzoyl esters, decreased cytotoxicity [35]. In this paper, the monosubstituted benzoyl esters with electron-withdrawing substituents (**R2-7**) and the *trans*-cinnamoyl esters with electron withdrawing-substituents (**R8-13**) exhibited either similar or slightly decreased cytotoxicity compared to RM. However, the nitrogen-heterocyclic esters, such as **R14-16** and **R18** exhibited highly increased cytotoxicity against H292 cell line with IC₅₀ values in the range of 1.1-6.4 nM, approximately 4- to 20-folds more potent than RM (IC₅₀ 22.5 nM) and H460 cell line with IC₅₀s in the range of 1.6-6.0 nM, approximately 2- to 5-folds more potent than RM (IC₅₀ 8.3 nM). Among them, **R14** possessing a 4-pyridinecarbonyl ester is the most potent cytotoxic analogue, exhibiting 20-fold and 5-fold increases in cytotoxicity to the H292 and H460 cell lines, respectively, relative to RM. In contrast, analogue **R17** possessing a 3-(4-pyridyl)acryloyl ester showed similar potency against H292 cell line and approximately 2-fold decreased cytotoxicity against H460 cell line compared to RM. Considering the present cytotoxicity results together with other previous reports [35-39], the ester side chain at C-22 of the renieramycin derivatives appears to be an important part responsible for the improved cytotoxicity profile. It should also be noted that the introduction of nitrogen-heterocyclic ring into the 22-*O*-ester analogue, which was proposed to overlay the right-hand quinone ring E, might mimic the third tetrahydroisoquinoline ring of ET 743 resulting in an increase in cytotoxic potency.

Table 6.1 Cytotoxicity of renieramycin M (RM), jorunnamycin A (JA), and 22-*O*-ester derivatives of JA against non-small cell lung cancer H292 and H460 cell lines

compound	R	cytotoxicity IC ₅₀ ± SD (nM)	
		H292	H460
RM	angeloyl	22.5 ± 3.9	8.3 ± 0.6
JA	H	217.4 ± 21.7	164.3 ± 11.1
R1	3,3,3-trifluoropropionyl	567.0 ± 48.1	321.3 ± 46.2
R2	4-fluorobenzoyl	56.2 ± 5.3	22.1 ± 2.0
R3	3-fluorobenzoyl	17.6 ± 2.0	11.2 ± 1.5
R4	2-fluorobenzoyl	29.8 ± 2.7	10.3 ± 0.5
R5	4-trifluoromethyl benzoyl	59.7 ± 1.3	23.8 ± 1.1
R6	3-trifluoromethyl benzoyl	48.6 ± 3.1	29.7 ± 2.8
R7	2-trifluoromethyl benzoyl	51.4 ± 1.5	22.0 ± 3.2
R8	cinnamoyl	19.4 ± 1.7	18.3 ± 2.1
R9	4-fluorocinnamoyl	44.3 ± 4.5	12.2 ± 0.2
R10	3-fluorocinnamoyl	11.3 ± 1.6	9.8 ± 0.3
R11	pentafluorocinnamoyl	21.0 ± 3.1	68.7 ± 0.4
R12	2-chlorocinnamoyl	25.0 ± 4.6	9.0 ± 0.1
R13	4-nitrocinnamoyl	21.5 ± 2.9	14.3 ± 1.0
R14	4-pyridinecarbonyl	1.1 ± 0.1	1.6 ± 0.3
R15	3-pyridinecarbonyl	6.4 ± 0.6	6.0 ± 0.8
R16	2-pyridinecarbonyl	3.7 ± 0.6	2.2 ± 0.3
R17	3-(4-pyridyl)acryloyl	20.4 ± 1.4	20.2 ± 1.2
R18	3-(3-pyridyl)acryloyl	4.9 ± 0.3	2.8 ± 0.4
cisplatin	-	12.1 ± 1.1 μM	8.2 ± 0.6 μM

H460 and H292: human non-small cell lung cancer cell lines.

4. Conclusion

In conclusion, eighteen 22-*O*-ester derivatives of JA were synthesized in moderate yields from JA, which was prepared by the three-step deangeloyl transformation of RM obtained from the Thai blue sponge *Xestospongia* sp. This study supports that the 22-*O*-ester derivatives of JA with a nitrogen-heterocyclic ring are potential candidates for development of new effective anticancer drugs to treat NSCLC patients. Among these analogues, **R14** showed the most potent cytotoxicity profile, exhibiting a 20-fold and 5-fold increases in cytotoxicity to H292 and H460 NSCLC cell lines, respectively, relative to RM. Further studies are needed to completely understand the molecular basis of the extraordinary cytotoxicity profiles of renieramycins.

5. References

- [1] Frincke, J. M., and Faulkner, D. J. Antimicrobial metabolites of the sponge *Reniera* sp. **Journal of the American Chemical Society** 104 (1982): 265-269.
- [2] He, H. Y., and Faulkner, D. J. Renieramycins E and F from the sponge *Reniera* sp.: Reassignment of the stereochemistry of the renieramycins. **The Journal of Organic Chemistry** 54 (1989): 5822-5824.
- [3] Davidson, B. S. Renieramycin G, a new alkaloid from the sponge *Xestospongia caycedoi*. **Tetrahedron Letters** 33 (1992): 3721-3724.
- [4] Suwanborirux, K., Amnuoypol, S., Plubrukarn, A., Pummangura, S., Kubo, A., Tanaka, C., and Saito, N. Chemistry of renieramycins. Part 3. Isolation and structure of stabilized renieramycin type derivatives possessing antitumor activity from Thai sponge *Xestospongia* species, pretreated with potassium cyanide. **Journal of Natural Products** 66 (2003): 1441-1446.
- [5] Amnuoypol, S., Suwanborirux, K., Pummangura, S., Kubo, A., Tanaka, C., and Saito, N. Chemistry of renieramycins. Part 5. Structure elucidation of renieramycin-type derivatives O, Q, R, and S from Thai marine sponge *Xestospongia* species pretreated with potassium cyanide. **Journal of Natural Products** 67 (2004): 1023-1028.

- [6] Daikuhara, N., Tada, Y., Yamaki, S., Charupant, K., Amnuoypol, S., Suwanborirux, K., and Saito, N. Chemistry of renieramycins. Part 7: Renieramycins T and U, novel renieramycin–ecteinascidin hybrid marine natural products from Thai sponge *Xestospongia* sp. **Tetrahedron Letters** 50 (2009): 4276-4278.
- [7] Saito, N., Yoshino, M., Charupant, K., and Suwanborirux, K. Chemistry of renieramycins. Part 10: Structure of renieramycin V, a novel renieramycin marine natural product having a sterol ether at C-14 position. **Heterocycles** 84 (2012): 309-314.
- [8] Tatsukawa, M., Punzalan, L. L. C., Magpantay, H. D. S., Villaseñor, I. M., Concepcion, G. P., Suwanborirux, K., Yokoya, M., and Saito, N. Chemistry of renieramycins. Part 13: Isolation and structure of stabilized renieramycin type derivatives, renieramycins W–Y, from Philippine blue sponge *Xestospongia* sp., pretreated with potassium cyanide. **Tetrahedron** 68 (2012): 7422-7428.
- [9] Parameswaran, P. S., Naik, C. G., Kamat, S. Y., and Pramanik, B. N. Renieramycins H and I, two novel alkaloids from the sponge *Haliclona cribricutis* Dendy. **Indian Journal of Chemistry** 37B (1998): 1258-1263.
- [10] Pettit, G. R., Knight, J. C., Collins, J. C., Herald, D. L., Pettit, R. K., Boyd, M. R., and Young, V. G. Antineoplastic agents 430. Isolation and structure of cribrostatins 3, 4, and 5 from the Republic of Maldives *Cribrochalina* species. **Journal of Natural Products** 63 (2000): 793-798.
- [11] Oku, N., Matsunaga, S., van Soest, R. W. M., and Fusetani, N. Renieramycin J, a highly cytotoxic tetrahydroisoquinoline alkaloid, from a marine sponge *Neopetrosia* sp. **Journal of Natural Products** 66 (2003): 1136-1139.
- [12] Fontana, A., Cavaliere, P., Wahidulla, S., Naik, C. G., and Cimino, G. A new antitumor isoquinoline alkaloid from the marine nudibranch *Jorunna funebris*. **Tetrahedron** 56 (2000): 7305-7308.
- [13] Charupant, K., Suwanborirux, K., Amnuoypol, S., Saito, E., Kubo, A., and Saito, N. Jorunnamycins A-C, new stabilized renieramycin-type bistetrahydroisoquinolines isolated from the Thai nudibranch *Jorunna funebris*. **Chemical and Pharmaceutical Bulletin** 55 (2007): 81-86.

- [14] He, W. F., Li, Y., Feng, M. T., Gavagnin, M., Mollo, E., Mao, S. C., and Guo, Y. W. New isoquinolinequinone alkaloids from the South China Sea nudibranch *Jorunna funebris* and its possible sponge-prey *Xestospongia* sp. **Fitoterapia** 96 (2014): 109-114.
- [15] Huang, R. Y., Chen, W. T., Kurtan, T., Mandi, A., Ding, J., Li, J., Li, X. W., and Guo, Y. W. Bioactive isoquinolinequinone alkaloids from the South China Sea nudibranch *Jorunna funebris* and its sponge-prey *Xestospongia* sp. **Future Medicinal Chemistry** 8 (2016): 17-27.
- [16] Scott, J. D., and Williams, R. M. Chemistry and biology of the tetrahydroisoquinoline antitumor antibiotics. **Chemical Reviews** 102 (2002): 1669-1730.
- [17] Le, V. H., Inai, M., Williams, R. M., and Kan, T. Ecteinascidins. A review of the chemistry, biology and clinical utility of potent tetrahydroisoquinoline antitumor antibiotics. **Natural Product Reports** 32 (2015): 328-347.
- [18] European Medicines Agency. Assessment report for Yondelis. London, UK: 2009.
- [19] U.S. Food and Drug Administration. FDA approves new therapy for certain types of advanced soft tissue sarcoma. Silver Spring, MD, USA: 2015.
- [20] Saito, N., Tanaka, C., Koizumi, Y., Suwanborirux, K., Amnuoypol, S., Pummangura, S., and Kubo, A. Chemistry of renieramycins. Part 6: Transformation of renieramycin M into jorumycin and renieramycin J including oxidative degradation products, mimosamycin, renierone, and renierol acetate. **Tetrahedron** 60 (2004): 3873-3881.
- [21] Fukuyama, T., Linton, S. D., and Tun, M. M. A stereocontrolled total synthesis of (±)-renieramycin A. **Tetrahedron Letters** 31 (1990): 5989-5992.
- [22] Chan, C., Heid, R., Zheng, S., Guo, J., Zhou, B., Furuuchi, T., and Danishefsky, S. J. Total Synthesis of Cribrostatin IV: Fine-Tuning the Character of an Amide Bond by Remote Control. **Journal of the American Chemical Society** 127 (2005): 4596-4598.

- [23] Lane, J. W., Chen, Y., and Williams, R. M. Asymmetric total syntheses of (-)-jorumycin, (-)-renieramycin G, 3-epi-jorumycin, and 3-epi-renieramycin G. **Journal of the American Chemical Society** 127 (2005): 12684-12690.
- [24] Magnus, P., and Matthews, K. S. Synthesis of the tetrahydroisoquinoline alkaloid (+/-)-renieramycin G and A (+/-)-lemonomycinone analogue from a common intermediate. **Journal of the American Chemical Society** 127 (2005): 12476-12477.
- [25] Chen, X., and Zhu, J. Total synthesis of the marine natural product (-)-cribrostatin 4 (renieramycin H). **Angewandte Chemie International Edition in English** 46 (2007): 3962-3965.
- [26] Vincent, G., and Williams, R. M. Asymmetric total synthesis of (-)-cribrostatin 4 (renieramycin H). **Angewandte Chemie International Edition in English** 46 (2007): 1517-1520.
- [27] Liao, X. W., Liu, W., Dong, W. F., Guan, B. H., Chen, S. Z., and Liu, Z. Z. Total synthesis of (-)-renieramycin G from L-tyrosine. **Tetrahedron** 65 (2009): 5709-5715.
- [28] Wu, Y. C., and Zhu, J. Asymmetric total syntheses of (-)-renieramycin M and G and (-)-jorumycin using aziridine as a lynchpin. **Organic Letters** 11 (2009): 5558-5561.
- [29] Yokoya, M., Ito, H., and Saito, N. Chemistry of renieramycins. Part 11: Total synthesis of (\pm)-cribrostatin 4. **Tetrahedron** 67 (2011): 9185-9192.
- [30] Yokoya, M., Shinada-Fujino, K., and Saito, N. Chemistry of renieramycins. Part 9: Stereocontrolled total synthesis of (\pm)-renieramycin G. **Tetrahedron Letters** 52 (2011): 2446-2449.
- [31] Yokoya, M., Shinada-Fujino, K., Yoshida, S., Mimura, M., Takada, H., and Saito, N. Chemistry of renieramycins. Part 12: An improved total synthesis of (\pm)-renieramycin G. **Tetrahedron** 68 (2012): 4166-4181.
- [32] Chen, R., Liu, H., and Chen, X. Asymmetric total synthesis of (-)-jorunnamycins A and C and (-)-jorumycin from L-tyrosine. **Journal of Natural Products** 76 (2013): 1789-1795.

- [33] Yokoya, M., Kobayashi, K., Sato, M., and Saito, N. Chemistry of renieramycins. Part 14: Total synthesis of renieramycin I and practical synthesis of cribrostatin 4 (renieramycin H). **Marine Drugs** 13 (2015): 4915-4933.
- [34] Yokoya, M., Toyoshima, R., Suzuki, T., Le, V. H., Williams, R. M., and Saito, N. Stereoselective total synthesis of (-)-renieramycin T. **The Journal of Organic Chemistry** (2016, in press).
- [35] Charupant, K., Daikuhara, N., Saito, E., Amnuoypol, S., Suwanborirux, K., Owa, T., and Saito, N. Chemistry of renieramycins. Part 8: Synthesis and cytotoxicity evaluation of renieramycin M-jorunnamycin A analogues. **Bioorganic & Medicinal Chemistry** 17 (2009): 4548-4558.
- [36] Halim, H., Chunhacha, P., Suwanborirux, K., and Chanvorachote, P. Anticancer and anti-metastatic activities of renieramycin M, a marine tetrahydroisoquinoline alkaloid, in human non-small cell lung cancer cells. **Anticancer Research** 31 (2011): 193-201.
- [37] Sirimangkalakitti, N., Chamni, S., Suwanborirux, K., and Chanvorachote, P. Renieramycin M sensitizes anoikis-resistant H460 lung cancer cells to anoikis. **Anticancer Research** 36 (2016): 1665-1671.
- [38] Liu, W., Dong, W., Liao, X., Yan, Z., Guan, B., Wang, N., and Liu, Z. Synthesis and cytotoxicity of (-)-renieramycin G analogs. **Bioorganic & Medicinal Chemistry Letters** 21 (2011): 1419-1421.
- [39] Liu, W., Liao, X., Dong, W., Yan, Z., Wang, N., and Liu, Z. Total synthesis and cytotoxicity of (-)-jorumycin and its analogues. **Tetrahedron** 68 (2012): 2759-2764.
- [40] Guo, J., Dong, W., Liu, W., Yan, Z., Wang, N., and Liu, Z. Synthesis and cytotoxicity of 3-aryl acrylic amide derivatives of the simplified saframycin-ecteinascidin skeleton prepared from L-dopa. **European Journal of Medicinal Chemistry** 62 (2013): 670-676.
- [41] International Agency for Research on Cancer. World Cancer Factsheet. London: Cancer Research UK, 2014.

- [42] Molina, J. R., Yang, P., Cassivi, S. D., Schild, S. E., and Adjei, A. A. Non-small cell lung cancer: Epidemiology, risk factors, treatment, and survivorship. **Mayo Clinic Proceedings** 83 (2008): 584-594.
- [43] Hirsh, V. Systemic therapies in metastatic non-small-cell lung cancer with emphasis on targeted therapies: The rational approach. **Current Oncology** 17 (2010): 13-23.
- [44] Esposito, L., Conti, D., Ailavajhala, R., Khalil, N., and Giordano, A. Lung cancer: Are we up to the challenge? **Current Genomics** 11 (2010): 513-518.
- [45] Tsujimoto, M., Lowtangkitcharoen, W., Mori, N., Pangkruang, W., Putongking, P., Suwanborirux, K., and Saito, N. Chemistry of ecteinascidins. Part 4: Preparation of 2'-N-acyl ecteinascidin 770 derivatives with improved cytotoxicity profiles. **Chemical and Pharmaceutical Bulletin** 61 (2013): 1052-1064.
- [46] Riss, T. L., Moravec, R. A., Niles, A. L., Benink, H. A., Worzella, T. J., and Minor, L. Cell viability assays. In G. S. Sittampalam, N. P. Coussens, H. Nelson (eds), **Assay Guidance Manual [Internet]**, Bethesda, MD: Eli Lilly & Company and the National Center for Advancing Translational Sciences, 2004.
- [47] Zucali, P. A., Ruiz, M. G., Giovannetti, E., Destro, A., Varella-Garcia, M., Floor, K., Ceresoli, G. L., Rodriguez, J. A., Garassino, I., Comoglio, P., Roncalli, M., Santoro, A., and Giaccone, G. Role of cMET expression in non-small-cell lung cancer patients treated with EGFR tyrosine kinase inhibitors. **Annals of Oncology** 19 (2008): 1605-1612.
- [48] Chunhacha, P., Sriuranpong, V., and Chanvorachote, P. Epithelial-mesenchymal transition mediates anoikis resistance and enhances invasion in pleural effusion-derived human lung cancer cells. **Oncology Letters** 5 (2013): 1043-1047.
- [49] Chanvorachote, P., Pongrakhananon, V., and Chunhacha, P. Prolonged nitric oxide exposure enhances anoikis resistance and migration through epithelial-mesenchymal transition and caveolin-1 upregulation. **BioMed Research International** 2014 (2014): 941359.

- [50] Yongsanguanchai, N., Pongrakhananon, V., Mutirangura, A., Rojanasakul, Y., and Chanvorachote, P. Nitric oxide induces cancer stem cell-like phenotypes in human lung cancer cells. **American Journal of Physiology - Cell Physiology** 308 (2015): C89-C100.



CHAPTER VII

RENIERAMYCIN M SENSITIZES

ANOIKIS-RESISTANT H460 LUNG CANCER CELLS TO ANOIKIS*

Natchanun Sirimangkalakitti,^a Supakarn Chamni,^a Khanit Suwanborirux,^a and Pithi Chanvorachote^b

^aCenter for Bioactive Natural Products from Marine Organisms and Endophytic Fungi, Department of Pharmacognosy and Pharmaceutical Botany; ^bCell-Based Drug and Health Product Development Research Unit and Department of Pharmacology and Physiology, Faculty of Pharmaceutical Sciences, Chulalongkorn University, Pathumwan, Bangkok, Thailand

1. Introduction

Lung cancer is the leading cause of cancer deaths in both men and women worldwide, with approximately 80% of all lung cancer comprising non-small cell lung cancer, and metastasis is the major cause of death from lung cancer [1-2]. Metastasis is a multistep process including detachment of cells from primary tissues, survival in the circulatory system, and subsequent formation of tumors in distant secondary organs [3-5]. In general, cells undergo apoptosis upon detachment from the extracellular matrix and neighboring cells, a process known as anoikis [6]. Metastatic cancer cells can develop resistance to anoikis through multiple mechanisms, allowing them to survive in the circulatory system. Therefore, circulating tumor cells (CTCs) which are anoikis-resistant have become a hot topic in cancer research fields [5, 7-9]. Numerous studies on anoikis-resistant mechanisms suggested that the survival and apoptotic pathways are primary mechanisms responsible for anoikis resistance, as well as cancer metastasis [3-5, 10-11]. The up-regulation of proteins in the survival

* Reproduced with permission from Anticancer Research, 36 (4), 1665-1671, 2016.

pathways, including activated extracellular signal-regulated kinase (ERK) and ATP-dependent tyrosine kinase (AKT), was shown to increase anoikis-resistant potential in lung cancer cells [12]. The proteins of the B-cell lymphoma-2 (BCL2) family in the apoptotic pathways play an important role in resistance to anoikis [4, 10]. For example, the up-regulation of the anti-apoptotic protein BCL2, together with down-regulation of the pro-apoptotic protein BCL2-associated X (BAX), provides anoikis resistance for CTCs in prostate cancer [13]. Moreover, the expression of BCL2 on CTCs is also associated with anoikis resistance and rapid progression in patients with metastatic breast cancer [8]. In addition, it has been found that the expression of the anti-apoptotic protein myeloid cell leukemia-1 (MCL1) mediates anoikis resistance of breast cancer and melanoma cells, and the knockdown of *MCL1* markedly both sensitized cancer cells to anoikis [14-15] and prevented metastasis *in vivo* [14].

In order to prevent cancer metastasis, our group focuses on searching for natural products with a capability of sensitizing anoikis-resistant cells to anoikis. Renieramycin M (RM), a bistetrahydroisoquinolinequinone alkaloid isolated from the Thai blue sponge *Xestospongia* sp., was reported to possess highly potent cytotoxicity against several human cancer cell lines, including lung, colon, prostate, breast, pancreatic, and oral cancer cells [16-19]. However, the effects on anoikis-resistant cells are still unknown. In this study, anoikis-resistant H460 lung cancer cells were established and used as a model of CTCs. The effects of RM on cell viability and cell morphology, and the role of survival and apoptotic proteins in the anoikis-resistant lung cancer cells were investigated.

2. Experimental

Renieramycin M (RM). RM was isolated from the Thai blue marine sponge *Xestospongia* sp. as previously reported, and its chemical structure was determined by comparison of the spectroscopic data with the literature [16]. RM was dissolved in dimethyl sulfoxide (DMSO; RCI Labscan, Bangkok, Thailand) as a 10 mM stock solution and diluted with serum-free medium to achieve concentrations containing less than 0.2% DMSO.

Cells and reagents. Human non-small cell H460 lung cancer cells and immortalized hair follicle dermal papilla (DP) cells were obtained from the American Type Culture Collection (Manassas, VA, USA) and Applied Biological Materials Inc. (Richmond, BC, Canada), respectively. Roswell Park Memorial Institute (RPMI)-1640 medium used for the culture of H460 cells and Dulbecco's modified Eagle's medium (DMEM) used for the culture of DP cells were supplemented with 10% fetal bovine serum (FBS), 2 mM L-glutamine, 100 units/ml penicillin, and 100 µg/ml streptomycin (Gibco, Carlsbad, CA, USA). Cell cultures were incubated in a humidified incubator at 37°C in an atmosphere of 5% CO₂. Primary antibodies to total ERK, phosphorylated ERK (p-ERK), total AKT, phosphorylated AKT (p-AKT), BCL2, MCL1, BAX, and α -tubulin and a secondary antibody: horseradish peroxidase (HRP)-linked anti-rabbit IgG were purchased from Cell Signaling Technology (Danvers, MA, USA).

Anoikis-resistant cells. Anoikis-resistant H460 cells (AR_H460) were established according to the method of Winitthana et al [20]. Briefly, attached H460 cells were trypsinized with 0.05% trypsin/0.02% EDTA (Gibco). Then the single-cell suspension in serum-free RPMI medium at a density of 2×10^5 cells/ml was seeded in a Costar 6-well plate with ultra-low attachment surface (Corning, New York, NY, USA) and cultured for 48 h. H460 cells were anoikis-resistant after 24-h detachment and called AR_H460. Cell viability, cell morphology, and the expression of the survival and apoptotic proteins of AR_H460 cells were determined compared to H460 cells under detached conditions. AR_H460 cells at 48 h were collected for further RM-treated experiments by centrifugation at $2,690 \times g$ for 10 min at room temperature and dissociation into single cells with 1 mM EDTA. Then the cells were washed with cultured RPMI medium.

Cell viability assay of attached cells. Cell viability was determined by water-soluble tetrazolium salt (WST) assay according to the manufacturer's instruction (Roche Diagnostic GmbH, Mannheim, Germany). H460 and DP cells were seeded in Costar 96-well plates (Corning) at a density of 1×10^5 cells/ml and allowed to adhere overnight in cultured RPMI and DMEM media, respectively. After the culture media were removed, cells were treated with different concentrations of RM (0-1 µM) and cultured

in the respective serum-free media for 24 h. Following the treatment, cells were incubated with 10% WST-1 for 2 h at 37°C. The intensity of the formazan product was determined by a VICTOR3 multilabel plate reader (PerkinElmer, Waltham, MA, USA) at 450 nm. Cell viability was calculated from optical density (OD) readings and represented as percentages with respect to the non-treated control value. Three concentrations of RM subtoxic to attached H460 cells were used for cell viability, cell morphology, and western blot assays on AR_H460 cells.

Cell viability assay of detached cells and anoikis assay. Cell viability was determined by WST assay. Cells in serum-free RPMI medium were seeded in a Costar 24-well plate with ultra-low attachment surface (Corning) at a density of 1×10^5 cells/ml. H460 cells in a detached condition were cultured and harvested at 0, 6, 12, 24, and 48 h for cell viability assay. AR_H460 cells in a detached condition were treated with subtoxic concentrations of RM (0-0.1 μ M) and harvested at 0, 6, 12, 24, and 48 h for cell viability assay. The harvested cells were incubated with 10% WST-1 for 2 h at 37°C. The intensity of the formazan product was measured at 450 nm using a plate reader. Cell viability was calculated from OD readings and represented as percentages with respect to the non-treated control value.

Cell morphology. Cells in serum-free RPMI medium were seeded in a 24-well plate with ultra-low attachment surface at a density of 2×10^5 cells/ml. H460 cells in a detached condition were cultured and observed at 0, 24, and 48 h. AR_H460 cells in a detached condition were treated with subtoxic concentrations of RM (0-0.1 μ M) and cultured for 24 h. Cell morphology was observed using a Nikon inverted phase contrast light microscope (Nikon, Tokyo, Japan) at $\times 40$ and $\times 100$ magnification equipped with a Sony NEX-5 camera (Sony, Tokyo, Japan).

Western blot analysis. Cells in serum-free RPMI medium were seeded in a 6-well plate with ultra-low attachment surface at a density of 2×10^5 cells/ml. H460 cells in a detached condition were cultured and harvested at 0, 24, and 48 h. AR_H460 cells in a detached condition were treated with subtoxic concentrations of RM (0-0.1 μ M), cultured and harvested at 24 h. The cells were harvested by centrifugation at $2,690 \times$

g for 10 min at 4°C and incubated in lysis buffer for 1 h on an ice box. Cell lysates were collected by centrifugation at 6,720 × g for 1 min at 4°C, and protein contents were analyzed using a BCA protein assay kit (Pierce Biotechnology, Rockford, IL, USA). An equal amount of protein from each sample (60 µg) was denatured by heating at 95°C for 5 min with Laemmli loading buffer and loaded onto 10% sodium dodecyl sulfate polyacrylamide gel electrophoresis (SDS-PAGE). After separation, proteins were transferred onto 0.45 µm nitrocellulose membranes (Bio-Rad, Hercules, CA, USA). The transferred membranes were blocked with 5% skim milk (Sigma-Aldrich, St. Louis, MO, USA) in TBST [20 mM Tris-HCl (pH 7.5), 138 mM NaCl, and 0.1% Tween 20] for 1 h at room temperature. The membranes were then washed with TBS and incubated with specific primary antibodies at 4°C overnight. After washing with TBST for 5 min (three times) to remove non-specific binding of the antibody, the membranes were further incubated with HRP-linked anti-rabbit IgG for 2 h at room temperature. The immune complexes were detected using a SuperSignal West Pico chemiluminescent substrate (Pierce Biotechnology) and exposed to Carestream Medical X-ray Blue/MXB film (Rochester, NY, USA). Relative protein levels were quantified by densitometric analysis using an ImageJ 1.48v software (<http://imagej.nih.gov/ij/index.html>, Bethesda, MD, USA). To confirm equal amounts of loaded proteins, α -tubulin was re-probed as a loading control in each treatment.

Statistical analysis. All data were obtained from at least three independent experiments and presented as means ± standard deviations (SD). Statistical differences were performed using one-way ANOVA with Turkey's *post hoc* test, unless otherwise stated, at a significance level of $p < 0.05$. IBM SPSS statistics version 20 (IBM Company, New York, NY, USA) was used for all statistical analyses.

3. Results

Characterization of anoikis-resistant H460 lung cancer cells. We first characterized the anoikis response of the lung cancer cells by culturing the cells in a detached condition for 0-48 h and cell viability at different times was determined. As shown in Figure 7.1A, cell viability gradually declined until 24 h after detachment and approximately 60% of the cells remained viable for a further 24 h. Therefore, we isolated the live cells after the first 24 h, and these anoikis-resistant H460 cells were named as AR_H460. Cell morphology in detached AR_H460 cells at 24 and 48 h was observed and compared to that of their parental H460 cells at 0 h as shown in Figure 7.1B. Interestingly, we found AR_H460 cells spontaneously formed multicellular aggregations while their parental H460 cells mostly exhibited a single-stage cell pattern.

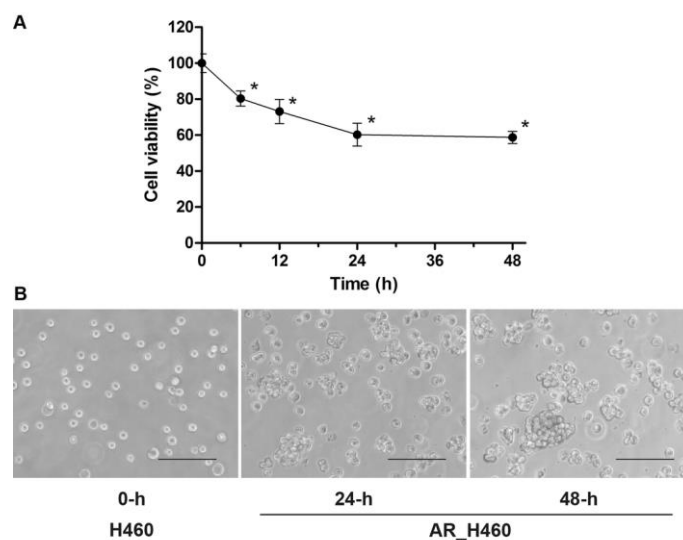


Figure 7.1 Cell viability and cell morphology of H460 lung cancer cells in a detached condition. A: H460 cells were cultured in a detached condition for 48 h. After detachment for 24 h, H460 cells were anoikis-resistant and named as AR_H460. Cell viability at each indicated time was evaluated by WST assay. Values are means \pm SD calculated as percentages compared to the control value at time 0 h. * $p < 0.05$ versus the control at time 0 h. B: Cell morphology of H460 cells at 0, 24, and 48 h after detachment was investigated using an inverted phase contrast light microscope at $\times 100$ magnification. Scale bar is 100 μm .

To study the proteins involved in anoikis resistance, the expression of the survival and apoptotic proteins in H460 and AR_H460 cells at 24 and 48 h under detached conditions was examined as illustrated in Figure 7.2. It is postulated that the declining viability of H460 cells during 0-24 h might mainly involve the reduced expression of the survival protein p-AKT, while the levels of the anti-apoptotic protein MCL1 and proapoptotic protein BAX were unchanged. Interestingly, it is clear that anoikis-resistant response of AR_H460 cells was mediated through the significant increase of the activation of ERK and AKT as well as the anti-apoptotic proteins BCL2 and MCL1 at 48 h compared with that at 24 h.

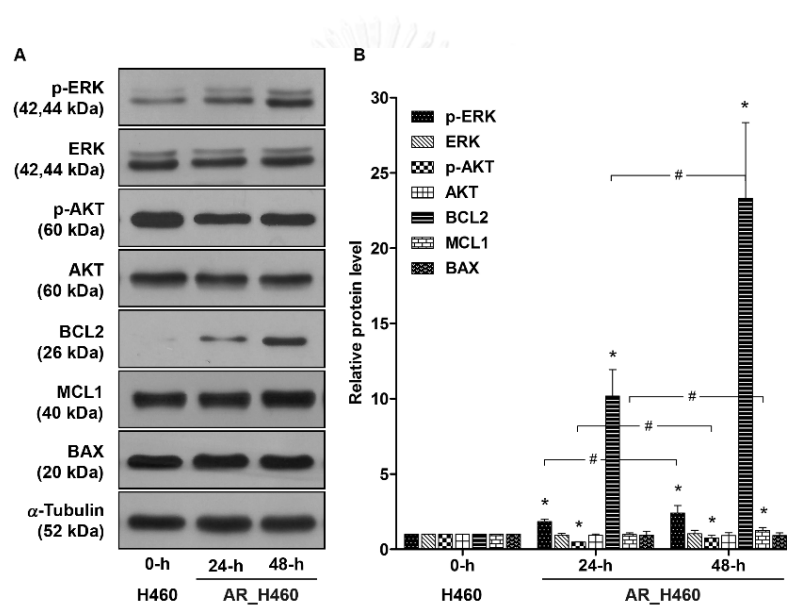


Figure 7.2 Expression of survival and apoptotic proteins of H460 lung cancer cells in a detached condition. A: At 0, 24, and 48 h after detachment, the indicated proteins of H460 cells were analyzed by western blotting. B: Relative protein levels were quantified by densitometric analysis. Values are means \pm SD calculated as values relative to those of H460 cells at 0 h, and statistically significant differences were analyzed by independent samples t-test. * $p < 0.05$ versus H460 cells at 0 h; # $p < 0.05$ cells at 24 h versus 48 h. ERK: Extracellular signal-regulated kinase; AKT: ATP-dependent tyrosine kinase; BCL2: B-cell lymphoma-2; MCL1: myeloid cell leukemia-1; BAX: BCL2-associated X.

Effect of RM on viability of H460 lung cancer and DP normal cells under attached conditions. To determine the appropriate concentrations for anoikis-resistant assay, concentrations of RM subtoxic to attached H460 lung cancer and DP normal cells were evaluated (Figure 7.3A). Cells were incubated with different concentrations of RM (0-1 μM) for 24 h, and cell viability was analyzed by WST assay. The results showed that RM at concentrations of 0-0.1 μM was non-toxic to both attached H460 and DP cells. Furthermore, RM at 1 μM was considered toxic to H460 cells but non-toxic to DP cells.

Effect of RM on viability of AR_H460 lung cancer cells. AR_H460 cells in a detached condition were established by culturing H460 cells on an ultra-low attachment plate for 48 h. AR_H460 cells were treated with subtoxic concentrations of RM (0-0.1 μM) and harvested at different times. Cell viability was evaluated by WST assay. Figure 7.3B shows that viability of non-treated AR_H460 cells was unchanged over the entire 48-h period. Interestingly, RM sensitized AR_H460 cells to anoikis in both time- and dose-dependent manners. RM at concentrations of 0.01-0.1 μM significantly reduced cell viability at 24 h, whilst cell viability was significantly decreased as early as 12 h after treatment with 0.1 μM RM, compared to the non-treated control.

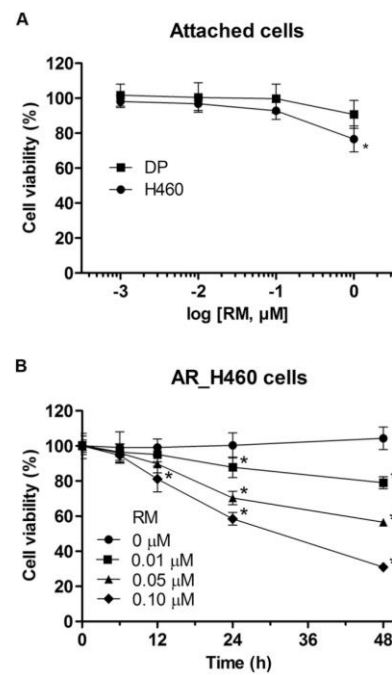


Figure 7.3 A: Cytotoxic effect of renieramycin M (RM) on H460 lung cancer and normal dermal papilla (DP) cells under attached conditions. Cells were treated with different concentrations of RM (0-1 μM) for 24 h. Cell viability was determined by WST assay. Values are means \pm SD calculated as percentages compared to the non-treated control value. * $p < 0.05$ versus the non-treated control. B: Cytotoxic effect of RM on AR_H460 cells in a detached condition. Cells were treated with RM at subtoxic concentrations (0-0.1 μM) for 48 h. Cell viability was determined by WST assay. Values are means \pm SD calculated as percentages compared to the non-treated control value at time 0 h. * $p < 0.05$ versus the non-treated control at the same time.

Effect of RM on cell morphology of AR_H460 lung cancer cells. AR_H460 cells in a detached condition were treated with subtoxic concentrations of RM (0-0.1 μM) and cultured in a plate with ultra-low attachment surface for 24 h. Cell morphology was observed under an inverted phase contrast light microscope (Figure 7.4). Non-treated AR_H460 cells spontaneously formed large aggregates. Treatment of AR_H460 cells with RM resulted in a dose-dependent suppression of aggregate formation.

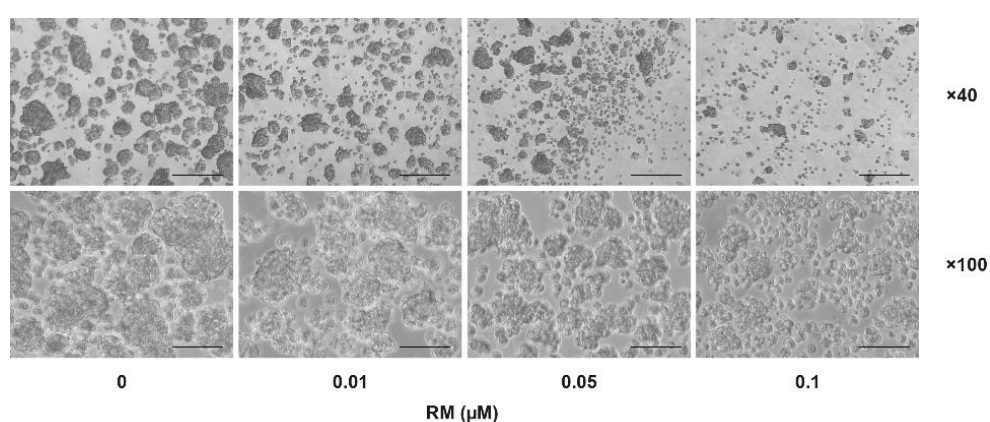


Figure 7.4 Cell morphology of AR_H460 lung cancer cells in a detached condition treated with renieramycin M (RM) at subtoxic concentrations. AR_H460 cells were treated with RM (0-0.1 μM) for 24 h and observed using an inverted phase contrast light microscope at $\times 40$ (upper panel, scale bar is 250 μm) and $\times 100$ (lower panel, scale bar is 100 μm) magnification.

RM sensitizes AR_H460 lung cancer cells to anoikis by decreasing anoikis-resistant pathways. To investigate the mechanisms of RM in sensitizing AR_H460 cells to anoikis, AR_H460 cells in a detached condition were treated with subtoxic concentrations of RM (0-0.1 μM) for 24 h. The expression of the survival proteins p-ERK, total ERK, p-AKT, and total AKT, anti-apoptotic proteins BCL2 and MCL1, and proapoptotic protein BAX was evaluated by western blot analysis. Figure 7.5 shows that the levels of p-ERK, p-AKT, total AKT, BCL2, and MCL1 were decreased in response to RM treatment in a dose-dependent manner. Treatment of RM at 0.01 μM resulted in a significant decrease of p-AKT and BCL2 levels, while a higher concentration of RM at 0.05 μM reduced the expression of total AKT and MCL1. Likewise, the protein level of p-ERK was only slightly reduced by RM at 0.1 μM . However, the expression of total ERK and BAX was not significantly altered.

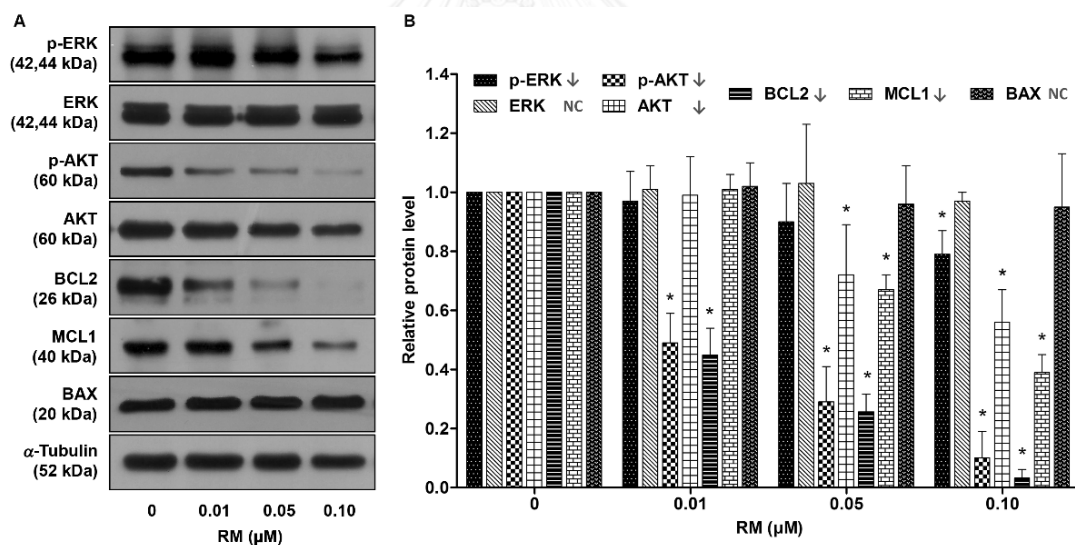


Figure 7.5 Expression of survival and apoptotic proteins of AR_H460 lung cancer cells treated with renieramycin M (RM) at subtoxic concentrations. A: After AR_H460 cells in a detached condition were treated with RM (0-0.1 μM) for 24 h, the indicated proteins were analyzed by western blotting. B: Relative protein levels were quantified by densitometric analysis. Values are means \pm SD calculated as values relative to the non-treated control value. * $p < 0.05$ versus the non-treated control. ERK: Extracellular signal-regulated kinase; AKT: ATP-dependent tyrosine kinase; BCL2: B-cell lymphoma-2; MCL1: myeloid cell leukemia-1; BAX: BCL2-associated X; NC: No change.

4. Discussion

Lung cancer is a significant cause of cancer-related deaths worldwide, with the majority of such a mortality due to metastasis [1-2]. To metastasize, cancer cells must have the capability to resist anoikis and survive within the circulatory system, and to initiate new tumors in distant secondary organs. Anoikis resistance plays an important role in promoting the survival of CTCs, which is one of the keys to cancer metastasis. Although fewer than 1% of cancer cells are still viable within 24 h after entering the circulation, very few surviving cells can give rise to metastases [21-22]. Not surprisingly, the presence of a high number of CTCs in blood is associated with poor survival in patients with lung metastatic cancer [23]. Targeting anoikis resistance in CTCs might represent a promising approach to reducing metastasis, thereby improving patient survival.

In this study, we employed anoikis-resistant H460 (AR_H460) lung cancer cells as a model of CTCs. Acquisition of anoikis resistance can be successfully developed in H460 lung cancer [12, 20, 24] by cell culturing under detached conditions. AR_H460 cells exhibited characteristics of anoikis resistance with unchanged cell viability for 24-48 h period after detachment and increased aggregate formation. These results were consistent with a previous study reporting that spontaneous aggregate formation of detached cells correlated with cell survival and growth [25]. Although the mechanisms of anoikis resistance are still largely unknown, many underlying mechanisms have been proposed, and the survival and apoptotic pathways were mentioned the most frequently [3-5, 10-11]. Our study showed that the survival proteins activated ERK and AKT, and anti-apoptotic proteins BCL2 and MCL1 were up-regulated, and that such proteins were likely responsible for anoikis resistance in these human lung cancer cells. Consistently, overexpression of BCL2 has been shown to be a marker of CTCs in patients with metastatic cancer [8-13]. The activation of ERK and AKT signals in these cells promotes cell survival by in part through the increase of BCL2 protein. Furthermore, several studies indicated that the inhibition of ERK and AKT signals, resulting in the decrease of BCL2 and MCL1, is able to restore anoikis sensitivity in several cancer types [14, 26-27].

Our investigations demonstrated that RM at subtoxic concentrations significantly reduced viability and suppressed spontaneous aggregate formation of AR_H460 cells. The molecular mechanisms indicate that RM sensitized AR_H460 cells to anoikis through the suppression of the survival proteins activated ERK and AKT, resulting in the reduction of expression of the anti-apoptotic proteins BCL2 and MCL1 (Figure 7.6). Inhibition of BCL2 and MCL1 protein expression of AR_H460 cells in a detached condition by RM were consistent with our previous finding for H460 cells in an attached condition [28].

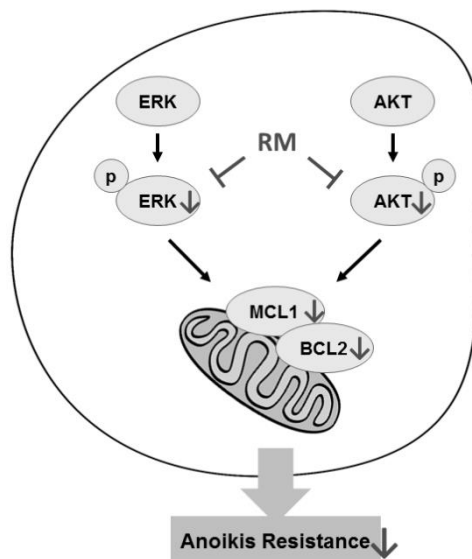


Figure 7.6 The scheme represents the effect of renieramyacin M (RM) on anoikis-resistant lung cancer cells. The present study proposed that RM has the ability to reduce anoikis resistance of AR_H460 cells through the suppression of survival signals of extracellular signal-regulated kinase (ERK) and ATP-dependent tyrosine kinase (AKT), which in turn reduce that of anti-apoptotic proteins B-cell lymphoma-2 (BCL2) and myeloid cell leukemia-1 (MCL1).

5. Conclusion

In conclusion, our findings highlight the potent effects of RM, a bistetrahydroisoquinolinequinone alkaloid isolated from the Thai blue sponge *Xestospongia* sp., on sensitization of anoikis-resistant lung cancer cells to anoikis through the reduction of the survival proteins activated ERK and AKT and anti-apoptotic proteins BCL2 and MCL1. Interestingly, the concentrations used caused no effect on viability of attached H460 and normal DP cells. A better understanding of molecular mechanisms of RM involved in anoikis resistance would assist in the development of anticancer drugs to kill CTCs and prevent metastasis in patients with lung cancer.

6. References

- [1] Esposito, L., Conti, D., Ailavajhala, R., Khalil, N., and Giordano, A. Lung cancer: Are we up to the challenge? **Current Genomics** 11 (2010): 513-518.
- [2] International Agency for Research on Cancer. World Cancer Factsheet. London: Cancer Research UK, 2014.
- [3] Mehlen, P., and Puisieux, A. Metastasis: A question of life or death. **Nature Reviews Cancer** 6 (2006): 449-458.
- [4] Simpson, C. D., Anyiwe, K., and Schimmer, A. D. Anoikis resistance and tumor metastasis. **Cancer Letters** 272 (2008): 177-185.
- [5] Kim, Y. N., Koo, K. H., Sung, J. Y., Yun, U. J., and Kim, H. Anoikis resistance: An essential prerequisite for tumor metastasis. **International Journal of Cell Biology** 2012 (2012): 306879.
- [6] Frisch, S. M., and Francis, H. Disruption of epithelial cell-matrix interactions induces apoptosis. **The Journal of Cell Biology** 124 (1994): 619-626.
- [7] Berezovskaya, O., Schimmer, A. D., Glinskii, A. B., Pinilla, C., Hoffman, R. M., Reed, J. C., and Glinsky, G. V. Increased expression of apoptosis inhibitor protein XIAP contributes to anoikis resistance of circulating human prostate cancer metastasis precursor cells. **Cancer Research** 65 (2005): 2378-2386.

- [8] Smerage, J. B., Budd, G. T., Doyle, G. V., Brown, M., Paoletti, C., Muniz, M., Miller, M. C., Repollet, M. I., Chianese, D. A., Connelly, M. C., Terstappen, L. W., and Hayes, D. F. Monitoring apoptosis and BCL2 on circulating tumor cells in patients with metastatic breast cancer. **Molecular Oncology** 7 (2013): 680-692.
- [9] Deng, S., Wu, Q., Zhao, Y., Zheng, X., Wu, N., Pang, J., Li, X., Bi, C., Liu, X., Yang, L., Liu, L., Su, W., Wei, Y., and Gong, C. Biodegradable polymeric micelle-encapsulated doxorubicin suppresses tumor metastasis by killing circulating tumor cells. **Nanoscale** 7 (2015): 5270-5280.
- [10] Taddei, M. L., Giannoni, E., Fiaschi, T., and Chiarugi, P. Anoikis: An emerging hallmark in health and diseases. **The Journal of Pathology** 226 (2012): 380-393.
- [11] Paoli, P., Giannoni, E., and Chiarugi, P. Anoikis molecular pathways and its role in cancer progression. **Biochimica et Biophysica Acta** 1833 (2013): 3481-3498.
- [12] Powan, P., and Chanvorachote, P. Nitric oxide mediates cell aggregation and mesenchymal to epithelial transition in anoikis-resistant lung cancer cells. **Molecular and Cellular Biochemistry** 393 (2014): 237-245.
- [13] Howard, E. W., Leung, S. C., Yuen, H. F., Chua, C. W., Lee, D. T., Chan, K. W., Wang, X., and Wong, Y. C. Decreased adhesiveness, resistance to anoikis and suppression of GRP94 are integral to the survival of circulating tumor cells in prostate cancer. **Clinical and Experimental Metastasis** 25 (2008): 497-508.
- [14] Woods, N. T., Yamaguchi, H., Lee, F. Y., Bhalla, K. N., and Wang, H. G. Anoikis, initiated by MCL1 degradation and BIM induction, is deregulated during oncogenesis. **Cancer Research** 67 (2007): 10744-10752.
- [15] Boisvert-Adamo, K., Longmate, W., Abel, E. V., and Aplin, A. E. MCL1 is required for melanoma cell resistance to anoikis. **Molecular Cancer Research** 7 (2009): 549-556.
- [16] Suwanborirux, K., Amnuoypol, S., Plubrukarn, A., Pummangura, S., Kubo, A., Tanaka, C., and Saito, N. Chemistry of renieramycins. Part 3. Isolation and structure of stabilized renieramycin type derivatives possessing antitumor

- activity from Thai sponge *Xestospongia* species, pretreated with potassium cyanide. **Journal of Natural Products** 66 (2003): 1441-1446.
- [17] Amnuoypol, S., Suwanborirux, K., Pummangura, S., Kubo, A., Tanaka, C., and Saito, N. Chemistry of renieramycins. Part 5. Structure elucidation of renieramycin-type derivatives O, Q, R, and S from Thai marine sponge *Xestospongia* species pretreated with potassium cyanide. **Journal of Natural Products** 67 (2004): 1023-1028.
- [18] Saito, N., Tanaka, C., Koizumi, Y., Suwanborirux, K., Amnuoypol, S., Pummangura, S., and Kubo, A. Chemistry of renieramycins. Part 6: Transformation of renieramycin M into jorumycin and renieramycin J including oxidative degradation products, mimosamycin, renierone, and renierol acetate. **Tetrahedron** 60 (2004): 3873-3881.
- [19] Charupant, K., Daikuhara, N., Saito, E., Amnuoypol, S., Suwanborirux, K., Owa, T., and Saito, N. Chemistry of renieramycins. Part 8: Synthesis and cytotoxicity evaluation of renieramycin M-jorunnamycin A analogues. **Bioorganic & Medicinal Chemistry** 17 (2009): 4548-4558.
- [20] Winitthana, T., Lawanprasert, S., and Chanvorachote, P. Triclosan potentiates epithelial-to-mesenchymal transition in anoikis-resistant human lung cancer cells. **PLoS One** 9 (2014): e110851.
- [21] Fidler, I. J. Metastasis: Quantitative analysis of distribution and fate of tumor emboli labeled with ¹²⁵I-5-iodo-2'-deoxyuridine. **Journal of the National Cancer Institute** 45 (1970): 773-782.
- [22] Fidler, I. J. The pathogenesis of cancer metastasis: The 'seed and soil' hypothesis revisited. **Nature Reviews Cancer** 3 (2003): 453-458.
- [23] Krebs, M. G., Sloane, R., Priest, L., Lancashire, L., Hou, J. M., Greystoke, A., Ward, T. H., Ferraldeschi, R., Hughes, A., Clack, G., Ranson, M., Dive, C., and Blackhall, F. H. Evaluation and prognostic significance of circulating tumor cells in patients with non-small-cell lung cancer. **Journal of Clinical Oncology** 29 (2011): 1556-1563.

- [24] Halim, H., Luanpitpong, S., and Chanvorachote, P. Acquisition of anoikis resistance up-regulates caveolin-1 expression in human non-small cell lung cancer cells. **Anticancer Research** 32 (2012): 1649-1658.
- [25] Zhang, X., Xu, L. H., and Yu, Q. Cell aggregation induces phosphorylation of PECAM1 and PYK2 and promotes tumor cell anchorage-independent growth. **Molecular Cancer** 9 (2010): 7.
- [26] Matsunaga, T., Takemoto, N., Sato, T., Takimoto, R., Tanaka, I., Fujimi, A., Akiyama, T., Kuroda, H., Kawano, Y., Kobune, M., Kato, J., Hirayama, Y., Sakamaki, S., Kohda, K., Miyake, K., and Niitsu, Y. Interaction between leukemic-cell VLA-4 and stromal fibronectin is a decisive factor for minimal residual disease of acute myelogenous leukemia. **Nature Medicine** 9 (2003): 1158-1165.
- [27] Galante, J. M., Mortenson, M. M., Bowles, T. L., Virudachalam, S., and Bold, R. J. ERK/BCL2 pathway in the resistance of pancreatic cancer to anoikis. **Journal of Surgical Research** 152 (2009): 18-25.
- [28] Halim, H., Chunhacha, P., Suwanborirux, K., and Chanvorachote, P. Anticancer and anti-metastatic activities of renieramycin M, a marine tetrahydroisoquinoline alkaloid, in human non-small cell lung cancer cells. **Anticancer Research** 31 (2011): 193-201.

CHAPTER VIII

RENIERAMYCIN M ATTENUATES CANCER STEM CELL-LIKE PHENOTYPES IN H460 LUNG CANCER CELLS*

Natchanun Sirimangkalakitti,^a Supakarn Chamni,^a Khanit Suwanborirux,^a and
Pithi Chanvorachote^b

^aCenter for Bioactive Natural Products from Marine Organisms and Endophytic Fungi, Department of Pharmacognosy and Pharmaceutical Botany; ^bCell-Based Drug and Health Product Development Research Unit and Department of Pharmacology and Physiology, Faculty of Pharmaceutical Sciences, Chulalongkorn University, Pathumwan, Bangkok, Thailand

1. Introduction

Cancer stem cells (CSCs) are a subpopulation of cancer cells possessing self-renewal capability and pluripotency. The existence of CSCs was first proven in human acute myeloid leukemia in 1997 [1] and was further extended to a broad spectrum of solid tumor types, including lung cancer [2-7]. In general, lung cancer has been accepted as one of leading causes of cancer deaths worldwide [8] with high degree of metastasis [9-10]. A number of studies show that CSCs within the tumors are major contributors responsible for drug-resistance, cancer recurrence, and metastasis after chemotherapy [11-13]. Since the clinical outcomes under current chemotherapeutic agents in non-small cell lung cancer (NSCLC) are not satisfied level (5-year survival is less than 15%) [9], researchers intensively investigate for the lung CSC-targeted therapies with the hope that they are promise means to improve the clinical outcomes.

* This draft manuscript will be submitted for publication to Anticancer Research.

Well-known characteristics of CSCs are the abilities to form colonies in an anchorage-independent condition and grow indefinitely as detached tumor spheroids in a serum-free condition [4, 7, 14-16]. Moreover, several studies have identified CD133, CD44, and aldehyde dehydrogenase (ALDH) as CSC markers, which are commonly used to distinguish CSCs from non-CSC populations [7, 11, 15-16]. In lung cancer research, CD133 is a potential marker for clinical prognosis. CD133 positive NSCLC patients had worse 5-year overall survival compared to the CD133 negative expression [17]. CD133 positive cancer cells have been found in several lung cancer subtypes [7] and shown higher tumorigenicity and chemoresistance than CD133 negative counterparts [14]. CD44 expression is commonly used as a marker for lung CSCs, and stem cell-like characteristics are enriched in CD44 positive cells of lung cancer cell lines [11, 15]. Aldehyde dehydrogenase 1 (ALDH1) is another cell surface marker connected with stem cell-like properties in NSCLC cell lines [18]. ALDH1A1 expression is associated with poor clinical outcome in NSCLC patients [16].

Most current anticancer agents are focused on the whole bulk of cancer cells. Interestingly, a number of natural products, such as curcumin, piperine [19], sulforaphane [20], 6-shogaol [21], and gigantol [22], have recently been reported to target CSCs. As renieramycin M (RM), a major bistetrahydroisoquinolinequinone alkaloid isolated from the Thai blue sponge *Xestospongia* sp., was reported to possess highly potent cytotoxicity against several human cancer cell lines [23-25], we further hypothesize that RM may have inhibitory effects on CSCs in human H460 NSCLC cells. In this study, CSC-like phenotypes, including colony and spheroid formations as well as cell surface CSC markers, were evaluated after RM treatment.

2. Experimental

Renieramycin M (RM). RM was isolated from the Thai blue marine sponge *Xestospongia* sp. as previously reported, and its chemical structure was identified by comparison of the spectroscopic data with the literature [23]. RM was dissolved in dimethyl sulfoxide (DMSO, RCI Labscan, Bangkok, Thailand), and 10 mM stock solution

of RM was further diluted in serum-free medium to achieve concentrations containing less than 0.2% DMSO.

Cells and reagents. Human non-small cell H460 lung cancer cells and immortalized hair follicle dermal papilla (DP) cells were obtained from the American Type Culture Collection (Manassas, VA, USA) and Applied Biological Materials Inc. (Richmond, BC, Canada), respectively. H460 and DP cells were cultured in Roswell Park Memorial Institute (RPMI)-1640 medium and Dulbecco's Modified Eagle's Medium (DMEM) medium, respectively. The media were supplemented with 10% fetal bovine serum (FBS), 2 mM L-glutamine, 100 units/ml penicillin, and 100 µg/ml streptomycin (Gibco, Carlsbad, CA, USA). Cell cultures were incubated in humidified atmosphere of 5% CO₂ at 37°C.

Cell viability assay. Cell viability was determined by water-soluble tetrazolium salt (WST) assay according to the manufacturer's instruction (Roche Diagnostic GmbH, Mannheim, Germany). H460 and DP cells were seeded at a density of 1×10^5 cells/ml in Costar 96-well plate (Corning, New York, NY, USA) and allowed to adhere overnight. The cells were treated with different concentrations of RM (0-1 µM) for 24 h. The detailed experimental procedure was described in our previous study [26]. The percentage of cell viability was calculated relative to the non-treated control value. Three concentrations of RM that was subtoxic to attached H460 cells were chosen for further experiments on lung CSC like-phenotypes.

Colony-formation assay. Anchorage-independent cell growth was determined in two-layer soft agar [27]. To prepare the lower layer, equal volumes of melted 1% agarose (Bio-Rad, Hercules, CA, USA) and the cultured RPMI medium were mixed (1:1), and then 500 µl of the mixture was put in a 24-well plate and allowed to solidify at 4°C for 15 min. To prepare the upper layer, melted 1% agarose and the cultured RPMI medium containing anoikis-resistant H460 cells at a density of 4×10^3 cells/ml and subtoxic concentrations of RM (0-0.1 µM) were mixed (1:2), and then 250 µl of the mixture was added as the upper layer. After the upper layer solidified, the cultured medium was added over the upper layer and incubated at 37°C for 2 weeks. Fresh

culture medium (200 μ l/well) was fed to the system every 3 days. Colony formation was photographed at day 7 and day 14 using a Nikon inverted phase contrast light microscope (Tokyo, Japan) at $\times 40$ magnification equipped with a Sony NEX-5 camera (Tokyo, Japan). Relative colony number and size were determined using ImageJ 1.48v software (<http://imagej.nih.gov/ij/index.html>, Bethesda, MD, USA) with respect to the non-treated control cells.

Spheroid-formation assay. H460 cells were seeded in a 24-well plate with ultra-low attachment surface at a density of 5×10^3 cells/ml in serum-free RPMI medium. Cells were treated with subtoxic concentrations of RM (0-0.1 μ M) and incubated at 37°C. Fresh serum-free medium was added to the system every 3 days. Primary spheroids were allowed to form and photographed at day 7 after treatment using an inverted phase contrast light microscope (Nikon) at $\times 40$ magnification equipped with a camera (Sony NEX-5). These primary spheroids were re-suspended into single cells and seeded in a 24-well ultra-low attachment plate. Secondary spheroids were allowed to form in the absence of RM and photographed at day 14, day 21, and day 30 after RM treatment.

Western blot analysis. Anoikis-resistant H460 cells in a detached condition were treated with subtoxic concentrations of RM (0-0.1 μ M), cultured and harvested at 24 h. Western blotting was analyzed according to the method of our previous study [26]. The primary antibodies to CD44 (Cell Signaling Technology, Danvers, MA, USA), CD133 (Cell Applications, San Diego, CA, USA), and ALDH1A1 (Cell Signaling Technology) were incubated with the membranes at 4°C for 2 days. After washing the membranes with TBST, the secondary antibody, horseradish peroxidase-conjugated either to anti-rabbit or to anti-mouse IgG (Cell Signaling Technology), was incubated for 2 h at room temperature. The immune complexes were detected using a SuperSignal West Pico chemiluminescent substrate (Pierce Biotechnology, Rockford, IL, USA) and exposed to carestream medical X-ray blue/MXB film (Rochester, NY, USA). Relative protein levels were quantified by densitometric analysis using an ImageJ 1.48v software. The blots

were reprobed with α -tubulin (Cell Signaling Technology) to confirm equal amounts of loaded proteins in each treatment.

Statistical analysis. Data were expressed in means \pm standard deviation (SD) obtained from at least three independent experiments. Statistical differences were performed using one-way ANOVA with Turkey's post hoc test at a significance level of $p < 0.05$. IBM SPSS statistics version 20 (IBM Company, New York, NY, USA) was used for all statistical analyses.

3. Results

Effect of RM on viability of H460 lung cancer and DP normal cells under attached conditions. To evaluate the effects of RM on CSC-like phenotypes, subtoxic concentrations of the compound on attached H460 lung cancer and DP normal cells were initially determined (Figure 8.1). Cells were treated with different concentrations of RM (0-1 μ M) for 24 h, and cell viability was measured by WST assay. The results showed that RM was considered non-toxic at the concentrations of 0-0.1 μ M to both H460 and DP cells (viability $\geq 93\%$). However, RM at 1 μ M was considered toxic to H460 cells (viability $\sim 83\%$) but non-toxic to DP cells (viability $\sim 93\%$).

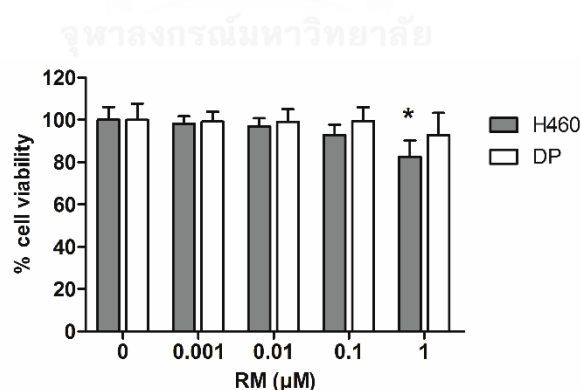


Figure 8.1 Cytotoxic effect of renieramycin M (RM) on H460 lung cancer and normal dermal papilla (DP) cells under normal culturing conditions. Cells were treated with different concentrations of RM (0-1 μ M) for 24 h. Cell viability was determined by WST assay. Values are means \pm SD calculated as percentages compared to the non-treated control value. * $p < 0.05$ versus the non-treated control.

RM suppressed colony formation. Anoikis-resistant H460 cells were subjected to soft agar colony-formation assay as a single-stage cell and treated with subtoxic concentrations of RM (0-0.1 μM). The colony formation was observed at day 7 and day 14 after RM treatment (Figure 8.2A). The colony number and size were determined and presented as relative values in comparison to those of non-treated control at day 7 (Figure 8.2B) and day 14 (Figure 8.2C). The results showed that non-treated control cells have certain ability to survive and grow in an anchorage-independent condition, while RM-treated cells exhibited significantly suppressed colony formation in a dose-dependent manner in terms of colony number and size on both observed days.

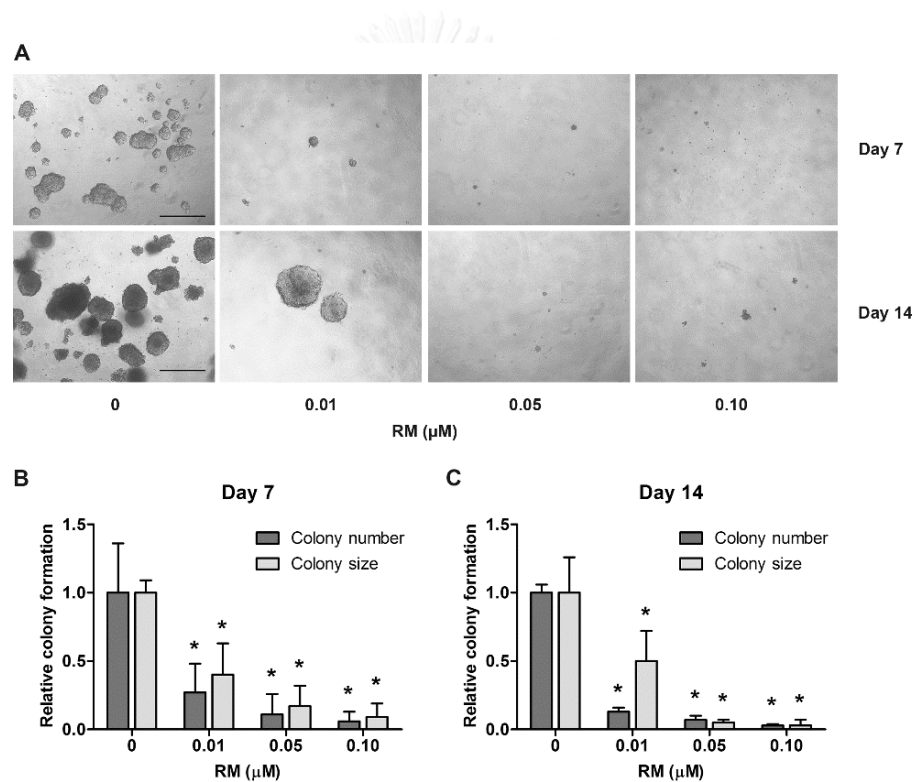


Figure 8.2 Colony formation of anoikis-resistant H460 cells treated with RM at subtoxic concentrations. Cells were treated with RM (0-0.1 μM) and subjected to soft agar colony-formation assay. The colony formation was observed using an inverted phase contrast light microscope with $\times 40$ magnification at day 7 and day 14, scale bar is 500 μm (A). Colony number and size at day 7 (B) and day 14 (C) were analyzed and calculated as relative values to the non-treated control values. * $p < 0.05$ versus the non-treated control.

RM suppressed spheroid formation. To evaluate whether RM could suppress the spheroid formation, H460 cells were seeded as a single-stage cell at a low density in serum-free RPMI medium and treated with subtoxic concentrations of RM (0-0.1 μM). The primary spheroids were allowed to form for 7 days in a detached condition and then resuspended into single cells and cultured for an additional passage under the absence of RM. The secondary spheroids were allowed to form for 30 days in a detached condition. As shown in Figure 8.3, non-treated control cells have an ability to survive and form spheroids in a serum starvation condition for long-term period. The number of secondary spheroids represented the presence of CSCs in H460 cells regarding their self-renewal ability and pluripotency. Interestingly, the results indicated that RM at the concentrations of 0.01-0.10 μM significantly suppressed the formation of primary spheroids in a dose-dependent manner and completely abolished the formation of secondary spheroids after day 30.

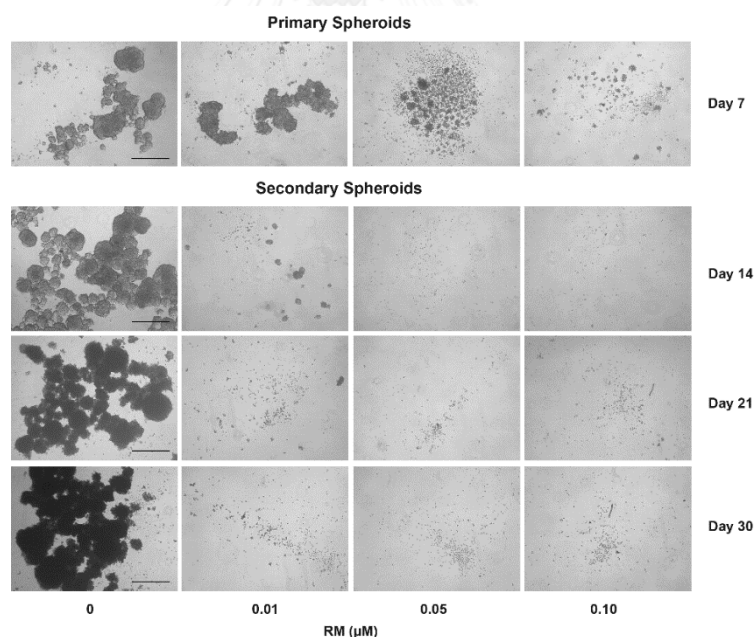


Figure 8.3 Spheroid formation of H460 lung cancer cells treated with RM at subtoxic concentrations. Cells at a low density in a serum-free condition were treated with RM (0-0.1 μM) and subjected to spheroid-formation assay. The primary spheroids were observed using an inverted phase contrast light microscope with $\times 40$ magnification at day 7 and then resuspended into single cells. The secondary spheroids were allowed to form and observed at day 14, day 21, and day 30. Scale bar is 500 μm .

RM reduced cancer stem cells (CSCs) markers. Having shown that treatment of the lung cancer cells with RM significantly suppressed the abilities of the cells to survive and grow in an anchorage-independent manner as well as to form spheroids, the molecular CSC markers in these cells in response to RM were further investigated. Cells in a detached condition were treated with subtoxic concentrations of RM (0-0.1 μM) for 24 h. The expression of CSC markers including CD133, CD44, and ALDH1A1 was evaluated by western blot analysis (Figure 8.4). The results showed that the expression of CD133, CD44, and ALDH1A1 significantly decreased in RM-treated cells at 0.1 μM compared to those of non-treated control.

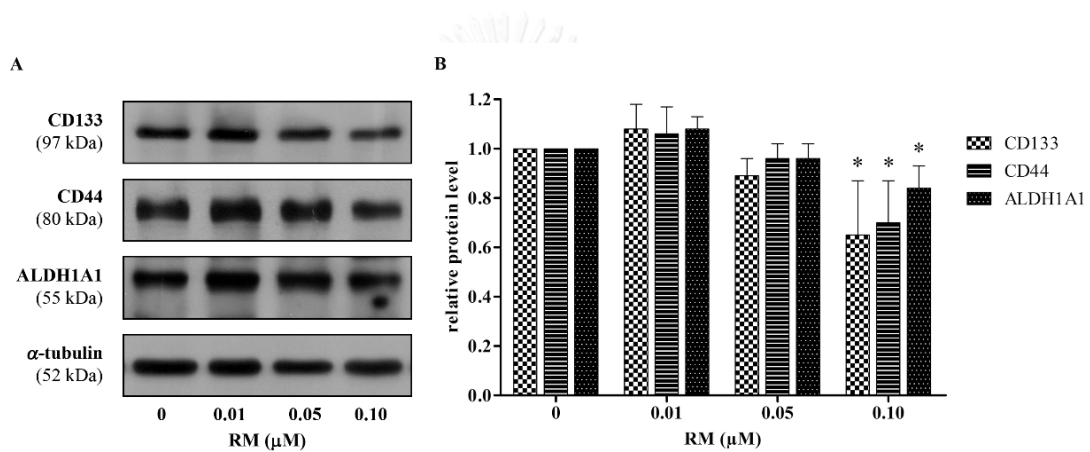


Figure 8.4 Expression of the lung cancer stem cell markers of anoikis-resistant H460 lung cancer cells treated with RM at subtoxic concentrations. A. After cells were treated with RM (0-0.1 μM) for 24 h, the indicated proteins were analyzed by western blotting. B. Relative protein levels were quantified by densitometric analysis. Values are means \pm SD calculated as relative values to the non-treated control values. * $p < 0.05$ versus the non-treated control.

4. Discussion

Lung cancer remains the most common cause of cancer deaths worldwide [8]. Limited outcomes of current chemotherapies are related to the metastatic potential of lung cancer [9, 14, 28]. These might be due to the presence of CSCs in lung cancer [29]. With a major role of CSCs in treatment failure and cancer recurrence [11-13], CSCs-targeting therapeutic strategy is an attractive approach for the effective cancer treatment. Small subpopulations of cancer cells with CSC properties have been also

identified within various cancers [1-7]. Based on the self-renewal capability and pluripotency, CSCs can initiate tumor development and maintain tumor growth. The colony- and spheroid-formation assays are commonly used to demonstrate these specific properties of CSCs [4, 7, 14-16] and assess the inhibitory activity against CSCs of anticancer agents [19-22]. CSCs possess high clonogenicity and produce more soft agar colonies compared to non-CSCs [4, 15-16]. Long-term cultures of spheroid-forming cells in the serum-free medium enrich with CSCs and exhibit high tumorigenicity [7, 14-15]. It has been demonstrated that the spheroids enhance the production of key angiogenic cytokines, preservation of extracellular matrix components, activation of survival signals as well as inhibition of apoptotic proteins leading to increase in survival and proliferation in culture time- and spheroid-size-dependent manners [30]. Furthermore, lung CSCs can be characterized by specific cell surface markers including CD133, CD44, and ALDH1A1 [7, 11, 15-16]. Lung cancer patients with high level of these CSC markers are related to poor prognosis and overall survival [17, 31]. The identification of CSCs provides a tool to investigate new anticancer drugs targeted to CSCs.

Previous research showed that RM, a major bistetrahydroisoquinoline-quinone alkaloid isolated from the blue sponge *Xestospongia* sp. [23], exhibited potent cytotoxicity against several human cancer cell lines [23-25], including H460 NSCLC [23]. In addition, RM exhibited other related anticancer activities, including anoikis sensitization, inhibition of migration, invasion, and anchorage-independent growth in H460 NSCLC cells [32]. Recently, our study has reported that RM is effective in targeting anoikis-resistant H460 NSCLC cells at concentrations of 0.01-0.10 μ M, which are subtoxic to the cancer cells in a normal culturing condition. Anoikis resistance plays an important role in promoting the survival of circulating tumor cells, which is one of the keys to cancer metastasis [26]. In the present investigation, the effects of RM on CSCs in H460 cells were examined. We found that treatment of H460 cells with RM at subtoxic concentrations (0.01-0.10 μ M) resulting in the decrease of CSCs indicated by the reduction of colony and spheroid formations along with the downregulation of lung CSC markers. RM markedly decreased colony-forming activity of CSCs in terms of

colony number and size at both observed days 7 and 14. RM also suppressed the formation of primary spheroids at day 7 and completely abolished the formation of secondary spheroids after day 30. Having shown that RM suppressed CSC-like phenotypes in H460 cells, we next confirmed these observations by using well-known lung CSC markers, including CD133, CD44, and ALDH1A1. The expression of these markers significantly decreased after treatment of RM at the highest concentration of 0.1 μM . Although these results did not strongly support the above colony- and spheroid-forming results due to the exposure time of RM to the cells for just 24 h, they addressed a potential role of RM treatment on CSCs in H460 cells. In this case, extending the exposure time of RM to the cells could sensitize most cells to anoikis, which was a problem to collect the cells and analyze their proteins.

In summary, RM plays a role in the attenuation of CSC-like phenotypes in H460 lung cancer cells by the reduction of colony- and spheroid-forming activities, along with the decrease in lung CSC markers. Our findings indicated that RM might be a potential candidate for prevention and treatment of metastasis in patients with lung cancer.

5. References

- [1] Bonnet, D., and Dick, J. E. Human acute myeloid leukemia is organized as a hierarchy that originates from a primitive hematopoietic cell. **Nature Medicine** 3 (1997): 730-737.
- [2] Al-Hajj, M., Wicha, M. S., Benito-Hernandez, A., Morrison, S. J., and Clarke, M. F. Prospective identification of tumorigenic breast cancer cells. **Proceedings of the National Academy of Sciences of the United States of America** 100 (2003): 3983-3988.
- [3] Singh, S. K., Clarke, I. D., Terasaki, M., Bonn, V. E., Hawkins, C., Squire, J., and Dirks, P. B. Identification of a cancer stem cell in human brain tumors. **Cancer Research** 63 (2003): 5821-5828.
- [4] Patrawala, L., Calhoun, T., Schneider-Broussard, R., Li, H., Bhatia, B., Tang, S., Reilly, J. G., Chandra, D., Zhou, J., Claypool, K., Coghlan, L., and Tang, D. G. Highly

- purified CD44⁺ prostate cancer cells from xenograft human tumors are enriched in tumorigenic and metastatic progenitor cells. **Oncogene** 25 (2006): 1696-1708.
- [5] Hermann, P. C., Huber, S. L., Herrler, T., Aicher, A., Ellwart, J. W., Guba, M., Bruns, C. J., and Heeschen, C. Distinct populations of cancer stem cells determine tumor growth and metastatic activity in human pancreatic cancer. **Cell Stem Cell** 1 (2007): 313-323.
- [6] Ricci-Vitiani, L., Lombardi, D. G., Pilozzi, E., Biffoni, M., Todaro, M., Peschle, C., and De Maria, R. Identification and expansion of human colon-cancer-initiating cells. **Nature** 445 (2007): 111-115.
- [7] Eramo, A., Lotti, F., Sette, G., Pilozzi, E., Biffoni, M., Di Virgilio, A., Conticello, C., Ruco, L., Peschle, C., and De Maria, R. Identification and expansion of the tumorigenic lung cancer stem cell population. **Cell Death & Differentiation** 15 (2008): 504-514.
- [8] International Agency for Research on Cancer. World Cancer Factsheet. London: Cancer Research UK, 2014.
- [9] Esposito, L., Conti, D., Ailavajhala, R., Khalil, N., and Giordano, A. Lung cancer: Are we up to the challenge? **Current Genomics** 11 (2010): 513-518.
- [10] Nichols, L., Saunders, R., and Knollmann, F. D. Causes of death of patients with lung cancer. **Archives of pathology & laboratory medicine** 136 (2012): 1552-1557.
- [11] Salama, R., Tang, J., Gadgeel, S. M., Ahmad, A., and Sarkar, F. H. Lung cancer stem cells: Current progress and future perspectives. **Journal of Stem Cell Research & Therapy** S7 (2012): 007.
- [12] Sampieri, K., and Fodde, R. Cancer stem cells and metastasis. **Seminars in Cancer Biology** 22 (2012): 187-193.
- [13] Vinogradov, S., and Wei, X. Cancer stem cells and drug resistance: the potential of nanomedicine. **Nanomedicine (Lond)** 7 (2012): 597-615.
- [14] Bertolini, G., Roz, L., Perego, P., Tortoreto, M., Fontanella, E., Gatti, L., Pratesi, G., Fabbri, A., Andriani, F., Tinelli, S., Roz, E., Caserini, R., Lo Vullo, S., Camerini, T., Mariani, L., Delia, D., Calabro, E., Pastorino, U., and Sozzi, G. Highly

- tumorigenic lung cancer CD133⁺ cells display stem-like features and are spared by cisplatin treatment. **Proceedings of the National Academy of Sciences of the United States of America** 106 (2009): 16281-16286.
- [15] Leung, E. L., Fiscus, R. R., Tung, J. W., Tin, V. P., Cheng, L. C., Sihoe, A. D., Fink, L. M., Ma, Y., and Wong, M. P. Non-small cell lung cancer cells expressing CD44 are enriched for stem cell-like properties. **PLoS One** 5 (2010): e14062.
- [16] Sullivan, J. P., Spinola, M., Dodge, M., Raso, M. G., Behrens, C., Gao, B., Schuster, K., Shao, C., Larsen, J. E., Sullivan, L. A., Honorio, S., Xie, Y., Scaglioni, P. P., DiMaio, J. M., Gazdar, A. F., Shay, J. W., Wistuba, II, and Minna, J. D. Aldehyde dehydrogenase activity selects for lung adenocarcinoma stem cells dependent on Notch signaling. **Cancer Research** 70 (2010): 9937-9948.
- [17] Qu, H., Li, R., Liu, Z., Zhang, J., and Luo, R. Prognostic value of cancer stem cell marker CD133 expression in non-small cell lung cancer: A systematic review. **International Journal of Clinical and Experimental Pathology** 6 (2013): 2644-2650.
- [18] Liang, D., and Shi, Y. Aldehyde dehydrogenase-1 is a specific marker for stem cells in human lung adenocarcinoma. **Medical Oncology** 29 (2012): 633-639.
- [19] Kakarala, M., Brenner, D. E., Korkaya, H., Cheng, C., Tazi, K., Ginestier, C., Liu, S., Dontu, G., and Wicha, M. S. Targeting breast stem cells with the cancer preventive compounds curcumin and piperine. **Breast Cancer Research and Treatment** 122 (2010): 777-785.
- [20] Li, Y., Zhang, T., Korkaya, H., Liu, S., Lee, H. F., Newman, B., Yu, Y., Clouthier, S. G., Schwartz, S. J., Wicha, M. S., and Sun, D. Sulforaphane, a dietary component of broccoli/broccoli sprouts, inhibits breast cancer stem cells. **Clinical Cancer Research** 16 (2010): 2580-2590.
- [21] Ray, A., Vasudevan, S., and Sengupta, S. 6-Shogaol inhibits breast cancer cells and stem cell-like spheroids by modulation of Notch signaling pathway and induction of autophagic cell death. **PLoS One** 10 (2015): e0137614.
- [22] Bhummaphan, N., and Chanvorachote, P. Gigantol suppresses cancer stem cell-like phenotypes in lung cancer cells. **Evidence-Based Complementary and Alternative Medicine** 2015 (2015): 836564.

- [23] Suwanborirux, K., Amnuoypol, S., Plubrukarn, A., Pummangura, S., Kubo, A., Tanaka, C., and Saito, N. Chemistry of renieramycins. Part 3. Isolation and structure of stabilized renieramycin type derivatives possessing antitumor activity from Thai sponge *Xestospongia* species, pretreated with potassium cyanide. **Journal of Natural Products** 66 (2003): 1441-1446.
- [24] Amnuoypol, S., Suwanborirux, K., Pummangura, S., Kubo, A., Tanaka, C., and Saito, N. Chemistry of renieramycins. Part 5. Structure elucidation of renieramycin-type derivatives O, Q, R, and S from Thai marine sponge *Xestospongia* species pretreated with potassium cyanide. **Journal of Natural Products** 67 (2004): 1023-1028.
- [25] Saito, N., Tanaka, C., Koizumi, Y., Suwanborirux, K., Amnuoypol, S., Pummangura, S., and Kubo, A. Chemistry of renieramycins. Part 6: Transformation of renieramycin M into jorumycin and renieramycin J including oxidative degradation products, mimosamycin, renierone, and renierol acetate. **Tetrahedron** 60 (2004): 3873-3881.
- [26] Sirimangkalakitti, N., Chamni, S., Suwanborirux, K., and Chanvorachote, P. Renieramycin M sensitizes anoikis-resistant H460 lung cancer cells to anoikis. **Anticancer Research** 36 (2016): 1665-1671.
- [27] Pengpaeng, P., Sritularak, B., and Chanvorachote, P. Dendrofalconerol A sensitizes anoikis and inhibits migration in lung cancer cells. **Journal of Natural Medicines** 69 (2015): 178-190.
- [28] Ohe, Y., Ohashi, Y., Kubota, K., Tamura, T., Nakagawa, K., Negoro, S., Nishiwaki, Y., Saijo, N., Ariyoshi, Y., and Fukuoka, M. Randomized phase III study of cisplatin plus irinotecan versus carboplatin plus paclitaxel, cisplatin plus gemcitabine, and cisplatin plus vinorelbine for advanced non-small-cell lung cancer: Four-Arm Cooperative Study in Japan. **Annals of Oncology** 18 (2007): 317-323.
- [29] Koren, A., Motaln, H., and Cufer, T. Lung cancer stem cells: A biological and clinical perspective. **Cellular Oncology** 36 (2013): 265-275.
- [30] Lee, J. H., Han, Y. S., and Lee, S. H. Long-duration three-dimensional spheroid culture promotes angiogenic activities of adipose-derived mesenchymal stem cells. **Biomolecules & therapeutics** 24 (2016): 260-267.

- [31] Liu, J., Xiao, Z., Wong, S. K.-M., Tin, V. P.-C., Ho, K.-Y., Wang, J., Sham, M.-H., and Wong, M. P. Lung cancer tumorigenicity and drug resistance are enhanced through ALDH^{hi}CD44^{hi} tumor initiating cells. **Oncotarget** 4 (2013): 1698-1711.
- [32] Halim, H., Chunhacha, P., Suwanborirux, K., and Chanvorachote, P. Anticancer and anti-metastatic activities of renieramycin M, a marine tetrahydroisoquinoline alkaloid, in human non-small cell lung cancer cells. **Anticancer Research** 31 (2011): 193-201.



CHAPTER IX

CONCLUSION

Twenty-one bromotyrosine-derived alkaloids, including two new compounds, 13-oxosubereamolline D (**B5**) and acanthodendrilline (**B21**), were isolated from the Thai sponge *Acanthodendrilla* sp. (Figure 9.1) This report is the first occurrence of bromotyrosine alkaloids from the sponge belonging to the order Dendroceratida. The structures were determined by analyses of 1D- and 2D-NMR, high-resolution mass, and optical rotation and circular dichroism (CD) data, together with literature comparisons. To resolve the absolute configuration of single chiral carbon of **B21**, the (*S*)- and (*R*)-synthetic enantiomers were obtained from the 4-step synthetic strategy using commercial tyramine and (*S*)- and (*R*)-epichlorohydrins as precursors. By comparing the specific rotation values of natural **B21** and the synthetic enantiomers, the stereocenter at C-11 was assigned as *S*. All isolated compounds were evaluated the acetylcholinesterase inhibitory activities by the modified Ellman's method. The most active compound was identified as **B7** with IC_{50} s 2.9 and 4.5 μ M against *EeAChE* and *hrAChE*, respectively. The *hrAChE* inhibition kinetics showed increased K_m and unchanged V_{max} values, suggesting its competitive mode of inhibition. The spirocyclohexadienylisoxazoline and specific length of the alkyl diamine linkage were proposed as the crucial parts for its strong inhibitory activity. On the other hand, the other compounds exhibited weak to moderate AChE inhibitory activity. Therefore, **B7** could be considered as a promising new lead for the development of new Alzheimer's drugs. In addition, the cytotoxicity of the synthetic enantiomers of **B21** evaluated by MTT assay indicated that (*S*)-enantiomer was approximately 3-fold more potent than (*R*)-enantiomer against human non-small cell lung cancer H292 cell line. The stereochemistry at C-11 of **B21** was, therefore, proposed as a key feature related to their cytotoxicity.

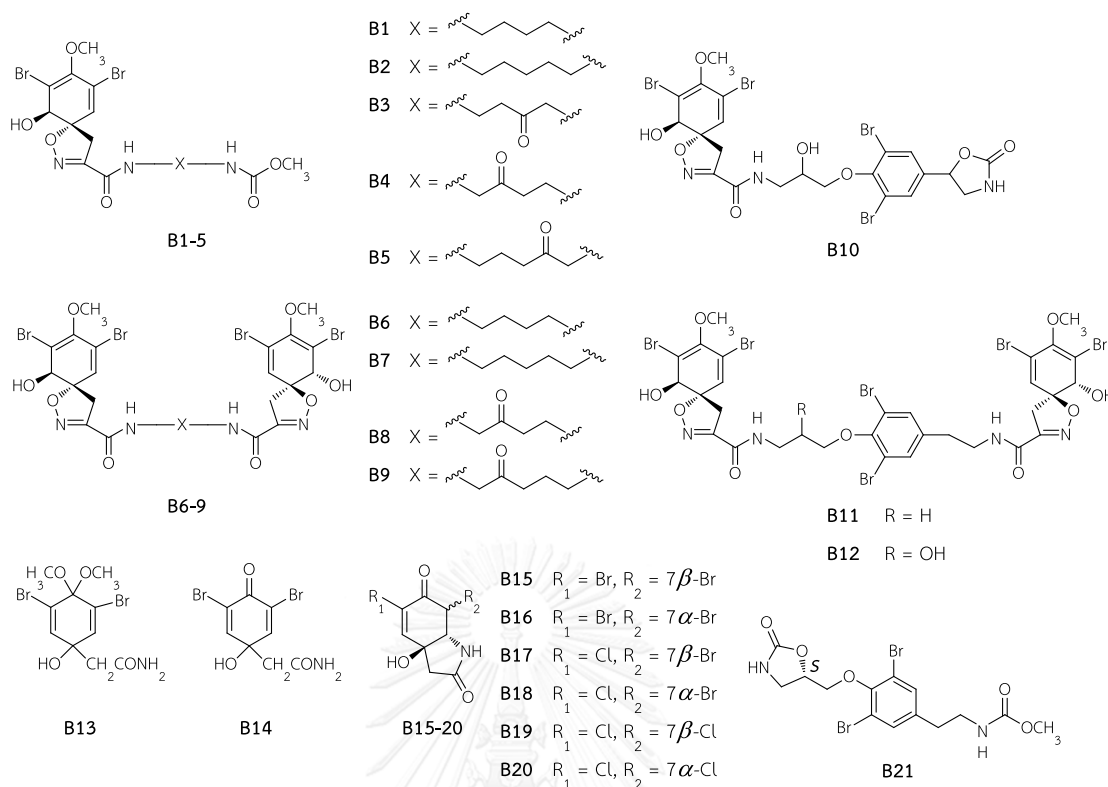


Figure 9.1 Bromotyrosine alkaloids isolated from the sponge *Acanthodendrilla* sp.

Eighteen 22-*O*-ester derivatives of jorunnamycin A (JA), including the 3,3,3-trifluoropropionyl ester (**R1**), six benzoyl (**R2-7**) and six cinnamoyl esters (**R8-13**) that vary in the electron-withdrawing groups, three pyridinecarbonyl esters (**R14-16**), and two pyridineacryloyl esters (**R17** and **R18**), were synthesized from JA (Figure 9.2). This starting material was prepared by the three-step deangeloyl transformation of renieramycin M (RM), a bistetrahydroisoquinolinequinone alkaloid which was obtained from the Thai blue sponge *Xestospongia* sp. The cytotoxicity of the derivatives emphasizing against human non-small cell lung cancer (NSCLC) cell lines was evaluated *in vitro* by measuring IC₅₀ using MTT assay. Our finding showed that the 22-*O*-ester derivatives of JA with nitrogen-heterocyclic aromatic ring, such as pyridinecarbonyl esters (**R14-16**) and 3-(3-pyridyl)acryloyl ester (**R18**), are potential candidates for development of new effective anticancer drugs to treat NSCLC patients. Among them, 22-*O*-(4-pyridinecarbonyl) ester (**R14**) is the most potent derivative,

exhibiting 5-fold and 20-fold increase in cytotoxicity to the H460 and H292 cell lines, respectively, relative to RM.

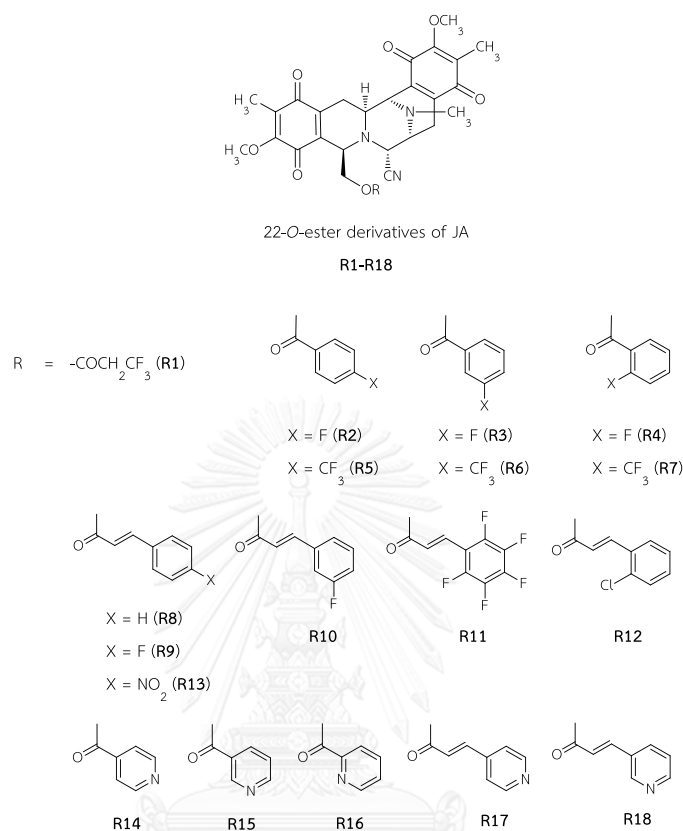


Figure 9.2 22-O-ester derivatives of jorunnamycin A prepared from renieramycin M (RM), isolated from the blue sponge *Xestospongia* sp.

RM was further investigated the effects on new therapeutic targets related to antimetastatic activity, including anoikis-resistant lung cancer cells and lung cancer stem-like cells. RM sensitized the anoikis-resistant lung cancer cells to anoikis through the reduction of the survival proteins activated ERK and AKT and anti-apoptotic proteins BCL2 and MCL1. RM also suppressed lung cancer stem cell-like phenotypes determining by the reduction of the colony and spheroid formations and the downregulation of lung CSC markers, including CD133, CD44, and ALDH1A1. A better understanding of molecular mechanisms of RM involved in anoikis resistance and stemness would assist in the development of anticancer drugs to kill circulating tumor cells and cancer stem cells in patients with metastatic lung cancer.

REFERENCES

- [1] Pawlik, J. R. Marine invertebrate chemical defenses. **Chemical Reviews** 93 (1993): 1911-1922.
- [2] Blunt, J. W., Copp, B. R., Keyzers, R. A., Munro, M. H., and Prinsep, M. R. Marine natural products. **Natural Product Reports** 30 (2013): 237-323.
- [3] Mehbub, M. F., Lei, J., Franco, C., and Zhang, W. Marine sponge derived natural products between 2001 and 2010: Trends and opportunities for discovery of bioactives. **Marine Drugs** 12 (2014): 4539-4577.
- [4] Bergmann, W., and Feeney, R. J. Contributions to the study of marine products. XXXII. The nucleosides of sponges. I. **The Journal of Organic Chemistry** 16 (1951): 981-987.
- [5] Proksch, P., Edrada, R. A., and Ebel, R. Drugs from the seas - current status and microbiological implications. **Applied Microbiology and Biotechnology** 59 (2002): 125-134.
- [6] Laport, M. S., Santos, O. C., and Muricy, G. Marine sponges: Potential sources of new antimicrobial drugs. **Current Pharmaceutical Biotechnology** 10 (2009): 86-105.
- [7] Weinheimer, A. J., and Spraggins, R. L. The occurrence of two new prostaglandin derivatives (15-epi-PGA₂ and its acetate, methyl ester) in the gorgonian *Plexaura homomalla* chemistry of coelenterates. XV. **Tetrahedron Letters** (1969): 5185-5188.
- [8] Martins, A., Vieira, H., Gaspar, H., and Santos, S. Marketed marine natural products in the pharmaceutical and cosmeceutical industries: tips for success. **Marine Drugs** 12 (2014): 1066-1101.
- [9] Mayer, A. M., Glaser, K. B., Cuevas, C., Jacobs, R. S., Kem, W., Little, R. D., McIntosh, J. M., Newman, D. J., Potts, B. C., and Shuster, D. E. The odyssey of marine pharmaceuticals: A current pipeline perspective. **Trends in Pharmacological Sciences** 31 (2010): 255-265.

- [10] Huyck, T. K., Gradishar, W., Manuguid, F., and Kirkpatrick, P. Eribulin mesylate. **Nature Reviews Drug Discovery** 10 (2011): 173-174.
- [11] Towle, M. J., Salvato, K. A., Budrow, J., Wels, B. F., Kuznetsov, G., Aalfs, K. K., Welsh, S., Zheng, W., Seletsky, B. M., Palme, M. H., Habgood, G. J., Singer, L. A., Dipietro, L. V., Wang, Y., Chen, J. J., Quincy, D. A., Davis, A., Yoshimatsu, K., Kishi, Y., Yu, M. J., and Littlefield, B. A. *In vitro* and *in vivo* anticancer activities of synthetic macrocyclic ketone analogues of halichondrin B. **Cancer Research** 61 (2001): 1013-1021.
- [12] Martin, M. J., Coello, L., Fernandez, R., Reyes, F., Rodriguez, A., Murcia, C., Garranzo, M., Mateo, C., Sanchez-Sancho, F., Bueno, S., de Eguilior, C., Francesch, A., Munt, S., and Cuevas, C. Isolation and first total synthesis of PM050489 and PM060184, two new marine anticancer compounds. **Journal of the American Chemical Society** 135 (2013): 10164-10171.
- [13] Sirimangkalakitti, N., Olatunji, O., Changwichit, K., Saesong, T., Chamni, S., Chanvorachote, P., Ingkaninan, K., Plubrukarn, A., and Suwanborirux, K. Bromotyrosine marine alkaloids with acetylcholinesterase inhibitory activity from the Thai sponge *Acanthodendrilla* sp. **Natural Product Communications** 10 (2015): 1945-1949.
- [14] Sirimangkalakitti, N., Yokoya, M., Chamni, S., Chanvorachote, P., Plubrukarn, A., Saito, N., and Suwanborirux, K. Synthesis and absolute configuration of acanthodendrilline, a new cytotoxic bromotyrosine alkaloid from the Thai marine sponge *Acanthodendrilla* sp. **Chemical and Pharmaceutical Bulletin** 64 (2016): 258-262.
- [15] Sirimangkalakitti, N., Chamni, S., Suwanborirux, K., and Chanvorachote, P. Renieramycin M sensitizes anoikis-resistant H460 lung cancer cells to anoikis. **Anticancer Research** 36 (2016): 1665-1671.
- [16] Uriz, M. J., and Maldonado, M. The genus *Acanthodendrilla* in the Mediterranean Sea with description of a new species. **Zoosystema** 22 (2000): 401-410.

- [17] Bergquist, P. R., and Cook, S. C. Family Dictyodendrillidae Bergquist, 1980. In J. N. A. Hooper, R. W. M. Soest, P. Willenz (eds), **Systema Porifera: A guide to the classification of sponges**, pp. 1072-1076. Boston, MA: Springer US, 2002.
- [18] Kozhemyako, V. B., Veremeichik, G. N., Shkryl, Y. N., Kovalchuk, S. N., Krasokhin, V. B., Rasskazov, V. A., Zhuravlev, Y. N., Bulgakov, V. P., and Kulchin, Y. N. Silicatein genes in spicule-forming and nonspicule-forming Pacific demosponges. **Marine biotechnology** 12 (2010): 403-409.
- [19] Tsukamoto, S., Matsunaga, S., Fusetani, N., and van Soest, R. W. Acanthosterol sulfates A-J: Ten new antifungal steroidal sulfates from a marine sponge *Acanthodendrilla* sp. **Journal of Natural Products** 61 (1998): 1374-1378.
- [20] Elkhyat, E., Edrada, R., Ebel, R., Wray, V., van Soest, R., Wiryowidagdo, S., Mohamed, M. H., Muller, W. E., and Proksch, P. New luffariellolide derivatives from the Indonesian sponge *Acanthodendrilla* sp. **Journal of Natural Products** 67 (2004): 1809-1817.
- [21] Ebada, S. S., Lin, W., and Proksch, P. Bioactive sesterterpenes and triterpenes from marine sponges: Occurrence and pharmacological significance. **Marine Drugs** 8 (2010): 313-346.
- [22] Tsukamoto, S., Tatsuno, M., van Soest, R. W., Yokosawa, H., and Ohta, T. New polyhydroxy sterols: Proteasome inhibitors from a marine sponge *Acanthodendrilla* sp. **Journal of Natural Products** 66 (2003): 1181-1185.
- [23] West, L. M., and Faulkner, D. J. Acanthosulfate, a sulfated hydroxyhydroquinone sesterterpenoid from the sponge *Acanthodendrilla* sp. **Journal of Natural Products** 71 (2008): 269-271.
- [24] Williams, D. E., Telliez, J. B., Liu, J., Tahir, A., van Soest, R., and Andersen, R. J. Meroterpenoid MAPKAP (MK2) inhibitors isolated from the Indonesian marine sponge *Acanthodendrilla* sp. **Journal of Natural Products** 67 (2004): 2127-2129.
- [25] Potts, B. C. M., Faulkner, D. J., De Carvalho, M. S., and Jacobs, R. S. Chemical mechanism of inactivation of bee venom phospholipase A2 by the marine natural products manoalide, luffariellolide, and scalaradiol. **Journal of the American Chemical Society** 114 (1992): 5093-5100.

- [26] Aoki, S., Yoshioka, Y., Miyamoto, Y., Higuchi, K., Setiawan, A., Murakami, N., Chen, Z.-S., Sumizawa, T., Akiyama, S.-i., and Kobayashi, M. Agosterol A, a novel polyhydroxylated sterol acetate reversing multidrug resistance from a marine sponge of *Spongia* sp. **Tetrahedron Letters** 39 (1998): 6303-6306.
- [27] Aoki, S., Setiawan, A., Yoshioka, Y., Higuchi, K., Fudetani, R., Chen, Z.-S., Sumizawa, T., Akiyama, S.-i., and Kobayashi, M. Reversal of multidrug resistance in human carcinoma cell line by agosterols, marine spongean sterols. **Tetrahedron** 55 (1999): 13965-13972.
- [28] Tallmadge, J. A., Butt, J. B., and Solomon, H. J. Minerals from sea salt. **Industrial & Engineering Chemistry** 56 (1964): 44-65.
- [29] Teeyapant, R., and Proksch, P. Biotransformation of brominated compounds in the marine sponge *Verongia aerophoba* — Evidence for an induced chemical defense? **Naturwissenschaften** 80 (1993): 369-370.
- [30] Ebel, R., Brenzinger, M., Kunze, A., Gross, H. J., and Proksch, P. Wound activation of protoxins in marine sponge *Aplysina aerophoba*. **Journal of Chemical Ecology** 23 (1997): 1451-1462.
- [31] Nuñez, C. V., Almeida, E. V. R., Granato, A. C., Marques, S. O., Santos, K. O., Pereira, F. R., Macedo, M. L., Ferreira, A. G., Hajdu, E., Pinheiro, U. S., Muricy, G., Peixinho, S., Freeman, C. J., Gleason, D. F., and Berlinck, R. G. S. Chemical variability within the marine sponge *Aplysina fulva*. **Biochemical Systematics and Ecology** 36 (2008): 283-296.
- [32] Nicholas, G. M., Newton, G. L., Fahey, R. C., and Bewley, C. A. Novel bromotyrosine alkaloids: Inhibitors of mycothiol S-conjugate amidase. **Organic Letters** 3 (2001): 1543-1545.
- [33] Park, Y., Liu, Y., Hong, J., Lee, C. O., Cho, H., Kim, D. K., Im, K. S., and Jung, J. H. New bromotyrosine derivatives from an association of two sponges, *Jaspis wondoensis* and *Poecillastra wondoensis*. **Journal of Natural Products** 66 (2003): 1495-1498.
- [34] Coleman, J. E., Van Soest, R., and Andersen, R. J. New geodiamolides from the sponge *Cymbastela* sp. collected in Papua New Guinea. **Journal of Natural Products** 62 (1999): 1137-1141.

- [35] Qi, S. H., Wang, Y. F., and Zhang, S. Steroids and alkaloids from the South China Sea sponge *Axinella* sp. **Journal of Asian Natural Products Research** 11 (2009): 1040-1044.
- [36] Rudi, A., Evan, T., Akinin, M., and Kashman, Y. Polycitone B and prepolycitrin A: Two novel alkaloids from the marine ascidian *Polycitor africanus*. **Journal of Natural Products** 63 (2000): 832-833.
- [37] Shao, N., Yao, G., and Chang, L. C. Bioactive constituents from the marine crinoid *Himerometra magnipinna*. **Journal of Natural Products** 70 (2007): 869-871.
- [38] Sharma, G. M., and Burkholder, P. R. Studies on the antimicrobial substances of sponges II. Structure and synthesis of a bromine-containing antibacterial compound from a marine sponge. **Tetrahedron Letters** 42 (1967): 4147-4150.
- [39] Peng, J., Li, J., and Hamann, M. T. The marine bromotyrosine derivatives. **The Alkaloids: Chemistry and Biology** 61 (2005): 59-262.
- [40] Tymiak, A. A., and Rinehart, K. L. Biosynthesis of dibromotyrosine-derived antimicrobial compounds by the marine sponge *Aplysina fistularis* (*Verongia aurea*). **Journal of the American Chemical Society** 103 (1981): 6763-6765.
- [41] Sharma, G. M., Vig, B., and Burkholder, P. R. Studies on the antimicrobial substances of sponges. IV. Structure of a bromine-containing compound from a marine sponge. **The Journal of Organic Chemistry** 35 (1970): 2823-2826.
- [42] Shestak, O. P., Novikov, V. L., Ivanova, E. P., and Gorshkova, N. M. Synthesis and antimicrobial activity of [3,5-dibromo(dichloro)-1-hydroxy-4-oxocyclohexa-2,5-dien-1-yl]acetic acids and their derivatives. **Pharmaceutical Chemistry Journal** 35 (2001): 366-369.
- [43] Koulman, A., Proksch, P., Ebel, R., Beekman, A. C., van Uden, W., Konings, A. W., Pedersen, J. A., Pras, N., and Woerdenbag, H. J. Cytotoxicity and mode of action of aeroplysinin-1 and a related dienone from the sponge *Aplysina aerophoba*. **Journal of Natural Products** 59 (1996): 591-594.
- [44] Gorshkov, B. A., Gorshkova, I. A., Makarieva, T. N., and Stonik, V. A. Inhibiting effect of cytotoxic bromine-containing compounds from sponges (Aplysinidae) on Na⁺-K⁺-ATPase activity. **Toxicon** 20 (1982): 1092-1094.

- [45] Moody, K., Thomson, R. H., Fattorusso, E., Minale, L., and Sodano, G. Aerothionin and homoaerothionin: Two tetrabromo spirocyclohexadienylisoxazoles from *Verongia* sponges. **Journal of the Chemical Society, Perkin Transactions 1** (1972): 18-24.
- [46] McMillan, J. A., Paul, I. C., Goo, Y. M., Rinehart Jr, K. L., Krueger, W. C., and Puschigoda, L. M. An X-ray study of aerothionin from *Aplysina fistularis* (pallas). **Tetrahedron Letters** 22 (1981): 39-42.
- [47] Benharref, A., Pais, M., and Debitus, C. Bromotyrosine alkaloids from the sponge *Pseudoceratina verrucosa*. **Journal of Natural Products** 59 (1996): 177-180.
- [48] Kernan, M. R., Cambie, R. C., and Bergquist, P. R. Chemistry of sponges, VII. 11, 19-Dideoxyfistularin 3 and 11-hydroxyaerothionin, bromotyrosine derivatives from *Pseudoceratina durissima*. **Journal of Natural Products** 53 (1990): 615-622.
- [49] Encarnación-Dimayuga, R., Ramírez, M. R., and Luna-Herrera, J. Aerothionin, a bromotyrosine derivative with antimycobacterial activity from the marine sponge *Aplysina gerardogreeni* (Demospongia). **Pharmaceutical Biology** 41 (2003): 384-387.
- [50] Kalaitzis, J. A., Leone Pde, A., Hooper, J. N., and Quinn, R. J. lanthesine E, a new bromotyrosine-derived metabolite from the Great Barrier Reef sponge *Pseudoceratina* sp. **Natural Product Research** 22 (2008): 1257-1263.
- [51] Shearman, J. **Bromotyrosine-derived natural products: Synthetic and biological studies**. Doctoral dissertation. University of Cambridge, 2011.
- [52] Liu, S., Fu, X., Schmitz, F. J., and Kelly-Borges, M. Psammaplysin F, a new bromotyrosine derivative from a sponge, *Aplysinella* sp. **J Nat Prod** 60 (1997): 614-615.
- [53] Yang, X., Davis, R. A., Buchanan, M. S., Duffy, S., Avery, V. M., Camp, D., and Quinn, R. J. Antimalarial bromotyrosine derivatives from the Australian marine sponge *Hyattella* sp. **Journal of Natural Products** 73 (2010): 985-987.
- [54] Copp, B. R., Ireland, C. M., and Barrows, L. R. Psammaplysin C: A new cytotoxic dibromotyrosine-derived metabolite from the marine sponge *Druinella*

- (=*Psammaplysilla*) *purpurea*. **Journal of Natural Products** 55 (1992): 822-823.
- [55] Tsukamoto, S., Kato, H., Hirota, H., and Fusetani, N. Ceratinamides A and B: New antifouling dibromotyrosine derivatives from the marine sponge *Pseudoceratina purpurea*. **Tetrahedron** 52 (1996): 8181-8186.
- [56] Xu, M., Andrews, K. T., Birrell, G. W., Tran, T. L., Camp, D., Davis, R. A., and Quinn, R. J. Psammaplysin H, a new antimalarial bromotyrosine alkaloid from a marine sponge of the genus *Pseudoceratina*. **Bioorganic & Medicinal Chemistry Letters** 21 (2011): 846-848.
- [57] Wright, A. D., Schupp, P. J., Schror, J. P., Engemann, A., Rohde, S., Kelman, D., de Voogd, N., Carroll, A., and Motti, C. A. Twilight zone sponges from Guam yield theonellin isocyanate and psammaplysin I and J. **Journal of Natural Products** 75 (2012): 502-506.
- [58] Arabshahi, L., and Schmitz, F. J. Brominated tyrosine metabolites from an unidentified sponge. **The Journal of Organic Chemistry** 52 (1987): 3584-3586.
- [59] Kobayashi, J. i., Tsuda, M., Agemi, K., Shigemori, H., Ishibashi, M., Sasaki, T., and Mikami, Y. Puralidins B and C, new bromotyrosine alkaloids from the Okinawan marine sponge *Psammaplysilla purea*. **Tetrahedron** 47 (1991): 6617-6622.
- [60] Olatunji, O. J., Ogundajo, A. L., Oladosu, I. A., Changwichit, K., Ingkaninan, K., Yuenyongsawad, S., and Plubrukarn, A. Non-competitive inhibition of acetylcholinesterase by bromotyrosine alkaloids. **Natural Product Communications** 9 (2014): 1559-1561.
- [61] Mierzwa, R., King, A., Conover, M. A., Tozzi, S., Puar, M. S., Patel, M., Coval, S. J., and Pomponi, S. A. Verongamine, a novel bromotyrosine-derived histamine H₃-antagonist from the marine sponge *Verongula gigantea*. **Journal of Natural Products** 57 (1994): 175-177.
- [62] Kim, D., Lee, I. S., Jung, J. H., Lee, C. O., and Choi, S. U. Psammaplin A, a natural phenolic compound, has inhibitory effect on human topoisomerase II and is cytotoxic to cancer cells. **Anticancer Research** 19 (1999): 4085-4090.

- [63] Pina, I. C., Gautschi, J. T., Wang, G. Y., Sanders, M. L., Schmitz, F. J., France, D., Cornell-Kennon, S., Sambucetti, L. C., Remiszewski, S. W., Perez, L. B., Bair, K. W., and Crews, P. Psammaplins from the sponge *Pseudoceratina purpurea*: inhibition of both histone deacetylase and DNA methyltransferase. **The Journal of Organic Chemistry** 68 (2003): 3866-3873.
- [64] Nicholas, G. M., Eckman, L. L., Ray, S., Hughes, R. O., Pfefferkorn, J. A., Barluenga, S., Nicolaou, K. C., and Bewley, C. A. Bromotyrosine-derived natural and synthetic products as inhibitors of mycothiol-S-conjugate amidase. **Bioorganic & Medicinal Chemistry Letters** 12 (2002): 2487-2490.
- [65] Miao, S., Andersen, R. J., and Allen, T. M. Cytotoxic metabolites from the sponge *lanthella basta* collected in Papua New Guinea. **Journal of Natural Products** 53 (1990): 1441-1446.
- [66] Gulavita, N. K., Pomponi, S. A., Wright, A. E., Garay, M., and Sills, M. A. Aplysillin A, a thrombin receptor antagonist from the marine sponge *Aplysina fistularis* fulva. **Journal of Natural Products** 58 (1995): 954-957.
- [67] Hirano, K., Kubota, T., Tsuda, M., Watanabe, K., Fromont, J., and Kobayashi, J. i. Ma'edamines A and B, cytotoxic bromotyrosine alkaloids with a unique 2(1H)pyrazinone ring from sponge *Suberea* sp. **Tetrahedron** 56 (2000): 8107-8110.
- [68] Lindquist, N., and Fenical, W. Polyandrocarpamides A-D, novel metabolites from the marine ascidian polyandrocarpa sp. **Tetrahedron Letters** 31 (1990): 2521-2524.
- [69] Chan, W. R., Tinto, W. F., Manchand, P. S., and Todaro, L. J. Stereostructures of geodiamolides A and B, novel cyclodepsipeptides from the marine sponge *Geodia* sp. **The Journal of Organic Chemistry** 52 (1987): 3091-3093.
- [70] de Silva, E. D., Andersen, R. J., and Allen, T. M. Geodiamolides C to F, new cytotoxic cyclodepsipeptides from the marine sponge *Pseudaxinyssa* sp. **Tetrahedron Letters** 31 (1990): 489-492.
- [71] Coleman, J. E., Dilip de Silva, E., Kong, F., Andersen, R. J., and Allen, T. M. Cytotoxic peptides from the marine sponge *Cymbastela* sp. **Tetrahedron** 51 (1995): 10653-10662.

- [72] Tinto, W. F., Lough, A. J., McLean, S., Reynolds, W. F., Yu, M., and Chan, W. R. Geodiamolides H and I, further cyclodepsipeptides from the marine sponge *Geodia* sp. **Tetrahedron** 54 (1998): 4451-4458.
- [73] Acosta, A. L., and Rodríguez, A. D. 11-Oxoerothionin: A cytotoxic antitumor bromotyrosine-derived alkaloid from the Caribbean marine sponge *Aplysina lacunosa*. **Journal of Natural Products** 55 (1992): 1007-1012.
- [74] Teeyapant, R., Woerdenbag, H. J., Kreis, P., Hacker, J., Wray, V., Witte, L., and Proksch, P. Antibiotic and cytotoxic activity of brominated compounds from the marine sponge *Verongia aerophoba*. **Zeitschrift für Naturforschung C** 48 (1993): 939-945.
- [75] Ankudey, F. J., Kiprof, P., Stromquist, E. R., and Chang, L. C. New bioactive bromotyrosine-derived alkaloid from a marine sponge *Aplysinella* sp. **Planta Medica** 74 (2008): 555-559.
- [76] Ross, S. A., Weete, J. D., Schinazi, R. F., Wirtz, S. S., Tharnish, P., Scheuer, P. J., and Hamann, M. T. Mololipids, a new series of anti-HIV bromotyramine-derived compounds from a sponge of the order Verongida. **Journal of Natural Products** 63 (2000): 501-503.
- [77] Mani, L., Jullian, V., Mourkazel, B., Valentin, A., Dubois, J., Cresteil, T., Folcher, E., Hooper, J. N., Erpenbeck, D., Aalbersberg, W., and Debitus, C. New antiplasmodial bromotyrosine derivatives from *Suberea ianthelliformis* Lendenfeld, 1888. **Chemistry & Biodiversity** 9 (2012): 1436-1451.
- [78] Tsukamoto, S., Kato, H., Hirota, H., and Fusetani, N. Ceratinamine: An unprecedented antifouling cyanoforamide from the marine sponge *Pseudoceratina purpurea*. **The Journal of Organic Chemistry** 61 (1996): 2936-2937.
- [79] Tabudravu, J. N., and Jaspars, M. Puralidin S and purpuramine J, bromotyrosine alkaloids from the Fijian marine sponge *Druinella* sp. **Journal of Natural Products** 65 (2002): 1798-1801.
- [80] Tran, T. D., Pham, N. B., Fechner, G., Hooper, J. N., and Quinn, R. J. Bromotyrosine alkaloids from the Australian marine sponge *Pseudoceratina verrucosa*. **Journal of Natural Products** 76 (2013): 516-523.

- [81] Shaala, L. A., Youssef, D. T., Badr, J. M., Sulaiman, M., and Khedr, A. Bioactive secondary metabolites from the Red Sea marine Verongid sponge *Suberea* species. **Marine Drugs** 13 (2015): 1621-1631.
- [82] de Medeiros, A. I., Gandolfi, R. C., Secatto, A., Falcucci, R. M., Faccioli, L. H., Hajdu, E., Peixinho, S., and Berlinck, R. G. 11-Oxoerothionin isolated from the marine sponge *Aplysina fistularis* shows anti-inflammatory activity in LPS-stimulated macrophages. **Immunopharmacol Immunotoxicol** 34 (2012): 919-924.
- [83] Carr, G., Berrue, F., Klaiklay, S., Pelletier, I., Landry, M., and Kerr, R. G. Natural products with protein tyrosine phosphatase inhibitory activity. **Methods** 65 (2014): 229-238.
- [84] Prince, M., Wimo, A., Guerchet, M., Ali, G., Wu, Y., and Prina, M. World Alzheimer report 2015: The global impact of dementia. London: Alzheimer's Disease International, 2015.
- [85] Silva, T., Reis, J., Teixeira, J., and Borges, F. Alzheimer's disease, enzyme targets and drug discovery struggles: From natural products to drug prototypes. **Ageing Research Reviews** 15 (2014): 116-145.
- [86] Sims, N. R., Bowen, D. M., Allen, S. J., Smith, C. C., Neary, D., Thomas, D. J., and Davison, A. N. Presynaptic cholinergic dysfunction in patients with dementia. **Journal of Neurochemistry** 40 (1983): 503-509.
- [87] Francis, P. T., Palmer, A. M., Snape, M., and Wilcock, G. K. The cholinergic hypothesis of Alzheimer's disease: A review of progress. **Journal of Neurology, Neurosurgery & Psychiatry** 66 (1999): 137-147.
- [88] Houghton, P. J., Ren, Y., and Howes, M. J. Acetylcholinesterase inhibitors from plants and fungi. **Natural Product Reports** 23 (2006): 181-199.
- [89] Giacobini, E. Cholinesterase inhibitors: New roles and therapeutic alternatives. **Pharmacological Research** 50 (2004): 433-440.
- [90] Bourne, Y., Taylor, P., Radić, Z., and Marchot, P. Structural insights into ligand interactions at the acetylcholinesterase peripheral anionic site. **The EMBO Journal** 22 (2003): 1-12.

- [91] Wiesner, J., Kriz Z Fau - Kuca, K., Kuca K Fau - Jun, D., Jun D Fau - Koca, J., and Koca, J. Acetylcholinesterases--the structural similarities and differences. **Journal of Enzyme Inhibition and Medicinal Chemistry** 22 (2007):
- [92] Dvir, H., Silman, I., Harel, M., Rosenberry, T. L., and Sussman, J. L. Acetylcholinesterase: from 3D structure to function. **Chemico-Biological Interactions** 187 (2010): 10-22.
- [93] Ellman, G. L., Courtney, K. D., Andres jr, V., and Featherstone, R. M. A new and rapid colorimetric determination of acetylcholinesterase activity. **Biochemical Pharmacology** 7 (1961): 88-95.
- [94] Ingkaninan, K., Temkitthawon, P., Chuenchom, K., Yuyaem, T., and Thongnoi, W. Screening for acetylcholinesterase inhibitory activity in plants used in Thai traditional rejuvenating and neurotonic remedies. **Journal of Ethnopharmacology** 89 (2003): 261-264.
- [95] Williams, P., Sorribas, A., and Howes, M. J. Natural products as a source of Alzheimer's drug leads. **Natural Product Reports** 28 (2011): 48-77.
- [96] Berkov, S., Georgieva, L., Kondakova, V., Atanassov, A., Viladomat, F., Bastida, J., and Codina, C. Plant sources of galanthamine: Phytochemical and biotechnological aspects. **Biotechnology & Biotechnological Equipment** 23 (2014): 1170-1176.
- [97] Langjae, R., Bussarawit, S., Yuenyongsawad, S., Ingkaninan, K., and Plubrukarn, A. Acetylcholinesterase-inhibiting steroidal alkaloid from the sponge *Corticium* sp. **Steroids** 72 (2007): 682-685.
- [98] Nukoolkarn, V. S., Saen-oon, S., Rungrotmongkol, T., Hannongbua, S., Ingkaninan, K., and Suwanborirux, K. Petrosamine, a potent anticholinesterase pyridoacridine alkaloid from a Thai marine sponge *Petrosia* n. sp. **Bioorganic & Medicinal Chemistry** 16 (2008): 6560-6567.
- [99] Yoon, N. Y., Chung, H. Y., Kim, H. R., and Choi, J. S. Acetyl- and butyrylcholinesterase inhibitory activities of sterols and phlorotannins from *Ecklonia stolonifera*. **Fisheries Science** 74 (2008): 200-207.
- [100] Sangnoi, Y., Sakulkeo, O., Yuenyongsawad, S., Kanjana-opas, A., Ingkaninan, K., Plubrukarn, A., and Suwanborirux, K. Acetylcholinesterase-inhibiting activity of

- pyrrole derivatives from a novel marine gliding bacterium, *Rapidithrix thailandica*. **Marine Drugs** 6 (2008): 578-586.
- [101] Desqueyroux-Faúndez, R., and Valentine, C. Family Petrosiidae Van Soest, 1980. In J. N. A. Hooper, R. W. M. Soest, P. Willenz (eds), **Systema Porifera: A Guide to the Classification of Sponges**, pp. 906-917. Boston, MA: Springer US, 2002.
- [102] Suwanborirux, K., Amnuoypol, S., Plubrukarn, A., Pummangura, S., Kubo, A., Tanaka, C., and Saito, N. Chemistry of renieramycins. Part 3. Isolation and structure of stabilized renieramycin type derivatives possessing antitumor activity from Thai sponge *Xestospongia* species, pretreated with potassium cyanide. **Journal of Natural Products** 66 (2003): 1441-1446.
- [103] Kluepfel, D., Baker, H. A., Piattoni, G., Sehgal, S. N., Sidorowicz, A., Singh, K., and Vezina, C. Naphthyridinomycin, a new broad-spectrum antibiotic. **The Journal of antibiotics** 28 (1975): 497-502.
- [104] Scott, J. D., and Williams, R. M. Chemistry and biology of the tetrahydroisoquinoline antitumor antibiotics. **Chemical Reviews** 102 (2002): 1669-1730.
- [105] Amnuoypol, S. **Cytotoxic bistetrahydroisoquinoline alkaloids from the Thai marine sponge, *Xestospongia* sp.** Doctoral dissertation. Pharmaceutical Chemistry and Natural Products, Faculty of Pharmaceutical Sciences, Chulalongkorn University, 2004.
- [106] Arai, T., Takahashi, K., and Kubo, A. New antibiotics saframycins A, B, C, D and E. **The Journal of antibiotics** 30 (1977): 1015-1018.
- [107] Mikami, Y., Takahashi, K., Yazawa, K., Arai, T., Namikoshi, M., Iwasaki, S., and Okuda, S. Biosynthetic studies on saframycin A, a quinone antitumor antibiotic produced by *Streptomyces lavendulae*. **The Journal of Biological Chemistry** 260 (1985): 344-348.
- [108] Arai, T., Yazawa, K., Takahashi, K., Maeda, A., and Mikami, Y. Directed biosynthesis of new saframycin derivatives with resting cells of *Streptomyces lavendulae*. **Antimicrobial Agents and Chemotherapy** 28 (1985): 5-11.

- [109] Irschik, H., Trowitzsch-Kienast, W., Gerth, K., Hofle, G., and Reichenbach, H. Saframycin Mx1, a new natural saframycin isolated from a myxobacterium. **The Journal of antibiotics** 41 (1988): 993-998.
- [110] Pospiech, A., Bietenhader, J., and Schupp, T. Two multifunctional peptide synthetases and an O-methyltransferase are involved in the biosynthesis of the DNA-binding antibiotic and antitumour agent saframycin Mx1 from *Myxococcus xanthus*. **Microbiology** 142 (Pt 4) (1996): 741-746.
- [111] Cheun-arom, T. **Renieramycins: Nonribosomal peptide synthetase gene and cytotoxicity against lung cancer cells**. Doctoral dissertation. Pharmacognosy, Department of Pharmacognosy and Pharmaceutical Botany, Faculty of Pharmaceutical Sciences, Chulalongkorn University, 2012.
- [112] Rinehart, K. L., Holt, T. G., Fregeau, N. L., Stroh, J. G., Keifer, P. A., Sun, F., Li, L. H., and Martin, D. G. Ecteinascidins 729, 743, 745, 759A, 759B, and 770: potent antitumor agents from the Caribbean tunicate *Ecteinascidia turbinata*. **The Journal of Organic Chemistry** 55 (1990): 4512-4515.
- [113] European Medicines Agency. Assessment report for Yondelis. London, UK: 2009.
- [114] U.S. Food and Drug Administration. FDA approves new therapy for certain types of advanced soft tissue sarcoma. Silver Spring, MD, USA: 2015.
- [115] D'Incalci, M., and Galmarini, C. M. A review of trabectedin (ET-743): a unique mechanism of action. **Molecular Cancer Therapeutics** 9 (2010): 2157-2163.
- [116] Le, V. H., Inai, M., Williams, R. M., and Kan, T. Ecteinascidins. A review of the chemistry, biology and clinical utility of potent tetrahydroisoquinoline antitumor antibiotics. **Natural Product Reports** 32 (2015): 328-347.
- [117] Romano, M., Frapolli, R., Zangarini, M., Bello, E., Porcu, L., Galmarini, C. M., Garcia-Fernandez, L. F., Cuevas, C., Allavena, P., Erba, E., and D'Incalci, M. Comparison of *in vitro* and *in vivo* biological effects of trabectedin, lurbinectedin (PM01183) and Zalypsis (PM00104). **International Journal of Cancer** 133 (2013): 2024-2033.
- [118] Frincke, J. M., and Faulkner, D. J. Antimicrobial metabolites of the sponge *Reniera* sp. **Journal of the American Chemical Society** 104 (1982): 265-269.

- [119] He, H. Y., and Faulkner, D. J. Renieramycins E and F from the sponge *Reniera* sp.: Reassignment of the stereochemistry of the renieramycins. **The Journal of Organic Chemistry** 54 (1989): 5822-5824.
- [120] Davidson, B. S. Renieramycin G, a new alkaloid from the sponge *Xestospongia caycedoi*. **Tetrahedron Letters** 33 (1992): 3721-3724.
- [121] Amnuoypol, S., Suwanborirux, K., Pummangura, S., Kubo, A., Tanaka, C., and Saito, N. Chemistry of renieramycins. Part 5. Structure elucidation of renieramycin-type derivatives O, Q, R, and S from Thai marine sponge *Xestospongia* species pretreated with potassium cyanide. **Journal of Natural Products** 67 (2004): 1023-1028.
- [122] Daikuhara, N., Tada, Y., Yamaki, S., Charupant, K., Amnuoypol, S., Suwanborirux, K., and Saito, N. Chemistry of renieramycins. Part 7: Renieramycins T and U, novel renieramycin–ecteinascidin hybrid marine natural products from Thai sponge *Xestospongia* sp. **Tetrahedron Letters** 50 (2009): 4276-4278.
- [123] Saito, N., Yoshino, M., Charupant, K., and Suwanborirux, K. Chemistry of renieramycins. Part 10: Structure of renieramycin V, a novel renieramycin marine natural product having a sterol ether at C-14 position. **Heterocycles** 84 (2012): 309-314.
- [124] Tatsukawa, M., Punzalan, L. L. C., Magpantay, H. D. S., Villaseñor, I. M., Concepcion, G. P., Suwanborirux, K., Yokoya, M., and Saito, N. Chemistry of renieramycins. Part 13: Isolation and structure of stabilized renieramycin type derivatives, renieramycins W–Y, from Philippine blue sponge *Xestospongia* sp., pretreated with potassium cyanide. **Tetrahedron** 68 (2012): 7422-7428.
- [125] Parameswaran, P. S., Naik, C. G., Kamat, S. Y., and Pramanik, B. N. Renieramycins H and I, two novel alkaloids from the sponge *Haliclona cribricutis* Dendy. **Indian Journal of Chemistry** 37B (1998): 1258-1263.
- [126] Pettit, G. R., Knight, J. C., Collins, J. C., Herald, D. L., Pettit, R. K., Boyd, M. R., and Young, V. G. Antineoplastic agents 430. Isolation and structure of cribrostatis 3, 4, and 5 from the Republic of Maldives *Cribochalina* species. **Journal of Natural Products** 63 (2000): 793-798.

- [127] Oku, N., Matsunaga, S., van Soest, R. W. M., and Fusetani, N. Renieramycin J, a highly cytotoxic tetrahydroisoquinoline alkaloid, from a marine sponge *Neopetrosia* sp. **Journal of Natural Products** 66 (2003): 1136-1139.
- [128] Fontana, A., Cavaliere, P., Wahidulla, S., Naik, C. G., and Cimino, G. A new antitumor isoquinoline alkaloid from the marine nudibranch *Jorunna funebris*. **Tetrahedron** 56 (2000): 7305-7308.
- [129] Charupant, K., Suwanborirux, K., Amnuoypol, S., Saito, E., Kubo, A., and Saito, N. Jorunnamycins A-C, new stabilized renieramycin-type bistetrahydroisoquinolines isolated from the Thai nudibranch *Jorunna funebris*. **Chemical and Pharmaceutical Bulletin** 55 (2007): 81-86.
- [130] He, W. F., Li, Y., Feng, M. T., Gavagnin, M., Mollo, E., Mao, S. C., and Guo, Y. W. New isoquinolinequinone alkaloids from the South China Sea nudibranch *Jorunna funebris* and its possible sponge-prey *Xestospongia* sp. **Fitoterapia** 96 (2014): 109-114.
- [131] Huang, R. Y., Chen, W. T., Kurtan, T., Mandi, A., Ding, J., Li, J., Li, X. W., and Guo, Y. W. Bioactive isoquinolinequinone alkaloids from the South China Sea nudibranch *Jorunna funebris* and its sponge-prey *Xestospongia* sp. **Future Medicinal Chemistry** 8 (2016): 17-27.
- [132] Saito, N., Tanaka, C., Koizumi, Y., Suwanborirux, K., Amnuoypol, S., Pummangura, S., and Kubo, A. Chemistry of renieramycins. Part 6: Transformation of renieramycin M into jorumycin and renieramycin J including oxidative degradation products, mimosamycin, renierone, and renierol acetate. **Tetrahedron** 60 (2004): 3873-3881.
- [133] Charupant, K., Daikuhara, N., Saito, E., Amnuoypol, S., Suwanborirux, K., Owa, T., and Saito, N. Chemistry of renieramycins. Part 8: Synthesis and cytotoxicity evaluation of renieramycin M-jorunnamycin A analogues. **Bioorganic & Medicinal Chemistry** 17 (2009): 4548-4558.
- [134] Liu, W., Liao, X., Dong, W., Yan, Z., Wang, N., and Liu, Z. Total synthesis and cytotoxicity of (-)-jorumycin and its analogues. **Tetrahedron** 68 (2012): 2759-2764.

- [135] Liu, W., Dong, W., Liao, X., Yan, Z., Guan, B., Wang, N., and Liu, Z. Synthesis and cytotoxicity of (-)-renieramycin G analogs. **Bioorganic & Medicinal Chemistry Letters** 21 (2011): 1419-1421.
- [136] Halim, H., Chunhacha, P., Suwanborirux, K., and Chanvorachote, P. Anticancer and anti-metastatic activities of renieramycin M, a marine tetrahydroisoquinoline alkaloid, in human non-small cell lung cancer cells. **Anticancer Research** 31 (2011): 193-201.
- [137] International Agency for Research on Cancer. World Cancer Factsheet. London: Cancer Research UK, 2014.
- [138] Esposito, L., Conti, D., Ailavajhala, R., Khalil, N., and Giordano, A. Lung cancer: Are we up to the challenge? **Current Genomics** 11 (2010): 513-518.
- [139] Nichols, L., Saunders, R., and Knollmann, F. D. Causes of death of patients with lung cancer. **Archives of pathology & laboratory medicine** 136 (2012): 1552-1557.
- [140] Ohe, Y., Ohashi, Y., Kubota, K., Tamura, T., Nakagawa, K., Negoro, S., Nishiwaki, Y., Saijo, N., Ariyoshi, Y., and Fukuoka, M. Randomized phase III study of cisplatin plus irinotecan versus carboplatin plus paclitaxel, cisplatin plus gemcitabine, and cisplatin plus vinorelbine for advanced non-small-cell lung cancer: Four-Arm Cooperative Study in Japan. **Annals of Oncology** 18 (2007): 317-323.
- [141] Molina, J. R., Yang, P., Cassivi, S. D., Schild, S. E., and Adjei, A. A. Non-small cell lung cancer: Epidemiology, risk factors, treatment, and survivorship. **Mayo Clinic Proceedings** 83 (2008): 584-594.
- [142] Hirsh, V. Systemic therapies in metastatic non-small-cell lung cancer with emphasis on targeted therapies: The rational approach. **Current Oncology** 17 (2010): 13-23.
- [143] Mehlen, P., and Puisieux, A. Metastasis: A question of life or death. **Nature Reviews Cancer** 6 (2006): 449-458.
- [144] Simpson, C. D., Anyiwe, K., and Schimmer, A. D. Anoikis resistance and tumor metastasis. **Cancer Letters** 272 (2008): 177-185.

- [145] Kim, Y. N., Koo, K. H., Sung, J. Y., Yun, U. J., and Kim, H. Anoikis resistance: An essential prerequisite for tumor metastasis. **International Journal of Cell Biology** 2012 (2012): 306879.
- [146] Krebs, M. G., Sloane, R., Priest, L., Lancashire, L., Hou, J. M., Greystoke, A., Ward, T. H., Ferraldeschi, R., Hughes, A., Clack, G., Ranson, M., Dive, C., and Blackhall, F. H. Evaluation and prognostic significance of circulating tumor cells in patients with non-small-cell lung cancer. **Journal of Clinical Oncology** 29 (2011): 1556-1563.
- [147] Frisch, S. M., and Francis, H. Disruption of epithelial cell-matrix interactions induces apoptosis. **The Journal of Cell Biology** 124 (1994): 619-626.
- [148] Taddei, M. L., Giannoni, E., Fiaschi, T., and Chiarugi, P. Anoikis: An emerging hallmark in health and diseases. **The Journal of Pathology** 226 (2012): 380-393.
- [149] Paoli, P., Giannoni, E., and Chiarugi, P. Anoikis molecular pathways and its role in cancer progression. **Biochimica et Biophysica Acta** 1833 (2013): 3481-3498.
- [150] Powan, P., and Chanvorachote, P. Nitric oxide mediates cell aggregation and mesenchymal to epithelial transition in anoikis-resistant lung cancer cells. **Molecular and Cellular Biochemistry** 393 (2014): 237-245.
- [151] Woods, N. T., Yamaguchi, H., Lee, F. Y., Bhalla, K. N., and Wang, H. G. Anoikis, initiated by MCL1 degradation and BIM induction, is deregulated during oncogenesis. **Cancer Research** 67 (2007): 10744-10752.
- [152] Howard, E. W., Leung, S. C., Yuen, H. F., Chua, C. W., Lee, D. T., Chan, K. W., Wang, X., and Wong, Y. C. Decreased adhesiveness, resistance to anoikis and suppression of GRP94 are integral to the survival of circulating tumor cells in prostate cancer. **Clinical and Experimental Metastasis** 25 (2008): 497-508.
- [153] Boisvert-Adamo, K., Longmate, W., Abel, E. V., and Aplin, A. E. MCL1 is required for melanoma cell resistance to anoikis. **Molecular Cancer Research** 7 (2009): 549-556.
- [154] Smerage, J. B., Budd, G. T., Doyle, G. V., Brown, M., Paoletti, C., Muniz, M., Miller, M. C., Repollet, M. I., Chianese, D. A., Connelly, M. C., Terstappen, L. W., and

- Hayes, D. F. Monitoring apoptosis and BCL2 on circulating tumor cells in patients with metastatic breast cancer. **Molecular Oncology** 7 (2013): 680-692.
- [155] Tanaka, F., Yoneda, K., Kondo, N., Hashimoto, M., Takuwa, T., Matsumoto, S., Okumura, Y., Rahman, S., Tsubota, N., Tsujimura, T., Kuribayashi, K., Fukuoka, K., Nakano, T., and Hasegawa, S. Circulating tumor cell as a diagnostic marker in primary lung cancer. **Clinical Cancer Research** 15 (2009): 6980-6986.
- [156] Negin, B. P., and Cohen, S. J. Circulating tumor cells in colorectal cancer: past, present, and future challenges. **Current Treatment Options in Oncology** 11 (2010): 1-13.
- [157] Danila, D. C., Fleisher, M., and Scher, H. I. Circulating tumor cells as biomarkers in prostate cancer. **Clinical Cancer Research** 17 (2011): 3903-3912.
- [158] Swaby, R. F., and Cristofanilli, M. Circulating tumor cells in breast cancer: A tool whose time has come of age. **BMC Medicine** 9 (2011): 1-7.
- [159] Deng, S., Wu, Q., Zhao, Y., Zheng, X., Wu, N., Pang, J., Li, X., Bi, C., Liu, X., Yang, L., Liu, L., Su, W., Wei, Y., and Gong, C. Biodegradable polymeric micelle-encapsulated doxorubicin suppresses tumor metastasis by killing circulating tumor cells. **Nanoscale** 7 (2015): 5270-5280.
- [160] Kim, J. B., Yu, J. H., Ko, E., Lee, K. W., Song, A. K., Park, S. Y., Shin, I., Han, W., and Noh, D. Y. The alkaloid Berberine inhibits the growth of Anoikis-resistant MCF-7 and MDA-MB-231 breast cancer cell lines by inducing cell cycle arrest. **Phytomedicine** 17 (2010): 436-440.
- [161] Salama, R., Tang, J., Gadgeel, S. M., Ahmad, A., and Sarkar, F. H. Lung cancer stem cells: Current progress and future perspectives. **Journal of Stem Cell Research & Therapy** S7 (2012): 007.
- [162] Sampieri, K., and Fodde, R. Cancer stem cells and metastasis. **Seminars in Cancer Biology** 22 (2012): 187-193.
- [163] Vinogradov, S., and Wei, X. Cancer stem cells and drug resistance: the potential of nanomedicine. **Nanomedicine** 7 (2012): 597-615.

- [164] Bonnet, D., and Dick, J. E. Human acute myeloid leukemia is organized as a hierarchy that originates from a primitive hematopoietic cell. **Nature Medicine** 3 (1997): 730-737.
- [165] Al-Hajj, M., Wicha, M. S., Benito-Hernandez, A., Morrison, S. J., and Clarke, M. F. Prospective identification of tumorigenic breast cancer cells. **Proceedings of the National Academy of Sciences of the United States of America** 100 (2003): 3983-3988.
- [166] Singh, S. K., Clarke, I. D., Terasaki, M., Bonn, V. E., Hawkins, C., Squire, J., and Dirks, P. B. Identification of a cancer stem cell in human brain tumors. **Cancer Research** 63 (2003): 5821-5828.
- [167] Patrawala, L., Calhoun, T., Schneider-Broussard, R., Li, H., Bhatia, B., Tang, S., Reilly, J. G., Chandra, D., Zhou, J., Claypool, K., Coghlan, L., and Tang, D. G. Highly purified CD44⁺ prostate cancer cells from xenograft human tumors are enriched in tumorigenic and metastatic progenitor cells. **Oncogene** 25 (2006): 1696-1708.
- [168] Hermann, P. C., Huber, S. L., Herrler, T., Aicher, A., Ellwart, J. W., Guba, M., Bruns, C. J., and Heeschen, C. Distinct populations of cancer stem cells determine tumor growth and metastatic activity in human pancreatic cancer. **Cell Stem Cell** 1 (2007): 313-323.
- [169] Ricci-Vitiani, L., Lombardi, D. G., Pilozzi, E., Biffoni, M., Todaro, M., Peschle, C., and De Maria, R. Identification and expansion of human colon-cancer-initiating cells. **Nature** 445 (2007): 111-115.
- [170] Eramo, A., Lotti, F., Sette, G., Pilozzi, E., Biffoni, M., Di Virgilio, A., Conticello, C., Ruco, L., Peschle, C., and De Maria, R. Identification and expansion of the tumorigenic lung cancer stem cell population. **Cell Death & Differentiation** 15 (2008): 504-514.
- [171] Bertolini, G., Roz, L., Perego, P., Tortoreto, M., Fontanella, E., Gatti, L., Pratesi, G., Fabbri, A., Andriani, F., Tinelli, S., Roz, E., Caserini, R., Lo Vullo, S., Camerini, T., Mariani, L., Delia, D., Calabro, E., Pastorino, U., and Sozzi, G. Highly tumorigenic lung cancer CD133⁺ cells display stem-like features and are

- spared by cisplatin treatment. **Proceedings of the National Academy of Sciences of the United States of America** 106 (2009): 16281-16286.
- [172] Leung, E. L., Fiskus, R. R., Tung, J. W., Tin, V. P., Cheng, L. C., Sihoe, A. D., Fink, L. M., Ma, Y., and Wong, M. P. Non-small cell lung cancer cells expressing CD44 are enriched for stem cell-like properties. **PLoS One** 5 (2010): e14062.
- [173] Sullivan, J. P., Spinola, M., Dodge, M., Raso, M. G., Behrens, C., Gao, B., Schuster, K., Shao, C., Larsen, J. E., Sullivan, L. A., Honorio, S., Xie, Y., Scaglioni, P. P., DiMaio, J. M., Gazdar, A. F., Shay, J. W., Wistuba, II, and Minna, J. D. Aldehyde dehydrogenase activity selects for lung adenocarcinoma stem cells dependent on Notch signaling. **Cancer Research** 70 (2010): 9937-9948.
- [174] Liang, D., and Shi, Y. Aldehyde dehydrogenase-1 is a specific marker for stem cells in human lung adenocarcinoma. **Medical Oncology** 29 (2012): 633-639.
- [175] Qu, H., Li, R., Liu, Z., Zhang, J., and Luo, R. Prognostic value of cancer stem cell marker CD133 expression in non-small cell lung cancer: A systematic review. **International Journal of Clinical and Experimental Pathology** 6 (2013): 2644-2650.
- [176] Gupta, P. B., Onder, T. T., Jiang, G., Tao, K., Kuperwasser, C., Weinberg, R. A., and Lander, E. S. Identification of selective inhibitors of cancer stem cells by high-throughput screening. **Cell** 138 (2009): 645-659.
- [177] Kakarala, M., Brenner, D. E., Korkaya, H., Cheng, C., Tazi, K., Ginestier, C., Liu, S., Dontu, G., and Wicha, M. S. Targeting breast stem cells with the cancer preventive compounds curcumin and piperine. **Breast Cancer Research and Treatment** 122 (2010): 777-785.
- [178] Li, Y., Zhang, T., Korkaya, H., Liu, S., Lee, H. F., Newman, B., Yu, Y., Clouthier, S. G., Schwartz, S. J., Wicha, M. S., and Sun, D. Sulforaphane, a dietary component of broccoli/broccoli sprouts, inhibits breast cancer stem cells. **Clinical Cancer Research** 16 (2010): 2580-2590.
- [179] Ray, A., Vasudevan, S., and Sengupta, S. 6-Shogaol inhibits breast cancer cells and stem cell-like spheroids by modulation of Notch signaling pathway and induction of autophagic cell death. **PLoS One** 10 (2015): e0137614.

- [180] Bhummaphan, N., and Chanvorachote, P. Gigantol suppresses cancer stem cell-like phenotypes in lung cancer cells. **Evidence-Based Complementary and Alternative Medicine** 2015 (2015): 836564.





APPENDICES

จุฬาลงกรณ์มหาวิทยาลัย
CHULALONGKORN UNIVERSITY

APPENDIX A

SPONGE MATERIALS, EXTRACTION, AND ISOLATION

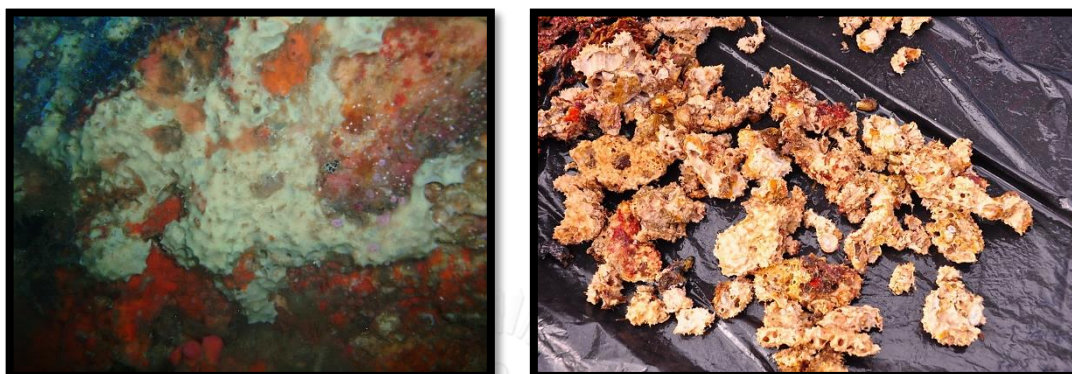


Figure A1 Underwater (left) and surface (right) photographs of the sponge *Acanthodendrilla* sp. collected from Ha Island, Krabi, Thailand (photographed by Dr. Khanit Suwanborirux)

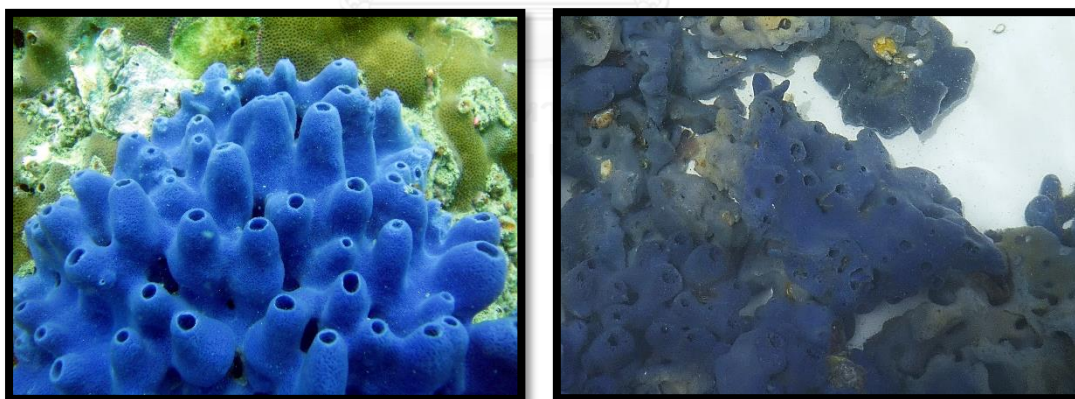


Figure A2 Underwater (left) and surface (right) photographs of the blue sponge *Xestospongia* sp. collected from Si Chang Island, Chonburi, Thailand (photographed by Dr. Khanit Suwanborirux)

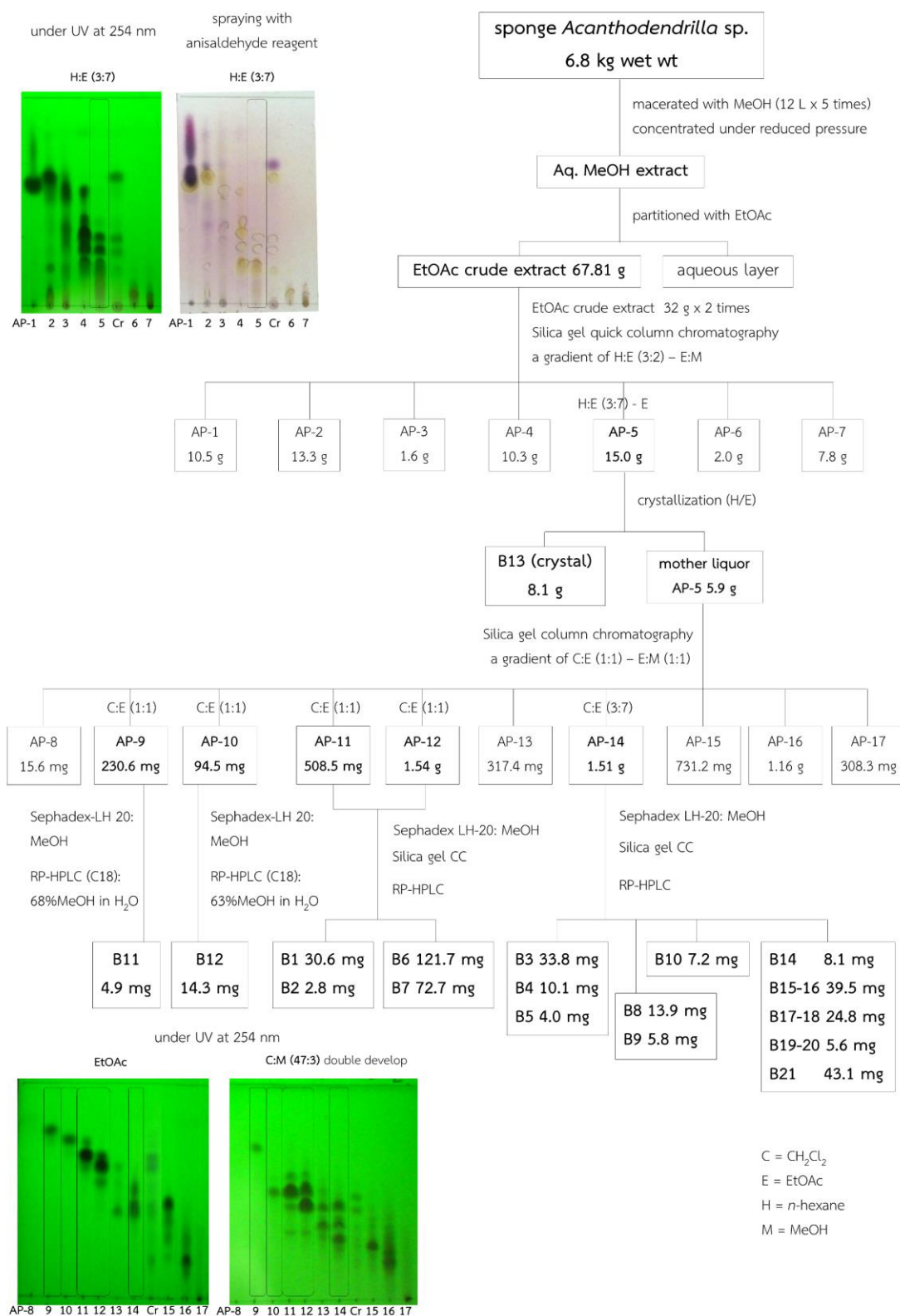
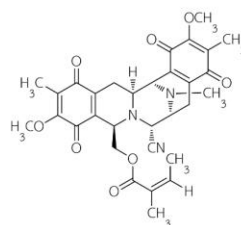
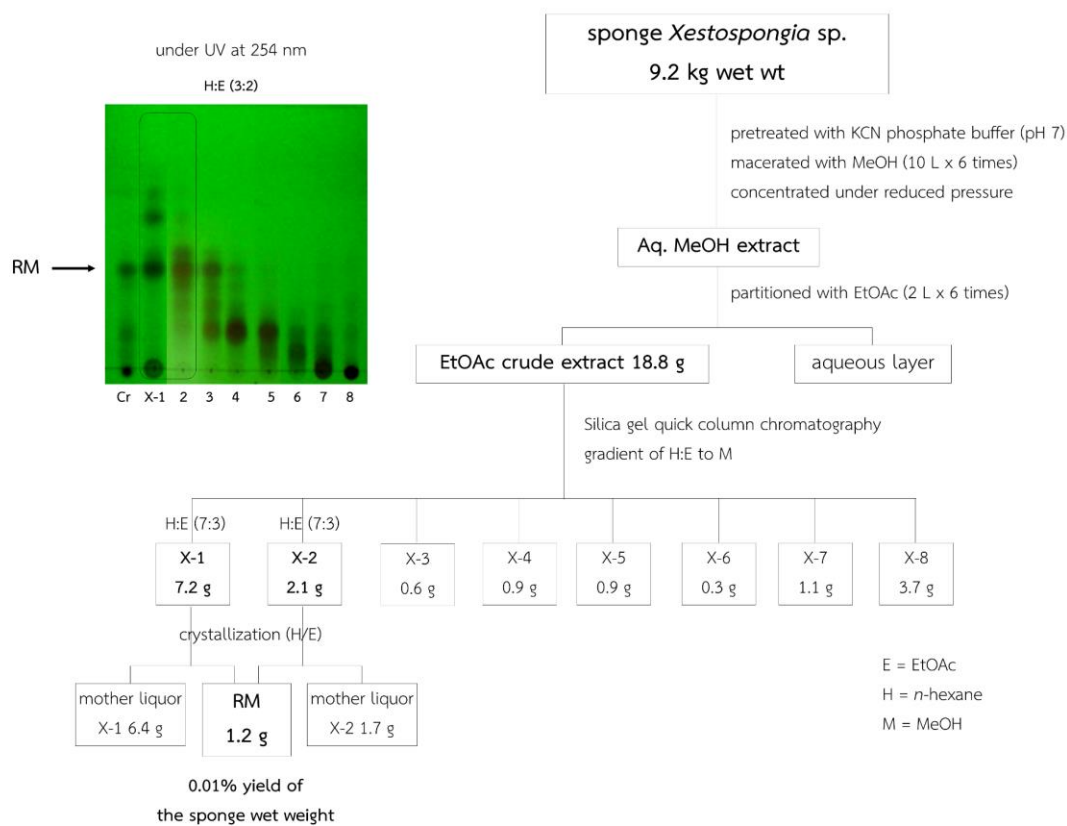


Figure A3 Extraction and isolation scheme of bromotyrosine alkaloids from the sponge *Acanthodendrilla* sp.

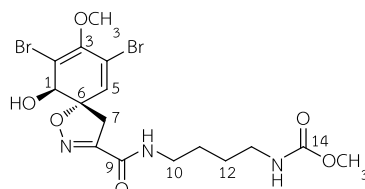


renieramycin M (RM)

Figure A4 Extraction and isolation scheme of renieramycin M (RM) from the blue sponge *Xestospongia* sp.

APPENDIX B

PHYSICAL AND SPECTROSCOPIC DATA OF BROMOTYROSINE ALKALOIDS

**Subereamolline C (B1):**

30.6 mg, 0.045% yield of EtOAc extract.

White amorphous powder.

$[\alpha]_D^{20}$ +185.0 (c 0.1, MeOH).

UV λ_{\max} (MeOH) nm (log ϵ): 230 (3.95), 283 (3.51).

IR (KBr) ν_{\max} 3339, 2940, 1701, 1653, 1541, 1263, and 989 cm^{-1}

^1H NMR (CDCl_3 , 300 MHz) δ 6.93 (1H, br, 9-NH), 6.31 (1H, s, H-5), 5.01 (1H, br, 14-NH), 4.36 (1H, s, H-1), 3.94 (1H, d, $J = 18.5$ Hz, H-7b), 3.75 (3H, s, 3-OCH₃), 3.66 (3H, s, 14-OCH₃), 3.35 (2H, dt, $J = 6.4, 6.1$ Hz, H₂-10), 3.19 (2H, q, $J = 5.0$ Hz, H₂-13), 3.01 (1H, d, $J = 18.5$ Hz, H-7a), 1.57 (2H, br, H₂-12), 1.56 (2H, br, H₂-11).

^{13}C NMR (CDCl_3 , 75 MHz) δ 159.4 (C, C-9), 157.4 (C, C-14), 154.2 (C, C-8), 148.0 (C, C-3), 130.9 (CH, C-5), 121.5 (C, C-4), 112.8 (C, C-2), 91.8 (C, C-6), 74.0 (CH, C-1), 60.1 (CH₃, 3-OCH₃), 52.2 (CH₃, 14-OCH₃), 40.5 (CH₂, C-13), 39.2 (CH₂, C-10), 38.9 (CH₂, C-7), 27.3 (CH₂, C-11), 26.5 (CH₂, C-12).

HREIMS: m/z 508.9790 [$\text{M}]^+$ (calcd for C₁₆H₂₁Br₂N₃O₆, 508.9797).

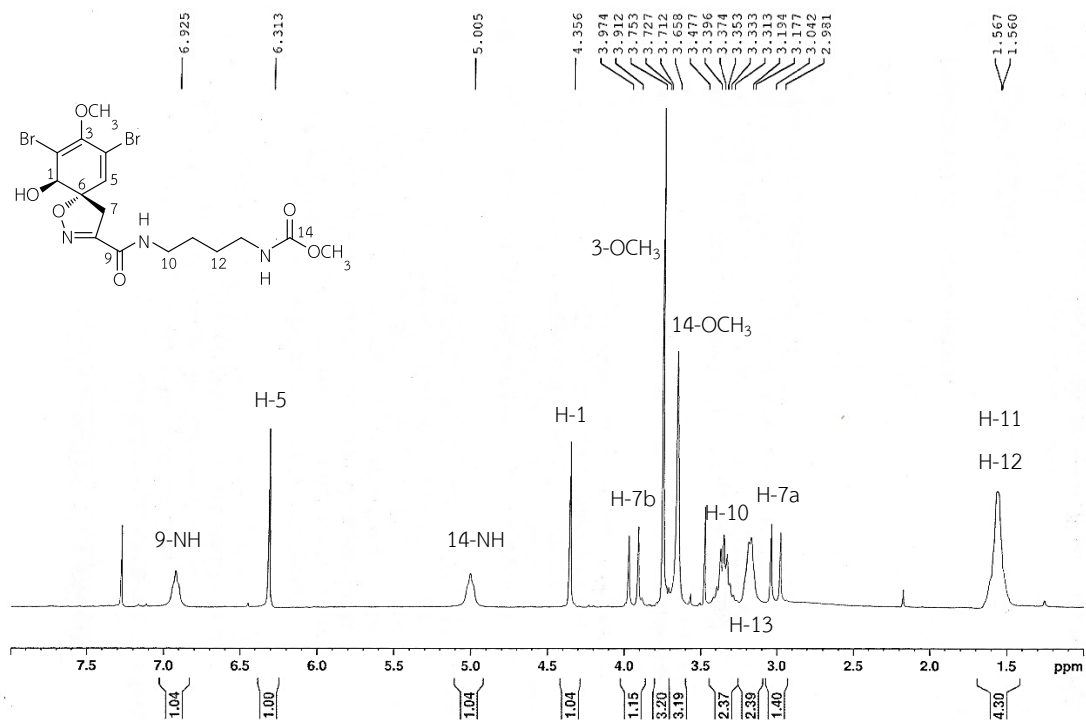


Figure B1 ^1H NMR spectrum (300 MHz) of subreamolline C (**B1**) in CDCl_3

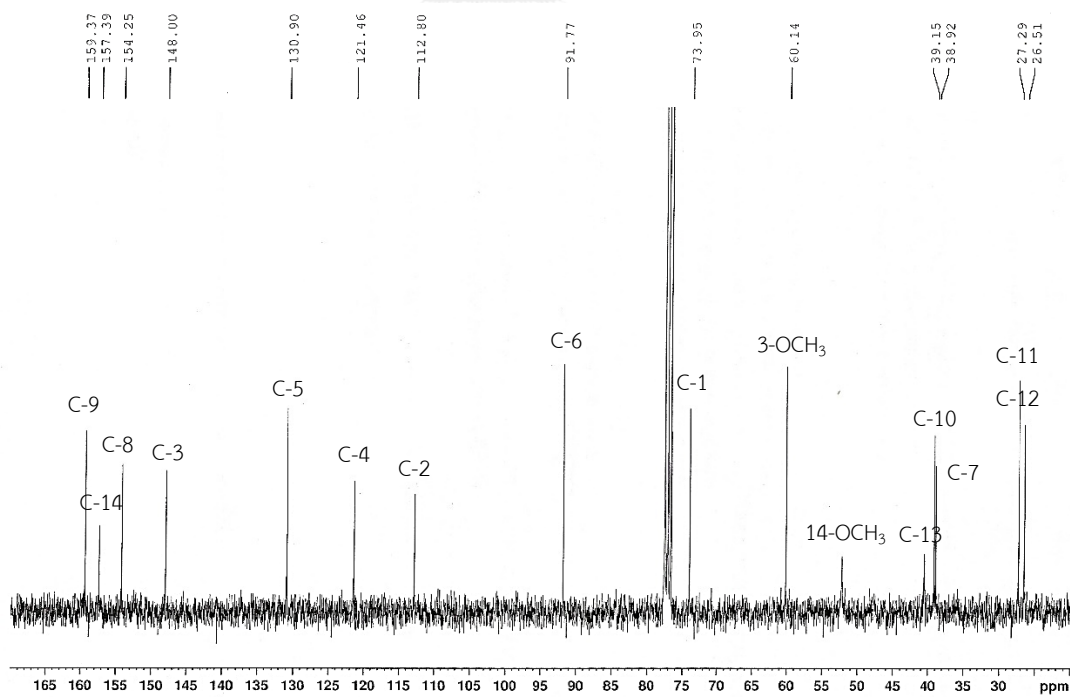
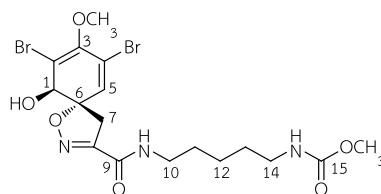


Figure B2 ^{13}C NMR spectrum (75 MHz) of subreamolline C (**B1**) in CDCl_3



Subereamolline D (B2):

2.8 mg, 0.004% yield of EtOAc extract.

White amorphous powder.

$[\alpha]_D^{28}$ +110.0 (c 0.1, MeOH).

UV λ_{\max} (MeOH) nm (log ϵ): 233 (3.68), 281 (3.36).

IR (CHCl₃) ν_{\max} 3017, 2938, 1717, 1676, 1522, and 1236 cm⁻¹

¹H NMR (CDCl₃, 300 MHz) δ 6.66 (1H, br, 9-NH), 6.33 (1H, s, H-5), 4.47 (1H, br, 15-NH), 4.41 (1H, s, H-1), 3.97 (1H, d, J = 18.8 Hz, H-7b), 3.77 (3H, s, 3-OCH₃), 3.68 (3H, s, 15-OCH₃), 3.36 (2H, br t, J = 6.8 Hz, H₂-10), 3.19 (2H, q, J = 6.3 Hz, H₂-14), 3.02 (1H, d, J = 18.8 Hz, H-7a), 1.60 (2H, m, H₂-11), 1.55 (2H, m, H₂-13), 1.41 (2H, m, H₂-12).

¹³C NMR (CDCl₃, 75 MHz) δ 159.1 (C, C-9), 157.2 (C-15), 154.3 (C, C-8), 148.1 (C, C-3), 131.1 (CH, C-5), 121.5 (C, C-4), 112.5 (C, C-2), 91.6 (C, C-6), 74.0 (CH, C-1), 60.2 (CH₃, 3-OCH₃), 52.1 (CH₃, 15-OCH₃), 40.8 (CH₂, C-14), 39.3 (CH₂, C-10), 38.8 (CH₂, C-7), 29.6 (CH₂, C-13), 28.9 (CH₂, C-11), 23.8 (CH₂, C-12).

HREIMS: m/z 522.9947 [M]⁺ (calcd for C₁₇H₂₃Br₂N₃O₆, 522.9954).

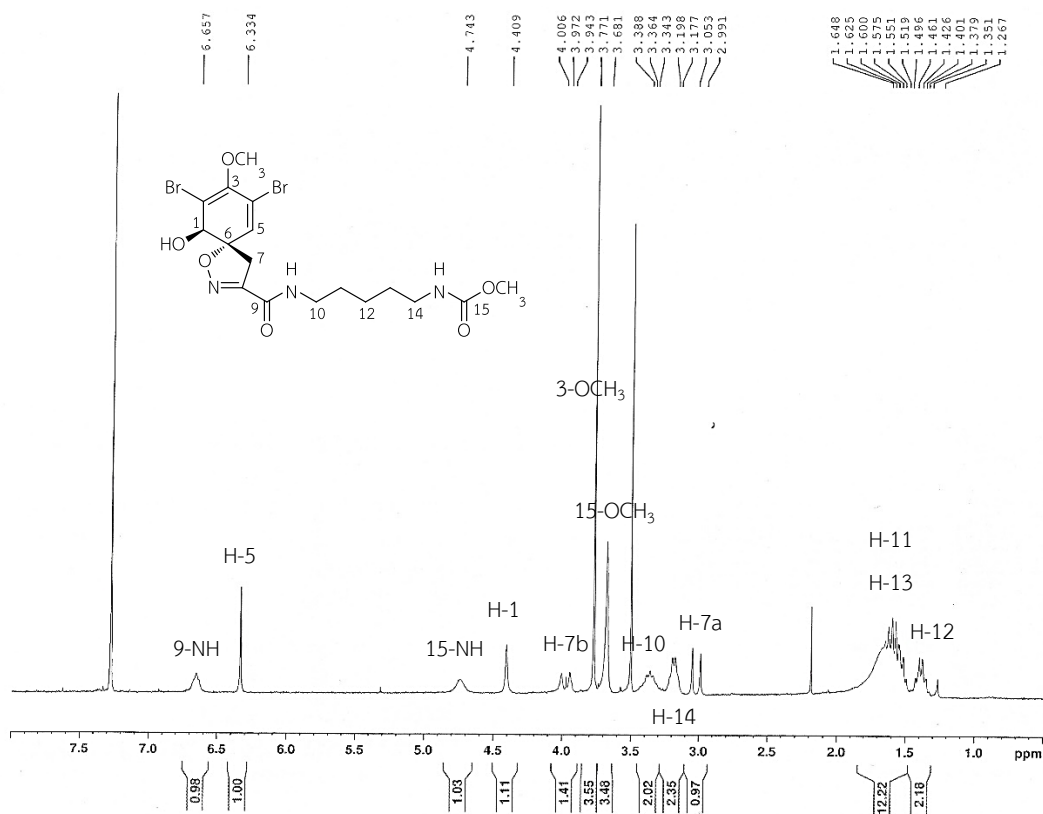


Figure B3 ^1H NMR spectrum (300 MHz) of subreamolline D (B2) in CDCl_3

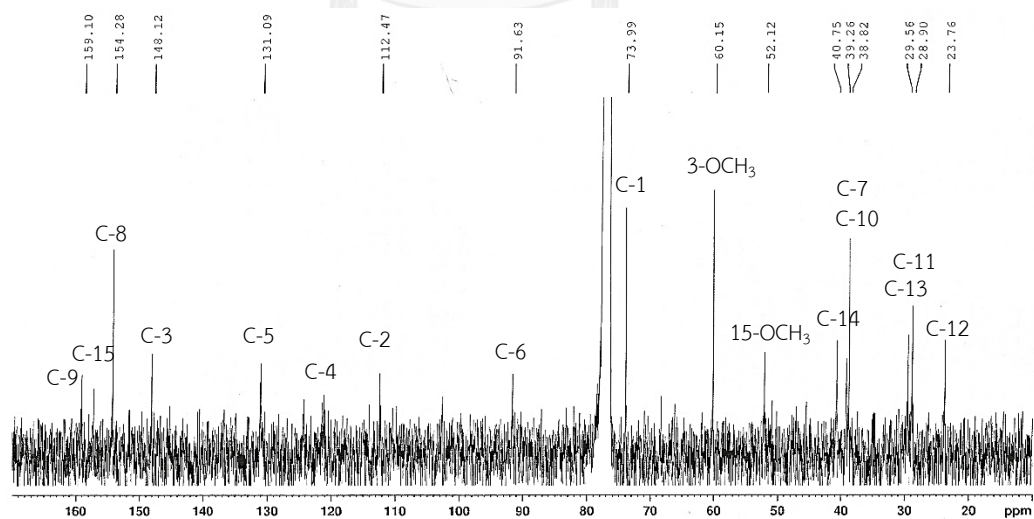
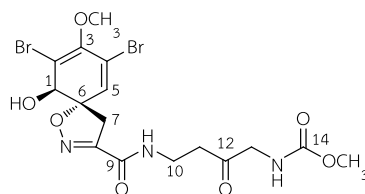


Figure B4 ^{13}C NMR spectrum (75 MHz) of subreamolline D (B2) in CDCl_3

**B3:**

33.8 mg, 0.050% yield of EtOAc extract.

White amorphous powder.

$[\alpha]_D^{20}$ +137.0 (c 2.4, MeOH).

UV λ_{\max} (MeOH) nm (log ϵ): 232 (4.12), 283 (3.87).

^1H NMR (acetone- d_6 , 500 MHz) δ 7.61 (1H, t, J = 5.9 Hz, 9-NH), 6.50 (1H, s, H-5), 6.41 (1H, br, 14-NH), 5.43 (1H, d, J = 8.2 Hz, 1-OH), 4.16 (1H, d, J = 8.2 Hz, H-1), 3.99 (2H, d, J = 5.5 Hz, H₂-13), 3.81 (1H, d, J = 18.3 Hz, H-7b), 3.71 (3H, s, 3-OCH₃), 3.59 (3H, s, 14-OCH₃), 3.54 (2H, dt, J = 6.5, 5.9 Hz, H₂-10), 3.15 (1H, d, J = 18.3 Hz, H-7a), 2.79 (2H, t, J = 6.5 Hz, H₂-11).

^{13}C NMR (acetone- d_6 , 125 MHz) δ 205.7 (C, C-12), 159.9 (C, C-9), 157.9 (C, C-14), 155.1 (C, C-8), 148.7 (C, C-3), 132.3 (CH, C-5), 122.0 (C, C-4), 113.8 (C, C-2), 91.6 (C, C-6), 75.1 (CH, C-1), 60.2 (CH₃, 3-OCH₃), 52.2 (CH₃, 14-OCH₃), 51.0 (CH₂, C-13), 40.0 (CH₂, C-11), 39.4 (CH₂, C-7), 34.9 (CH₂, C-10).

HREIMS: m/z 522.9586 [M]⁺ (calcd for C₁₆H₁₉Br₂N₃O₇, 522.9590).

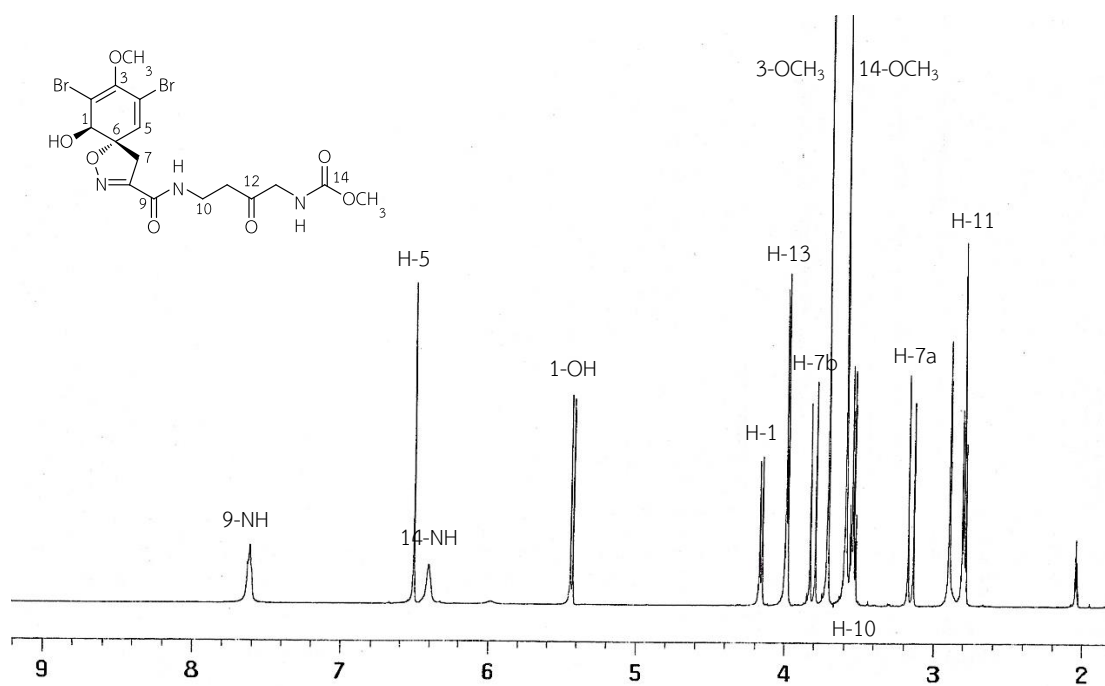


Figure B5 ^1H NMR spectrum (500 MHz) of **B3** in acetone- d_6

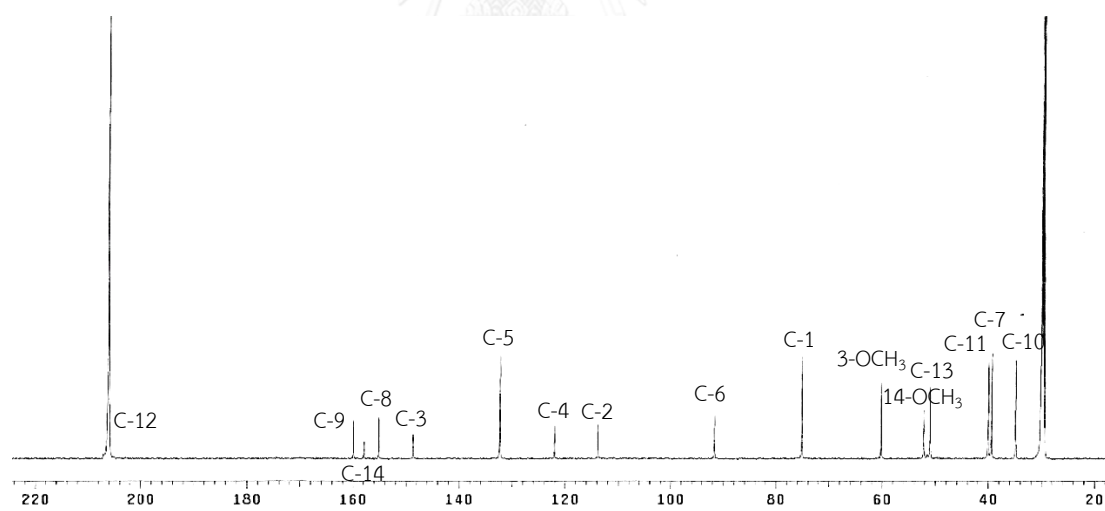
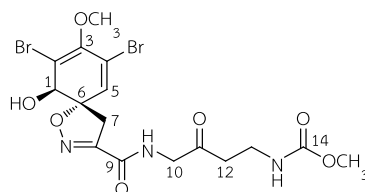


Figure B6 ^{13}C NMR spectrum (125 MHz) of **B3** in acetone- d_6

**B4:**

10.1 mg, 0.015% yield of EtOAc extract.

White amorphous powder.

$[\alpha]_D^{20} +156.4$ (c 0.7, MeOH).

UV λ_{\max} (MeOH) nm (log ϵ): 231 (4.12), 283 (3.89).

^1H NMR (acetone- d_6 , 500 MHz) δ 7.77 (1H, t, $J = 5.3$ Hz, 9-NH), 6.54 (1H, s, H-5), 6.18 (1H, br, 14-NH), 5.45 (1H, d, $J = 7.7$ Hz, 1-OH), 4.20 (1H, d, $J = 7.7$ Hz, H-1), 4.18 (2H, d, $J = 5.3$ Hz, H₂-10), 3.83 (1H, d, $J = 18.5$ Hz, H-7b), 3.71 (3H, s, 3-OCH₃), 3.55 (3H, s, 14-OCH₃), 3.37 (2H, td, $J = 6.8, 6.3$ Hz, H₂-13), 3.19 (1H, d, $J = 18.5$ Hz, H-7a), 2.75 (2H, t, $J = 6.8$ Hz, H₂-12).

^{13}C NMR (acetone- d_6 , 125 MHz) δ 204.9 (C, C-11), 159.9 (C, C-9), 157.9 (C, C-14), 155.1 (C, C-8), 148.7 (C, C-3), 132.3 (CH, C-5), 122.1 (C, C-4), 113.9 (C, C-2), 91.9 (C, C-6), 75.2 (CH, C-1), 60.2 (CH₃, 3-OCH₃), 51.8 (CH₃, 14-OCH₃), 49.4 (CH₂, C-10), 39.9 (CH₂, C-7), 40.5 (CH₂, C-12), 36.5 (CH₂, C-13).

HREIMS: m/z 522.9583 [M]⁺ (calcd for C₁₆H₁₉Br₂N₃O₇, 522.9590).

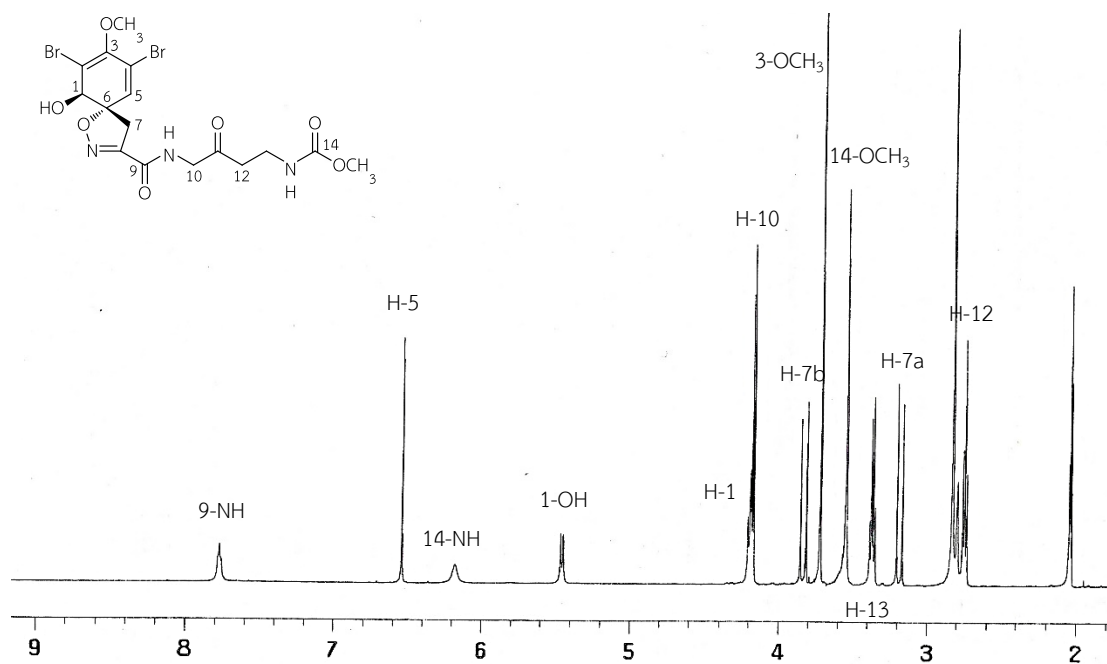


Figure B7 ^1H NMR spectrum (500 MHz) of **B4** in acetone-*d*₆

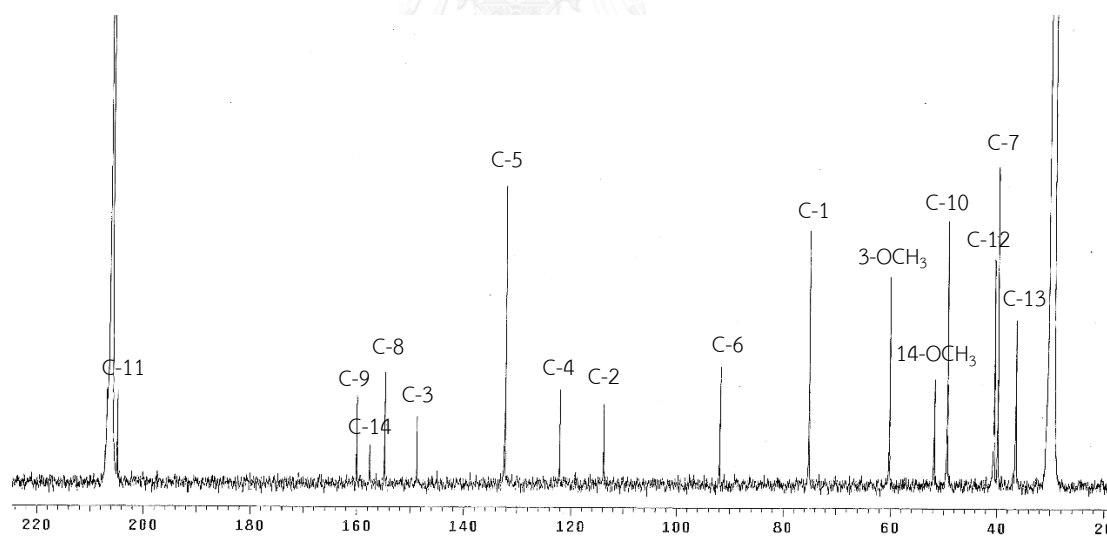


Figure B8 ^{13}C NMR spectrum (125 MHz) of **B4** in acetone-*d*₆

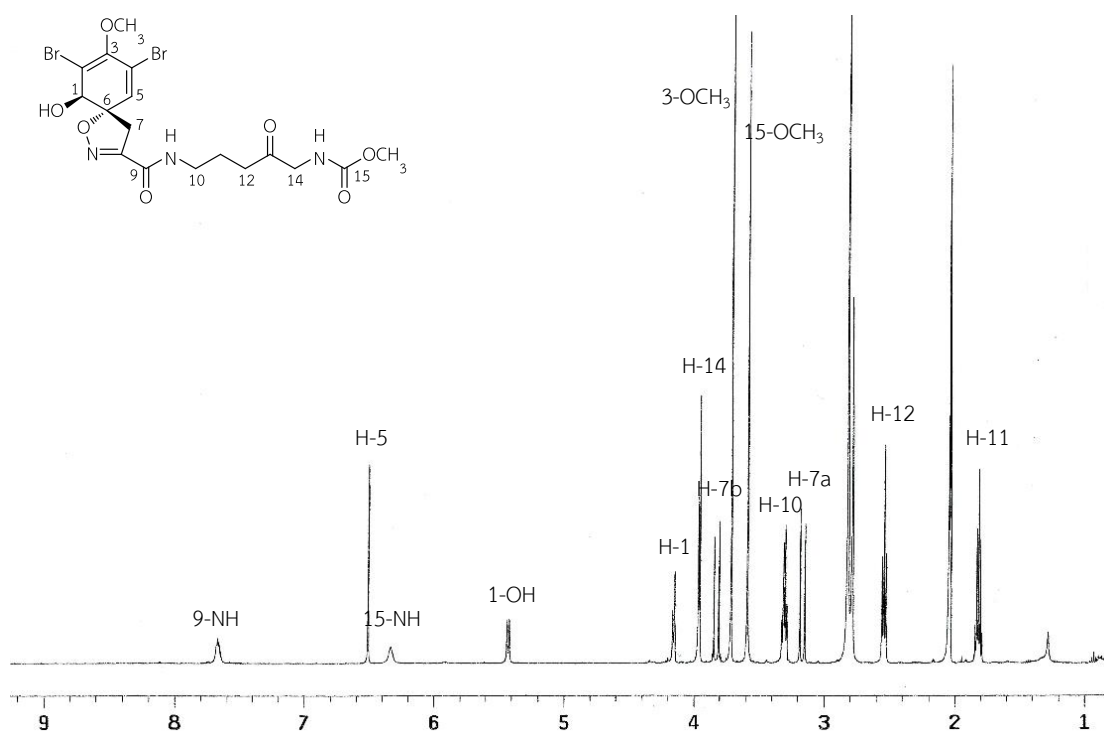


Figure B9 ^1H NMR spectrum (500 MHz) of 13-oxosubereamolline D (B5) in acetone- d_6

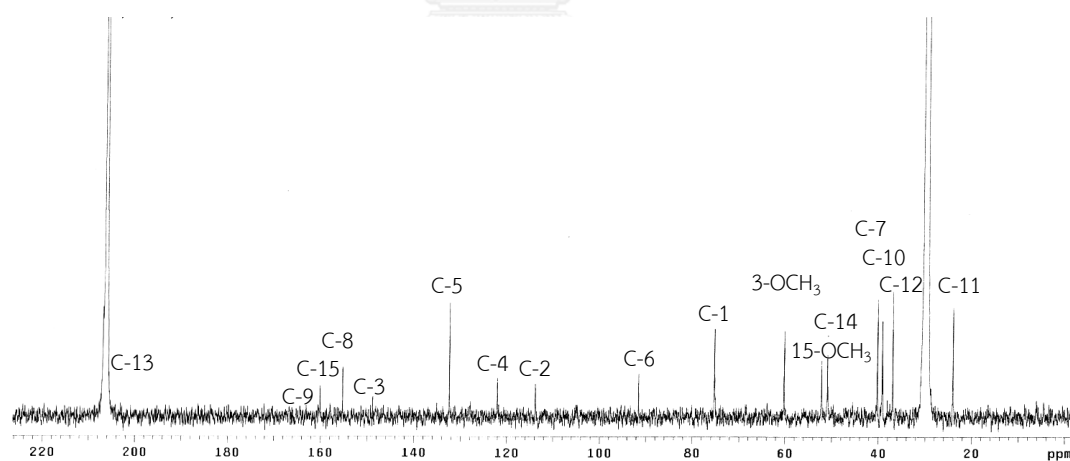


Figure B10 ^{13}C NMR spectrum (125 MHz) of 13-oxosubereamolline D (B5) in acetone- d_6

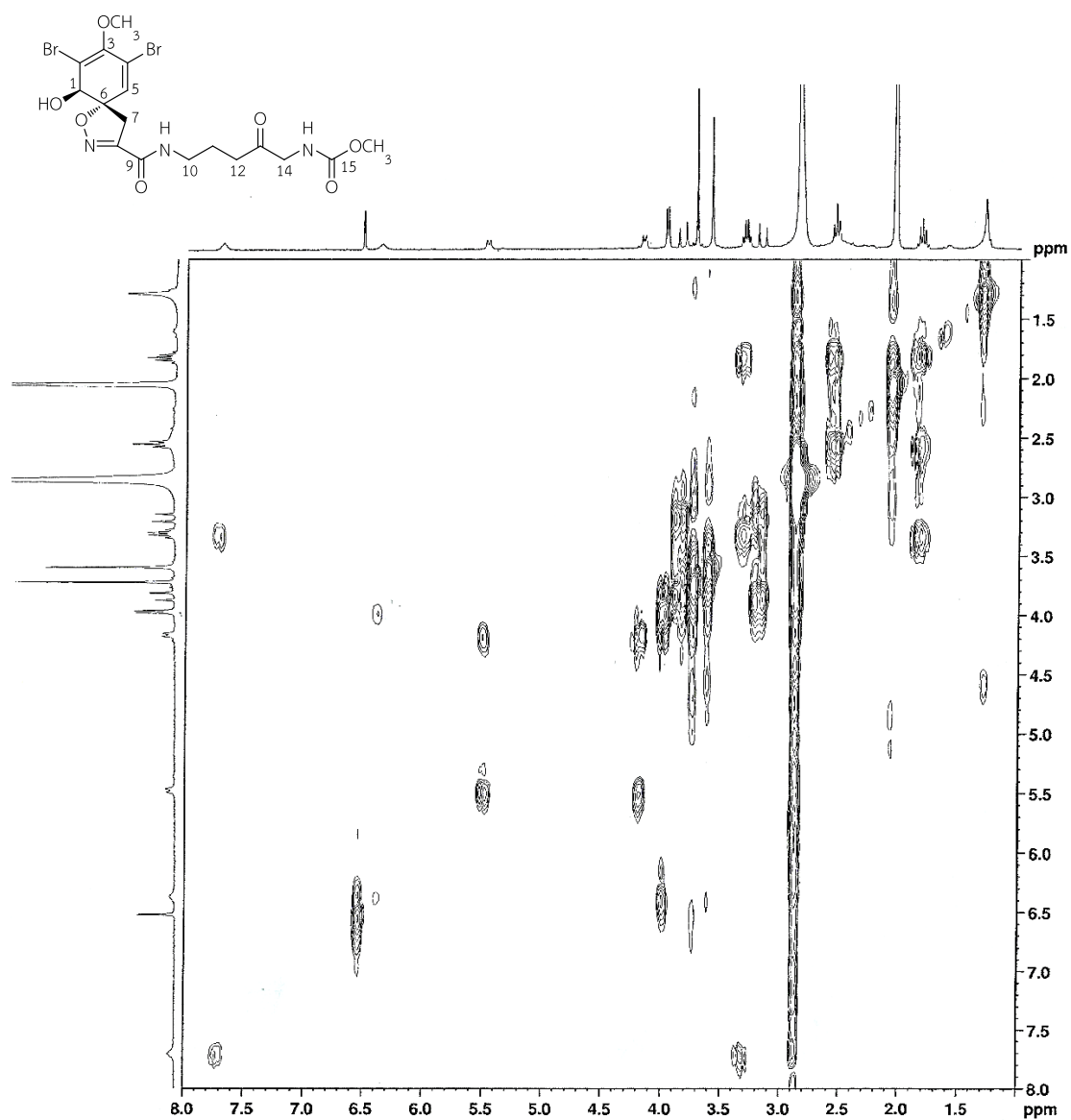


Figure B11 ^1H - ^1H COSY spectrum (300 MHz) of 13-oxosubereamolline D (B5) in acetone- d_6

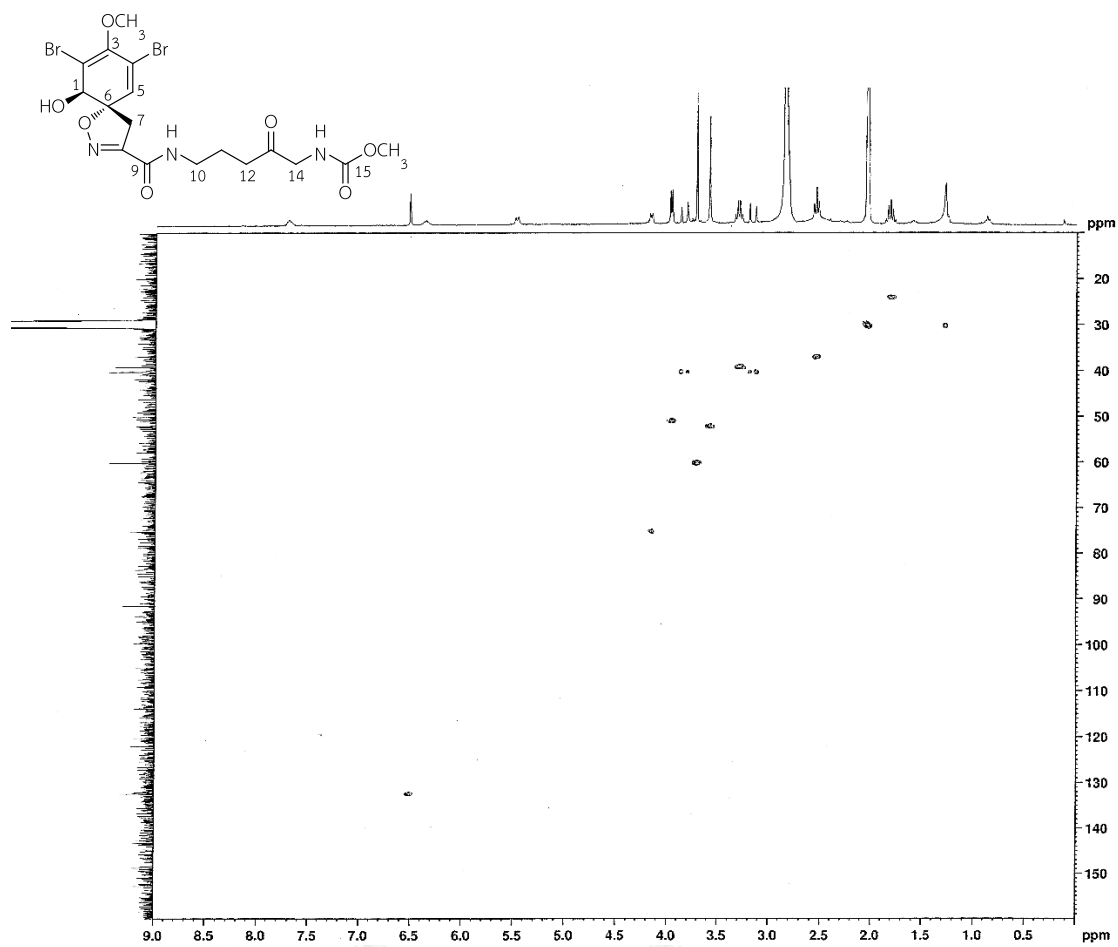


Figure B12 HSQC spectrum (300 MHz) of 13-oxosubereamolline D (B5) in acetone- d_6

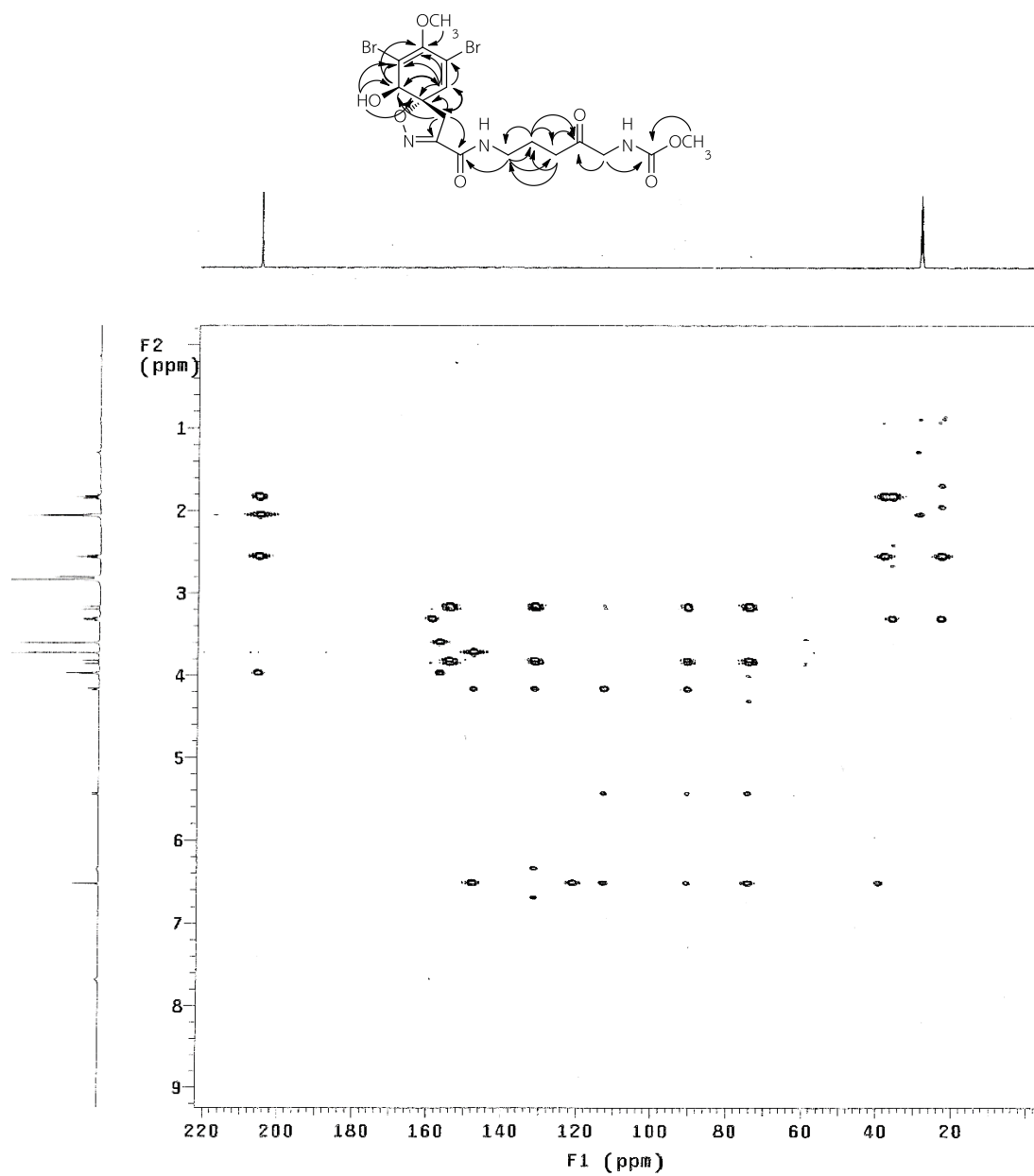


Figure B13 HMBC spectrum (500 MHz) of 13-oxosubereamolline D (B5) in acetone- d_6

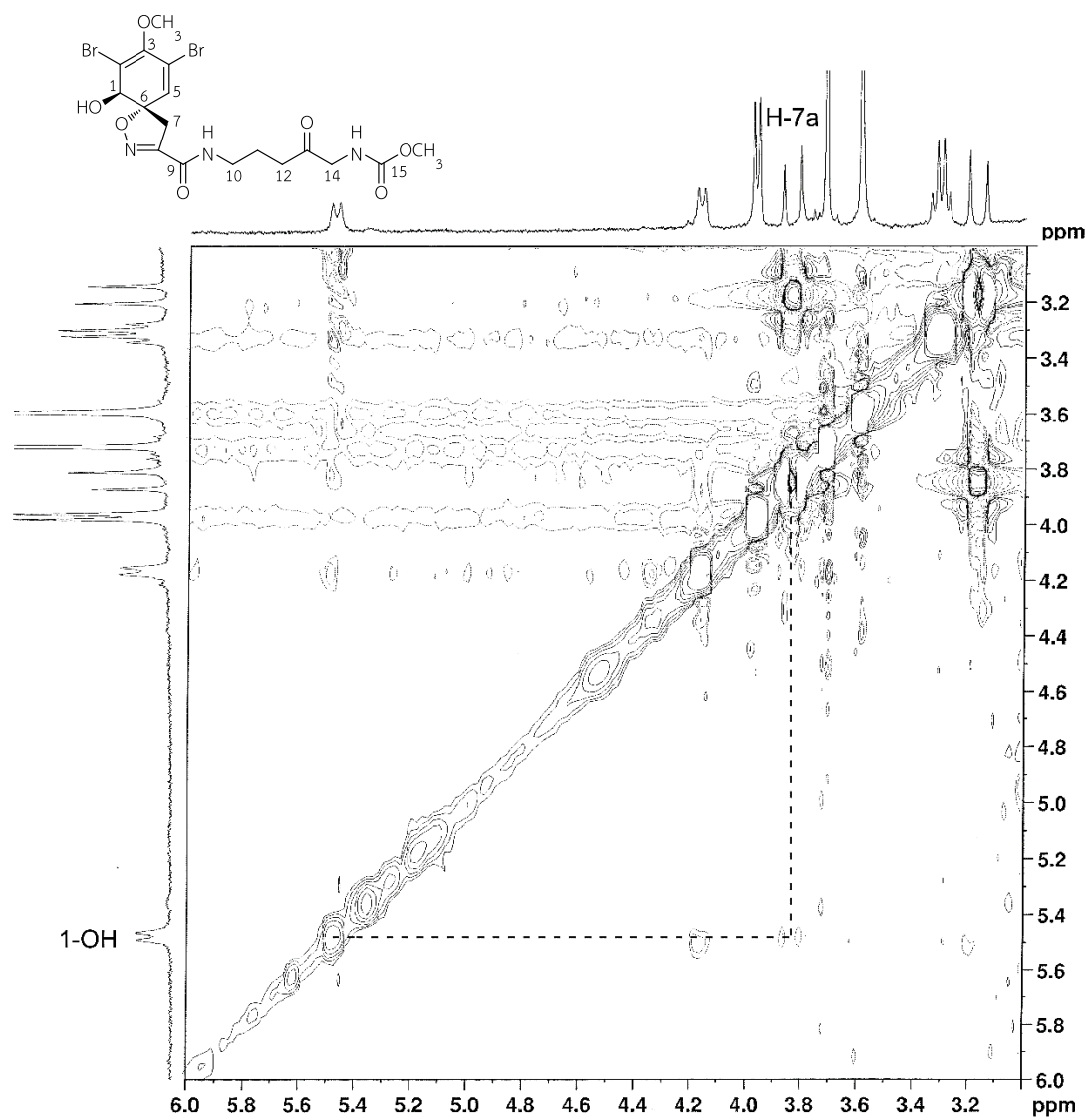


Figure B14 NOESY spectrum (300 MHz) of 13-oxosubereamolline D (B5) in acetone- d_6

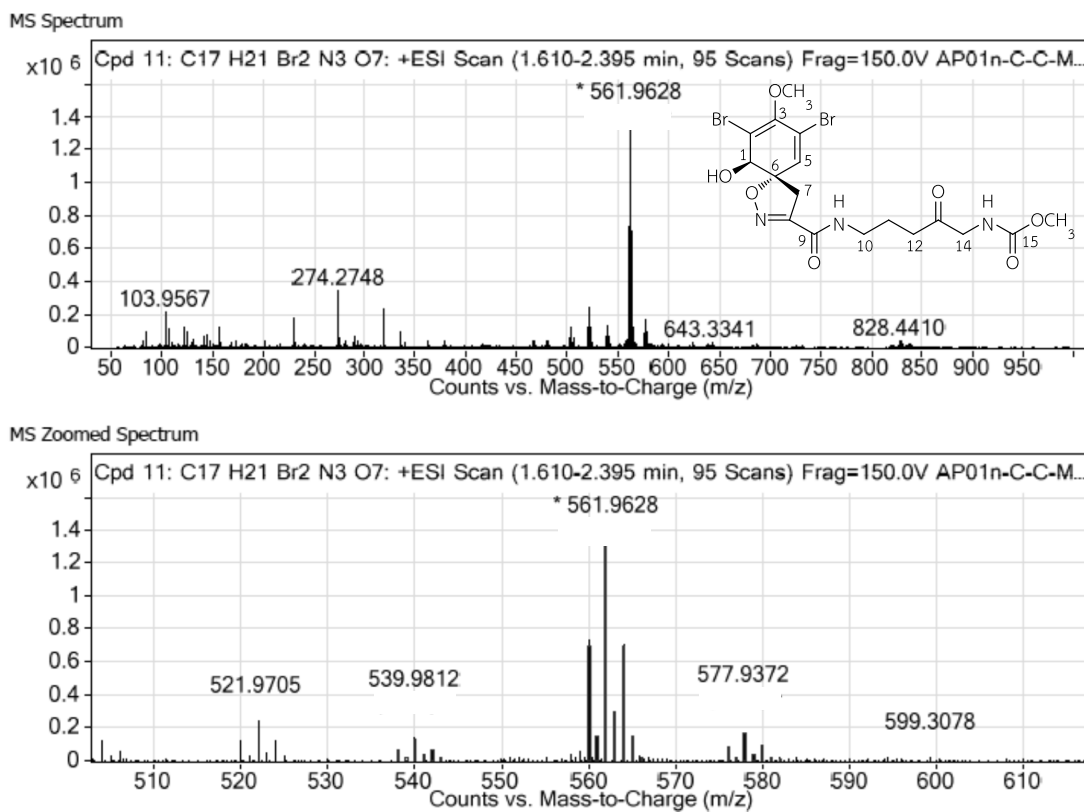


Figure B15 HRESIMS spectrum of 13-oxosubereamolline D (B5)

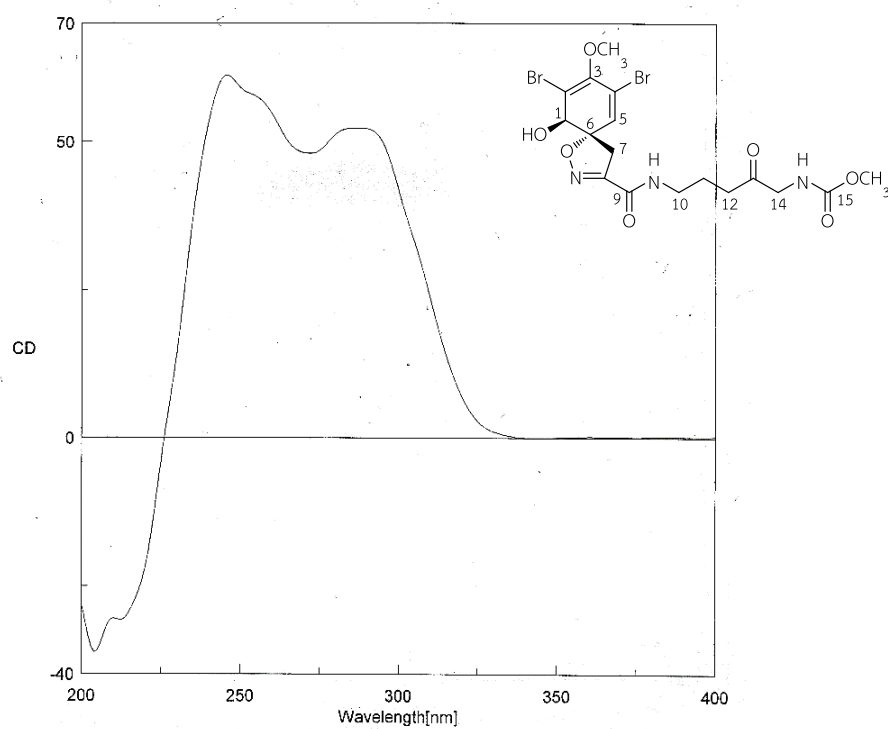
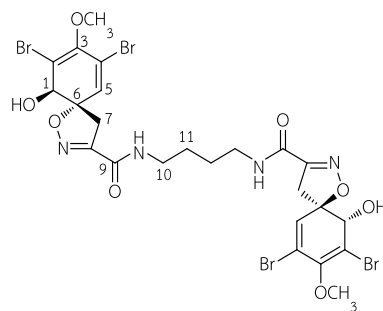


Figure B16 CD spectrum of 13-oxosubereamolline D (B5)



Aerothionin (B6):

121.7 mg, 0.179% yield of EtOAc extract.

White amorphous powder.

$[\alpha]_D^{20}$ +245.0 (c 0.1, MeOH).

^1H NMR (acetone- d_6 , 300 MHz) δ 7.69 (2H, br, 9-NH), 6.53 (2H, s, H-5), 5.47 (2H, d, J = 7.8 Hz, 1-OH), 4.18 (2H, d, J = 7.8 Hz, H-1), 3.84 (2H, d, J = 18.0 Hz, H-7b), 3.72 (6H, s, 3-OCH₃), 3.33 (4H, m, H₂-10), 3.19 (2H, d, J = 18.0 Hz, H-7a), 1.62 (4H, m, H₂-11).

^{13}C NMR (acetone- d_6 , 75 MHz) δ 159.9 (C, C-9), 155.3 (C, C-8), 148.7 (C, C-3), 132.4 (CH, C-5), 122.0 (C, C-4), 113.9 (C, C-2), 91.5 (C, C-6), 75.2 (CH, C-1), 60.2 (CH₃, 3-OCH₃), 40.2 (CH₂, C-7), 39.5 (CH₂, C-10), 27.5 (CH₂, C-11).

HRFABMS: m/z 836.8387 [M+Na]⁺ (calcd for C₂₄H₂₆Br₄N₄O₈Na, 836.8382).

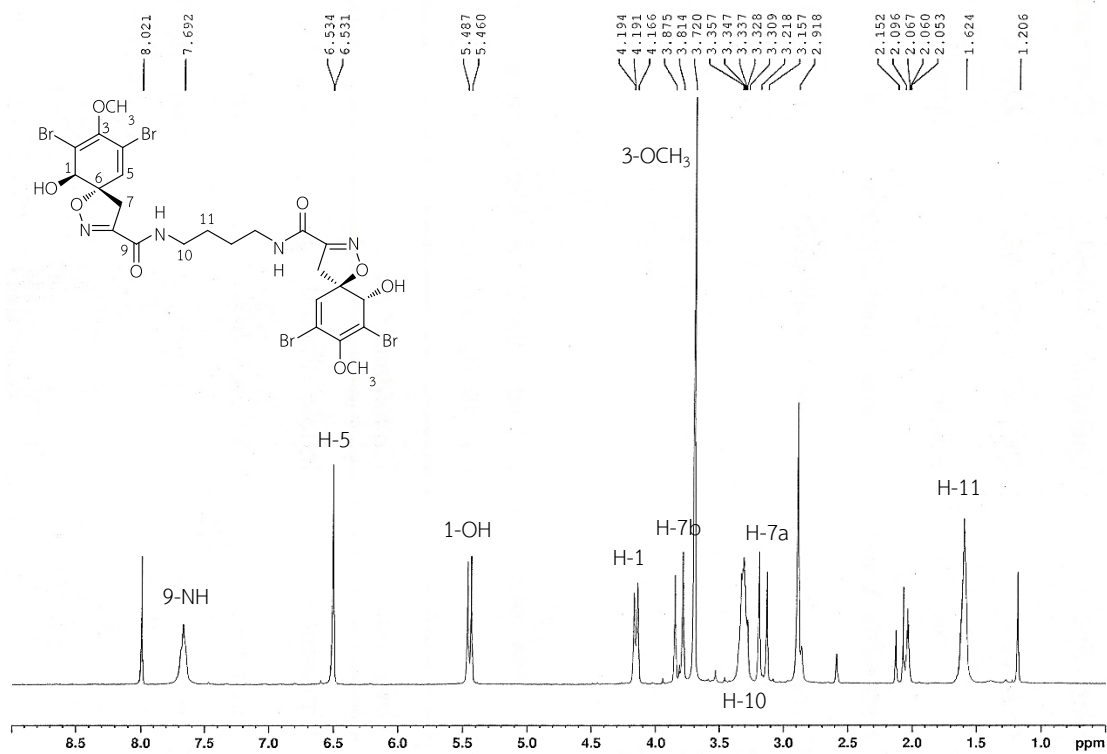


Figure B17 ^1H NMR spectrum (300 MHz) of aeriothionin (B6) in acetone- d_6

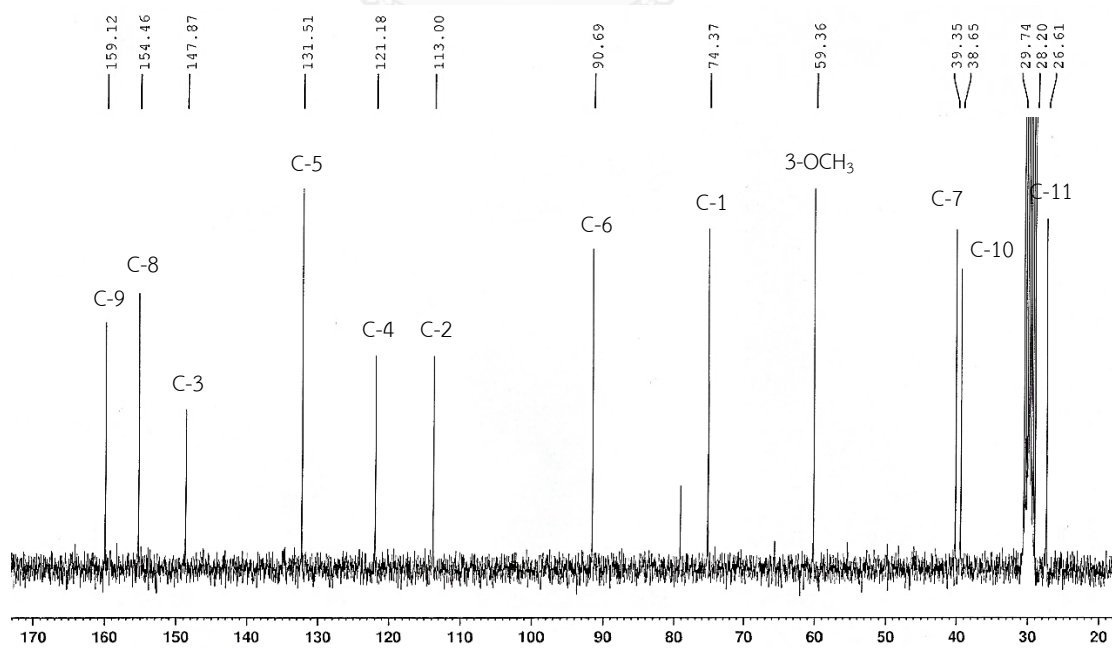
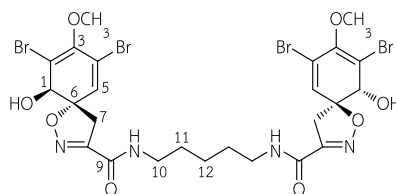


Figure B18 ^{13}C NMR spectrum (75 MHz) of aeriothionin (B6) in acetone- d_6



Homoaerotherionin (B7):

72.7 mg, 0.107% yield of EtOAc extract.

White amorphous powder.

$[\alpha]_D^{20}$ +153.0 (*c* 0.1, MeOH).

$^1\text{H NMR}$ (CDCl_3 , 300 MHz) δ 6.90 (2H, t, J = 6.0 Hz, 9-NH), 6.34 (2H, s, H-5), 4.39 (2H, s, H-1), 3.94 (2H, d, J = 18.5 Hz, H-7b), 3.76 (6H, s, 3-OCH₃), 3.35 (4H, m, H₂-10), 3.03 (2H, d, J = 18.5 Hz, H-7a), 1.60 (4H, quin, J = 6.8 Hz, H₂-11), 1.39 (2H, m, H₂-12).

$^{13}\text{C NMR}$ (CDCl_3 , 75 MHz) δ 159.5 (C, C-9), 154.3 (C, C-8), 148.0 (C, C-3), 131.0 (CH, C-5), 121.4 (C, C-4), 112.8 (C, C-2), 91.9 (C, C-6), 74.0 (CH, C-1), 60.0 (CH₃, 3-OCH₃), 39.2 (CH₂, C-7), 38.9 (CH₂, C-10), 28.7 (CH₂, C-11), 23.7 (CH₂, C-12).

HRFABMS: m/z 850.8553 $[\text{M}+\text{Na}]^+$ (calcd for $\text{C}_{25}\text{H}_{28}\text{Br}_4\text{N}_4\text{O}_8\text{Na}$, 850.8538).

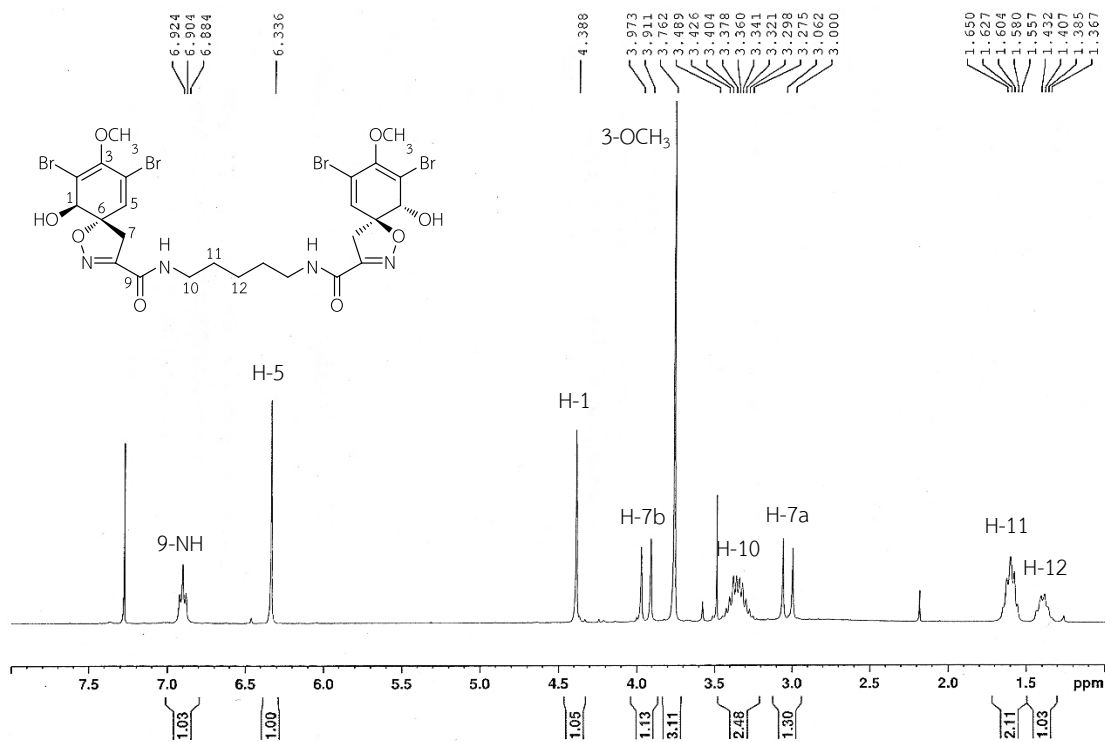


Figure B19 ¹H NMR spectrum (300 MHz) of homoaerthionin (B7) in CDCl₃

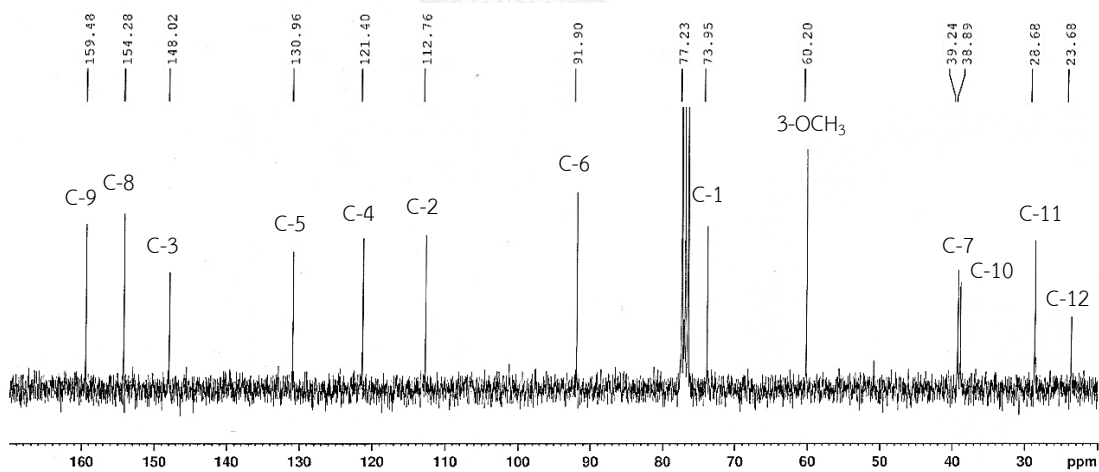
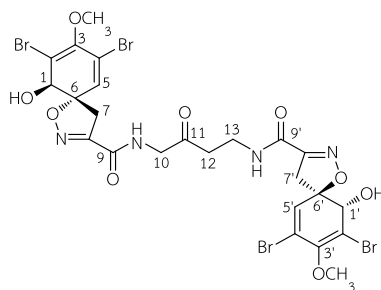


Figure B20 ¹³C NMR spectrum (75 MHz) of homoaerthionin (B7) in CDCl₃



11-Oxo-aerothionin (B8):

13.9 mg, 0.020% yield of EtOAc extract.

White amorphous powder.

$[\alpha]_D^{20}$ +175.0 (c 0.2, MeOH).

UV λ_{\max} (MeOH) nm (log ϵ): 233 (4.26), 283 (4.04).

^1H NMR (acetone- d_6 , 500 MHz) δ 7.81 and 7.63 (each 1H, t, J = 5.7 Hz, 9-NH and 9'-NH), 6.54 and 6.51 (each 1H, d, J = 0.9 Hz, H-5 and H'-5), 5.46 and 5.43 (each 1H, d, J = 7.8 Hz, 1-OH and 1'-OH), 4.20 and 4.16 (each 1H, d, J = 7.8 Hz, H-1 and H'-1'), 3.89 and 3.77 (each 1H, d, J = 18.0 Hz, H-7b and H-7'b), 3.72 and 3.71 (each 3H, s, 3-OCH₃ and 3'-OCH₃), 4.19 (2H, d, J = 5.7 Hz, H₂-10), 3.56 (2H, td, J = 6.9, 5.7 Hz, H₂-13), 3.20 and 3.14 (each 1H, d, J = 18.0 Hz, H-7a and H-7'a), 2.82 (2H, overlapped, H₂-12).

^{13}C NMR (acetone- d_6 , 125 MHz,) δ 205.0 (C, C-11), 160.1 and 160.0 (C, C-9 and C-9'), 155.1 and 154.8 (C, C-8 and C-8'), 148.7 (C, C-3 and C-3'), 132.3 (CH, C-5 and C-5'), 122.1 (C, C-4 and C-4'), 113.9 (C, C-2 and C-2'), 92.0 and 91.7 (C, C-6 and C-6'), 75.2 (CH, C-1 and C-1'), 60.2 (CH₃, 3-OCH₃ and 3'-OCH₃), 49.4 (CH₂, C-10), 40.0 and 39.9 (CH₂, C-7 and C-7'), 39.8 (CH₂, C-12), 34.9 (CH₂, C-13).

HRFABMS: m/z 850.8181 $[\text{M}+\text{Na}]^+$ (calcd for C₂₄H₂₄Br₄N₄O₉Na, 850.8174).

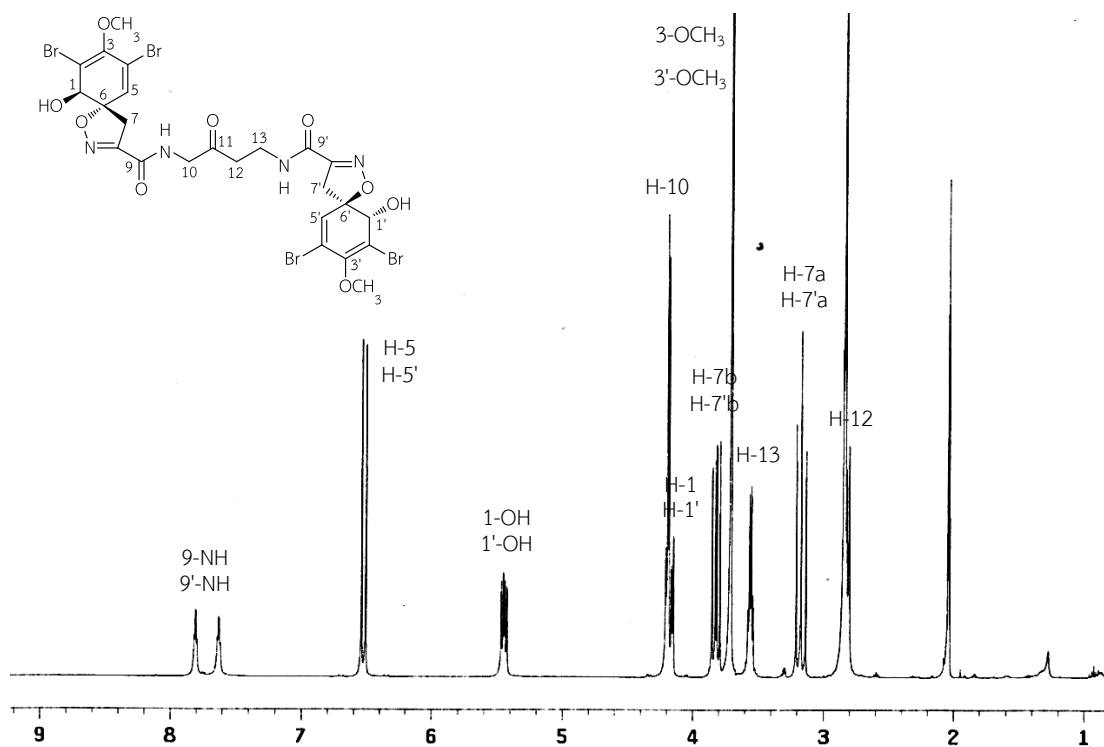


Figure B21 ^1H NMR spectrum (500 MHz) of 11-oxoaerithionin (**B8**) in acetone- d_6

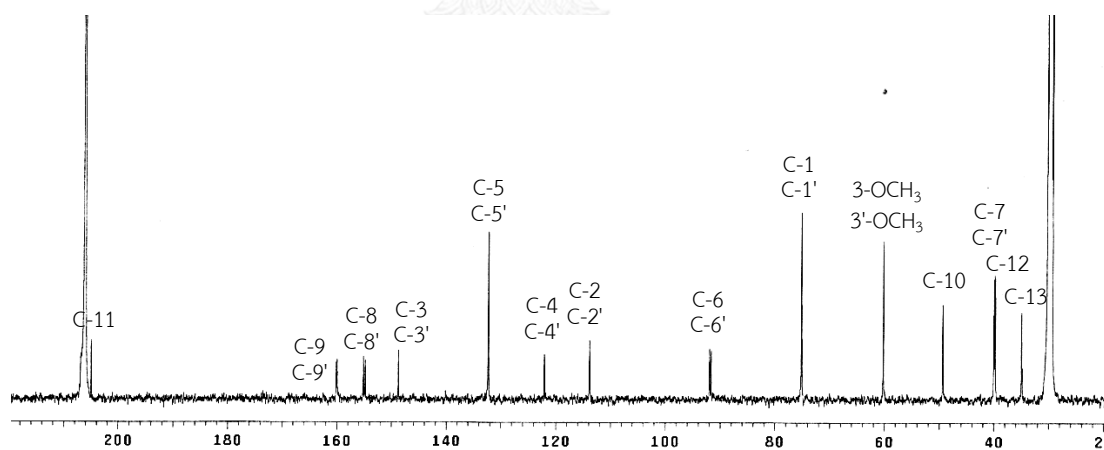
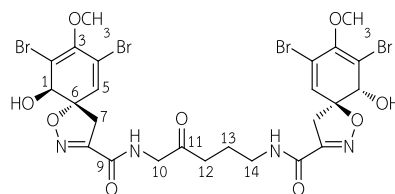


Figure B22 ^{13}C NMR spectrum (125 MHz) of 11-oxoaerithionin (**B8**) in acetone- d_6



Oxohomoaerotherionin (B9):

5.8 mg, 0.009% yield of EtOAc extract.

White amorphous powder.

$[\alpha]_D^{20}$ +215.2 (c 0.3, MeOH).

UV λ_{\max} (MeOH) nm (log ϵ): 231 (4.48), 283 (4.23).

^1H NMR (acetone- d_6 , 500 MHz) δ 7.76 and 7.68 (each 1H, t, J = 5.7 Hz, 9-NH and 9'-NH), 6.54 and 6.51 (each 1H, d, J = 0.9 Hz, H-5 and H'-5), 5.46 and 5.43 (each 1H, d, J = 8.3 Hz, 1-OH and 1'-OH), 4.17 and 4.16 (each 1H, d, J = 8.3 Hz, H-1 and H'-1'), 3.84 and 3.82 (each 1H, d, J = 18.3 Hz, H-7b and H'-7b), 3.72 and 3.71 (each 3H, s, 3-OCH₃ and 3'-OCH₃), 4.17 (2H, d, J = 5.7 Hz, H₂-10), 3.31 (2H, td, J = 6.8, 5.7 Hz, H₂-14), 3.21 and 3.15 (each 1H, d, J = 18.3 Hz, H-7a and H'-7a), 2.60 (2H, t, J = 6.8 Hz, H₂-12), 1.84 (2H, quin, J = 6.8 Hz, H₂-13).

^{13}C NMR (acetone- d_6 , 125 MHz) δ 205.4 (C, C-11), 160.2 and 160.1 (C, C-9 and C-9'), 155.3 and 154.8 (C, C-8 and C-8'), 148.8 (C, C-3 and C-3'), 132.4 and 132.3 (CH, C-5 and C-5'), 122.1 (C, C-4 and C-4'), 113.9 (C, C-2 and C-2'), 92.0 and 91.6 (C, C-6 and C-6'), 75.2 (CH, C-1 and C-1'), 60.2 (CH₃, 3-OCH₃ and 3'-OCH₃), 49.3 (CH₂, C-10), 40.2 and 39.9 (CH₂, C-7 and C-7'), 39.1 (CH₂, C-14), 37.3 (CH₂, C-12), 24.1 (CH₂, C-13).

HRFABMS: m/z 864.8331 [M+Na]⁺ (calcd for C₂₅H₂₆Br₄N₄O₉Na, 864.8331).

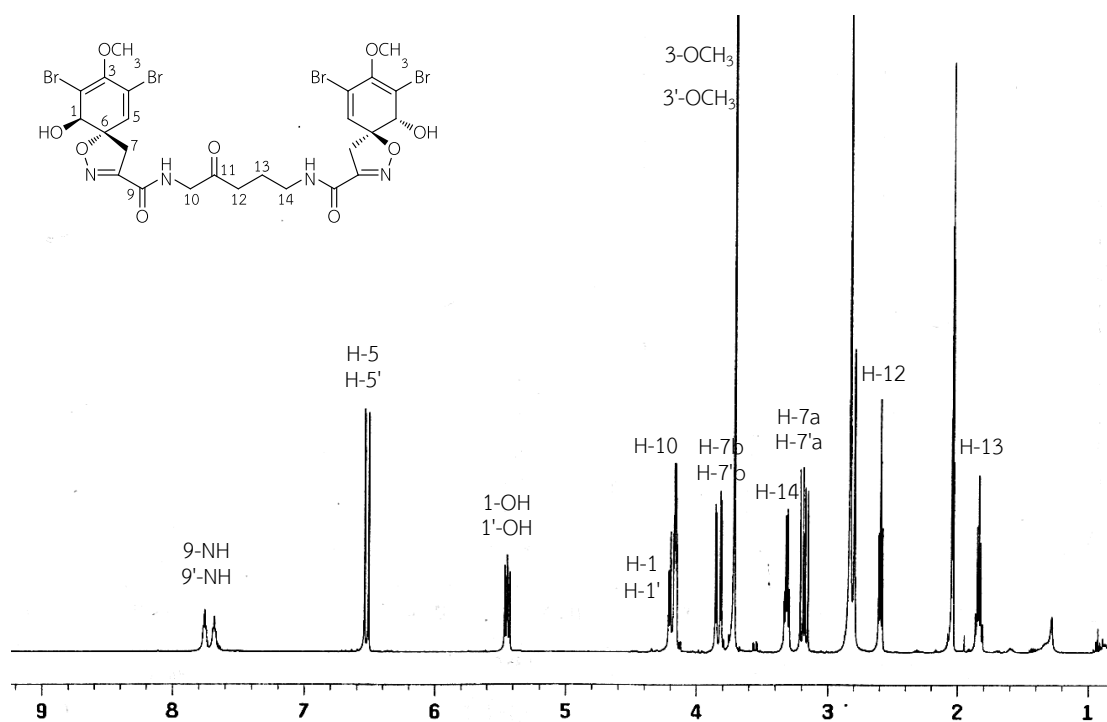


Figure B23 ^1H NMR spectrum (500 MHz) of oxohomoaerthionin (**B9**) in acetone- d_6

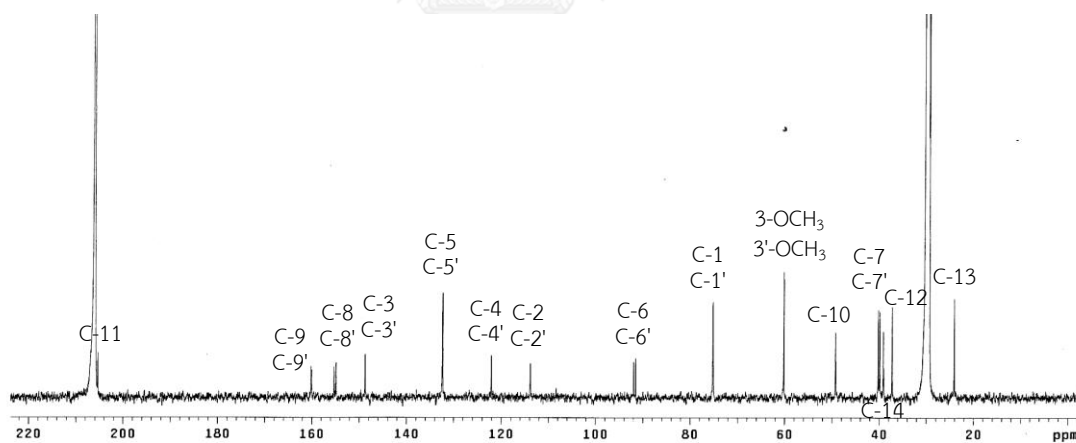
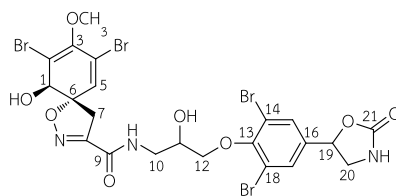


Figure B24 ^{13}C NMR spectrum (125 MHz) of oxohomoaerthionin (**B9**) in acetone- d_6



Fistularin 1 (B10):

7.2 mg, 0.011% yield of EtOAc extract.

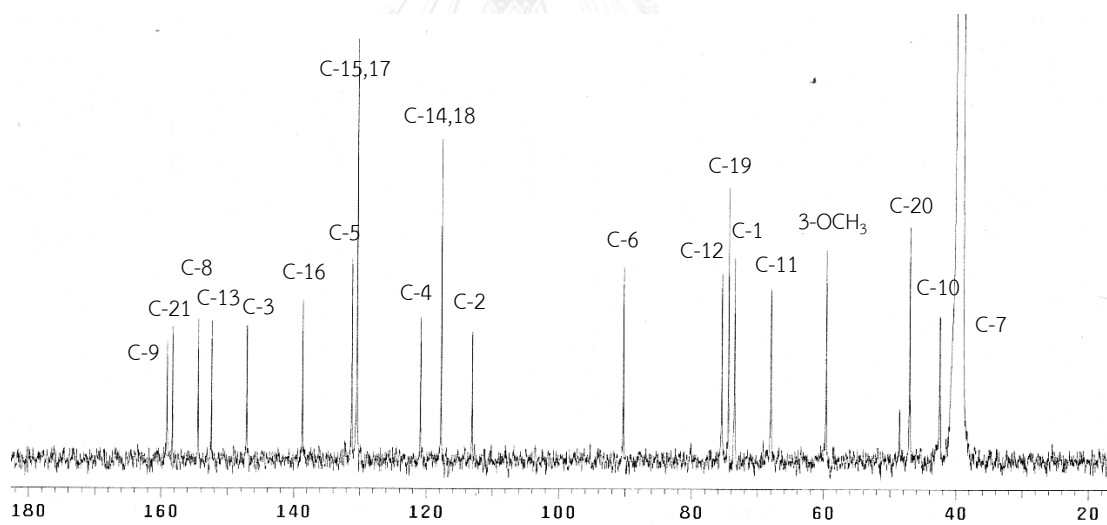
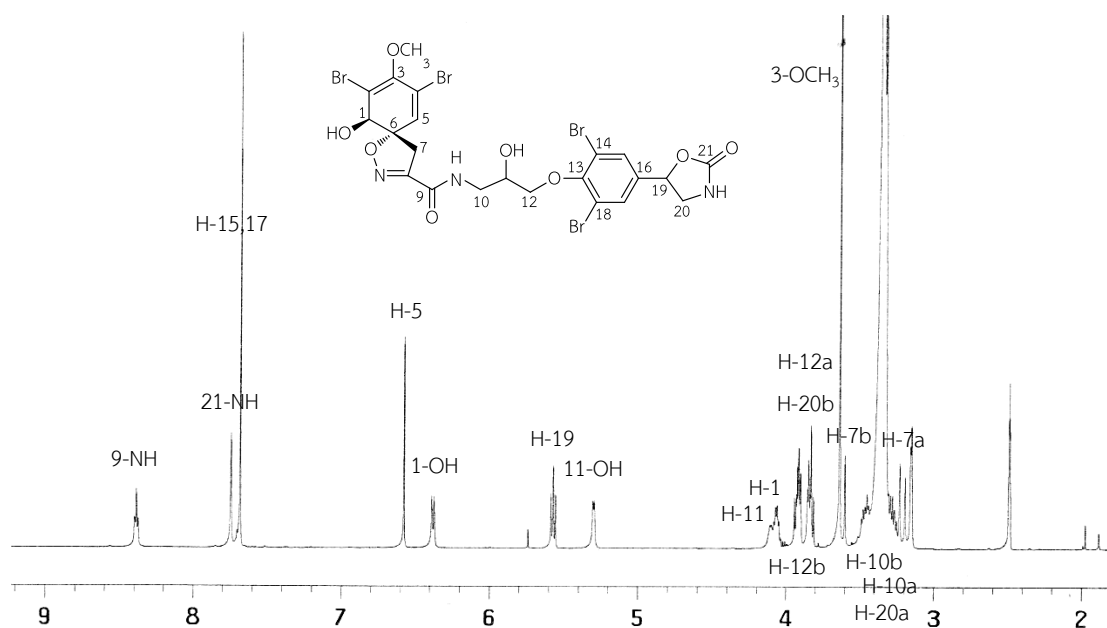
White amorphous powder.

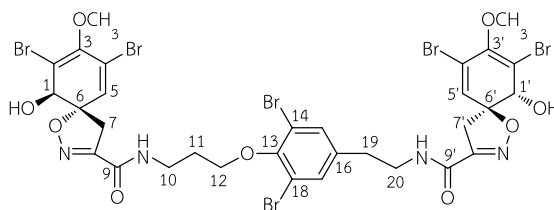
$[\alpha]_D^{26} +76.6$ (*c* 0.2, MeOH).

^1H NMR (DMSO-*d*₆, 500 MHz) δ 8.39 (1H, t, *J* = 5.9 Hz, 9-NH), 7.75 (1H, br, 21-NH), 7.68 (2H, s, H-15 and H-17), 6.58 (1H, s, H-5), 6.38 (1H, d, *J* = 8.0 Hz, 1-OH), 5.57 (1H, t, *J* = 7.9 Hz, H-19), 5.30 (1H, d, *J* = 5.4 Hz, 11-OH), 4.07 (1H, m, H-11), 3.93 (1H, overlapped, H-1), 3.93 (1H, overlapped, H-12b), 3.84 (each 1H, overlapped, H-12a and H-20b), 3.64 (3H, s, 3-OCH₃), 3.62 (1H, d, *J* = 18.0 Hz, H-7b), 3.47 (1H, overlapped, H-10b), 3.37 (1H, overlapped, H-20a), 3.30 (1H, overlapped, H-10a), 3.21 (1H, d, *J* = 18.0 Hz, H-7a).

^{13}C NMR (DMSO-*d*₆, 125 MHz) δ 159.1 (C, C-9), 158.3 (C-21), 154.4 (C, C-8), 152.4 (C, C-13), 147.1 (C, C-3), 138.7 (C, C-16), 131.2 (CH, C-5), 130.4 (CH, C-15 and C-17), 120.9 (C, C-4), 117.8 (C, C-14 and C-18), 113.1 (C, C-2), 90.3 (C, C-6), 75.5 (CH₂, C-12), 74.5 (CH₂, C-19), 73.6 (CH, C-1), 68.0 (CH, C-11), 59.6 (CH₃, 3-OCH₃), 47.1 (CH₂, C-20), 42.5 (CH₂, C-10), 39.8 (CH₂, C-7).

FABMS: *m/z* 794 [M+Na]⁺ (calcd for C₂₂H₂₁Br₄N₃O₈Na, 793.7960).





11, 19-Dideoxyfistularin 3 (B11):

4.9 mg, 0.007% yield of EtOAc extract.

Pale yellow amorphous powder.

$[\alpha]_D^{27} +188.1$ (c 0.1, MeOH).

^1H NMR (acetone- d_6 , 300 MHz) δ 7.78 (1H, t, $J = 7.2$ Hz, 9'-NH), 7.73 (1H, t, $J = 6.9$ Hz, 9-NH), 7.53 (2H, s, H-15 and H-17), 6.54 and 6.52 (each 1H, s, H-5 and H-5'), 5.45 (2H, d, $J = 7.5$ Hz, 1-OH and 1'-OH), 4.18 (2H, d, $J = 7.5$ Hz, H-1 and H-1'), 4.10 (2H, t, $J = 6.0$ Hz, H₂-12), 3.86 and 3.83 (each 1H, d, $J = 18.0$ Hz, H-7b and H-7'b), 3.73 (6H, s, 3-OCH₃ and 3'-OCH₃), 3.62 (2H, m, H₂-10), 3.58 (2H, m, H₂-20), 3.19 and 3.17 (each 1H, d, $J = 18.0$ Hz, H-7a and H-7'a), 2.87 (2H, overlapped, H₂-19), 2.16 (2H, quin, $J = 6.0$ Hz, H₂-11).

^{13}C NMR (acetone- d_6 , 75 MHz) δ 159.1 (C, C-9 and C-9'), 154.4 and 154.3 (C, C-8 and C-8'), 151.4 (C, C-13), 147.9 (C, C-3 and C-3'), 138.9 (C, C-16), 133.2 (CH, C-15 and C-17), 131.5 and 131.4 (CH, C-5 and C-5'), 121.23 and 121.18 (C, C-4 and C-4'), 117.6 (C, C-14 and C-18), 113.0 (C, C-2 and C-2'), 90.7 (C, C-6 and C-6'), 74.4 (CH, C-1 and C-1'), 71.3 (CH₂, C-12), 59.3 (CH₃, 3-OCH₃ and 3'-OCH₃), 40.1 (CH₂, C-20), 39.3 (CH₂, C-7 and C-7'), 36.6 (CH₂, C-10), 33.9 (CH₂, C-19), 29.8 (CH₂, C-11).

HRFABMS: m/z 1098.7070 $[\text{M}+\text{Na}]^+$ (calcd for C₃₁H₃₀Br₆N₄O₉Na, 1098.7011).

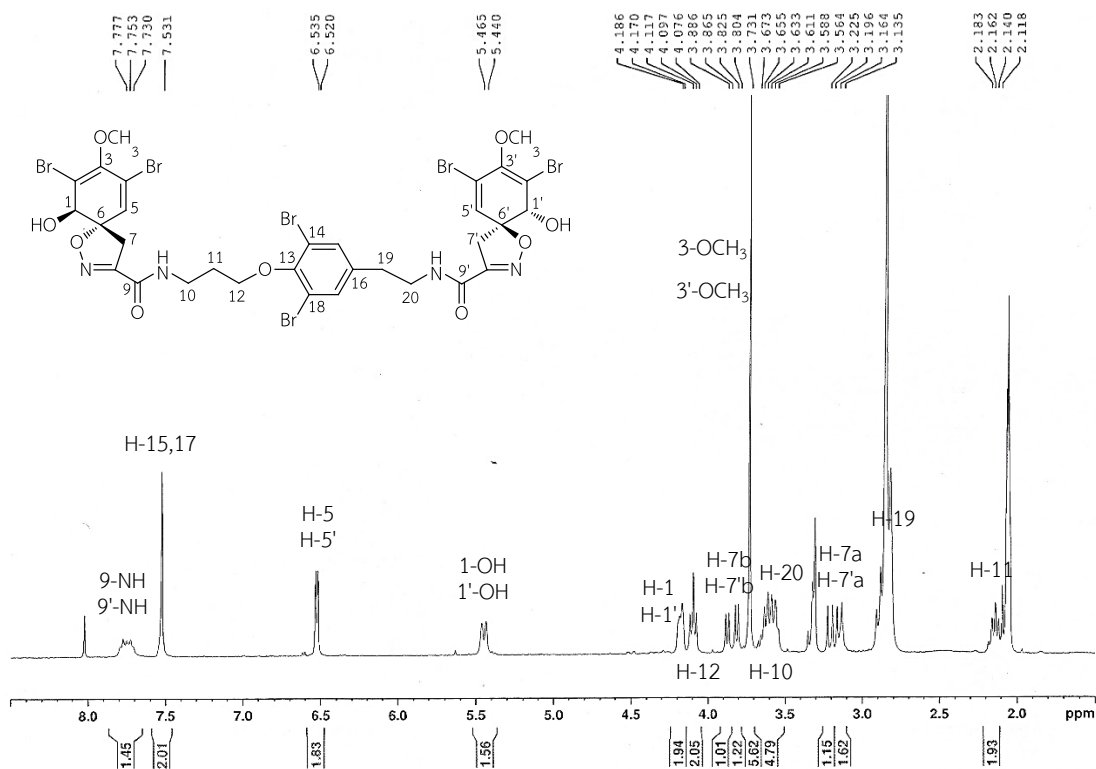


Figure B27 ^1H NMR spectrum (300 MHz) of 11,19-dideoxyfistularin 3 (B11) in acetone- d_6

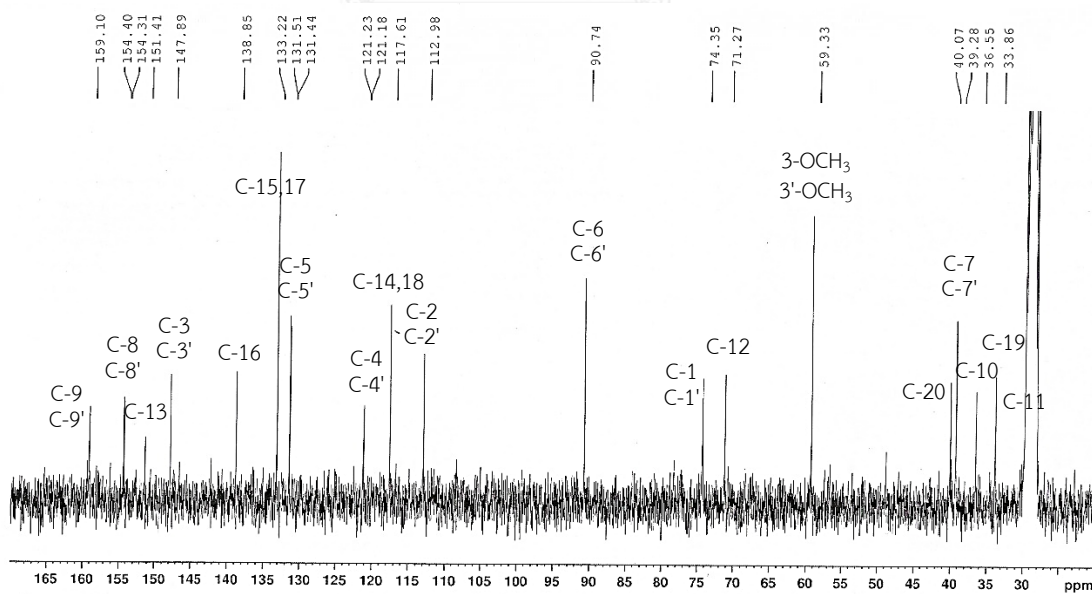
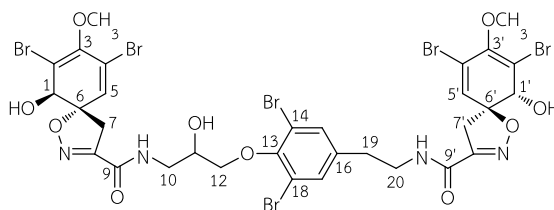


Figure B28 ^{13}C NMR spectrum (75 MHz) of 11,19-dideoxyfistularin 3 (B11) in acetone- d_6



19-Deoxyfistularin 3 (B12):

14.3 mg, 0.021% yield of EtOAc extract.

Pale yellow amorphous powder.

$[\alpha]_D^{27} +122.4$ (c 0.6, MeOH).

^1H NMR (acetone- d_6 , 300 MHz) δ 7.79 (1H, t, $J = 6.0$ Hz, 9'-NH), 7.66 (1H, t, $J = 5.7$ Hz, 9-NH), 7.53 (2H, s, H-15 and H-17), 6.54 and 6.52 (each 1H, d, $J = 0.6$ Hz, H-5 and H-5'), 5.48 and 5.46 (each 1H, d, $J = 7.8$ Hz, 1-OH and 1'-OH), 4.49 (1H, br, 11-OH), 4.25 (1H, m, H-11), 4.20 and 4.19 (each 1H, d, $J = 7.8$ Hz, H-1 and H-1'), 4.04 (2H, m, H₂-12), 3.87 and 3.84 (each 1H, d, $J = 18.3$ Hz, H-7b and H-7'b), 3.73 (6H, s, 3-OCH₃ and 3'-OCH₃), 3.59 (2H, m, H₂-20), 3.57 (1H, m, H-10b), 3.31 (1H, br, H-10a), 3.21 and 3.17 (each 1H, d, $J = 18.3$ Hz, H-7a and H-7'a), 2.89 (2H, overlapped, H₂-19).

^{13}C NMR (acetone- d_6 , 75 MHz) δ 160.1 and 159.7 (C, C-9 and C-9'), 154.8 (C, C-8 and C-8'), 151.6 (C, C-13), 148.4 (C, C-3 and C-3'), 139.5 (C, C-16), 133.8 (CH, C-15 and C-17), 131.9 (CH, C-5 and C-5'), 121.7 (C, C-4 and C-4'), 118.0 (C, C-14 and C-18), 113.5 (C, C-2 and C-2'), 91.4 and 91.2 (C, C-6 and C-6'), 75.5 (CH₂, C-12), 74.9 (CH, C-1 and C-1'), 69.4 (CH, C-11), 59.8 (CH₃, 3-OCH₃ and 3'-OCH₃), 43.2 (CH₂, C-10), 40.6 (CH₂, C-20), 39.74 and 39.70 (CH₂, C-7 and C-7'), 34.4 (CH₂, C-19).

HRFABMS: m/z 1114.7019 $[\text{M}+\text{Na}]^+$ (calcd for C₃₁H₃₀Br₆N₄O₁₀Na, 1114.6960).

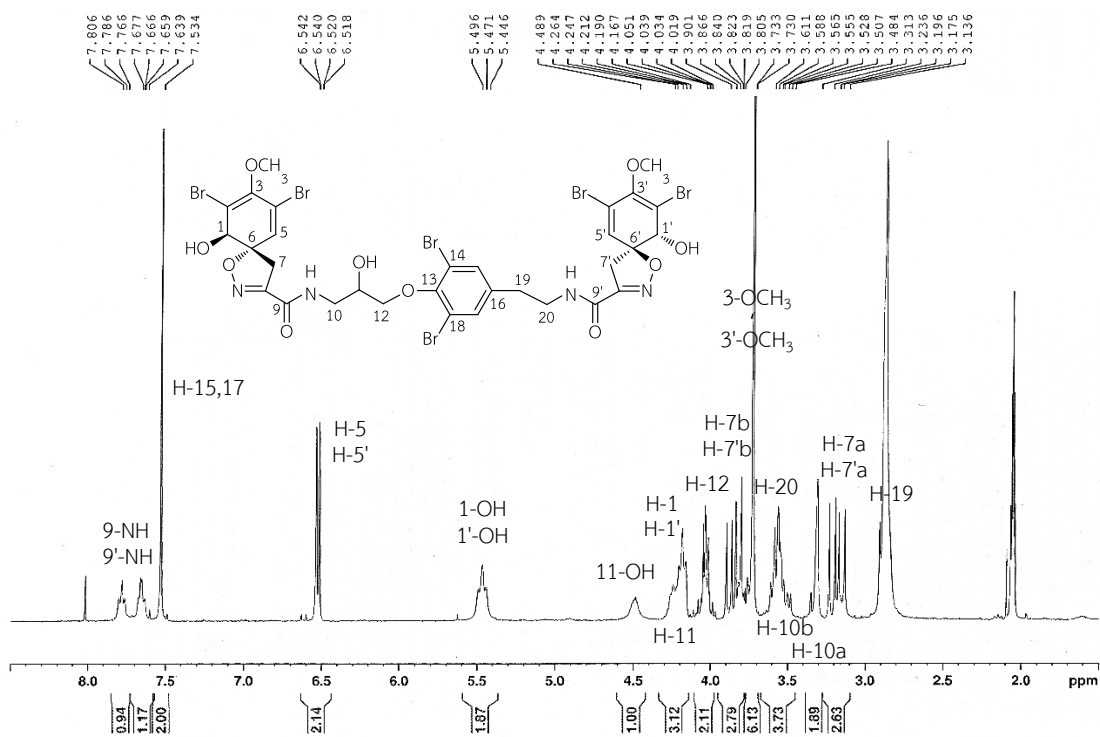


Figure B29 ^1H NMR spectrum (300 MHz) of 19-deoxyfistularin 3 (B12) in acetone- d_6

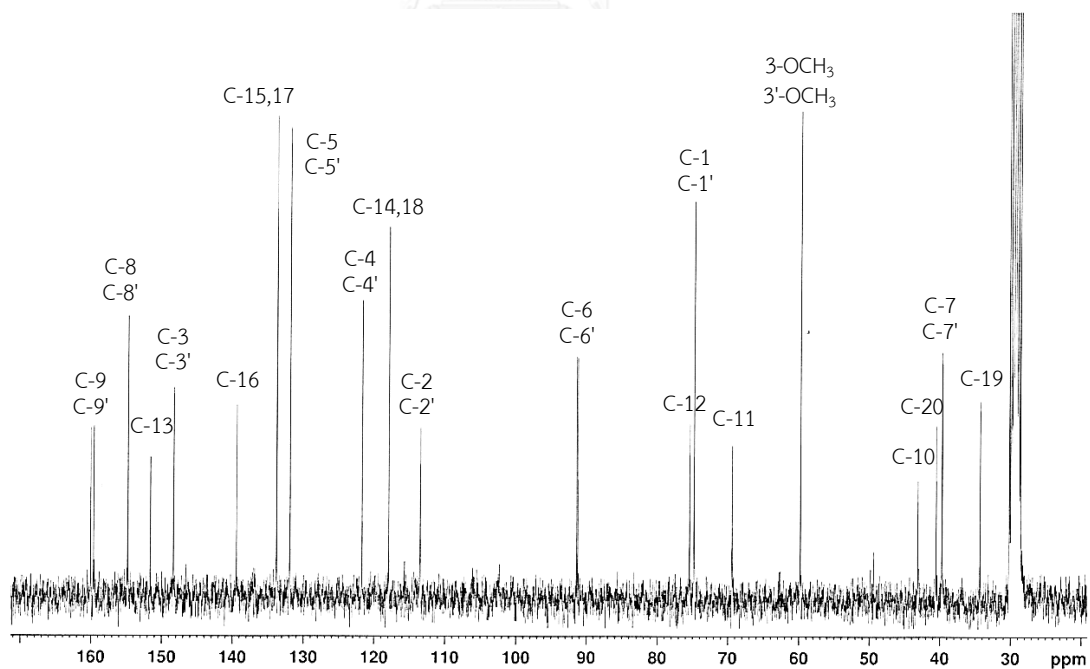
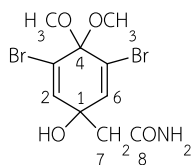


Figure B30 ^{13}C NMR spectrum (75 MHz) of 19-deoxyfistularin 3 (B12) in acetone- d_6



3,5-dibromo-1-hydroxy-4,4-dimethoxy-2,5-cyclohexadiene-1-acetamide (B13):

8.12 g, 11.975% yield of EtOAc extract.

White crystal.

^1H NMR (DMSO- d_6 , 300 MHz) δ 7.40 and 6.99 (each 1H, br s, NH_2), 6.80 (2H, s, H-2 and H-6), 6.01 (1H, br s, 1-OH), 3.04 and 2.97 (each 3H, s, 4- $\text{OCH}_3 \times 2$), 2.40 (2H, s, H_2 -7).

^{13}C NMR (DMSO- d_6 , 75 MHz) δ 171.0 (C, C-8), 143.6 (CH, C-2 and C-6), 121.4 (C, C-3 and C-5), 97.5 (C, C-4), 71.4 (C, C-1), 51.6 and 51.3 (CH_3 , 4- $\text{OCH}_3 \times 2$), 47.5 (CH_2 , C-7).

EIMS: m/z 369 $[\text{M}]^+$ (calcd for $\text{C}_{10}\text{H}_{13}\text{Br}_2\text{NO}_4$, 368.9211).

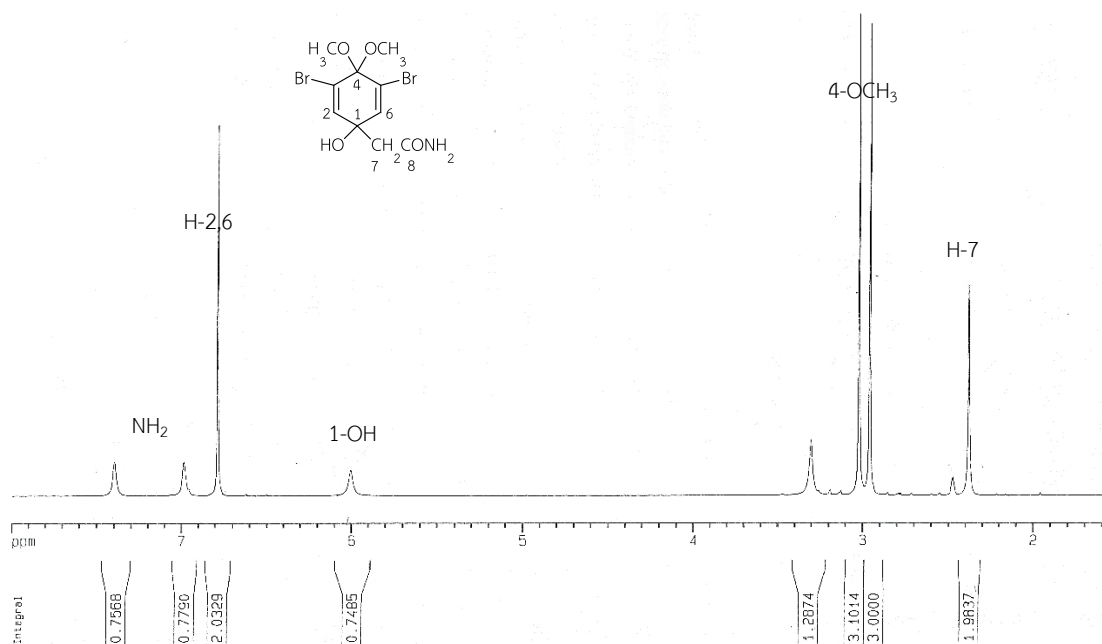


Figure B31 ¹H NMR spectrum (300 MHz) of 3,5-dibromo-1-hydroxy-4,4-dimethoxy-2,5-cyclohexadiene-1-acetamide (**B13**) in DMSO-*d*₆

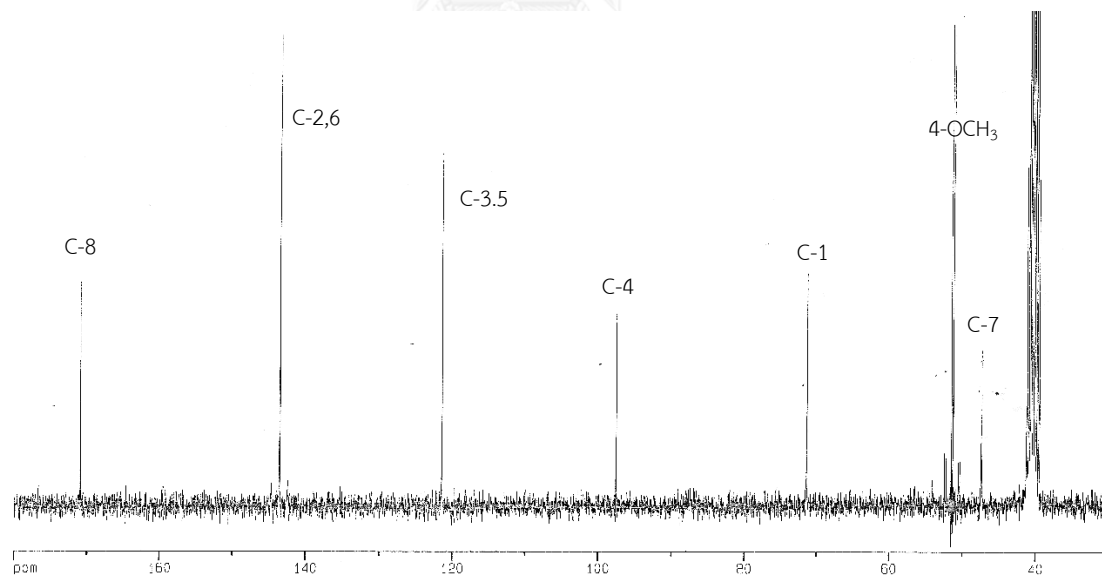
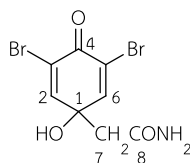


Figure B32 ¹³C NMR spectrum (75 MHz) of 3,5-dibromo-1-hydroxy-4,4-dimethoxy-2,5-cyclohexadiene-1-acetamide (**B13**) in DMSO-*d*₆



Verongiaquinol (B14):

8.1 mg, 0.012% yield of EtOAc extract.

White amorphous powder.

UV λ_{\max} (MeOH) nm (log ϵ): 258 (3.87).

^1H NMR (DMSO- d_6 , 500 MHz) δ 7.58 (2H, s, H-2 and H-6), 7.41 and 6.95 (each 1H, br s, NH_2), 6.37 (1H, s, 1-OH), 2.58 (2H, s, H_2 -7).

^{13}C NMR (DMSO- d_6 , 125 MHz) δ 172.5 (C, C-4), 169.4 (C, C-8), 153.6 (CH, C-2 and C-6), 119.2 (C, C-3 and C-5), 72.0 (C, C-1), 45.2 (CH_2 , C-7).

HREIMS: m/z 322.8794 [M] $^+$ (calcd for $\text{C}_8\text{H}_7\text{Br}_2\text{NO}_3$, 322.8793).

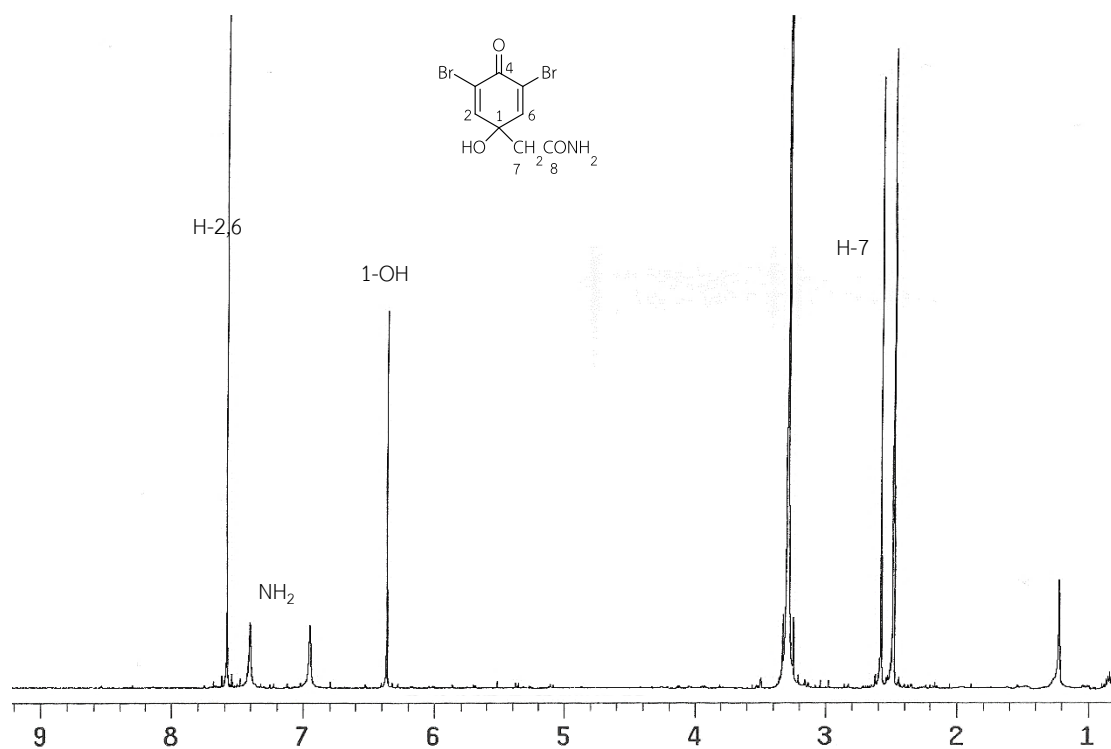


Figure B33 ^1H NMR spectrum (500 MHz) of verongiaquinol (B14) in $\text{DMSO-}d_6$

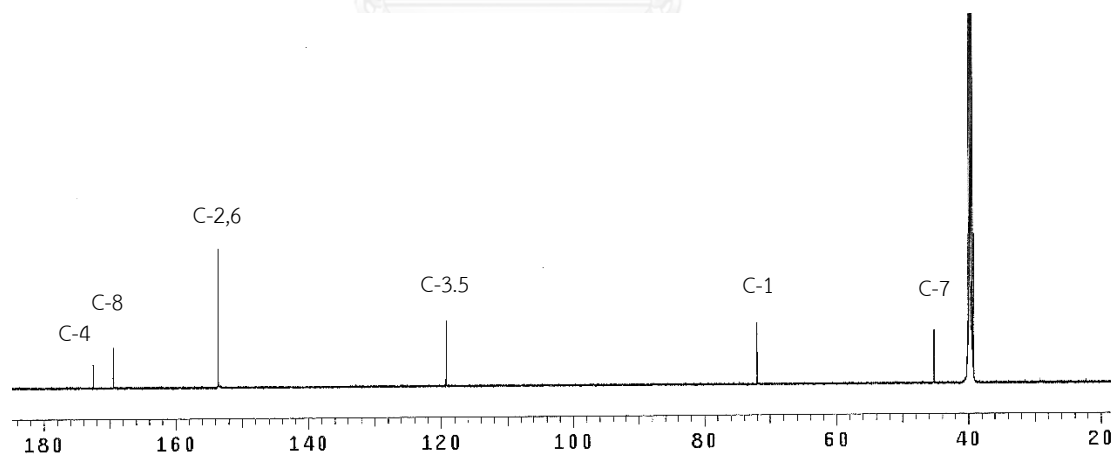
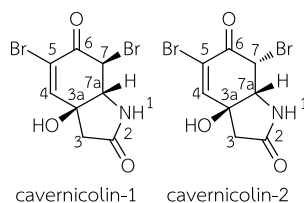


Figure B34 ^{13}C NMR spectrum (125 MHz) of verongiaquinol (B14) in $\text{DMSO-}d_6$



Cavernicolin-1 (B15) and cavernicolin-2 (B16)

An epimeric mixture, 39.5 mg, 0.058% yield of EtOAc extract.

White amorphous powder.

UV λ_{\max} (MeOH) nm (log ϵ): 257 (3.84).

^1H NMR (300 MHz, acetone- d_6) of **B15**: δ 7.65 (1H, br, NH), 7.45 (1H, s, H-4), 5.52 (1H, s, OH), 5.18 (1H, d, $J = 10.2$ Hz, H-7), 4.21 (1H, d, $J = 10.2$ Hz, H-7a), 2.91 and 2.47 (each 1H, d, $J = 16.5$ Hz, H-3).

^1H NMR (300 MHz, acetone- d_6) of **B16**: δ 7.33 (1H, s, H-4), 7.21 (1H, br, NH), 5.67 (1H, s, OH), 5.34 (1H, d, $J = 3.9$ Hz, H-7), 4.45 (1H, d, $J = 3.9$ Hz, H-7a), 2.74 and 2.57 (each 1H, d, $J = 17.1$ Hz, H-3).

^{13}C NMR (75 MHz, acetone- d_6) of **B15**: δ 183.5 (C-6), 174.3 (C-2), 150.2 (C-4), 120.4 (C-5), 76.5 (C-3a), 69.0 (C-7a), 53.3 (C-7), 43.1 (C-3).

^{13}C NMR (75 MHz, acetone- d_6) of **B16**: δ 183.9 (C-6), 173.2 (C-2), 149.2 (C-4), 120.5 (C-5), 75.5 (C-3a), 64.8 (C-7a), 56.8 (C-7), 45.1 (C-3).

HREIMS: m/z 322.8790 $[\text{M}]^+$ (calcd for $\text{C}_8\text{H}_7\text{Br}_2\text{NO}_3$, 322.8793).

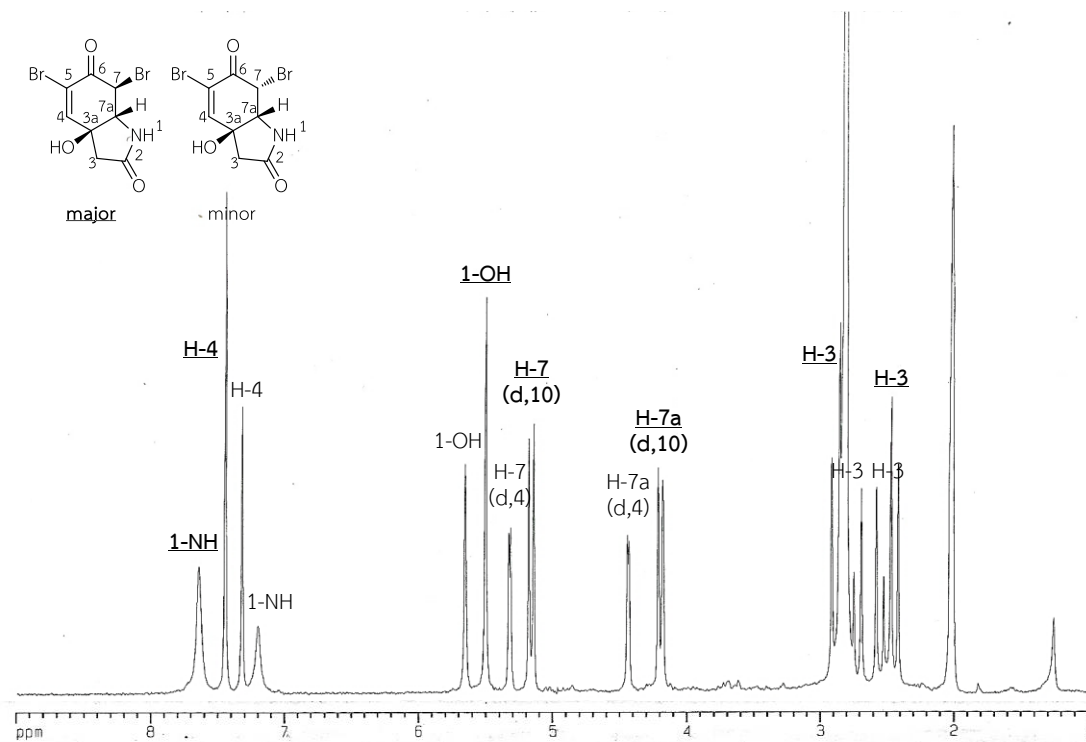


Figure B35 ^1H NMR spectrum (300 MHz) of cavemicolins-1 and -2 (B15 and B16) mixture in acetone- d_6

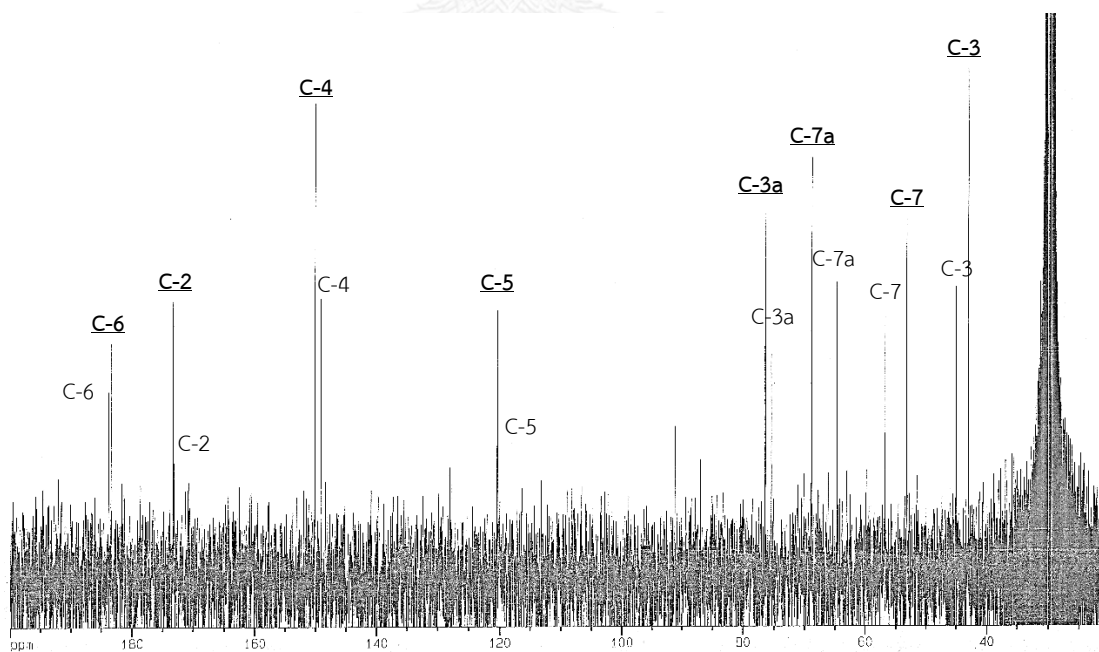
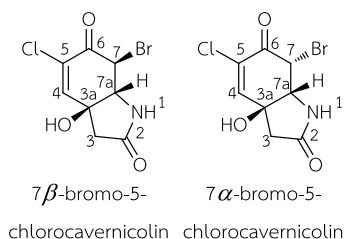


Figure B36 ^{13}C NMR spectrum (75 MHz) of cavemicolins-1 and -2 (B15 and B16) mixture in acetone- d_6



7β -Bromo-5-chlorocavernicolins (B17) and 7α -bromo-5-chlorocavernicolin (B18)

An epimeric mixture, 24.8 mg, 0.037% yield of EtOAc extract.

White amorphous powder.

UV λ_{\max} (MeOH) nm (log ϵ): 247 (3.71).

^1H NMR (500 MHz, DMSO- d_6) of **B17**: δ 8.55 (1H, br, NH), 7.21 (1H, s, H-4), 6.23 (1H, d, $J = 0.6$ Hz, OH), 5.36 (1H, d, $J = 10.2$ Hz, H-7), 3.94 (1H, dd, $J = 10.2, 2.1$ Hz, H-7a), 2.84 and 2.25 (each 1H, d, $J = 17.1$ Hz, H-3).

^1H NMR (500 MHz, DMSO- d_6) of **B18**: δ 8.14 (1H, br, NH), 7.11 (1H, s, H-4), 6.29 (1H, s, OH), 5.22 (1H, d, $J = 3.9$ Hz, H-7), 4.21 (1H, d, $J = 3.9$ Hz, H-7a), 2.63 and 2.44 (each 1H, d, $J = 17.1$ Hz, H-3).

^{13}C NMR (125 MHz, DMSO- d_6) of **B17**: δ 183.6 (C-6), 173.7 (C-2), 146.5 (C-4), 128.1 (C-5), 74.5 (C-3a), 68.1 (C-7a), 58.3 (C-7), 42.5 (C-3).

^{13}C NMR (125 MHz, DMSO- d_6) of **B18**: δ 183.7 (C-6), 173.2 (C-2), 145.2 (C-4), 127.5 (C-5), 73.3 (C-3a), 63.3 (C-7a), 53.5 (C-7), 44.4 (C-3).

HREIMS: m/z 278.9296 $[\text{M}]^+$ (calcd for $\text{C}_8\text{H}_7\text{BrClNO}_3$, 278.9298).

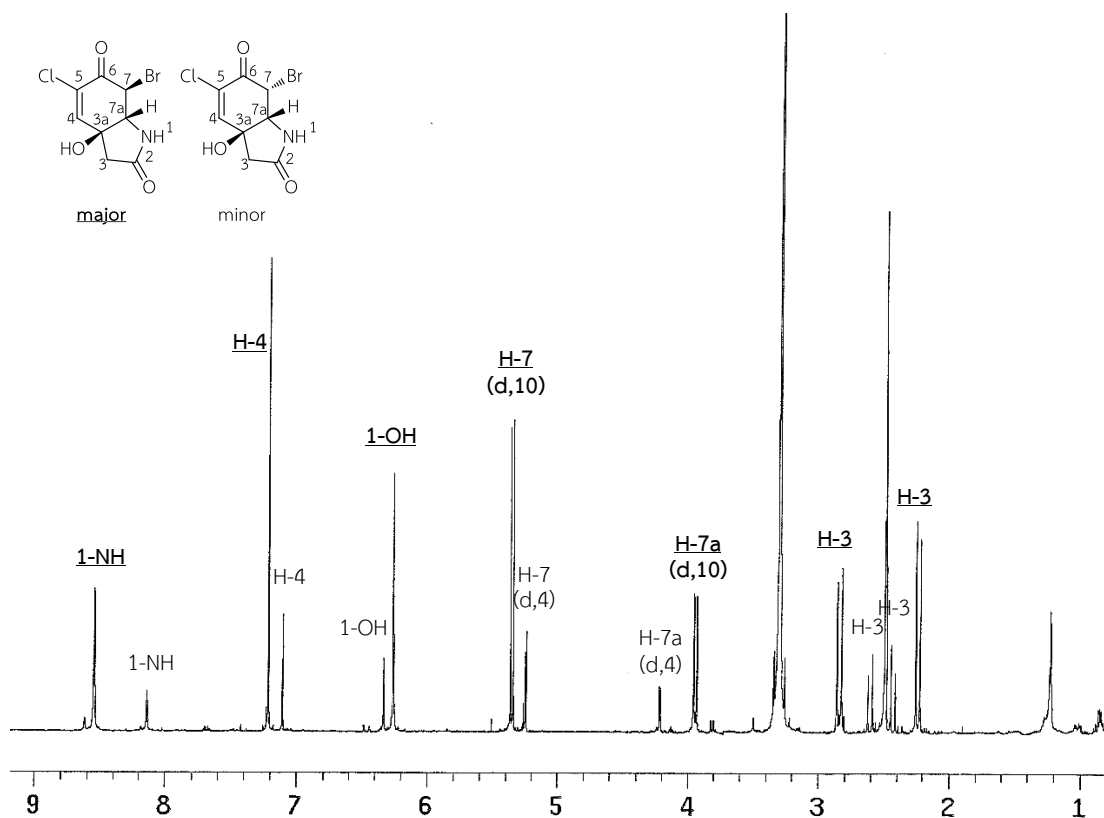


Figure B37 ^1H NMR spectrum (500 MHz) of 7β - and 7α -bromo-5-chlorocavernicolins (B17 and B18) mixture in $\text{DMSO-}d_6$

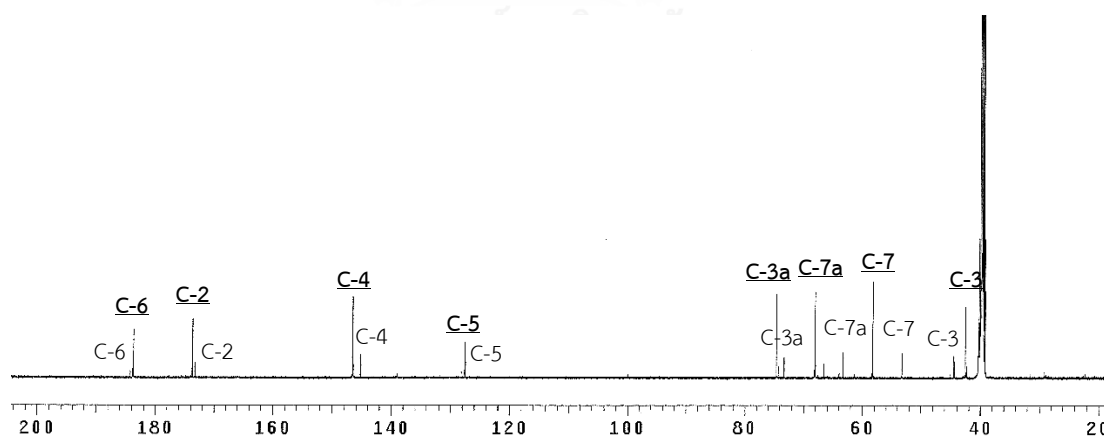


Figure B38 ^{13}C NMR spectrum (125 MHz) of 7β - and 7α -bromo-5-chlorocavernicolins (B17 and B18) mixture in $\text{DMSO-}d_6$.

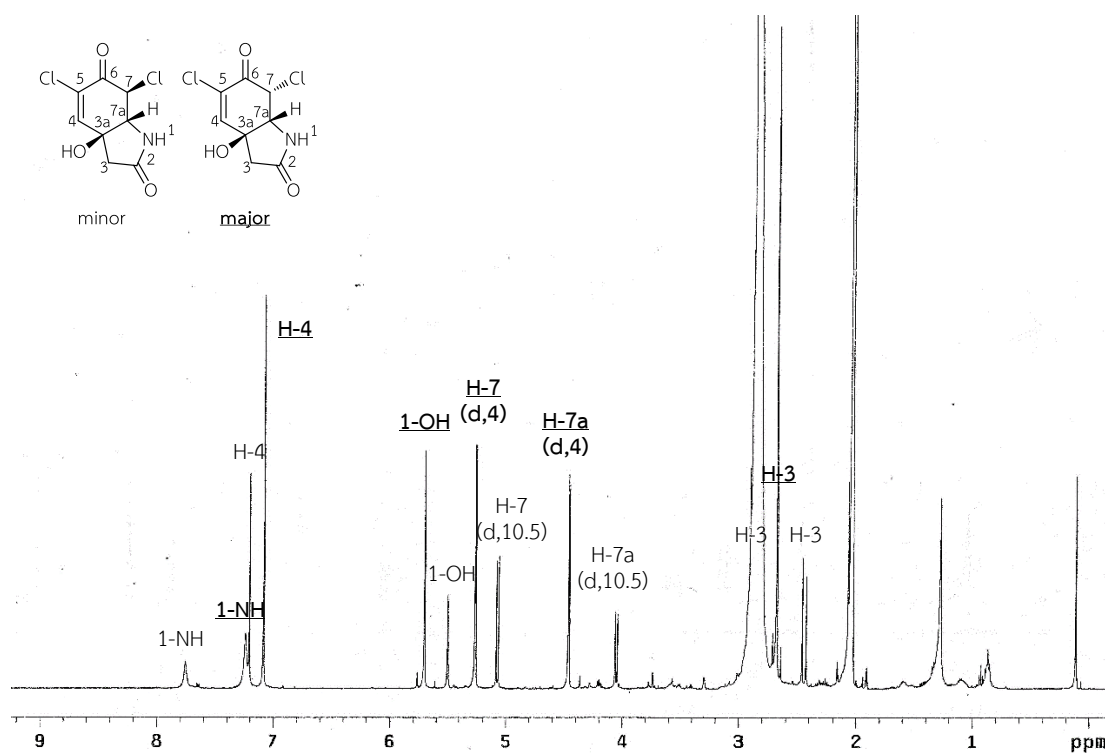


Figure B39 ^1H NMR spectrum (500 MHz) of 5,7 β - and 5,7 α -dichlorocavernicolins (B19 and B20) mixture in acetone- d_6

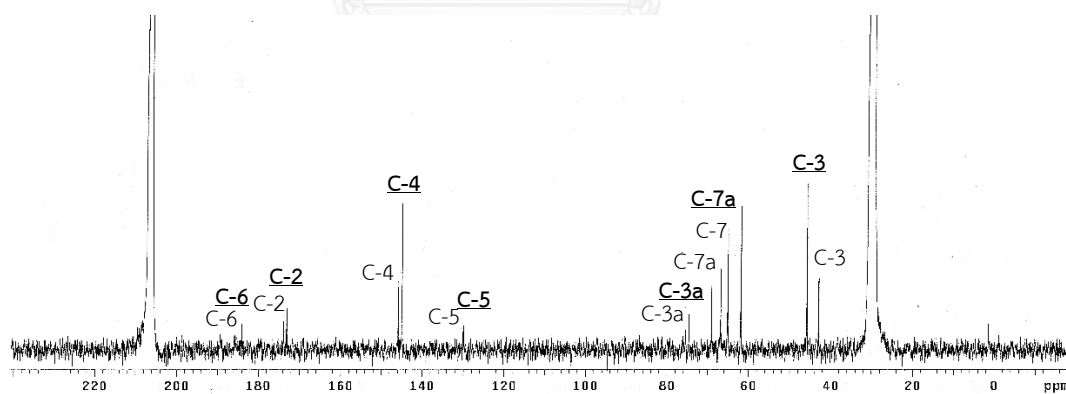
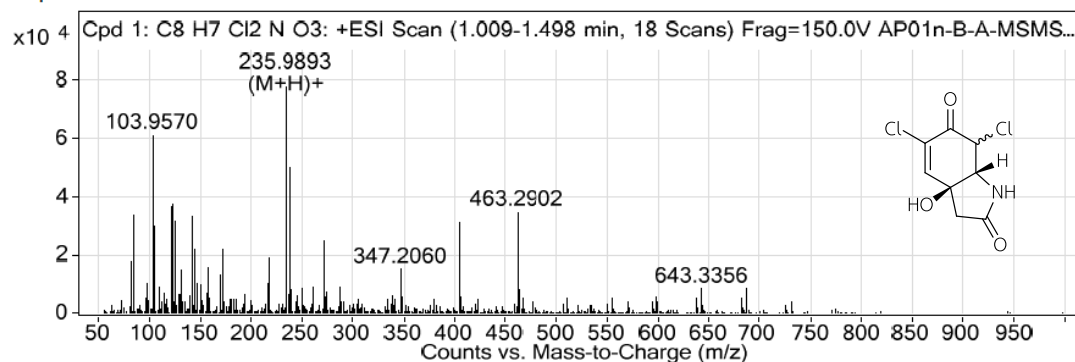


Figure B40 ^{13}C NMR spectrum (125 MHz) of 5,7 β - and 5,7 α -dichlorocavernicolins (B19 and B20) mixture in acetone- d_6

MS Spectrum



MS Zoomed Spectrum

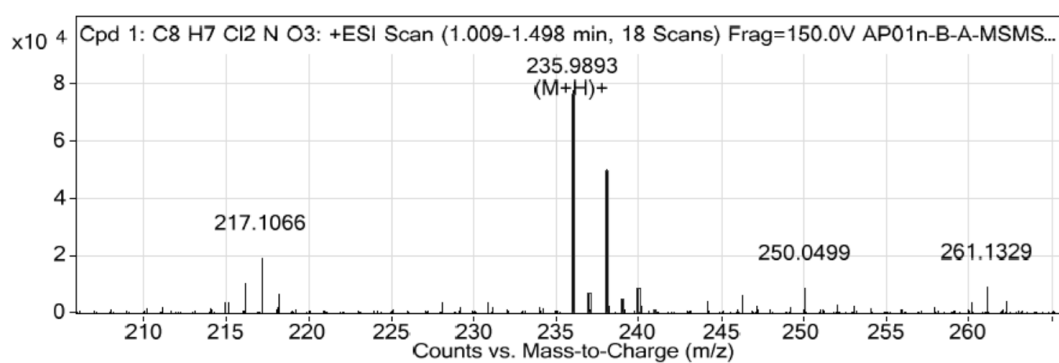


Figure B41 HRESIMS spectrum of 5,7 β - and 5,7 α -dichlorocavernicolins (B19 and B20) mixture

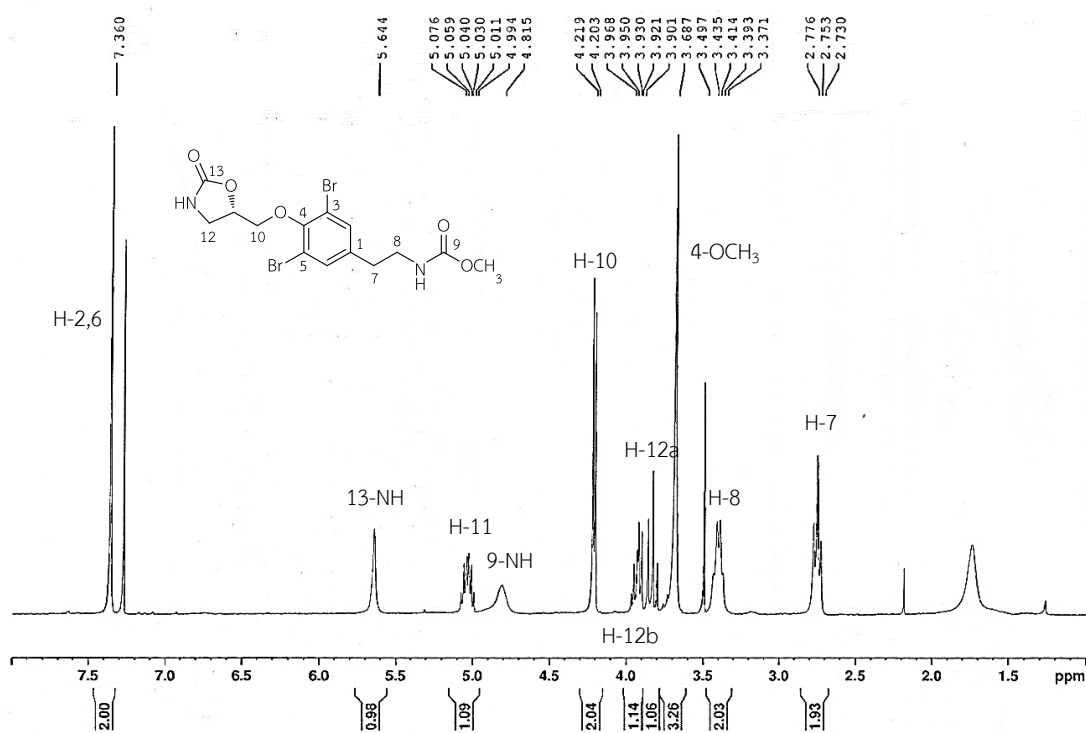


Figure B42 ^1H NMR spectrum (300 MHz) of 11S-acanthodendrilline [(S)-B21] in CDCl_3

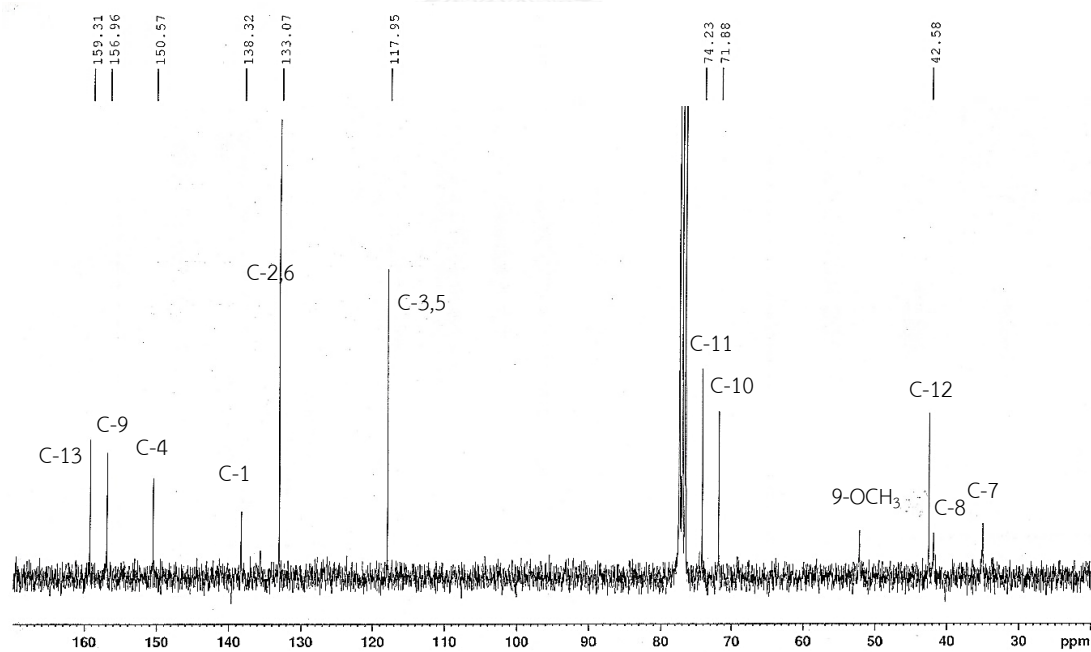


Figure B43 ^{13}C NMR spectrum (75 MHz) of 11S-acanthodendrilline [(S)-B21] in CDCl_3

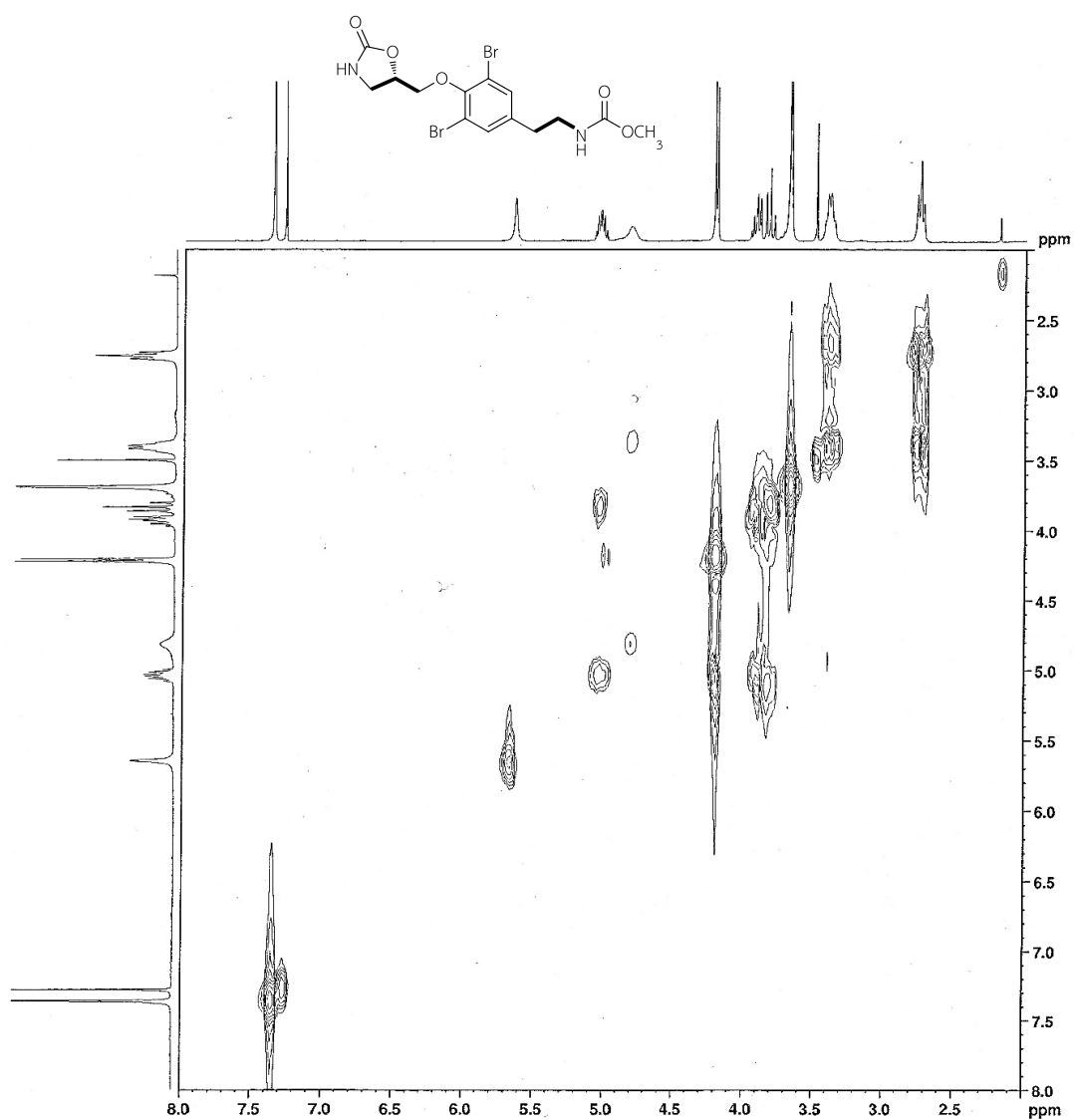


Figure B44 ^1H - ^1H COSY spectrum (300 MHz) of 11S-acanthodendrilline [(S)-B21] in CDCl_3

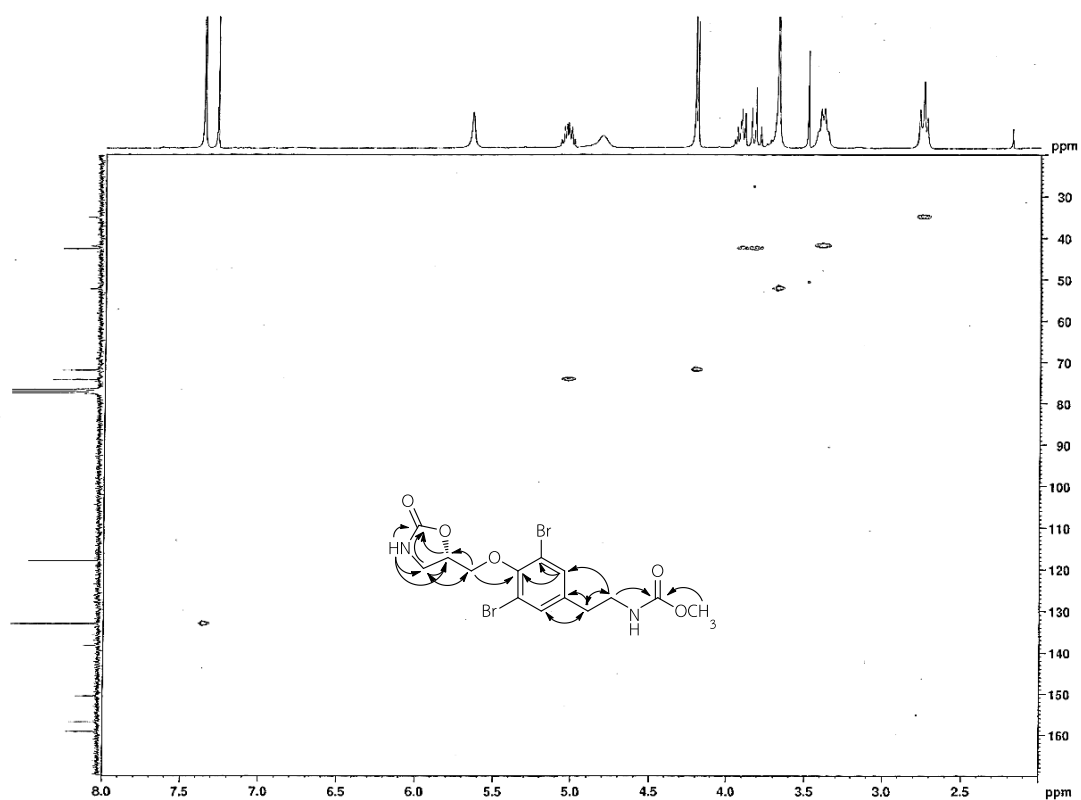


Figure B45 HSQC spectrum (300 MHz) of 11S-acanthodendrilline [(S)-B21] in CDCl₃

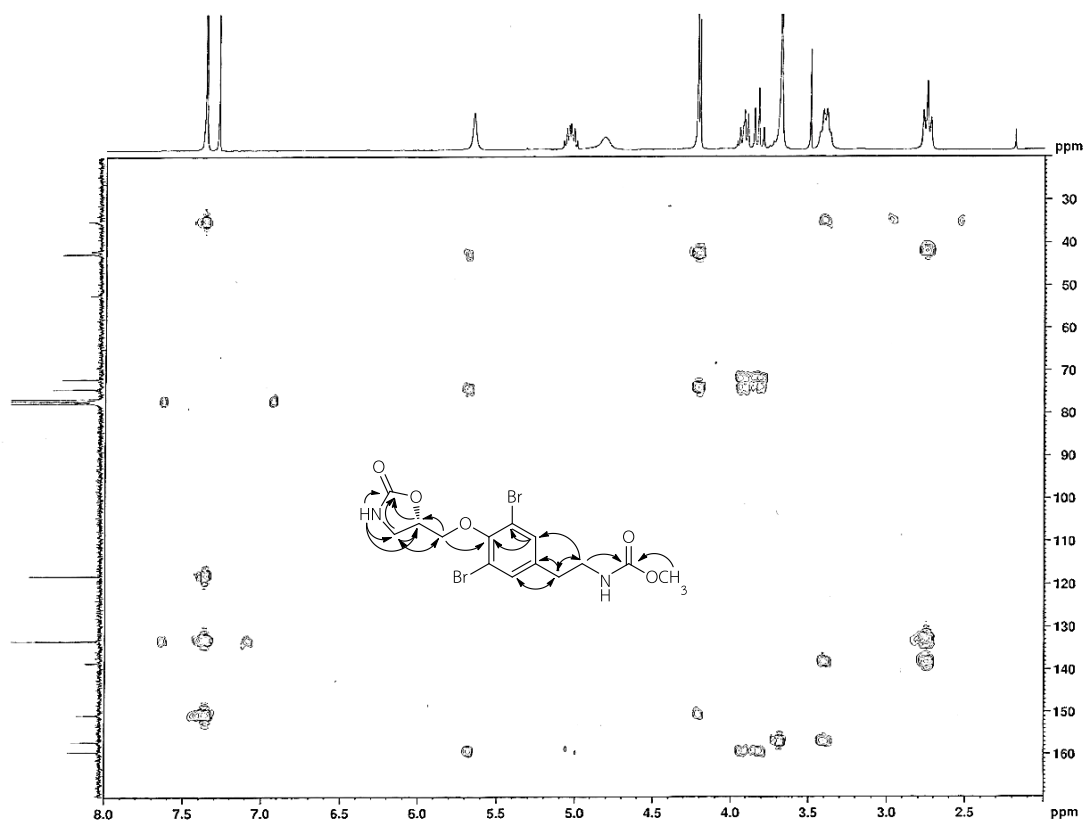


Figure B46 HMBC spectrum (300 MHz) of 11S-acanthodendrilline [(S)-B21] in CDCl₃

[Elemental Composition]

Data : 469FH001

Date : 11-Nov-2013 18:39

Sample: AP01-CD

Note : -

Inlet : Direct

Ion Mode : FAB+

RT : 7.08 min

Scan#: (31,35)

Elements : C 40/5, H 40/5, O 8/2, N 2/0, Br 2/1

Mass Tolerance : 5mmu

Unsaturation (U.S.) : 0.0 - 10.0

Observed m/z	Int%	Err[ppm / mmu]	U.S.	Composition
450.9512	52.1	+1.7 / +0.8	6.5	C 14 H 17 O 5 N 2 Br 2

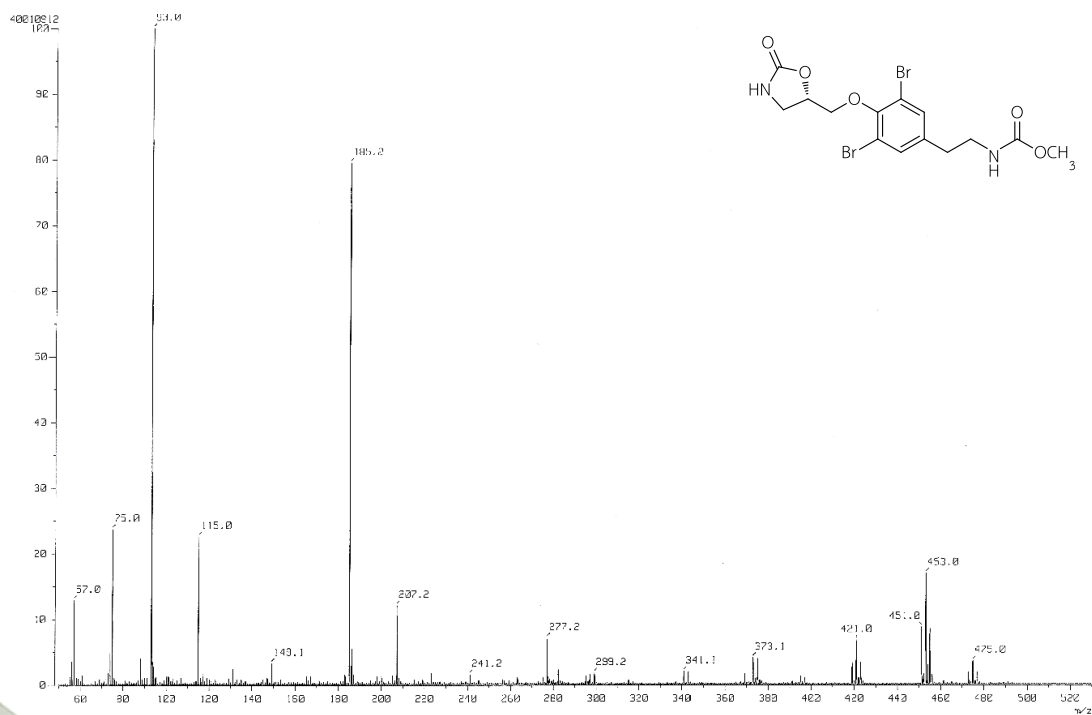


Figure B47 HRFABMS spectrum of 11S-acanthodendrilline [(S)-B21]

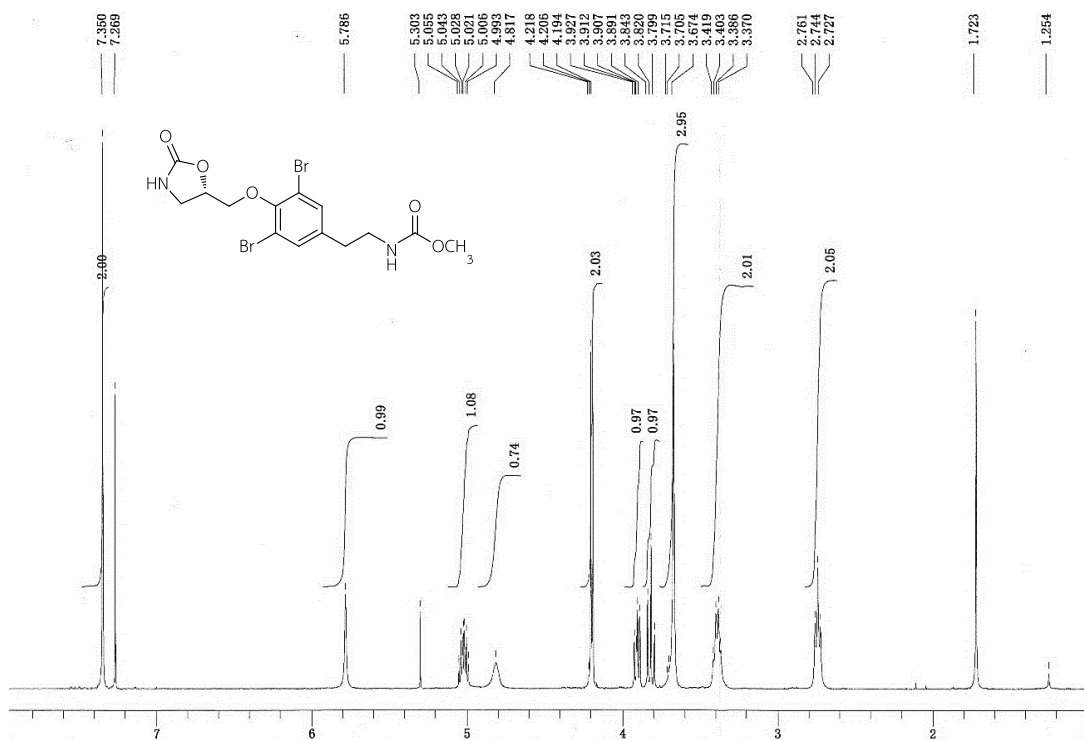


Figure B48 ¹H NMR spectrum (400 MHz) of synthetic acanthodendrin [(S)-B21] in CDCl₃

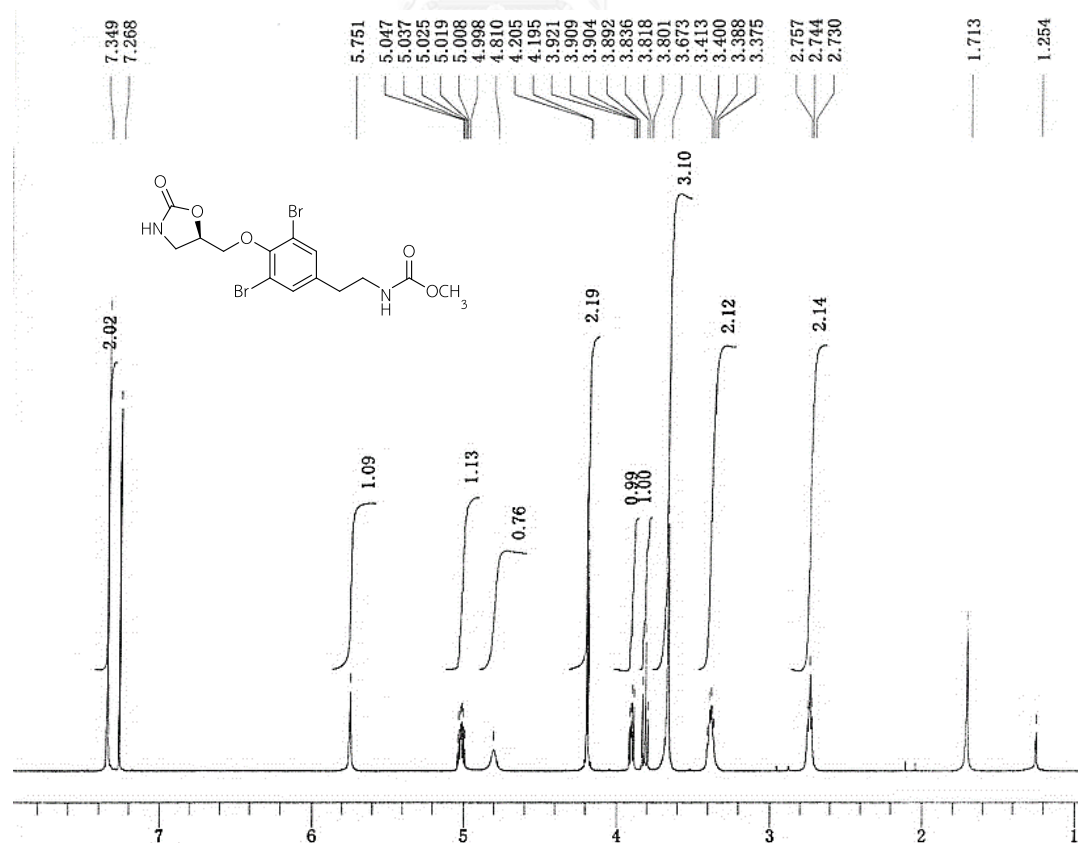
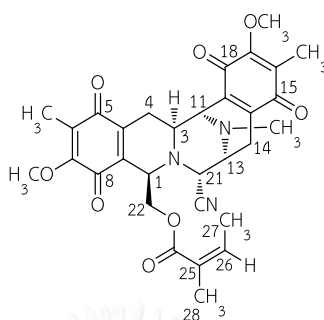


Figure B49 ¹H NMR spectrum (400 MHz) of synthetic acanthodendrin [(R)-B21] in CDCl₃

APPENDIX C

PHYSICAL AND SPECTROSCOPIC DATA OF RENIARAMYCIN DERIVATIVES



Renieramycin M: orange prisms; ¹H NMR (CDCl₃, 300 MHz) δ 5.96 (1H, qq, $J = 7.4, 1.5$ Hz, 26-H), 4.54 (1H, dd, $J = 11.7, 3.0$ Hz, H-22b), 4.10 (1H, dd, $J = 11.7, 2.7$ Hz, H-22a), 4.07 (1H, d, $J = 2.4$ Hz, H-21), 4.02 (2H, overlapped, H-1 and H-11), 4.02 and 3.99 (each 3H, each s, 7-OCH₃ and 17-OCH₃), 3.40 (1H, ddd, $J = 7.5, 2.4, 1.8$ Hz, H-13), 3.11 (1H, ddd, $J = 11.4, 3.0, 2.6$ Hz, H-3), 2.89 (1H, dd, $J = 17.3, 2.6$ Hz, H-4 α), 2.76 (1H, dd, $J = 20.8, 7.5$ Hz, H-14 α), 2.30 (1H, d, $J = 20.8$ Hz, H-14 β), 2.28 (3H, s, NCH₃), 1.94 and 1.90 (each 3H, each s, 6-CH₃ and 16-CH₃), 1.82 (3H, dq, $J = 7.4, 1.5$ Hz, 27-CH₃), 1.58 (3H, dq, $J = 1.5, 1.2$ Hz, 28-CH₃), 1.36 (1H, ddd, $J = 17.3, 11.4, 2.7$ Hz, H-4 β).

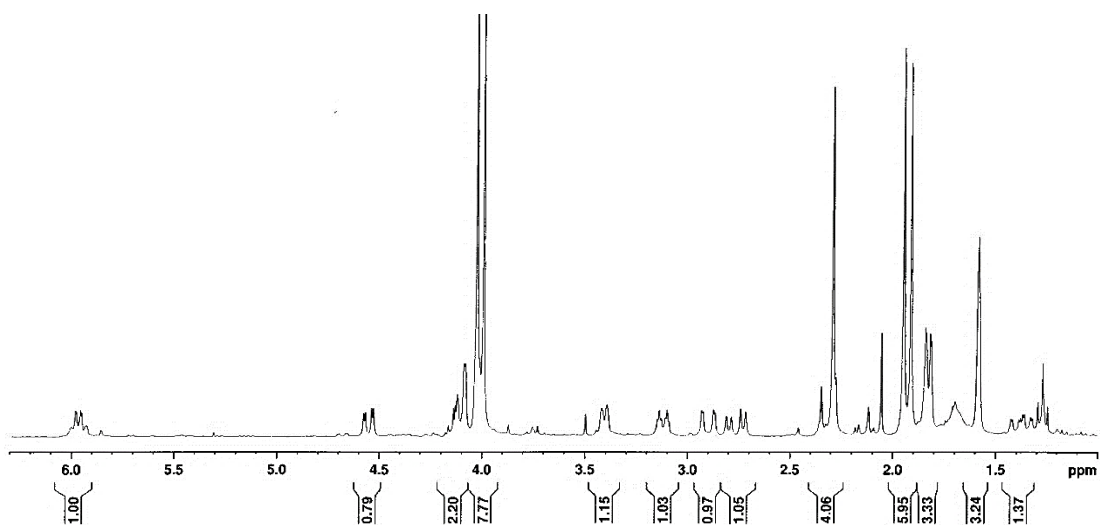
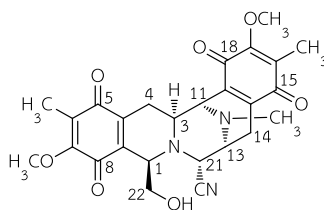


Figure C1 ¹H NMR spectrum (300 MHz) of renieramycin M (RM)



Jorunnamycin A: yield 44.0%; yellow amorphous powder; ^1H NMR (CDCl_3 , 500 MHz) δ 4.14 (1H, d, $J = 2.1$ Hz, H-21), 4.08 (1H, d, $J = 2.7$ Hz, H-11), 4.03 and 3.99 (each 3H, each s, 7-OCH₃ and 17-OCH₃), 3.89 (1H, br d, $J = 2.4$ Hz, H-1), 3.71 (1H, dd, $J = 11.6, 2.6$ Hz, H-22b), 3.49 (1H, br, H-22a), 3.42 (1H, br d, $J = 7.5$ Hz, H-13), 3.18 (1H, ddd, $J = 11.7, 2.7, 2.3$ Hz, H-3), 2.93 (1H, dd, $J = 17.4, 2.3$ Hz, H-4 α), 2.83 (1H, dd, $J = 21.2, 7.5$ Hz, H-14 α), 2.31 (3H, s, NCH₃), 2.27 (1H, d, $J = 21.2$ Hz, H-14 β), 1.94 (6H, s, 6-CH₃ and 16-CH₃), 1.41 (1H, ddd, $J = 17.4, 11.7, 2.1$ Hz, H-4 β).

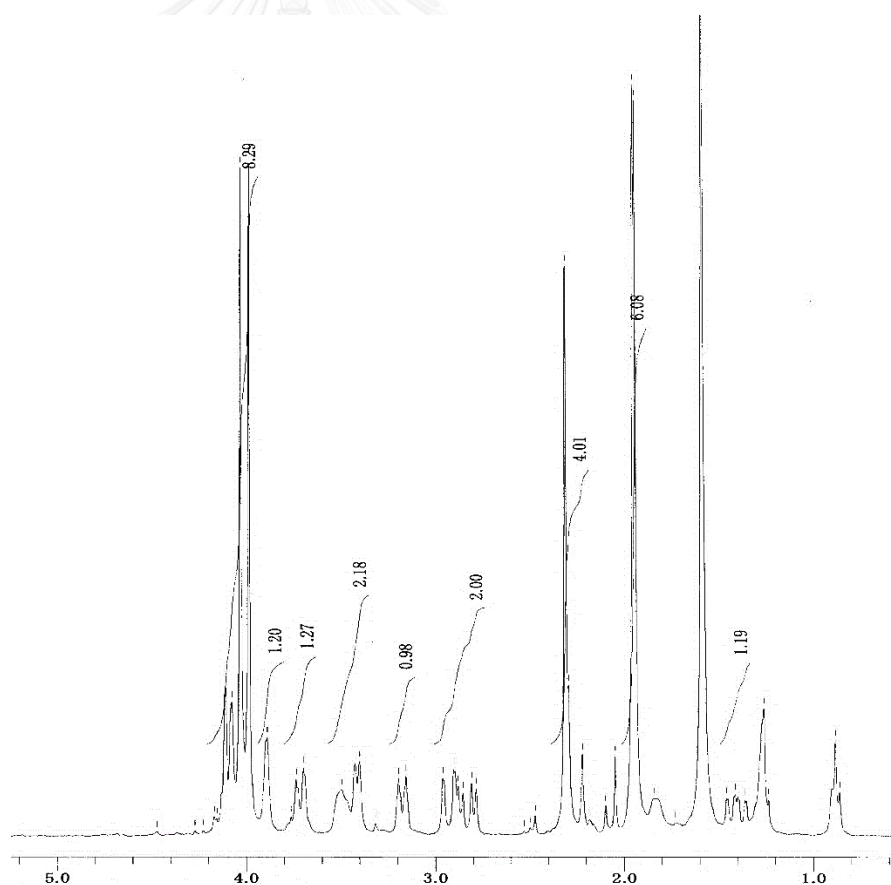
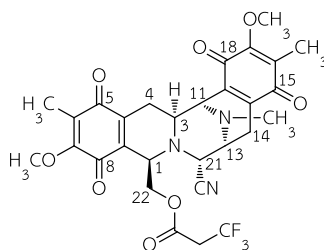


Figure C2 ^1H NMR spectrum (500 MHz) of jorunnamycin A (JA)



22-O-(3,3,3-Trifluoropropionyl)jorunnamycin A (R1): yield 78.5%; yellow amorphous solid; $[\alpha]_D^{23}$ -129.1 (c 0.1, CHCl_3); CD $\Delta\epsilon$ nm (c 13.3 μM , MeOH, 24°C) 0 (400), -6.5 (353), -3.1 (306), -21.4 (280), 0 (264), $+7.2$ (254), $+0.5$ (229), $+8.7$ (207); IR (KBr) ν_{max} 2955, 2926, 2855, 1751, 1655, 1618, 1375, 1298, 1263, 1236, 1150, 1121 cm^{-1} ; ^1H NMR (CDCl_3 , 500 MHz) δ 4.40 (1H, dd, $J = 11.8, 2.9$ Hz, H-22b), 4.23 (1H, dd, $J = 11.8, 3.4$ Hz, H-22a), 4.04 (1H, d, $J = 2.3$ Hz, H-21), 4.03 (1H, overlapped, H-1), 4.03 (1H, overlapped, H-11), 4.003 (3H, s, 7-OCH₃), 3.997 (3H, s, 17-OCH₃), 3.41 (1H, ddd, $J = 7.7, 2.3, 1.7$ Hz, H-13), 3.11 (1H, ddd, $J = 11.5, 2.9, 2.0$ Hz, H-3), 2.97 (2H, qd, $J = 20.6, 3.5$, COCH₂CF₃), 2.90 (1H, dd, $J = 17.8, 2.0$ Hz, H-4 α), 2.78 (1H, dd, $J = 21.4, 7.7$ Hz, H-14 α), 2.30 (3H, s, NCH₃), 2.27 (1H, d, $J = 21.4$ Hz, H-14 β), 1.95 (3H, s, 6-CH₃), 1.94 (3H, s, 16-CH₃), 1.37 (1H, ddd, $J = 17.8, 11.5, 2.7$ Hz, H-4 β); ^{13}C NMR (CDCl_3 , 125 MHz) δ 186.4 (C, C-15), 185.2 (C, C-5), 182.4 (C, C-18), 181.0 (C, C-8), 163.4 (C, OCO), 155.6 (C, C-7), 155.4 (C, C-17), 142.0 (C, C-10), 141.8 (C, C-20), 135.0 (C, C-19), 134.6 (C, C-9), 128.8 (C, C-6 and C, C-16), 124.1 (C, CH₂CF₃), 116.7 (C, CN), 64.5 (CH₂, C-22), 61.1 (CH₃, 17-OCH₃), 60.9 (CH₃, 7-OCH₃), 58.7 (CH, C-21), 55.9 (CH, C-1), 54.5 (CH, C-13), 54.4 (CH, C-3), 54.1 (CH, C-11), 41.5 (CH₃, NCH₃), 39.5 (CH₂, CH₂CF₃), 25.1 (CH₂, C-4), 21.1 (CH₂, C-14), 8.8 (CH₃, 6-CH₃), 8.5 (CH₃, 16-CH₃); HREIMS m/z 603.1829 [M]⁺ (calcd for C₂₉H₂₈O₈N₃F₃, 603.1828).

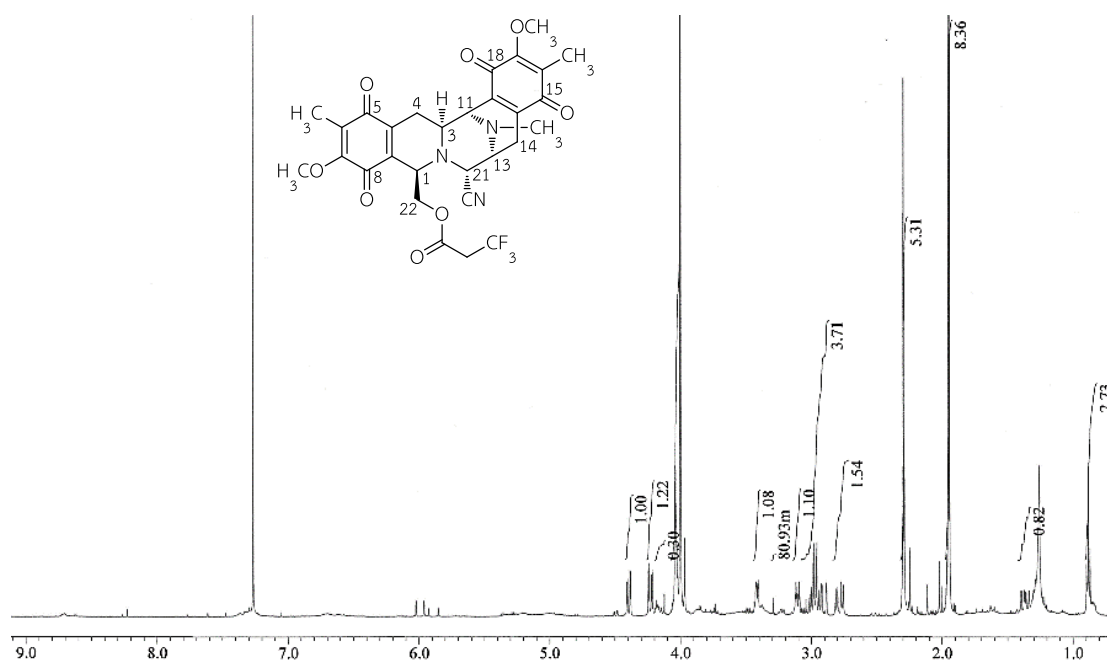


Figure C3 ¹H NMR spectrum (500 MHz) of 22-O-(3,3,3-trifluoropropionyl) jorunnamycin A (R1) in CDCl₃

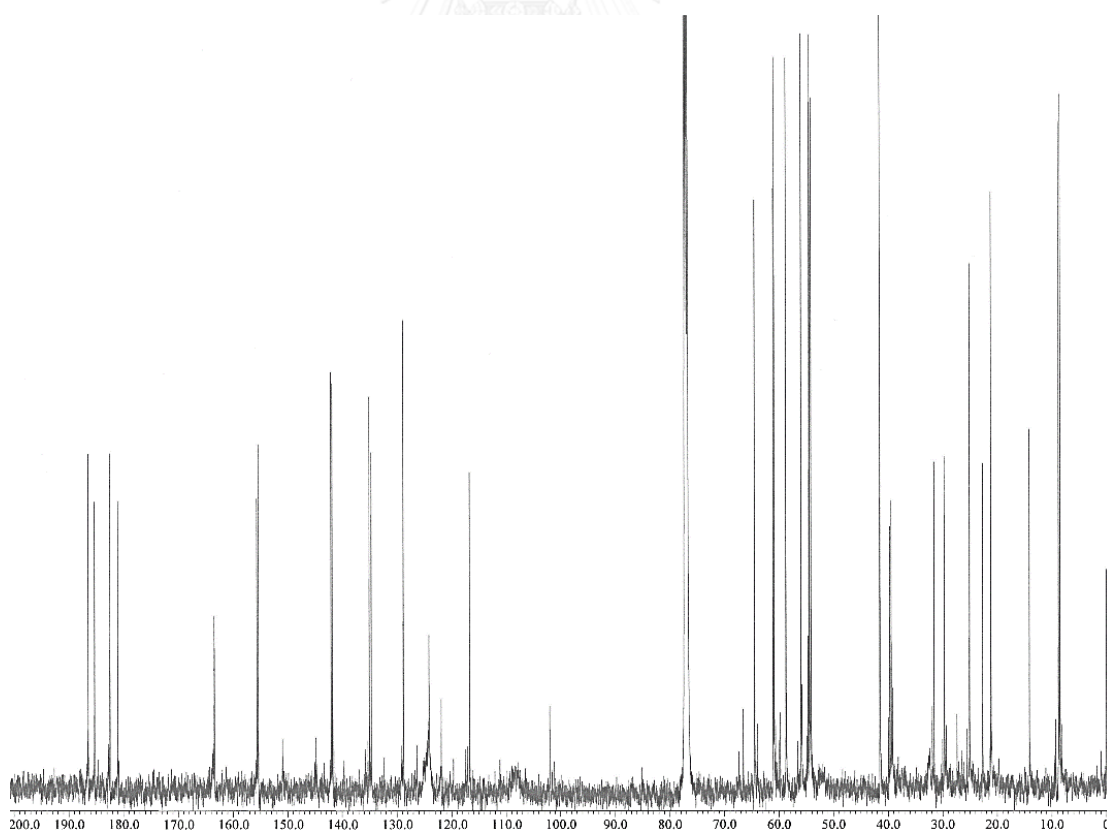


Figure C4 ¹³C NMR spectrum (125 MHz) of 22-O-(3,3,3-trifluoropropionyl) jorunnamycin A (R1) in CDCl₃

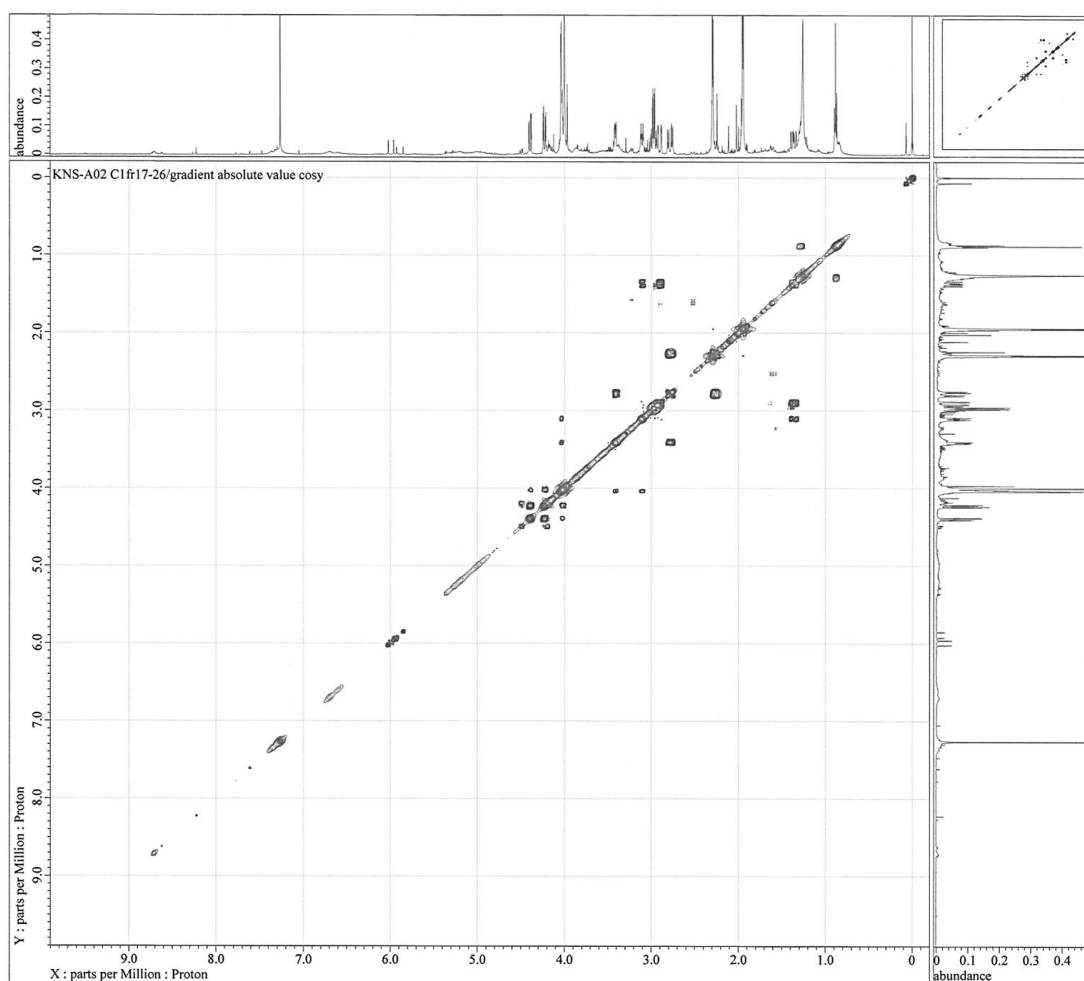


Figure C5 ^1H - ^1H COSY spectrum (500 MHz) of 22-O-(3,3,3-trifluoropropionyl) jorunnamycin A (**R1**) in CDCl_3

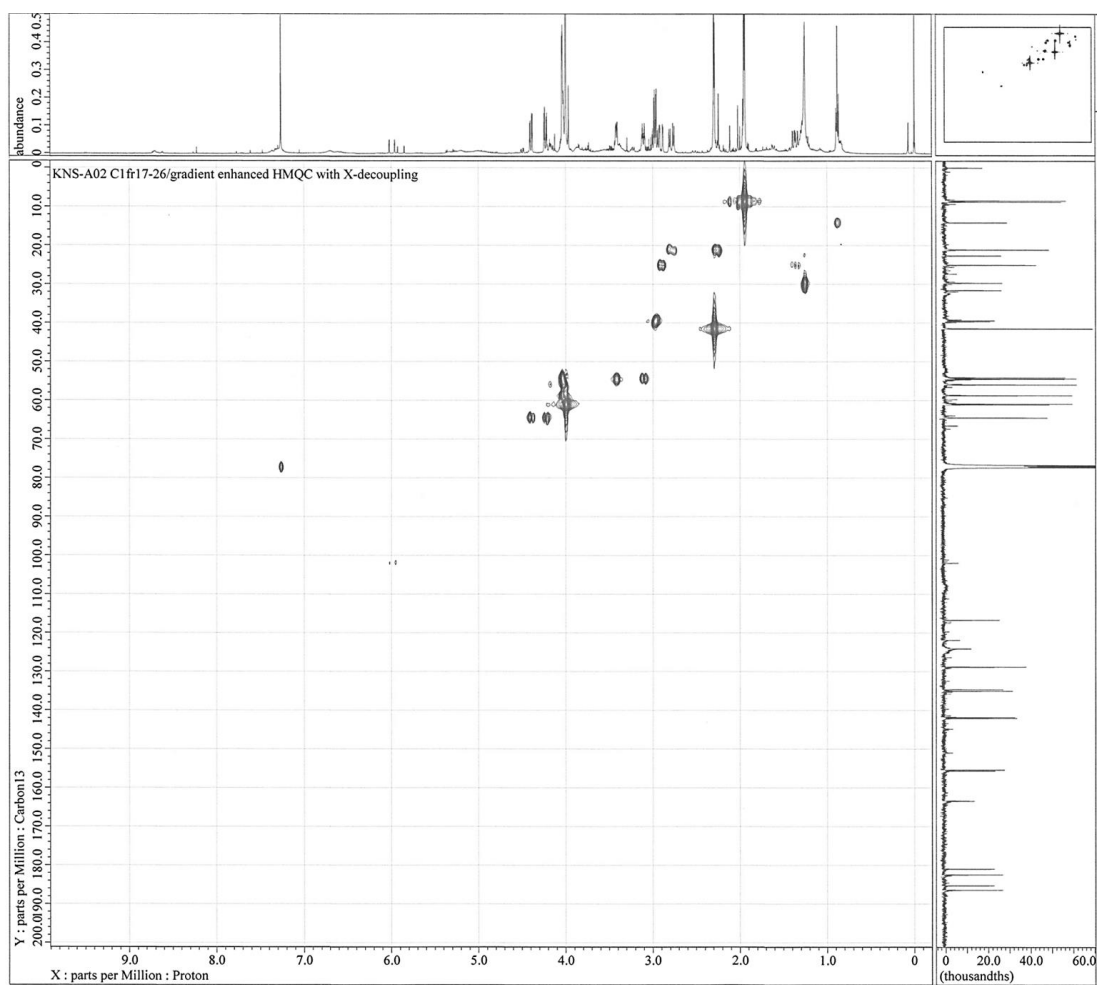


Figure C6 HMQC spectrum (500 MHz) of 22-O-(3,3,3-trifluoropropionyl)
jorunnamycin A (**R1**) in CDCl₃

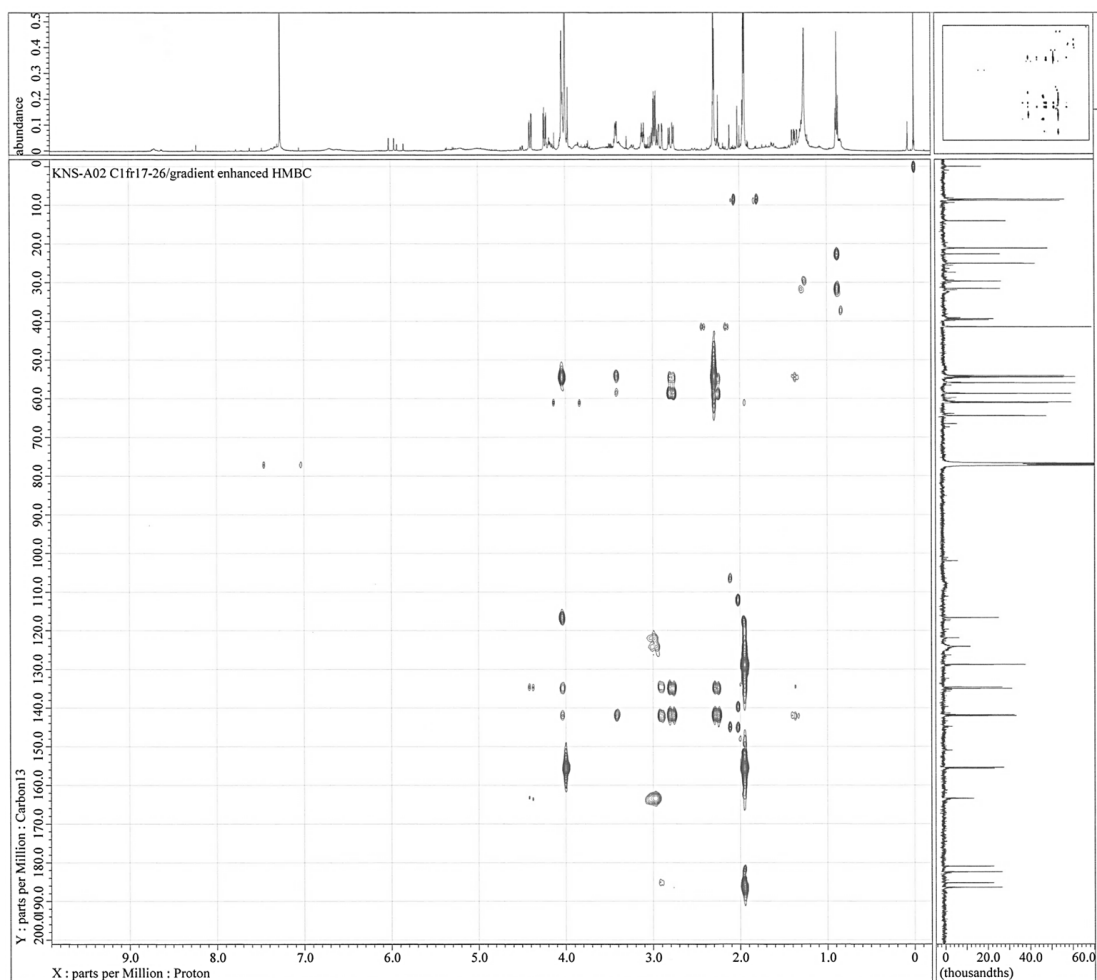


Figure C7 HMBC spectrum (500 MHz) of 22-O-(3,3,3-trifluoropropionyl)
jorunnamycin A (**R1**) in CDCl₃

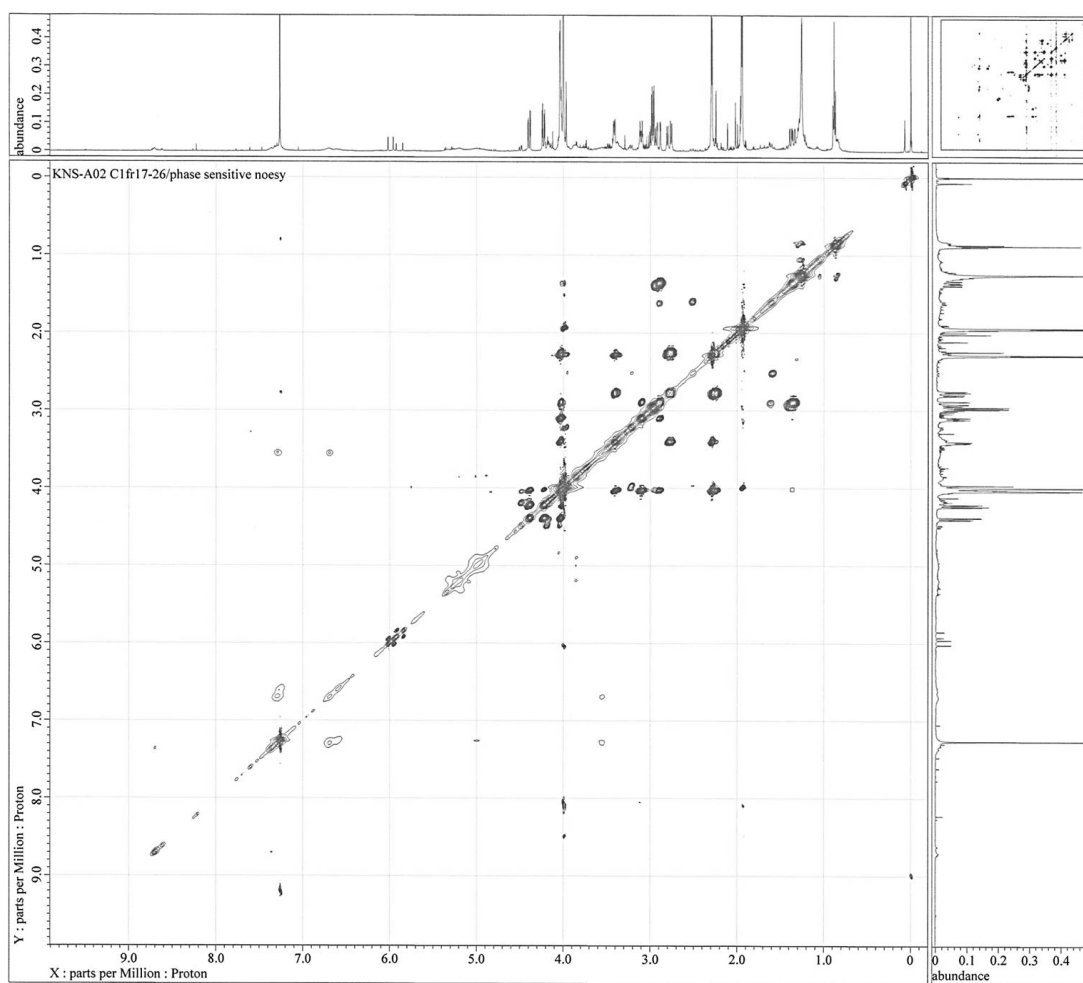
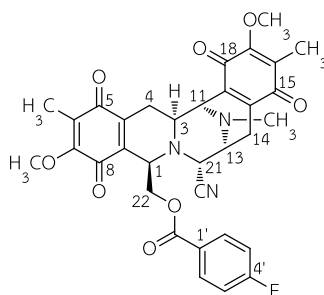


Figure C8 NOESY spectrum (500 MHz) of 22-O-(3,3,3-trifluoropropionyl) jorunnamycin A (**R1**) in CDCl₃



22-O-(4-Fluorobenzoyl)jorunnamycin A (R2): yield 72.1%; yellow amorphous solid; $[\alpha]_D^{24}$ -67.6 (c 0.3, CHCl_3); CD $\Delta\epsilon$ nm (c 9.8 μM , MeOH, 24°C) 0 (403), -5.7 (359), -2.5 (309), -13.9 (284), 0 (272), $+13.2$ (261), 0 (244), -6.1 (234), 0 (219), $+6.0$ (206), 0 (203), -11.6 (201); IR (KBr) ν_{max} 2959, 2940, 2855, 1721, 1655, 1614, 1605, 1508, 1450, 1373, 1310, 1263, 1234, 1153, 1117, 1090, 802, 766 cm^{-1} ; ^1H NMR (CDCl_3 , 500 MHz) δ 7.66 (2H, dd, $J = 8.9, 5.4$ Hz, H-2' and H-6'), 7.01 (2H, dd, $J = 8.9, 8.6$ Hz, H-3' and H-5'), 4.99 (1H, dd, $J = 11.6, 2.7$ Hz, H-22b), 4.10 (1H, dd, $J = 11.6, 2.3$ Hz, H-22a), 4.09 (1H, d, $J = 2.4$ Hz, H-21), 4.05 (3H, s, 7-OCH₃), 4.07 (1H, ddd, $J = 2.7, 2.6, 2.3$ Hz, H-1), 3.94 (1H, d, $J = 2.3$ Hz, H-11), 3.77 (3H, s, 17-OCH₃), 3.39 (1H, ddd, $J = 7.8, 2.4, 1.7$ Hz, H-13), 3.09 (1H, ddd, $J = 11.7, 2.6, 2.3$ Hz, H-3), 2.90 (1H, dd, $J = 17.6, 2.6$ Hz, H-4 α), 2.71 (1H, dd, $J = 21.2, 7.8$ Hz, H-14 α), 2.35 (1H, d, $J = 21.2$ Hz, H-14 β), 2.22 (3H, s, NCH₃), 2.00 (3H, s, 6-CH₃), 1.75 (3H, s, 16-CH₃), 1.26 (1H, ddd, $J = 17.6, 11.7, 2.6$ Hz, H-4 β); ^{13}C NMR (CDCl_3 , 125 MHz) δ 185.8 (C, C-15), 185.2 (C, C-5), 182.2 (C, C-18), 181.1 (C, C-8), 165.7 (C, C-4'), 164.5 (C, OCO), 155.6 (C, C-7), 154.9 (C, C-17), 142.1 (C, C-10), 142.0 (C, C-20), 135.4 (C, C-9), 134.5 (C, C-19), 132.0 (CH, C-2' and C-6'), 128.7 (C, C-6), 128.1 (C, C-16), 125.4 (C, C-1'), 116.9 (C, CN), 115.7 (CH, C-3' and C-5'), 62.0 (CH₂, C-22), 61.2 (CH₃, 7-OCH₃), 60.8 (CH₃, 17-OCH₃), 58.4 (CH, C-21), 56.7 (CH, C-1), 54.5 (CH, C-13), 54.3 (CH, C-3), 54.1 (CH, C-11), 41.4 (CH₃, NCH₃), 25.5 (CH₂, C-4), 20.9 (CH₂, C-14), 8.9 (CH₃, 6-CH₃), 8.7 (CH₃, 16-CH₃); HREIMS m/z 615.2020 [$\text{M}]^+$ (calcd for $\text{C}_{33}\text{H}_{30}\text{O}_8\text{N}_3\text{F}_3$, 615.2017).

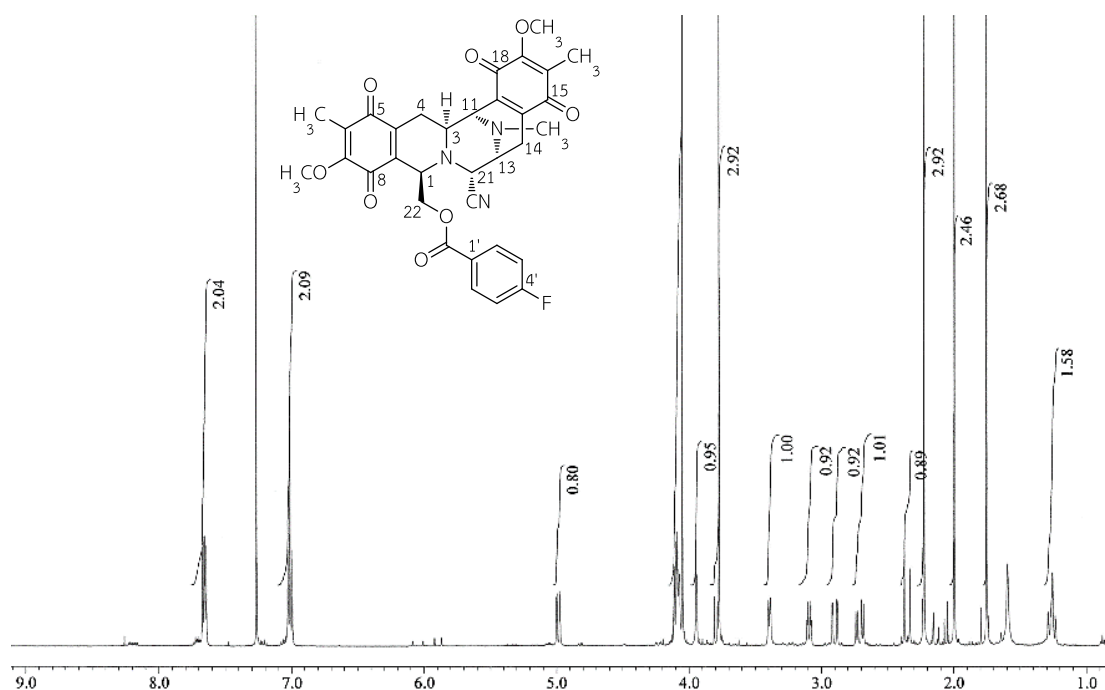


Figure C9 ^1H NMR spectrum (500 MHz) of 22-O-(4-fluorobenzoyl)jorunnamycin A (R2) in CDCl_3

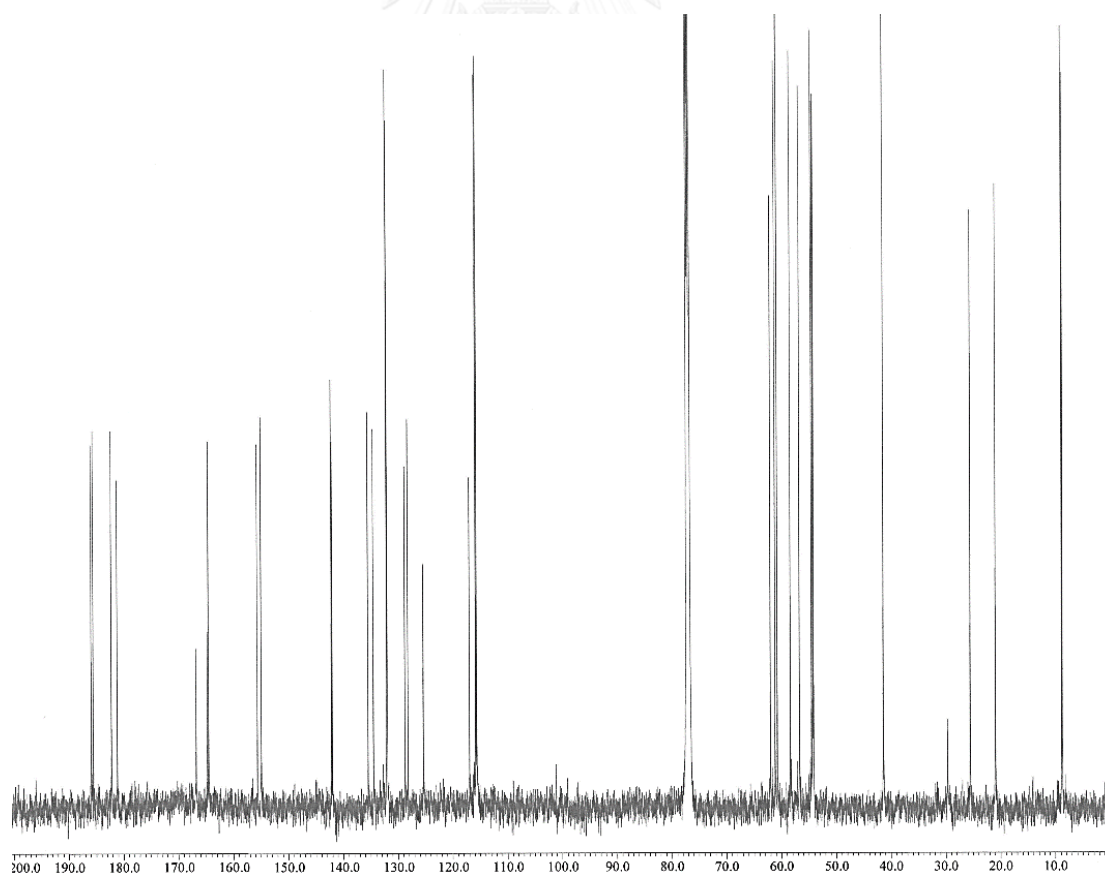


Figure C10 ^{13}C NMR spectrum (125 MHz) of 22-O-(4-fluorobenzoyl)jorunnamycin A (R2) in CDCl_3

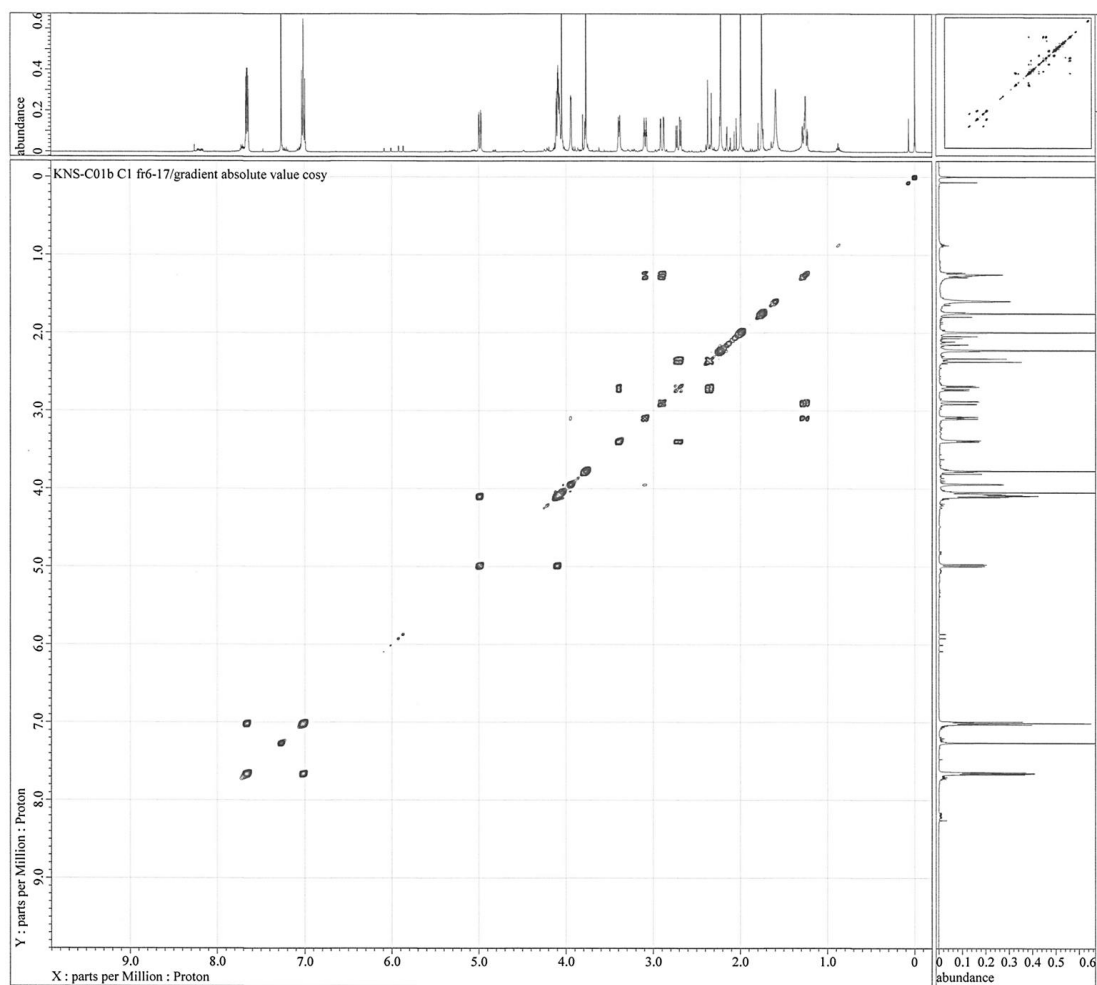


Figure C11 ^1H - ^1H COSY spectrum (500 MHz) of 22-O-(4-fluorobenzoyl) jorunnamycin A (R2) in CDCl_3

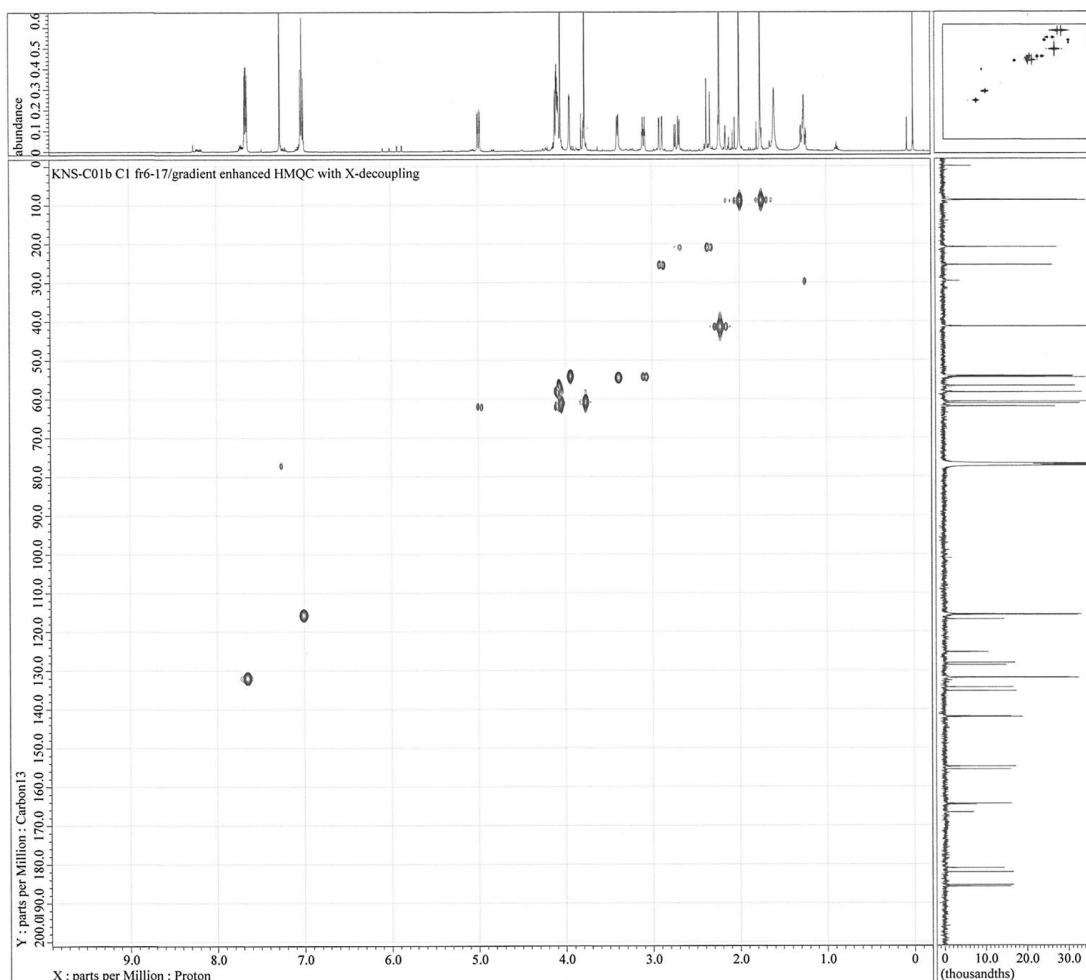


Figure C12 HMQC spectrum (500 MHz) of 22-O-(4-fluorobenzoyl) jorunnamycin A (**R2**) in CDCl_3

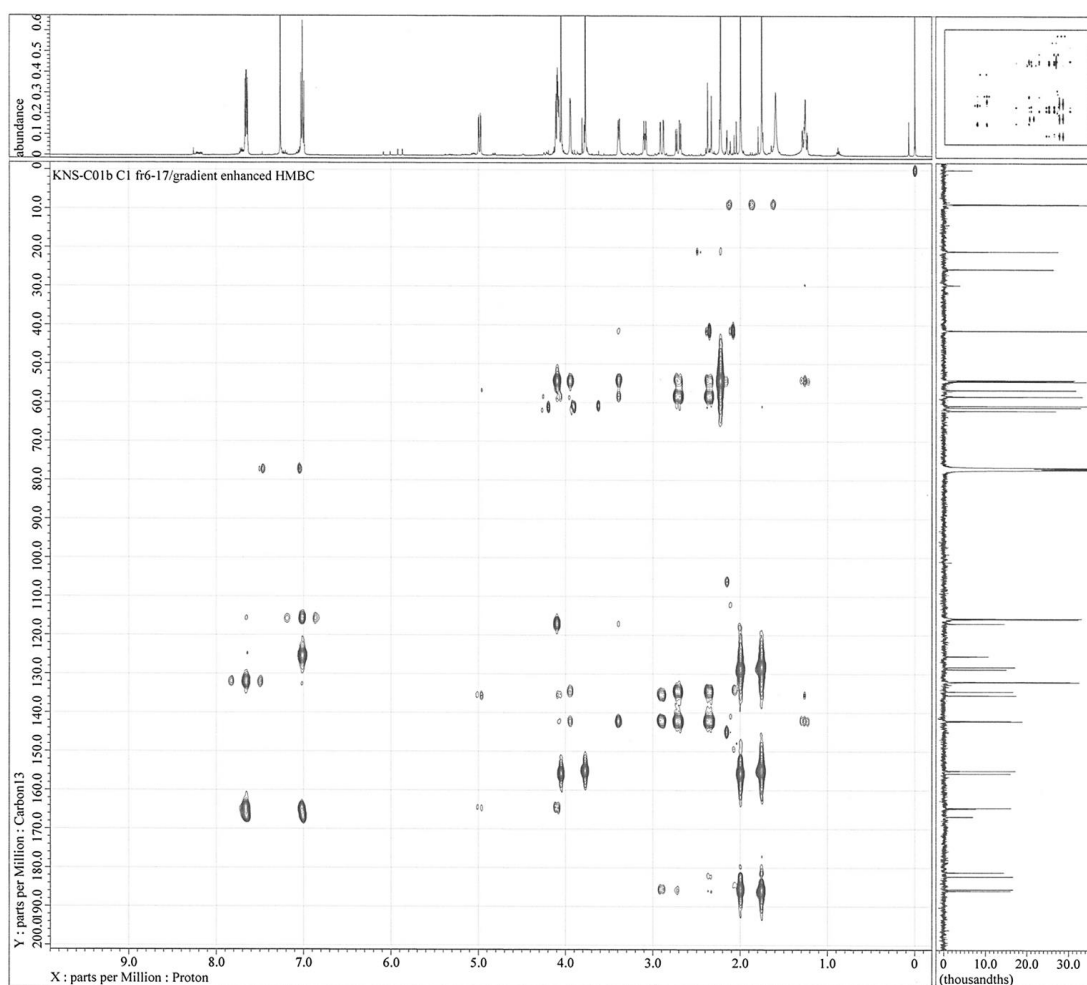


Figure C13 HMBC spectrum (500 MHz) of 22-O-(4-fluorobenzoyl) jorunnamycin A (**R2**) in CDCl₃

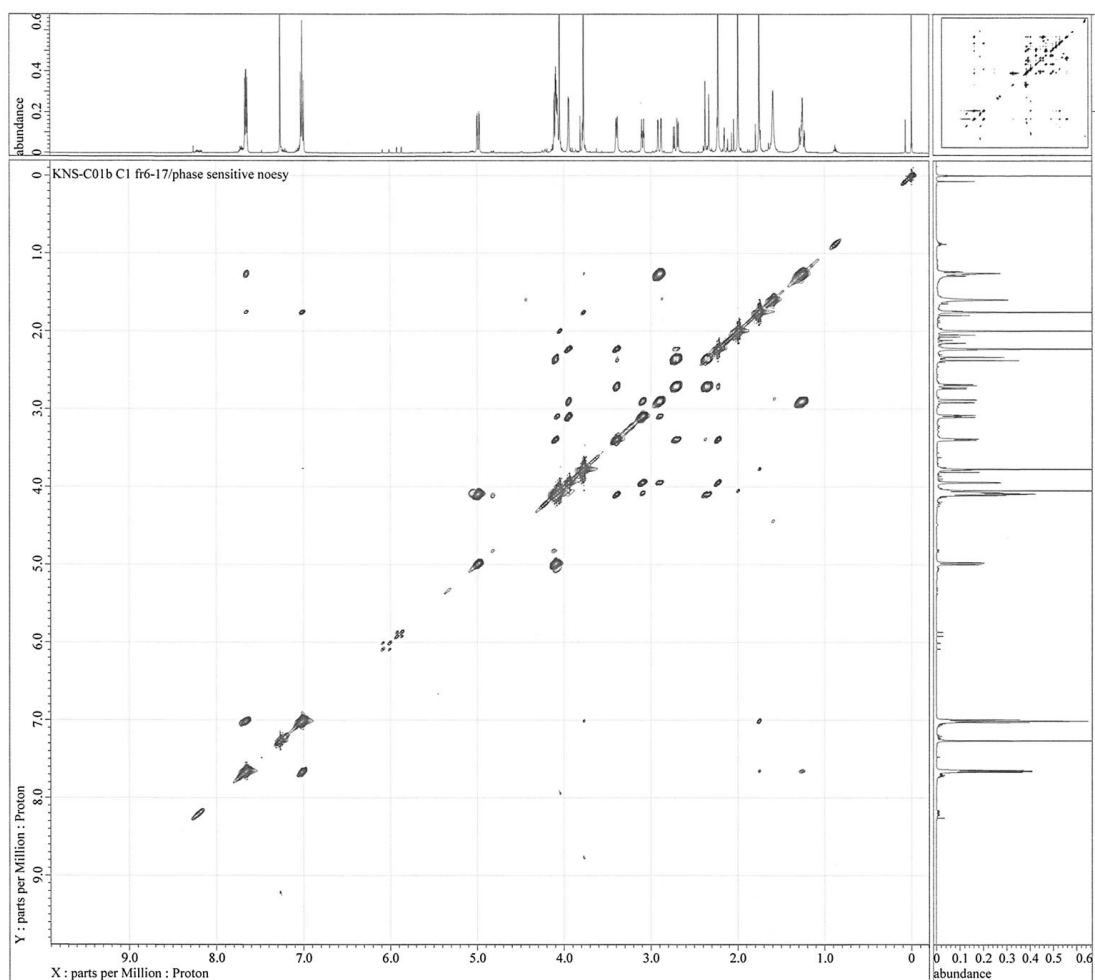
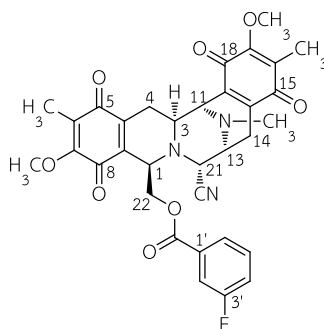


Figure C14 NOESY spectrum (500 MHz) of 22-O-(4-fluorobenzoyl) jorunnamycin A (R2) in CDCl₃



22-O-(3-Fluorobenzoyl)jorunnamycin A (R3): yield 81.8%; yellow amorphous solid; $[\alpha]_D^{24}$ -65.3 (c 0.4, CHCl_3); CD $\Delta\epsilon$ nm (c 13.0 μM , MeOH, 24°C) 0 (404), -4.4 (360), -1.7 (312), -9.7 (282), 0 (270), $+9.7$ (259), 0 (241), -3.5 (230), -0.3 (211); IR (KBr) ν_{max} 2947, 2853, 1726, 1655, 1616, 1593, 1447, 1373, 1271, 1236, 1200, 1152, 957, 907, 754 cm^{-1} ; ^1H NMR (CDCl_3 , 500 MHz) δ 7.40 (1H, ddd, J = 7.8, 1.6, 1.2 Hz, H-6'), 7.34 (1H, ddd, J = 9.5, 2.6, 1.6 Hz, H-2'), 7.32 (1H, ddd, J = 8.3, 7.8, 5.5 Hz, H-5'), 7.22 (1H, tdd, J = 8.3, 2.6, 1.2 Hz, H-4'), 5.00 (1H, dd, J = 11.7, 3.0 Hz, H-22b), 4.12 (1H, dd, J = 11.7, 2.0 Hz, H-22a), 4.10 (1H, d, J = 2.4 Hz, H-21), 4.08 (1H, ddd, J = 3.0, 2.5, 2.0 Hz, H-1), 4.05 (3H, s, 7-OCH₃), 3.95 (1H, d, J = 2.3 Hz, H-11), 3.75 (3H, s, 17-OCH₃), 3.40 (1H, ddd, J = 7.7, 2.4, 1.7 Hz, H-13), 3.10 (1H, ddd, J = 11.5, 2.6, 2.3 Hz, H-3), 2.91 (1H, dd, J = 17.6, 2.6 Hz, H-4 α), 2.72 (1H, dd, J = 21.2, 7.7 Hz, H-14 α), 2.36 (1H, d, J = 21.2 Hz, H-14 β), 2.23 (3H, s, NCH₃), 2.00 (3H, s, 6-CH₃), 1.74 (3H, s, 16-CH₃), 1.27 (1H, ddd, J = 17.6, 11.5, 2.5 Hz, H-4 β); ^{13}C NMR (CDCl_3 , 125 MHz) δ 185.9 (C, C-15), 185.4 (C, C-5), 182.2 (C, C-18), 181.1 (C, C-8), 164.4 (C, OCO), 162.4 (C, C-3'), 155.6 (C, C-7), 154.9 (C, C-17), 142.1 (C, C-10), 142.0 (C, C-20), 135.3 (C, C-9), 134.5 (C, C-19), 131.4 (C, C-1'), 130.2 (CH, C-5'), 128.8 (C, C-6), 128.3 (C, C-16), 124.9 (CH, C-6'), 120.3 (CH, C-4'), 116.9 (C, CN), 116.4 (CH, C-2'), 62.2 (CH₂, C-22), 61.2 (CH₃, 7-OCH₃), 60.8 (CH₃, 17-OCH₃), 58.4 (CH, C-21), 56.7 (CH, C-1), 54.5 (CH, C-13), 54.3 (CH, C-3), 54.1 (CH, C-11), 41.4 (CH₃, NCH₃), 25.5 (CH₂, C-4), 21.0 (CH₂, C-14), 8.9 (CH₃, 6-CH₃), 8.6 (CH₃, 16-CH₃); HREIMS m/z 615.2013 [M]⁺ (calcd for C₃₃H₃₀O₈N₃F₃, 615.2017).

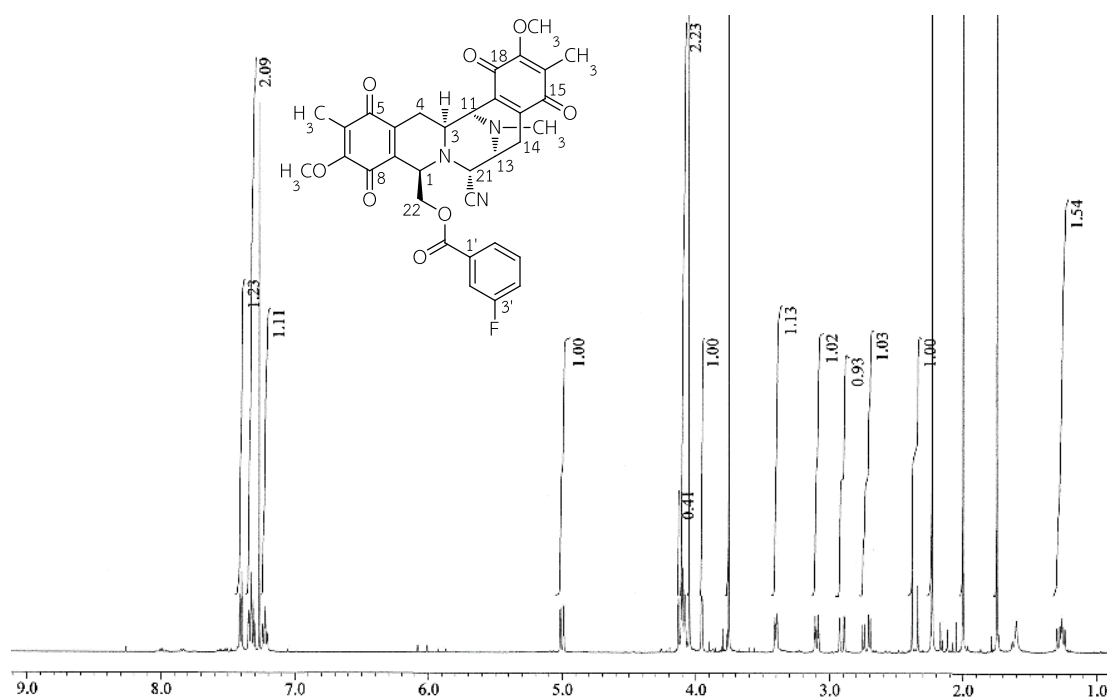


Figure C15 ^1H NMR spectrum (500 MHz) of 22-O-(3-fluorobenzoyl)jorunnamycin A (R3) in CDCl_3

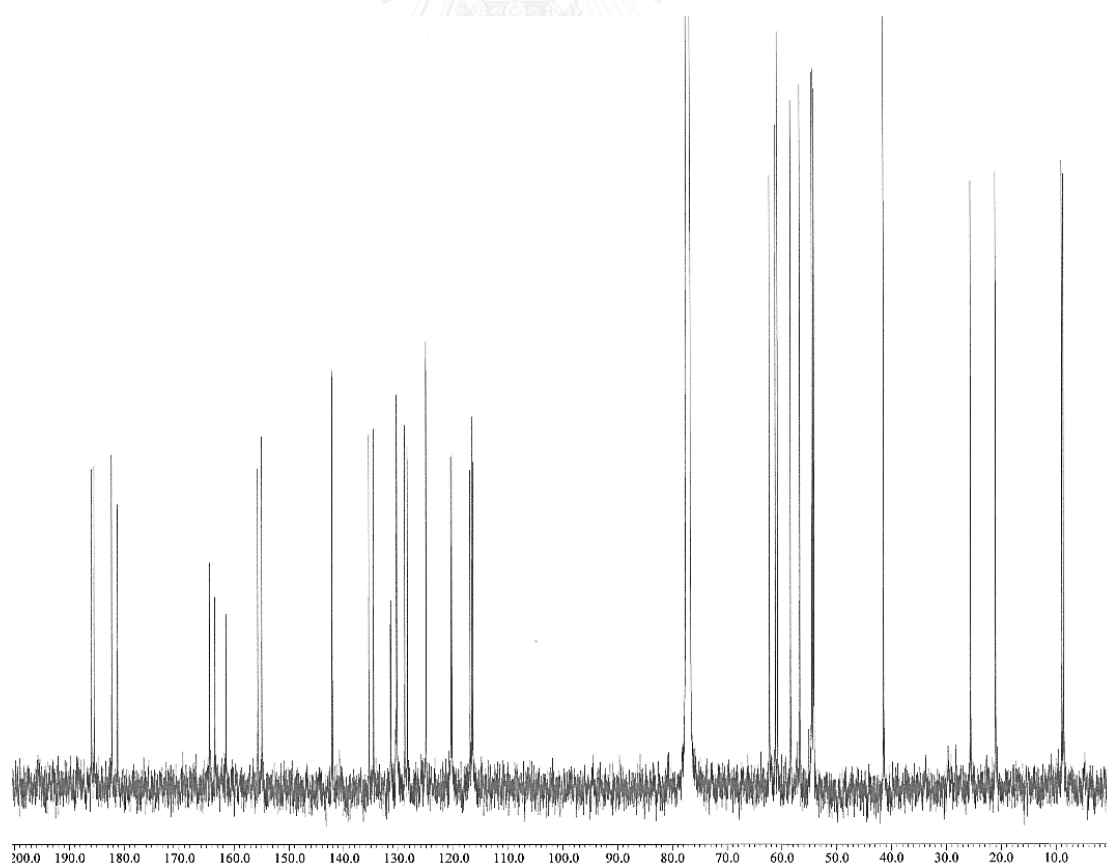
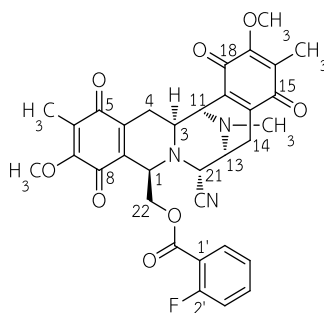


Figure C16 ^{13}C NMR spectrum (125 MHz) of 22-O-(3-fluorobenzoyl)jorunnamycin A (R3) in CDCl_3



22-O-(2-Fluorobenzoyl)jorunnamycin A (R4): yield 79.4%; yellow amorphous solid; $[\alpha]_D^{25}$ -67.5 (c 0.3, CHCl_3); CD $\Delta\epsilon$ nm (c 13.0 μM , MeOH, 24°C) 0 (402), -4.7 (355), -2.1 (311), -9.2 (282), 0 (269), $+7.4$ (259), 0 (244), -5.6 (231), 0 (219), $+1.6$ (212), 0 (207), -3.4 (203); IR (KBr) ν_{max} 2945, 2853, 1721, 1655, 1614, 1498, 1456, 1373, 1294, 1236, 1150, 1128, 1080, 760 cm^{-1} ; ^1H NMR (CDCl_3 , 500 MHz) δ 7.69 (1H, td, $J = 7.7, 1.9$ Hz, H-6'), 7.49 (1H, m, H-4'), 7.15 (1H, td, $J = 7.7, 1.0$ Hz, H-5'), 6.98 (1H, ddd, $J = 11.0, 8.4, 1.0$ Hz, H-3'), 4.94 (1H, dd, $J = 11.7, 2.6$ Hz, H-22b), 4.15 (1H, dd, $J = 11.7, 2.5$ Hz, H-22a), 4.14 (1H, d, $J = 2.5$ Hz, H-21), 4.07 (1H, ddd, $J = 2.8, 2.6, 2.5$ Hz, H-1), 4.02 (3H, s, 7-OCH₃), 3.99 (1H, d, $J = 2.2$ Hz, H-11), 3.82 (3H, s, 17-OCH₃), 3.40 (1H, ddd, $J = 7.7, 2.5, 1.4$ Hz, H-13), 3.13 (1H, ddd, $J = 11.6, 2.3, 2.2$ Hz, H-3), 2.88 (1H, dd, $J = 17.6, 2.3$ Hz, H-4 α), 2.72 (1H, dd, $J = 21.1, 7.7$ Hz, H-14 α), 2.36 (1H, d, $J = 21.1$ Hz, H-14 β), 2.25 (3H, s, NCH₃), 1.97 (3H, s, 6-CH₃), 1.62 (3H, s, 16-CH₃), 1.44 (1H, ddd, $J = 17.6, 11.6, 2.8$ Hz, H-4 β); ^{13}C NMR (CDCl_3 , 125 MHz) δ 185.8 (C, C-15), 185.5 (C, C-5), 182.4 (C, C-18), 181.2 (C, C-8), 163.9 (C, OCO), 161.3 (C, C-2'), 155.6 (C, C-7), 154.9 (C, C-17), 142.3 (C, C-10), 142.0 (C, C-20), 135.1 (C, C-9), 134.9 (CH, C-4'), 134.7 (C, C-19), 132.6 (CH, C-6'), 128.7 (C, C-6), 128.2 (C, C-16), 124.3 (CH, C-5'), 117.5 (C, C-1'), 117.0 (C, CN), 116.9 (CH, C-3'), 62.9 (CH₂, C-22), 61.1 (CH₃, 7-OCH₃), 60.8 (CH₃, 17-OCH₃), 58.4 (CH, C-21), 56.4 (CH, C-1), 54.6 (CH, C-13), 54.2 (CH, C-3 and CH, C-11), 41.4 (CH₃, NCH₃), 25.2 (CH₂, C-4), 21.0 (CH₂, C-14), 8.8 (CH₃, 6-CH₃), 8.5 (CH₃, 16-CH₃); HREIMS m/z 615.2013 [$\text{M}]^+$ (calcd for $\text{C}_{33}\text{H}_{30}\text{O}_8\text{N}_3\text{F}_3$, 615.2017).

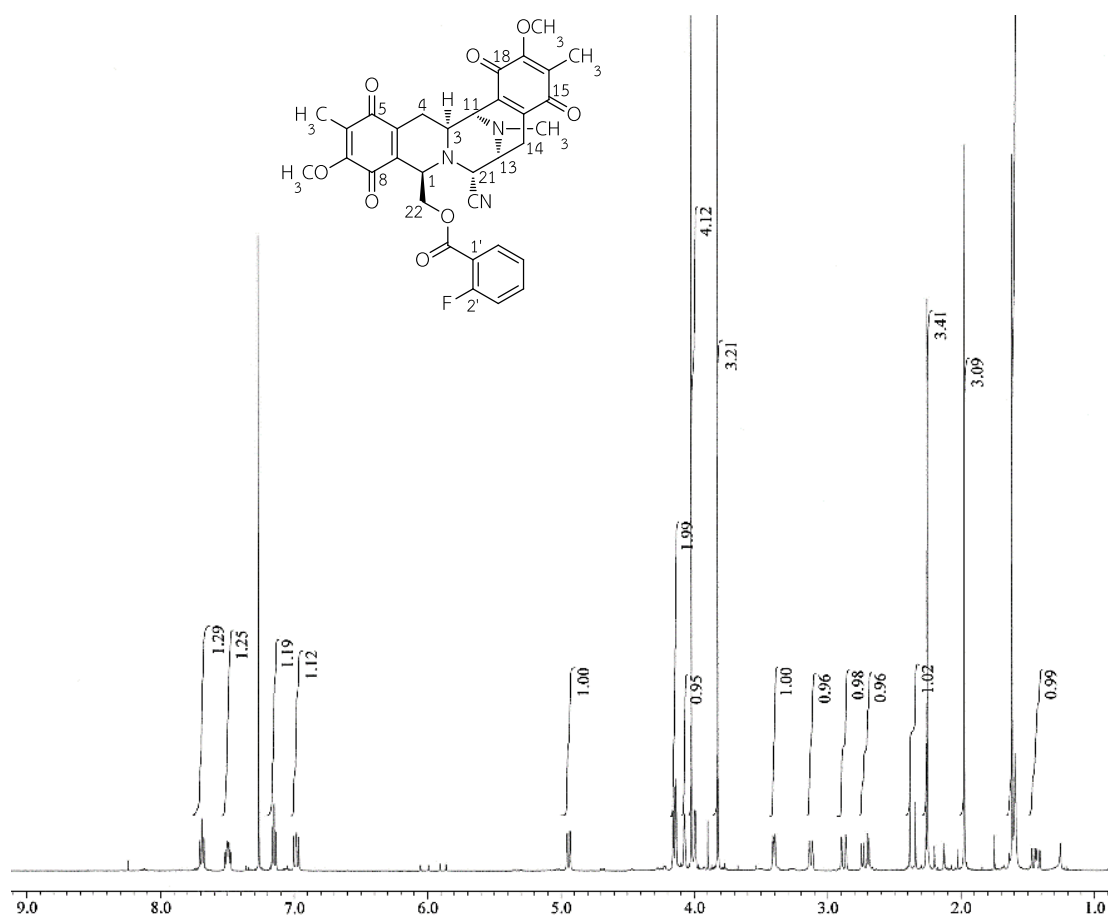


Figure C17 ¹H NMR spectrum (500 MHz) of 22-O-(2-fluorobenzoyl)jorunnamycin A (R4) in CDCl₃

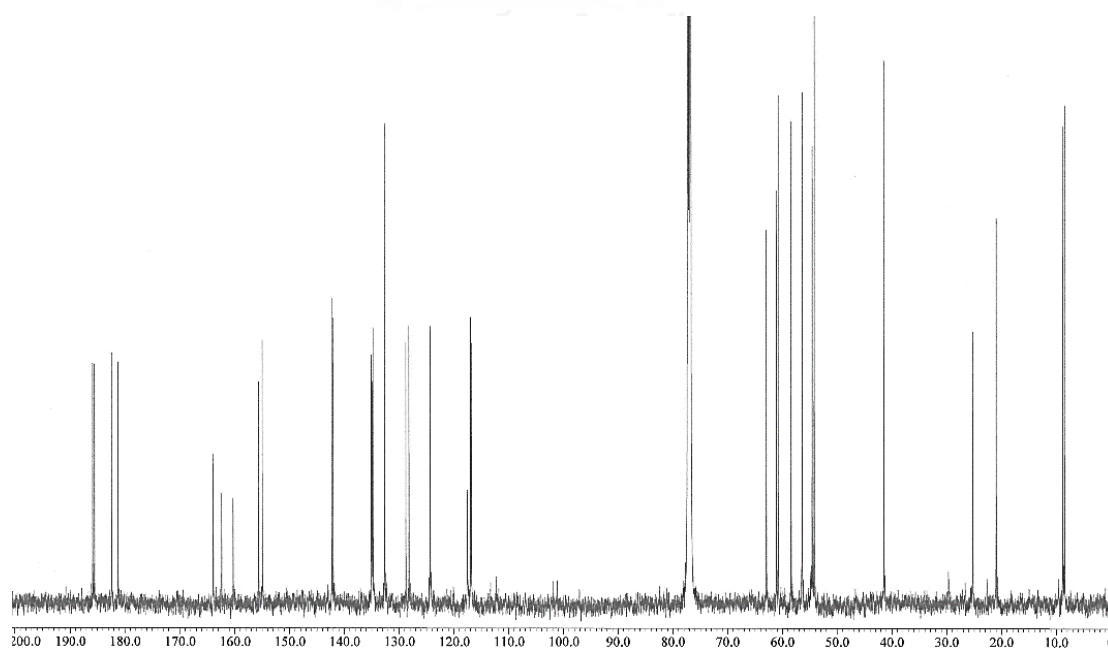
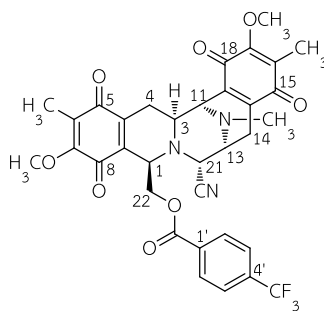
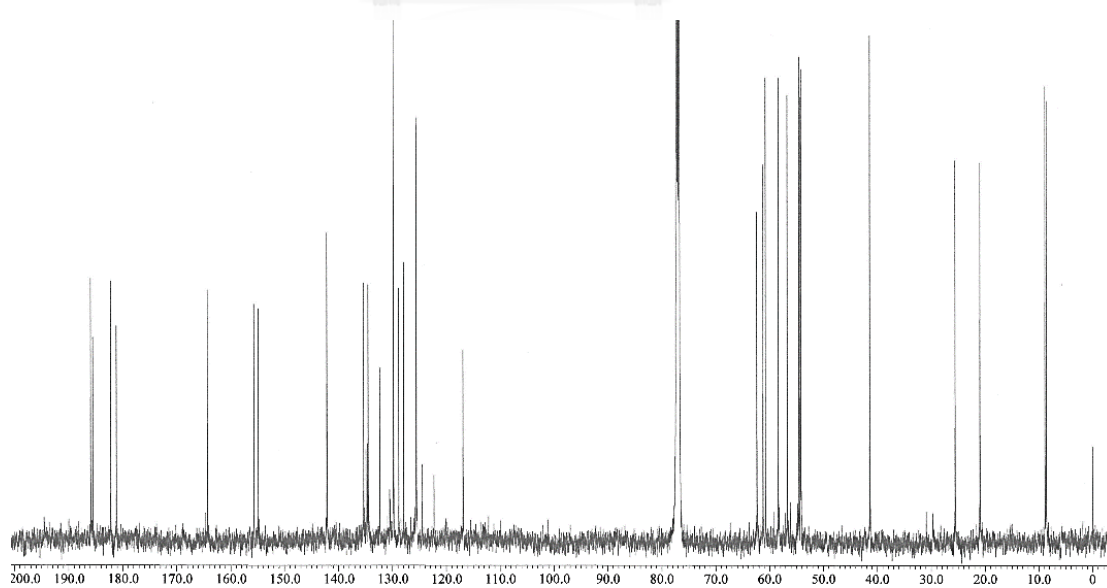
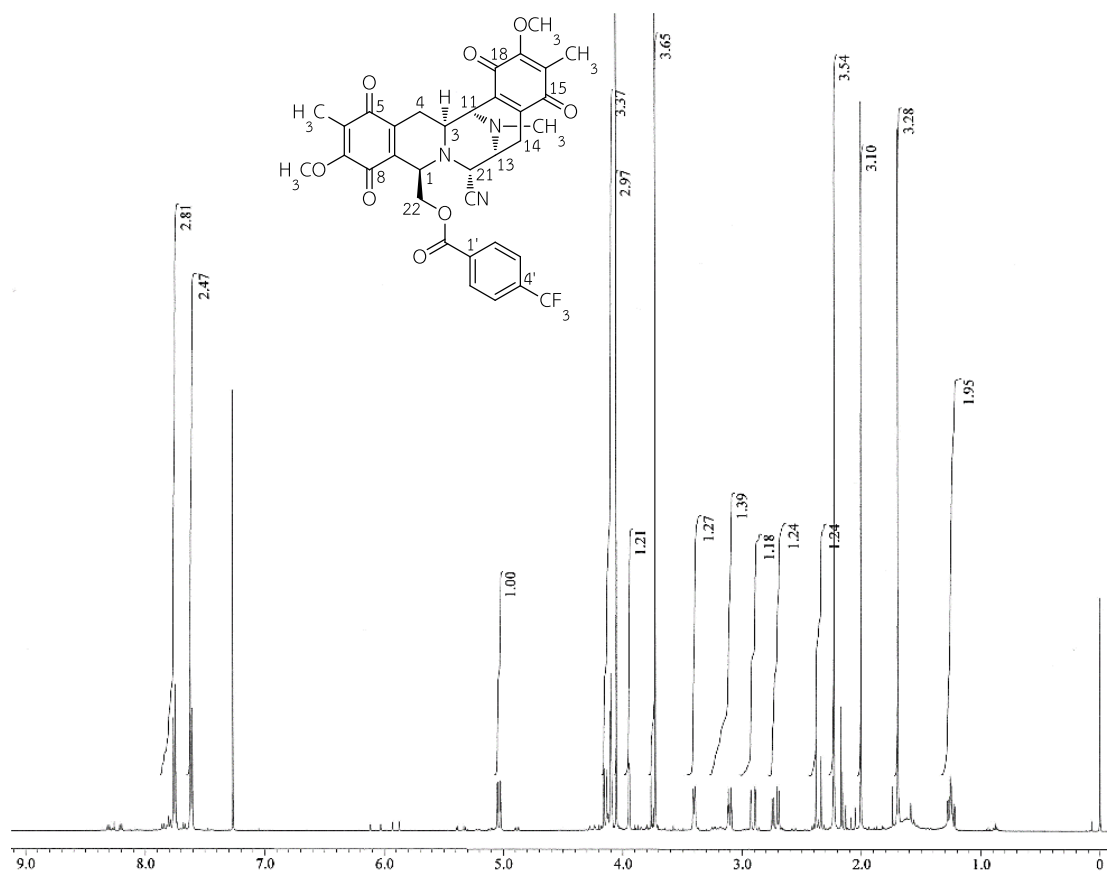
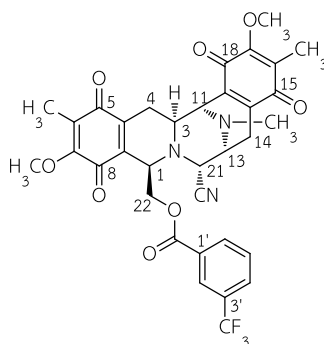


Figure C18 ¹³C NMR spectrum (125 MHz) of 22-O-(2-fluorobenzoyl)jorunnamycin A (R4) in CDCl₃



22-O-(4-Trifluoromethyl benzoyl)jorunnamycin A (R5): yield 68.2%; yellow amorphous solid; $[\alpha]_D^{24}$ -91.3 (c 0.3, CHCl_3); CD $\Delta\epsilon$ nm (c 12.0 μM , MeOH, 23°C) 0 (404), -3.9 (358), -1.4 (306), -8.6 (281), 0 (270), $+6.7$ (259), 0 (242), -4.3 (227), 0 (214), $+1.4$ (211), 0 (205), -1.8 (203); IR (KBr) ν_{max} 2945, 2855, 1728, 1655, 1616, 1450, 1412, 1375, 1325, 1275, 1236, 1132, 1067, 1018, 773, 702 cm^{-1} ; ^1H NMR (CDCl_3 , 500 MHz) δ 7.75 (2H, d, J = 8.5 Hz, H-2' and H-6'), 7.61 (2H, d, J = 8.5 Hz, H-3' and H-5'), 5.03 (1H, dd, J = 11.8, 3.1 Hz, H-22b), 4.15 (1H, dd, J = 11.8, 2.0 Hz, H-22a), 4.10 (1H, d, J = 2.3 Hz, H-21), 4.09 (1H, overlapped, H-1), 4.05 (3H, s, 7-OCH₃), 3.95 (1H, d, J = 2.3 Hz, H-11), 3.73 (3H, s, 17-OCH₃), 3.40 (1H, ddd, J = 7.7, 2.3, 1.7 Hz, H-13), 3.10 (1H, ddd, J = 11.5, 2.7, 2.3 Hz, H-3), 2.91 (1H, dd, J = 17.6, 2.7 Hz, H-4 α), 2.72 (1H, dd, J = 21.2, 7.7 Hz, H-14 α), 2.36 (1H, d, J = 21.2 Hz, H-14 β), 2.23 (3H, s, NCH₃), 2.00 (3H, s, 6-CH₃), 1.70 (3H, s, 16-CH₃), 1.25 (1H, ddd, J = 17.6, 11.5, 2.7 Hz, H-4 β); ^{13}C NMR (CDCl_3 , 125 MHz) δ 185.9 (C, C-15), 185.5 (C, C-5), 182.2 (C, C-18), 181.1 (C, C-8), 164.2 (C, OCO), 155.6 (C, C-7), 154.9 (C, C-17), 142.12 (C, C-20), 142.07 (C, C-10), 135.3 (C, C-9), 134.7 (C, C-4'), 134.5 (C, C-19), 132.3 (C, C-1'), 129.8 (CH, C-2' and C-6'), 128.8 (C, C-6), 127.9 (C, C-16), 125.6 (CH, C-3' and C-5'), 123.4 (C, 4'-CF₃), 116.9 (C, CN), 62.4 (CH₂, C-22), 61.2 (CH₃, 7-OCH₃), 60.8 (CH₃, 17-OCH₃), 58.4 (CH, C-21), 56.7 (CH, C-1), 54.5 (CH, C-13), 54.3 (CH, C-3), 54.1 (CH, C-11), 41.4 (CH₃, NCH₃), 25.6 (CH₂, C-4), 21.0 (CH₂, C-14), 8.9 (CH₃, 6-CH₃), 8.6 (CH₃, 16-CH₃); HRFABMS m/z 666.2065 $[\text{M}+\text{H}]^+$ (calcd for C₃₄H₃₁O₈N₃F₃, 666.2063).





22-O-(3-Trifluoromethyl benzoyl)jorunnamycin A (R6): yield 66.0%; yellow amorphous solid; $[\alpha]_D^{25}$ -68.0 (c 0.4, CHCl_3); CD $\Delta\epsilon$ nm (c 12.0 μM , MeOH, 23°C) 0 (404), -3.9 (357), -1.8 (306), -10.0 (285), 0 (271), $+9.0$ (259), 0 (240), -1.9 (234), 0 (219), 0.9 (209), 0 (205); IR (KBr) ν_{max} 2947, 2855, 1728, 1655, 1616, 1449, 1375, 1335, 1238, 1167, 1132, 1072, 957, 756, 696 cm^{-1} ; ^1H NMR (CDCl_3 , 500 MHz) δ 7.92 (1H, s, H-2'), 7.84 (1H, d, $J = 7.8$ Hz, H-6'), 7.78 (1H, d, $J = 8.1$ Hz, H-4'), 7.51 (1H, dd, $J = 8.1$, 7.8 Hz, H-5'), 4.96 (1H, dd, $J = 11.8$, 3.2 Hz, H-22b), 4.12 (1H, dd, $J = 11.8$, 2.3 Hz, H-22a), 4.11 (1H, d, $J = 2.4$ Hz, H-21), 4.11 (1H, overlapped, H-1), 4.04 (3H, s, 7-OCH₃), 3.97 (1H, d, $J = 2.4$ Hz, H-11), 3.76 (3H, s, 17-OCH₃), 3.40 (1H, ddd, $J = 7.7$, 2.4, 1.6 Hz, H-13), 3.11 (1H, ddd, $J = 11.6$, 2.6, 2.4 Hz, H-3), 2.92 (1H, dd, $J = 17.6$, 2.2 Hz, H-4 α), 2.71 (1H, dd, $J = 21.2$, 7.7 Hz, H-14 α), 2.33 (1H, d, $J = 21.2$ Hz, H-14 β), 2.24 (3H, s, NCH₃), 2.00 (3H, s, 6-CH₃), 1.69 (3H, s, 16-CH₃), 1.26 (1H, ddd, $J = 17.6$, 11.6, 2.7 Hz, H-4 β); ^{13}C NMR (CDCl_3 , 125 MHz) δ 185.7 (C, C-15), 185.2 (C, C-5), 182.2 (C, C-18), 181.1 (C, C-8), 164.2 (C, OCO), 155.6 (C, C-7), 154.8 (C, C-17), 142.0 (C, C-10 and C, C-20), 135.3 (C, C-9), 134.5 (C, C-19), 132.6 (CH, C-6'), 131.3 (C, C-3'), 130.1 (C, C-1'), 129.7 (CH, C-4'), 129.3 (CH, C-5'), 128.9 (C, C-6), 127.9 (C, C-16), 126.1 (CH, C-2'), 123.3 (C, 3'-CF₃), 116.8 (C, CN), 62.8 (CH₂, C-22), 61.2 (CH₃, 7-OCH₃), 60.7 (CH₃, 17-OCH₃), 58.5 (CH, C-21), 56.5 (CH, C-1), 54.5 (CH, C-13), 54.2 (CH, C-3), 54.0 (CH, C-11), 41.4 (CH₃, NCH₃), 25.5 (CH₂, C-4), 21.0 (CH₂, C-14), 8.8 (CH₃, 6-CH₃), 8.5 (q, 16-CH₃); HRFABMS m/z 666.2065 $[\text{M}+\text{H}]^+$ (calcd for C₃₄H₃₁O₈N₃F₃, 666.2063).

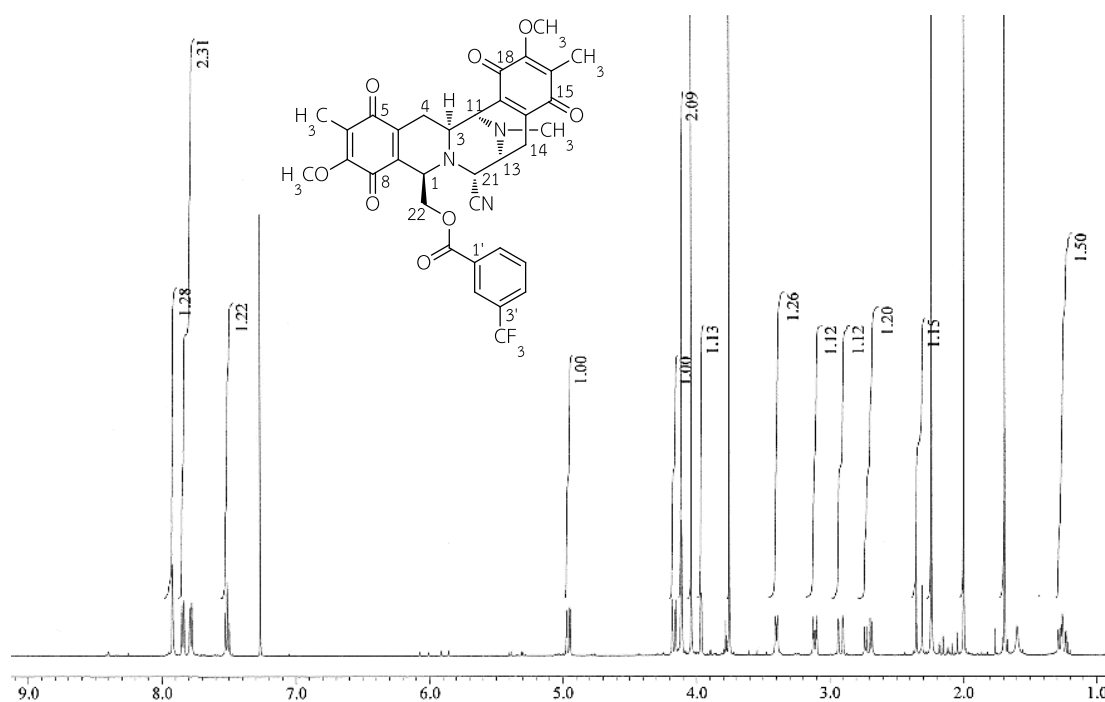


Figure C21 ¹H NMR spectrum (500 MHz) of 22-O-(3-trifluoromethyl benzoyl) jorunnamycin A (R6) in CDCl₃

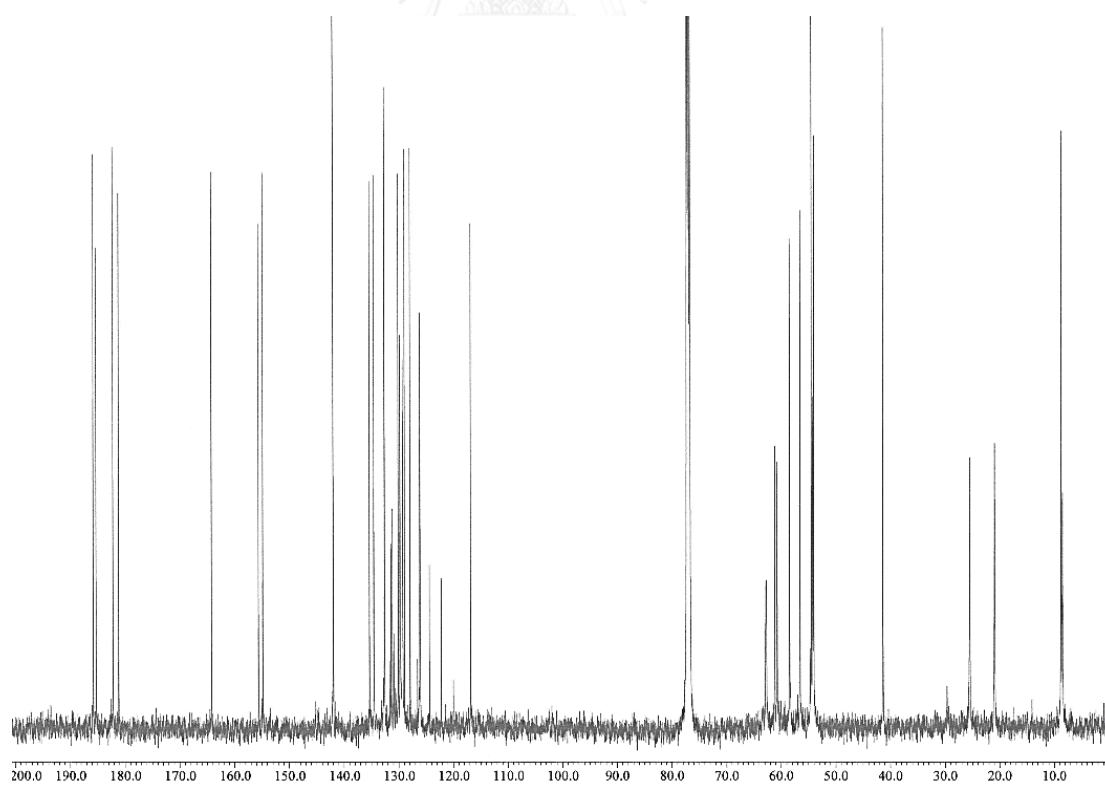
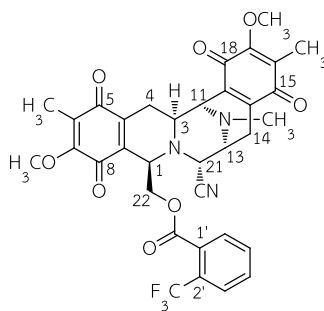


Figure C22 ¹³C NMR spectrum (125 MHz) of 22-O-(3-trifluoromethyl benzoyl) jorunnamycin A (R6) in CDCl₃



22-O-(2-Trifluoromethyl benzoyl)jorunnamycin A (R7): yield 69.0%; yellow amorphous solid; $[\alpha]_D^{25}$ -64.9 (c 0.3, CHCl_3); CD $\Delta\epsilon$ nm (c 13.0 μM , MeOH, 24°C) 0 (400), -4.0 (355), -1.7 (303), -10.0 (281), 0 (267), $+6.5$ (257), 0 (240), -3.4 (228), 0 (219), $+4.3$ (209), $+2.1$ (203); IR (KBr) ν_{max} 2934, 2857, 1736, 1655, 1616, 1449, 1375, 1314, 1236, 1165, 1146, 1053, 1036, 770 cm^{-1} ; ^1H NMR (CDCl_3 , 500 MHz) δ 7.68 (1H, d, J = 8.0 Hz, H-3'), 7.59 (1H, ddd, J = 8.0, 7.7, 0.8 Hz, H-4'), 7.53 (1H, ddd, J = 7.7, 7.3, 1.0 Hz, H-5'), 7.47 (1H, d, J = 7.3 Hz, H-6'), 4.57 (1H, dd, J = 11.8, 2.9 Hz, H-22b), 4.39 (1H, dd, J = 11.8, 3.2 Hz, H-22a), 4.103 (1H, ddd, J = 3.2, 2.9, 2.7 Hz, H-1), 4.097 (1H, d, J = 2.5 Hz, H-21), 4.00 (1H, overlapped, H-11), 3.99 (3H, s, 7-OCH₃), 3.86 (3H, s, 17-OCH₃), 3.40 (1H, ddd, J = 7.6, 2.5, 1.6 Hz, H-13), 3.13 (1H, ddd, J = 11.4, 2.9, 2.6 Hz, H-3), 2.88 (1H, dd, J = 17.6, 2.6 Hz, H-4 α), 2.74 (1H, dd, J = 21.2, 7.6 Hz, H-14 α), 2.27 (3H, s, NCH₃), 2.26 (1H, d, J = 21.2 Hz, H-14 β), 1.95 (3H, s, 6-CH₃), 1.79 (3H, s, 16-CH₃), 1.30 (1H, ddd, J = 17.6, 11.4, 2.7 Hz, H-4 β); ^{13}C NMR (CDCl_3 , 125 MHz) δ 186.0 (C, C-15), 185.5 (C, C-5), 182.3 (C, C-18), 180.9 (C, C-8), 165.9 (C, OCO), 155.8 (C, C-7), 155.1 (C, C-17), 141.9 (C, C-20), 141.5 (C, C-10), 135.1 (C, C-9), 134.9 (C, C-19), 131.7 (CH, C-5'), 131.6 (CH, C-4'), 130.2 (CH, C-6'), 129.8 (C, C-1'), 128.9 (C, C-6), 128.7 (C, C-2'), 128.6 (C, C-16), 126.9 (CH, C-3'), 123.0 (C, 2'-CF₃), 116.7 (C, CN), 64.6 (CH₂, C-22), 61.0 (CH₃, 7-OCH₃), 60.9 (CH₃, 17-OCH₃), 58.6 (CH, C-21), 56.1 (CH, C-1), 54.5 (CH, C-3 and CH, C-13), 54.2 (CH, C-11), 41.5 (CH₃, NCH₃), 25.2 (CH₂, C-4), 21.2 (CH₂, C-14), 8.7 (CH₃, 6-CH₃), 8.6 (CH₃, 16-CH₃); HRFABMS m/z 666.2059 $[\text{M}+\text{H}]^+$ (calcd for C₃₄H₃₁O₈N₃F₃, 666.2063).

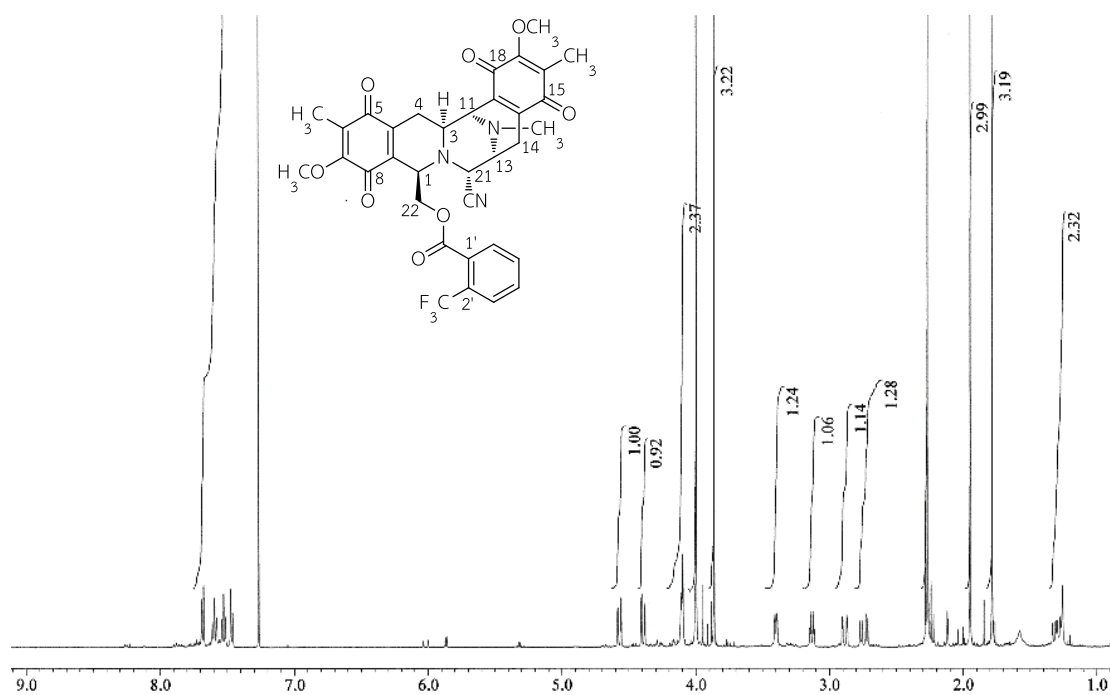


Figure C23 ^1H NMR spectrum (500 MHz) of 22-O-(2-trifluoromethyl benzoyl) jorunnamycin A (R7) in CDCl_3

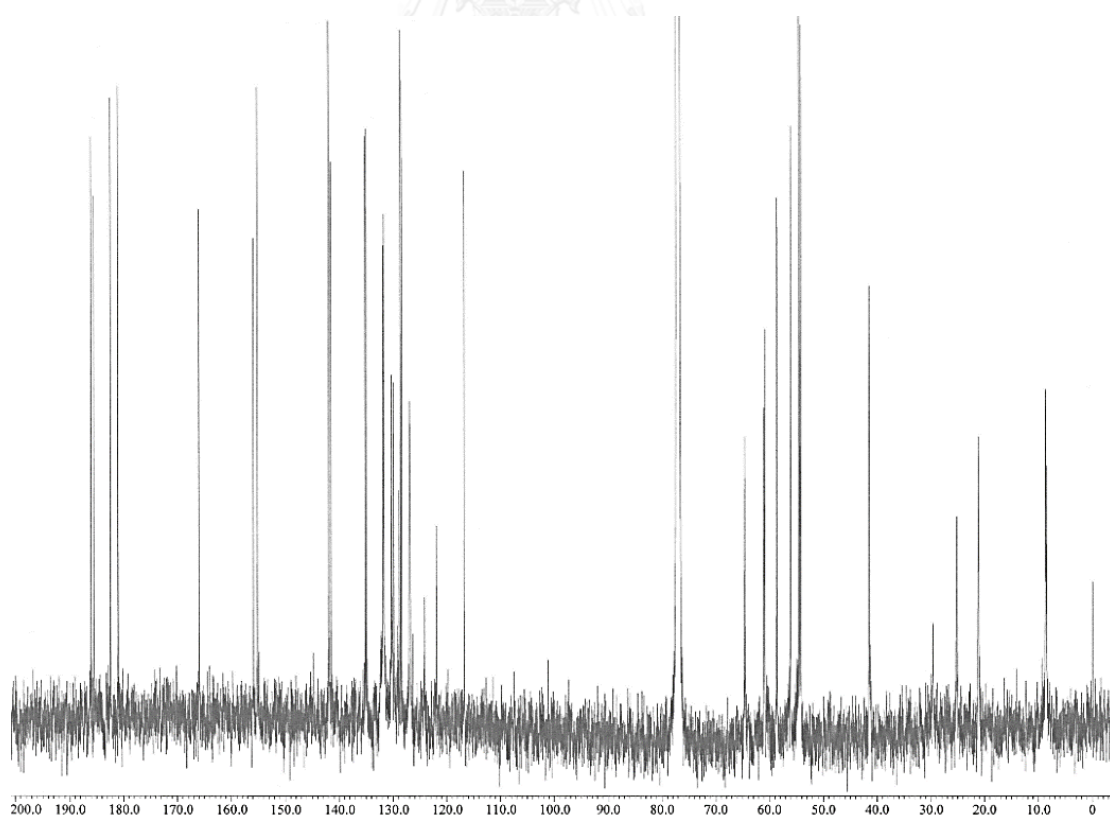
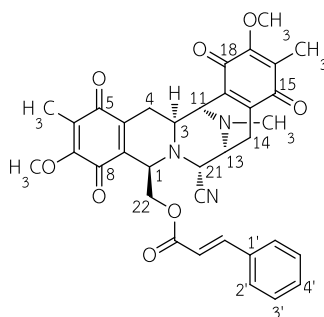


Figure C24 ^{13}C NMR spectrum (125 MHz) of 22-O-(2-trifluoromethyl benzoyl) jorunnamycin A (R7) in CDCl_3



22-O-Cinnamoyl jorunnamycin A (R8): yield 67.3%; yellow amorphous solid; $[\alpha]_D^{28}$ -156.7 (c 0.2, CHCl_3); CD $\Delta\epsilon$ nm (c 12.8 μM , MeOH, 25°C) 0 (403), -4.8 (355), -3.1 (307), -18.2 (282), 0 (269), $+13.1$ (258), $+1.1$ sh (231), 0 (228), -4.3 (219), -9.7 (206); IR (KBr) ν_{max} 2941, 2853, 1715, 1655, 1616, 1450, 1373, 1310, 1236, 1161, 770 cm^{-1} ; ^1H NMR (CDCl_3 , 500 MHz) δ 7.39 (5H, m, ArH), 7.38 (1H, d, $J = 16.1$ Hz, $\text{COCH}=\text{CH}$), 6.08 (1H, d, $J = 16.1$ Hz, $\text{COCH}=\text{CH}$), 4.89 (1H, dd, $J = 11.8, 3.2$ Hz, H-22b), 4.10 (1H, d, $J = 2.5$ Hz, H-21), 4.04 (3H, s, 7-OCH₃), 4.03 (1H, ddd, $J = 3.2, 2.7, 2.5$ Hz, H-1), 3.98 (1H, d, $J = 2.6$ Hz, H-11), 3.93 (1H, dd, $J = 11.8, 2.5$ Hz, H-22a), 3.69 (3H, s, 17-OCH₃), 3.39 (1H, ddd, $J = 7.7, 2.5, 1.7$ Hz, H-13), 3.10 (1H, ddd, $J = 11.6, 2.6, 2.3$ Hz, H-3), 2.92 (1H, dd, $J = 17.4, 2.3$ Hz, H-4 α), 2.72 (1H, dd, $J = 21.2, 7.7$ Hz, H-14 α), 2.42 (1H, d, $J = 21.2$ Hz, H-14 β), 2.25 (3H, s, NCH₃), 1.99 (3H, s, 6-CH₃), 1.60 (3H, s, 16-CH₃), 1.37 (1H, ddd, $J = 17.4, 11.6, 2.7$ Hz, H-4 β); ^{13}C NMR (CDCl_3 , 125 MHz) δ 186.0 (C, C-15), 185.7 (C, C-5), 182.4 (C, C-18), 181.1 (C, C-8), 165.8 (C, OCO), 155.6 (C, C-7), 154.5 (C, C-17), 144.5 (CH, COCH=CH), 142.3 (C, C-10), 142.1 (C, C-20), 135.5 (C, C-9), 134.6 (C, C-19), 133.7 (C, C-1'), 130.8 (CH, C-4'), 129.0 (CH, C-2' and C-6'), 128.7 (C, C-6), 128.4 (C, C-16), 128.2 (CH, C-3' and C-5'), 117.0 (C, CN), 116.5 (CH, COCH=CH), 61.7 (CH₂, C-22), 61.2 (CH₃, 7-OCH₃), 60.6 (CH₃, 17-OCH₃), 58.4 (CH, C-21), 56.6 (CH, C-1), 54.6 (CH, C-13), 54.3 (CH, C-3), 54.1 (CH, C-11), 41.4 (CH₃, NCH₃), 25.6 (CH₂, C-4), 20.9 (CH₂, C-14), 8.8 (CH₃, 6-CH₃), 8.4 (CH₃, 16-CH₃); HREIMS m/z 623.2268 $[\text{M}]^+$ (calcd for $\text{C}_{35}\text{H}_{33}\text{O}_8\text{N}_3$, 623.2268).

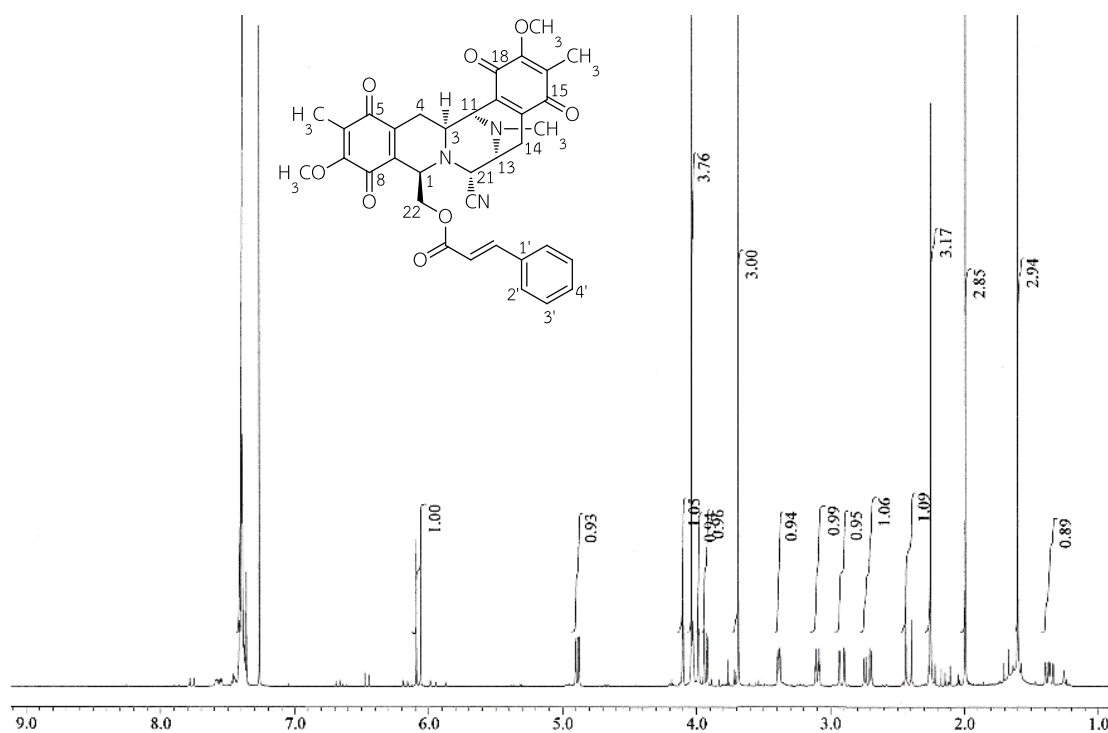


Figure C25 ^1H NMR spectrum (500 MHz) of 22-O-cinnamoyl jorunnamycin A (**R8**) in CDCl_3

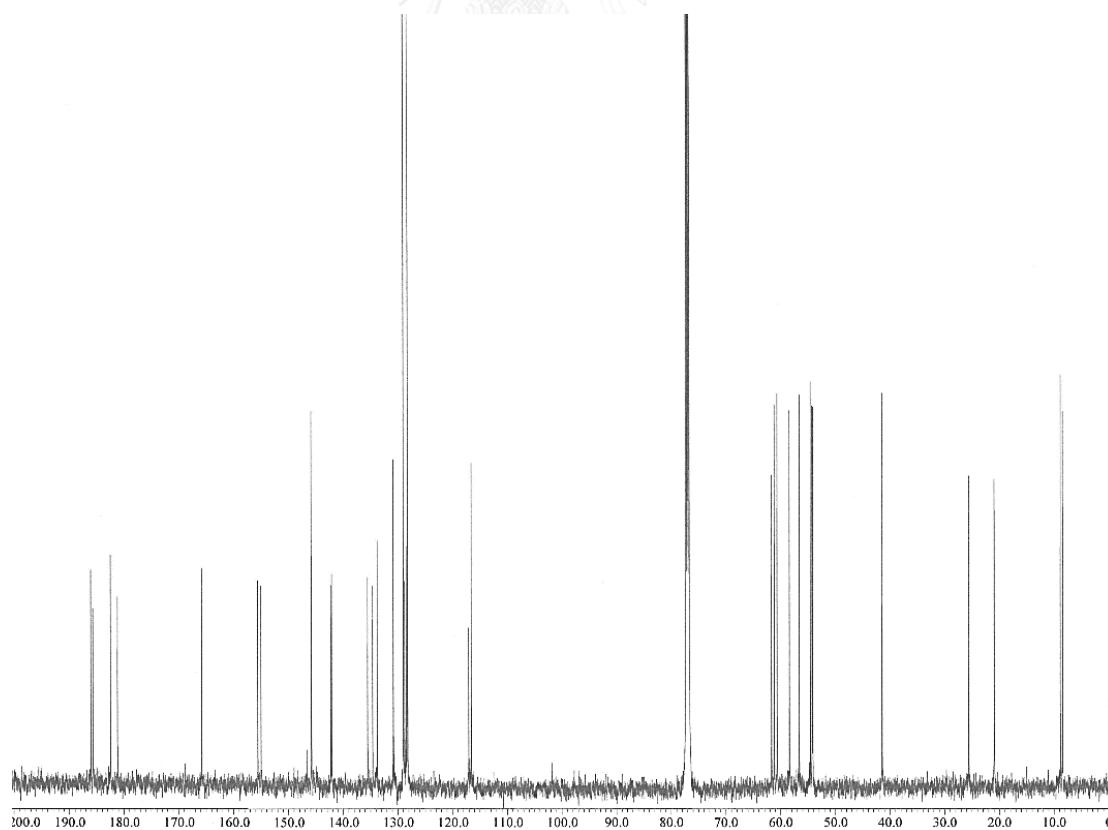


Figure C26 ^{13}C NMR spectrum (125 MHz) of 22-O-cinnamoyl jorunnamycin A (**R8**) in CDCl_3

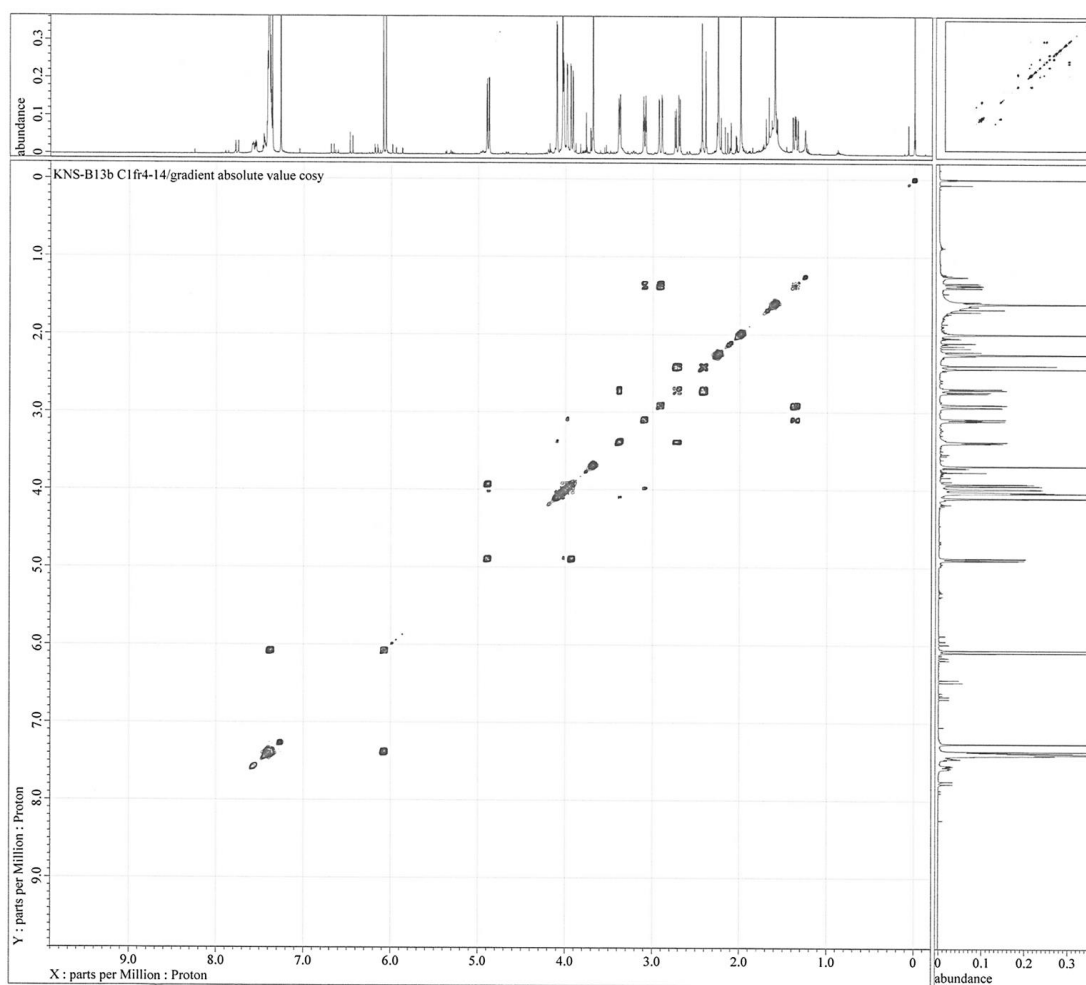


Figure C27 ^1H - ^1H COSY spectrum (500 MHz) of 22-*O*-cinnamoyl jorunnamycin A (**R8**) in CDCl_3

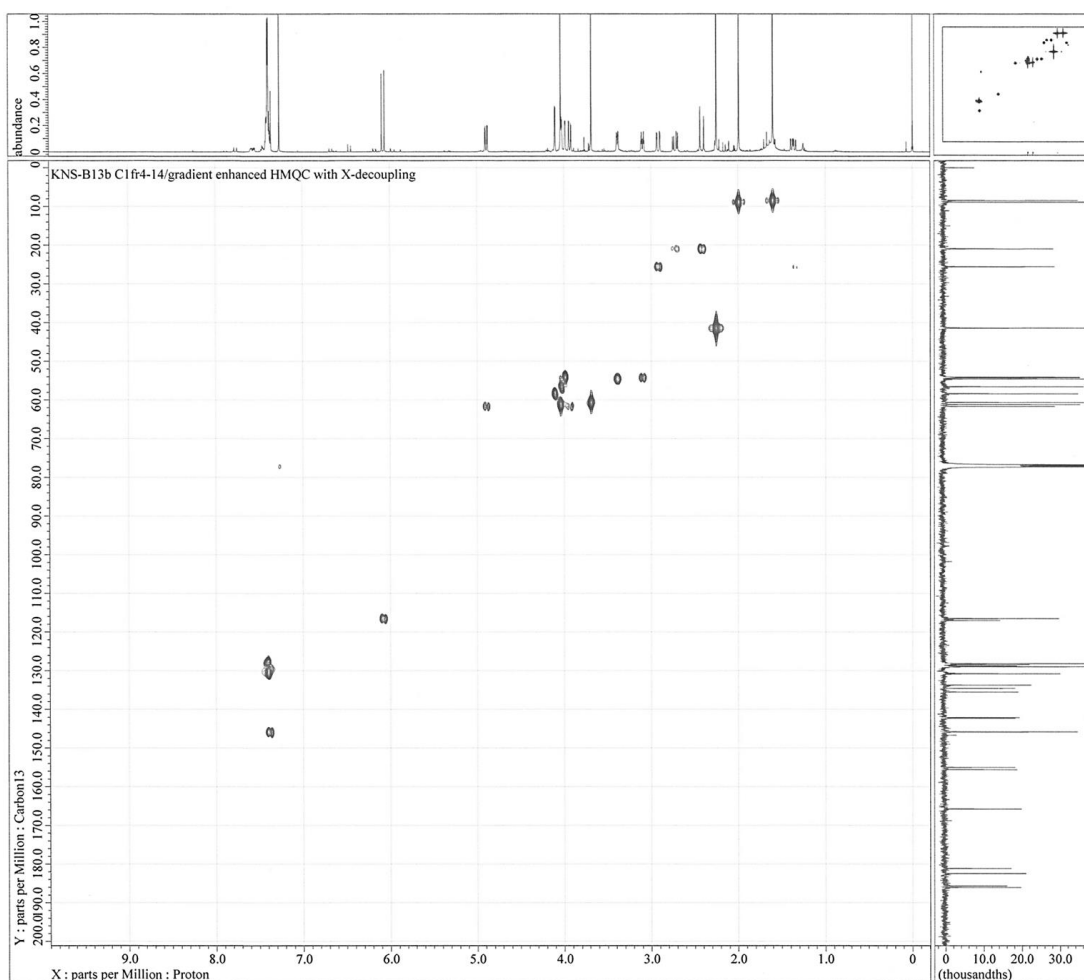


Figure C28 HMQC spectrum (500 MHz) of 22-O-cinnamoyl jorunnamycin A (**R8**) in CDCl₃

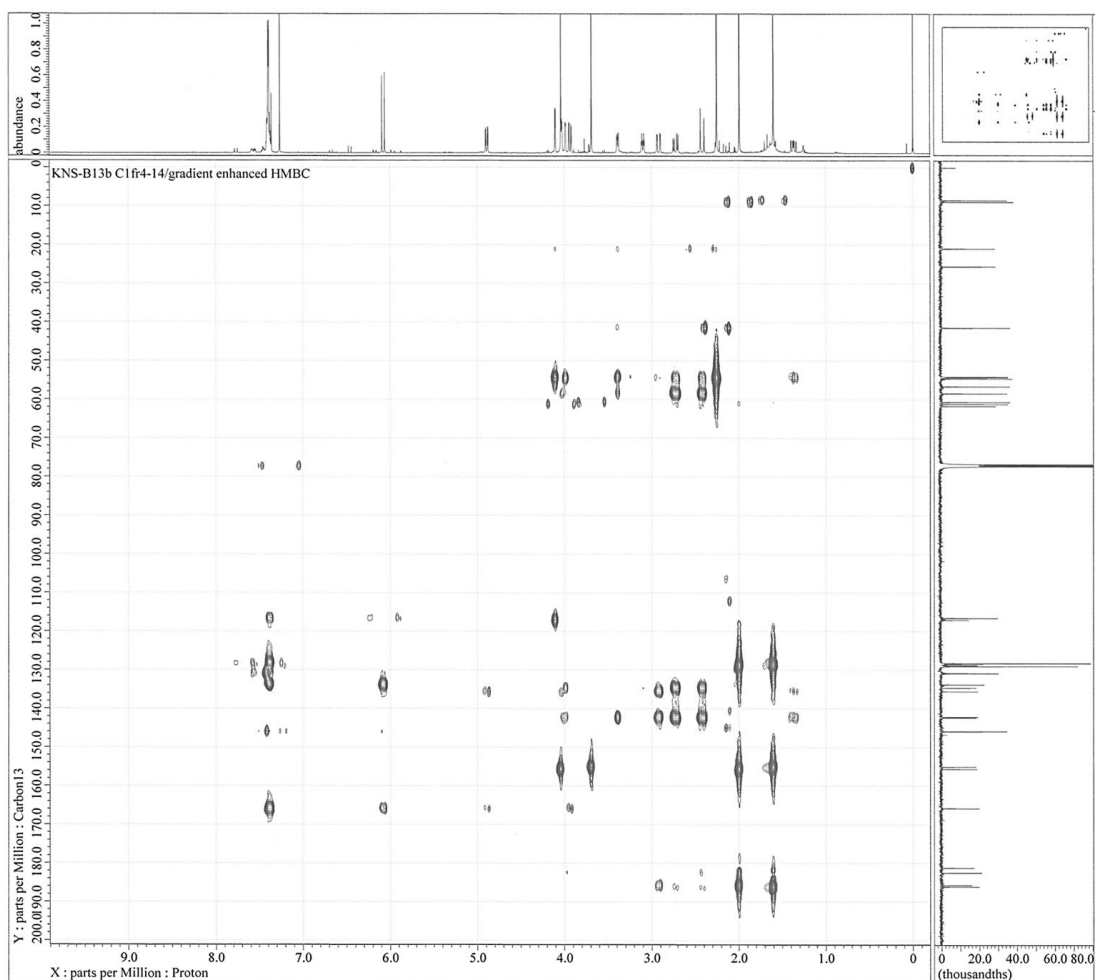


Figure C29 HMBC spectrum (500 MHz) of 22-*O*-cinnamoyl jorunnamycin A (**R8**) in CDCl_3

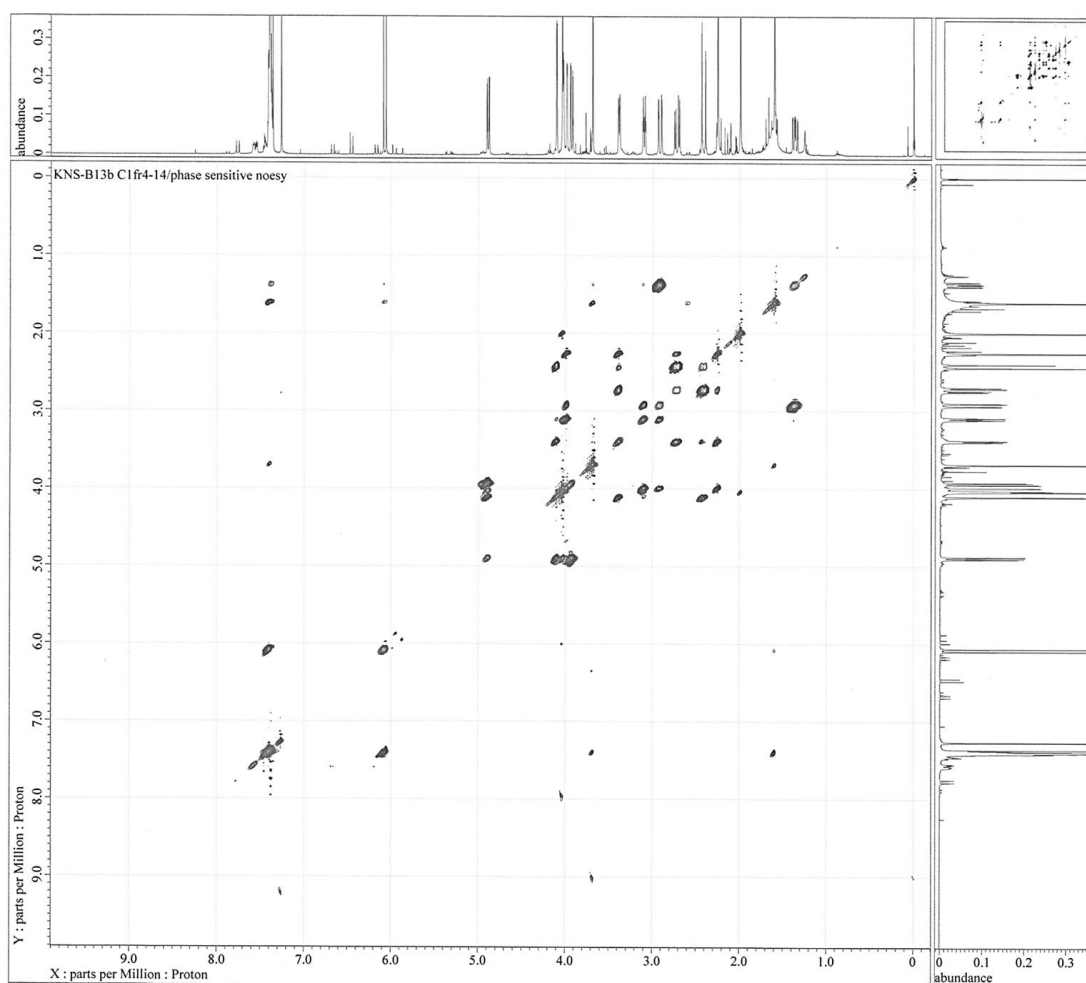
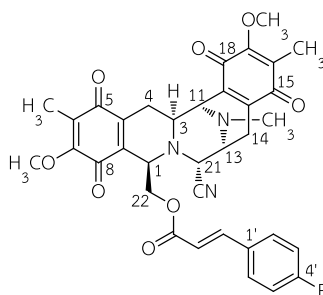
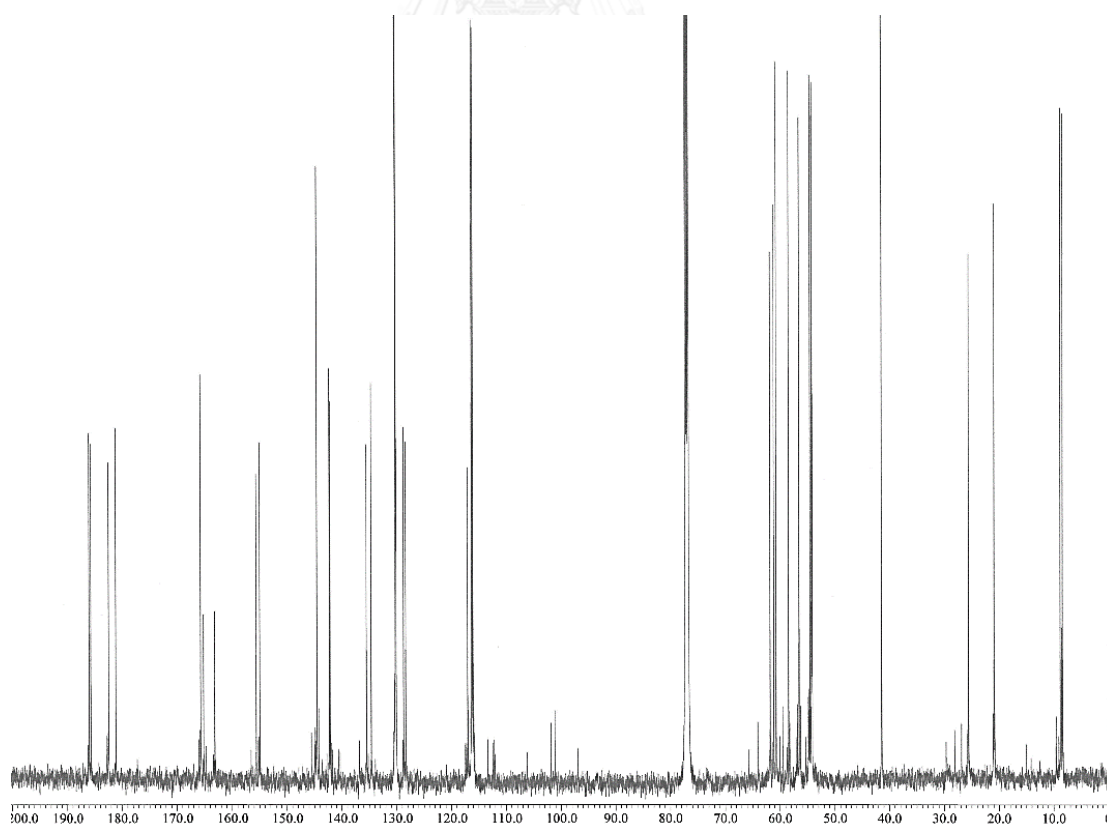
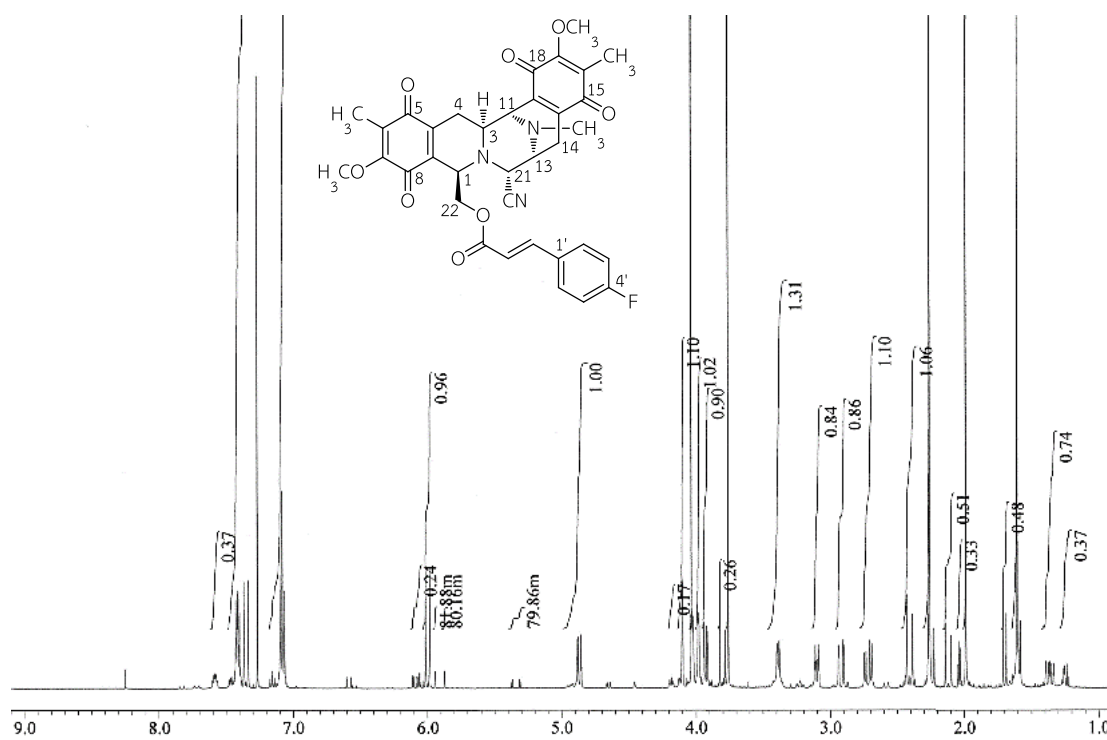
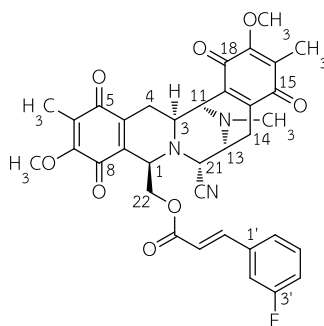


Figure C30 NOESY spectrum (500 MHz) of 22-O-cinnamoyl jorunnamycin A (**R8**) in CDCl_3



22-O-(4-Fluorocinnamoyl)jorunnamycin A (R9): yield 61.5%; yellow amorphous solid; $[\alpha]_D^{21}$ -159.2 (c 0.4, CHCl_3); CD $\Delta\epsilon$ nm (c 12.5 μM , MeOH, 25°C) 0 (402), -5.8 (355), -3.1 (308), -19.4 (283), 0 (270), $+16.5$ (258), $+1.8$ sh (233), 0 (227), -5.0 (218), -4.0 (214), -12.7 (205); IR (KBr) ν_{max} 2926, 2853, 1717, 1655, 1616, 1601, 1510, 1450, 1373, 1312, 1234, 1159, 835 cm^{-1} ; ^1H NMR (CDCl_3 , 500 MHz) δ 7.41 (2H, dd, $J = 8.9, 5.5$ Hz, H-2' and H-6'), 7.35 (1H, d, $J = 16.1$ Hz, $\text{COCH}=\text{CH}$), 7.08 (2H, t, $J = 8.6$ Hz, H-3' and H-5'), 6.00 (1H, d, $J = 16.1$ Hz, $\text{COCH}=\text{CH}$), 4.87 (1H, dd, $J = 11.9, 3.2$ Hz, H-22b), 4.10 (1H, d, $J = 2.2$ Hz, H-21), 4.03 (3H, s, 7-OCH₃), 4.02 (1H, ddd, $J = 3.2, 2.7, 2.6$ Hz, H-1), 3.98 (1H, d, $J = 2.9$ Hz, H-11), 3.93 (1H, dd, $J = 11.9, 2.7$ Hz, H-22a), 3.76 (3H, s, 17-OCH₃), 3.39 (1H, ddd, $J = 7.8, 2.2, 1.7$ Hz, H-13), 3.10 (1H, ddd, $J = 11.7, 2.9, 2.6$ Hz, H-3), 2.92 (1H, dd, $J = 17.4, 2.6$ Hz, H-4 α), 2.72 (1H, dd, $J = 21.2, 7.8$ Hz, H-14 α), 2.41 (1H, d, $J = 21.2$ Hz, H-14 β), 2.26 (3H, s, NCH₃), 1.94 (3H, s, 6-CH₃), 1.61 (3H, s, 16-CH₃), 1.36 (1H, ddd, $J = 17.4, 11.7, 2.6$ Hz, H-4 β); ^{13}C NMR (CDCl_3 , 125 MHz) δ 186.0 (C, C-15), 185.7 (C, C-5), 182.4 (C, C-18), 181.1 (C, C-8), 165.7 (C, OCO), 164.1 (C, C-4'), 155.6 (C, C-7), 154.5 (C, C-17), 144.5 (CH, $\text{COCH}=\text{CH}$), 142.3 (C, C-10), 142.1 (C, C-20), 135.5 (C, C-9), 134.6 (C, C-19), 130.1 (CH, C-2' and C-6'), 130.1 (C, C-1'), 128.7 (C, C-6), 128.3 (C, C-16), 117.0 (C, CN), 116.3 (CH, $\text{COCH}=\text{CH}$), 116.1 (CH, C-3' and C-5'), 61.8 (CH₂, C-22), 61.2 (CH₃, 7-OCH₃), 60.7 (CH₃, 17-OCH₃), 58.4 (CH, C-21), 56.5 (CH, C-1), 54.5 (CH, C-13), 54.3 (CH, C-3), 54.1 (CH, C-11), 41.4 (CH₃, NCH₃), 25.6 (CH₂, C-4), 20.9 (CH₂, C-14), 8.8 (CH₃, 6-CH₃), 8.4 (CH₃, 16-CH₃); HRFABMS m/z 642.2255 [$\text{M}+\text{H}$]⁺ (calcd for C₃₅H₃₃O₈N₃F, 642.2252).





22-O-(3-fluorocinnamoyl)jorunnamycin A (R10): yield 69.2%; yellow amorphous solid; $[\alpha]_D^{24}$ -150.8 (c 0.5, CHCl_3); CD $\Delta\epsilon$ nm (c 12.5 μM , MeOH, 24°C) 0 (408), -4.5 (367), -4.14 (319), -15.9 (282), 0 (269), $+10.3$ (258), $+1.0$ sh (236), 0 (230), -2.8 (220), -2.9 sh (213), -6.4 (205); IR (KBr) ν_{max} 2945, 2853, 2228, 1717, 1655, 1614, 1584, 1449, 1373, 1318, 1275, 1236, 1159, 1150, 980, 966, 787, 770, 756 cm^{-1} ; ^1H NMR (CDCl_3 , 500 MHz) δ 7.36 (1H, m, H-5'), 7.35 (1H, d, $J = 16.2$ Hz, COCH=CH), 7.19 (1H, br d, $J = 7.7$ Hz, H-6'), 7.12 (1H, br d, $J = 8.9$ Hz, H-2'), 7.11 (1H, m, H-4'), 6.07 (1H, d, $J = 16.2$ Hz, COCH=CH), 4.86 (1H, dd, $J = 11.8, 3.2$ Hz, H-22b), 4.10 (1H, d, $J = 2.3$ Hz, H-21), 4.03 (3H, s, 7-OCH₃), 4.03 (1H, overlapped, H-1), 3.99 (1H, d, $J = 2.3$ Hz, H-11), 3.96 (1H, dd, $J = 11.8, 2.6$ Hz, H-22a), 3.78 (3H, s, 17-OCH₃), 3.39 (1H, ddd, $J = 7.3, 2.3, 1.9$ Hz, H-13), 3.10 (1H, ddd, $J = 11.8, 2.6, 2.6$ Hz, H-3), 2.92 (1H, dd, $J = 17.4, 2.6$ Hz, H-4 α), 2.72 (1H, dd, $J = 21.2, 7.3$ Hz, H-14 α), 2.40 (1H, d, $J = 21.2$ Hz, H-14 β), 2.26 (3H, s, NCH₃), 1.99 (3H, s, 6-CH₃), 1.69 (3H, s, 16-CH₃), 1.36 (1H, ddd, $J = 17.4, 11.8, 2.6$ Hz, H-4 β); ^{13}C NMR (CDCl_3 , 125 MHz) δ 186.0 (C, C-15), 185.6 (C, C-5), 182.4 (C, C-18), 181.1 (C, C-8), 165.4 (C, OCO), 163.0 (C, C-3'), 155.6 (C, C-7), 155.0 (C, C-17), 144.4 (CH, COCH=CH), 142.2 (C, C-10), 142.1 (C, C-20), 136.0 (C, C-1'), 135.4 (C, C-9), 134.6 (C, C-19), 130.6 (CH, C-5'), 128.7 (C, C-6), 128.3 (C, C-16), 124.4 (CH, C-6'), 117.9 (CH, COCH=CH), 117.6 (CH, C-2'), 117.0 (C, CN), 114.2 (CH, C-4'), 62.0 (CH₂, C-22), 61.1 (CH₃, 7-OCH₃), 60.7 (CH₃, 17-OCH₃), 58.4 (CH, C-21), 56.5 (CH, C-1), 54.5 (CH, C-13), 54.3 (CH, C-3), 54.1 (CH, C-11), 41.4 (CH₃, NCH₃), 25.5 (CH₂, C-4), 20.9 (CH₂, C-14), 8.8 (CH₃, 6-CH₃), 8.4 (CH₃, 16-CH₃); HRFABMS m/z 642.2255 $[\text{M}+\text{H}]^+$ (calcd for C₃₅H₃₃O₈N₃F, 642.2252).

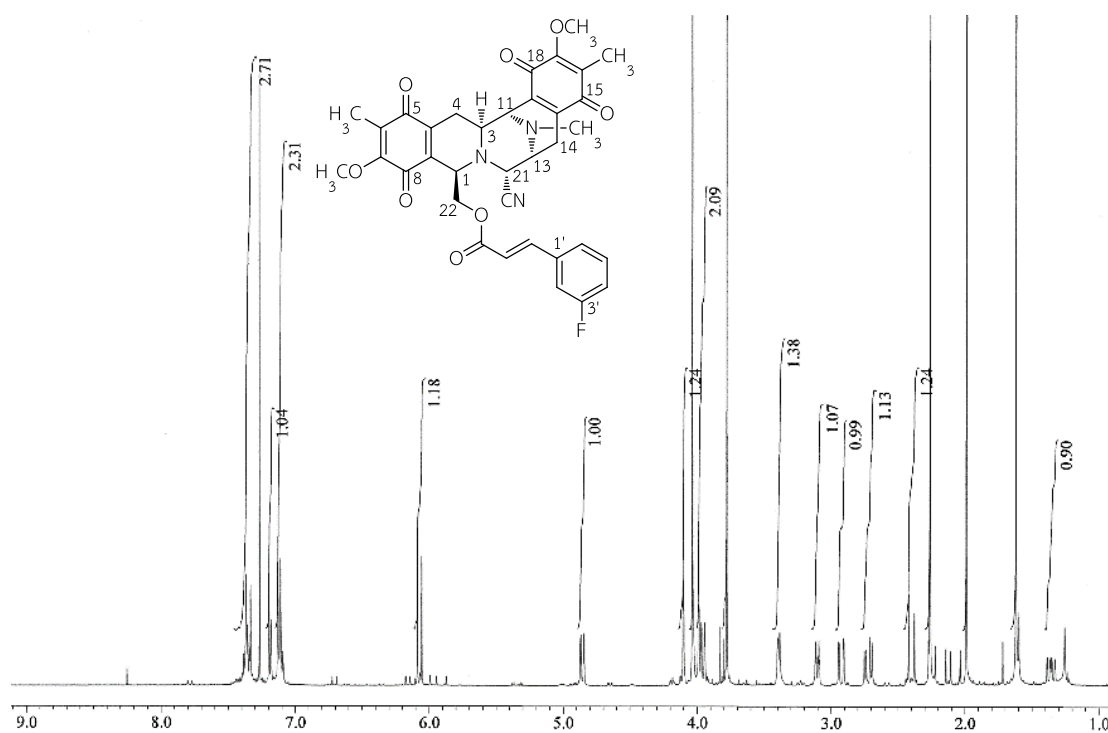


Figure C33 ¹H NMR spectrum (500 MHz) of 22-O-(3-fluorocinnamoyl) jorunnamycin A (R10) in CDCl₃

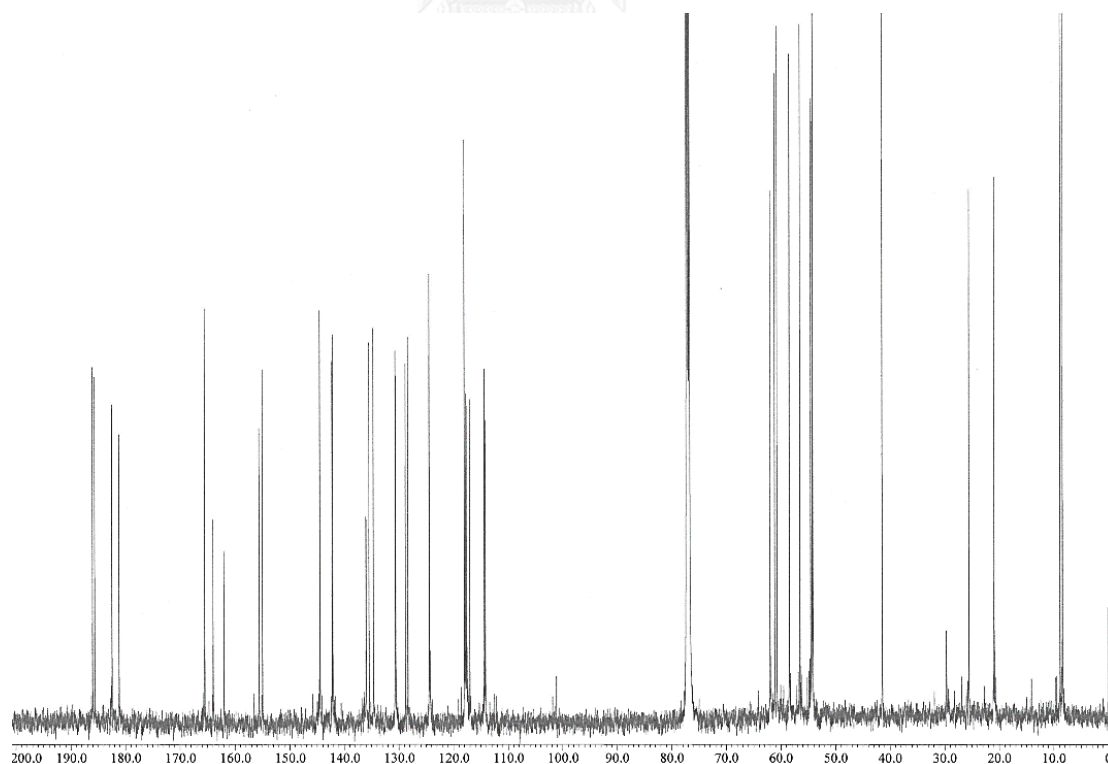
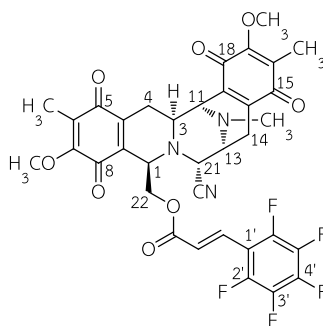


Figure C34 ¹³C NMR spectrum (125 MHz) of 22-O-(3-fluorocinnamoyl) jorunnamycin A (R10) in CDCl₃



22-O-Pentafluorocinnamoyl jorunnamycin A (R11): yield 64.9%; yellow amorphous solid; $[\alpha]_D^{24}$ -123.9 (c 0.6, CHCl_3); CD $\Delta\epsilon$ nm (c 11.2 μM , MeOH, 24°C) 0 (396), -2.4 (357), -1.7 (320), -8.7 (285), 0 (268), $+4.6$ (259), $+0.6$ sh (240), -1.3 (224), 0 (214), $+3.4$ (206); IR (KBr) ν_{max} 2949, 2855, 1724, 1655, 1616, 1524, 1501, 1375, 1296, 1236, 1151, 964 cm^{-1} ; ^1H NMR (CDCl_3 , 500 MHz) δ 7.35 (1H, d, J = 16.6 Hz, COCH=CH), 6.40 (1H, d, J = 16.6 Hz, COCH=CH), 4.74 (1H, dd, J = 11.5, 3.1 Hz, H-22b), 4.08 (1H, d, J = 2.4 Hz, H-21), 4.05 (1H, ddd, J = 3.1, 3.1, 2.5 Hz, H-1), 4.03 (3H, s, 7-OCH₃), 4.02 (1H, dd, J = 11.5, 3.1 Hz, H-22a), 3.99 (1H, d, J = 2.5 Hz, H-11), 3.94 (3H, s, 17-OCH₃), 3.39 (1H, ddd, J = 7.7, 2.4, 1.7 Hz, H-13), 3.12 (1H, ddd, J = 11.6, 2.8, 2.5 Hz, H-3), 2.96 (1H, dd, J = 17.5, 2.8 Hz, H-4 α), 2.73 (1H, dd, J = 21.2, 7.7 Hz, H-14 α), 2.33 (1H, d, J = 21.2 Hz, H-14 β), 2.27 (3H, s, NCH₃), 1.98 (3H, s, 6-CH₃), 1.70 (3H, s, 16-CH₃), 1.36 (1H, ddd, J = 17.5, 11.6, 2.5 Hz, H-4 β); ^{13}C NMR (CDCl_3 , 125 MHz) δ 185.9 (C, C-15), 185.7 (C, C-5), 182.4 (C, C-18), 181.1 (C, C-8), 164.9 (C, OCO), 155.5 (C, C-7), 154.9 (C, C-17), 145.5 (C, C-2' and C-6'), 142.2 (C, C-10), 142.1 (C, C-20), 142.0 (C, C-4'), 137.8 (C, C-3' and C-5'), 135.2 (C, C-9), 134.7 (C, C-19), 129.2 (CH, COCH=CH), 128.9 (C, C-6), 127.9 (C, C-16), 124.7 (CH, COCH=CH), 116.9 (C, CN), 109.3 (C, C-1'), 63.1 (CH₂, C-22), 61.1 (CH₃, 7-OCH₃), 60.9 (CH₃, 17-OCH₃), 58.7 (CH, C-21), 56.2 (CH, C-1), 54.5 (CH, C-13), 54.4 (CH, C-3), 54.2 (CH, C-11), 41.5 (CH₃, NCH₃), 25.4 (CH₂, C-4), 21.1 (CH₂, C-14), 8.8 (CH₃, 6-CH₃), 8.2 (CH₃, 16-CH₃); HRFABMS m/z 714.1880 $[\text{M}+\text{H}]^+$ (calcd for C₃₅H₂₉O₈N₃F₅, 714.1875).

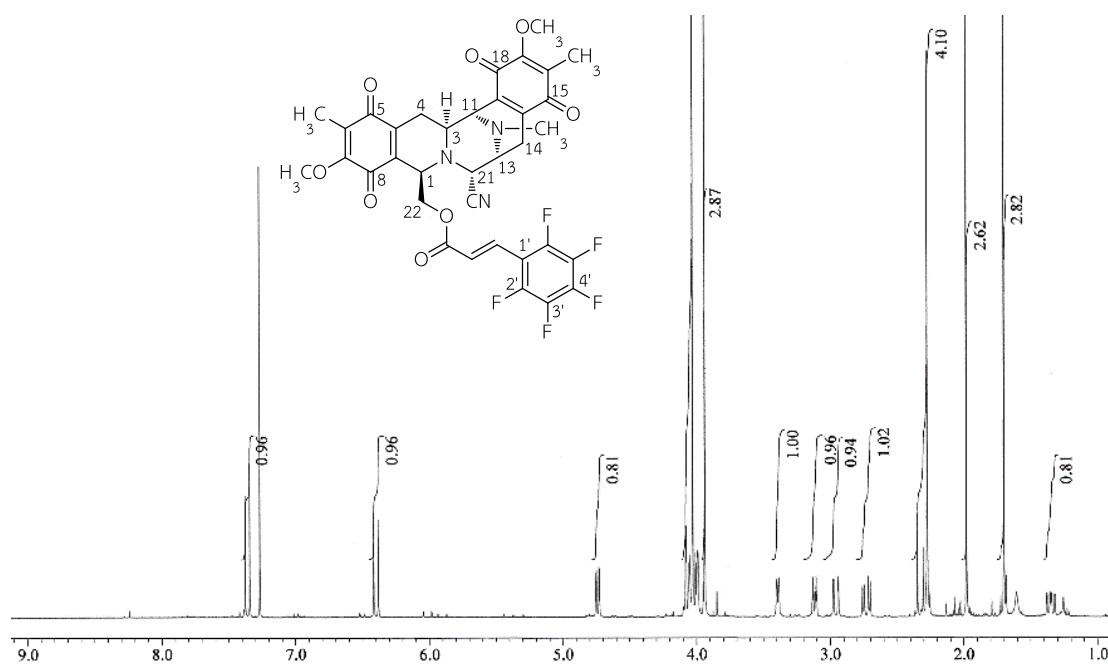


Figure C35 ¹H NMR spectrum (500 MHz) of 22-O-pentafluorocinnamoyl jorunnamycin A (R11) in CDCl₃

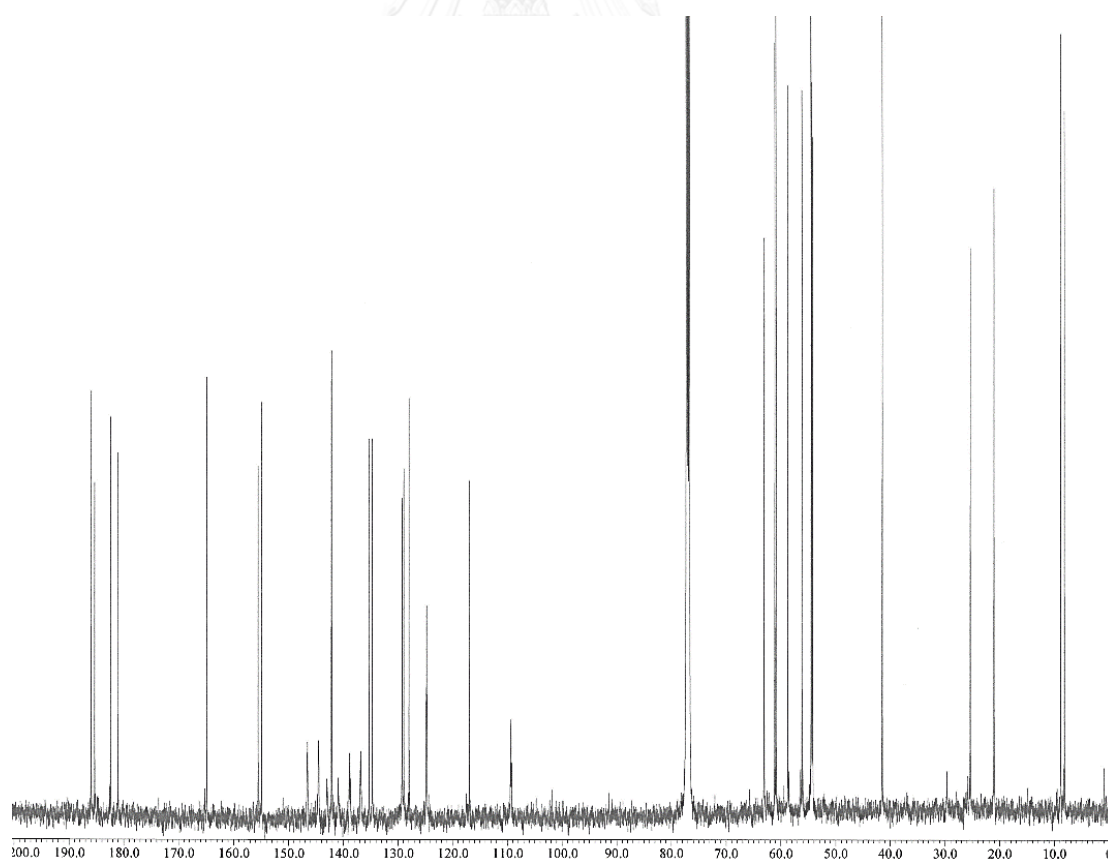
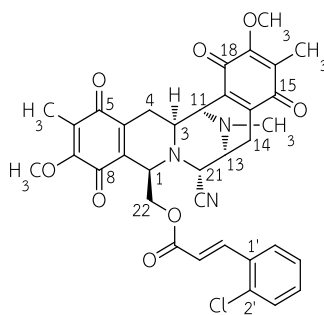


Figure C36 ¹³C NMR spectrum (125 MHz) of 22-O-pentafluorocinnamoyl jorunnamycin A (R11) in CDCl₃



22-O-(2-Chlorocinnamoyl)jorunnamycin A (R12): yield 55.2%; yellow amorphous solid; $[\alpha]_D^{23}$ -94.4 (c 0.4, CHCl_3); CD $\Delta\epsilon$ nm (c 9.1 μM , MeOH, 24°C) 0 (396), -5.2 (351), -3.8 (315), -18.5 (287), 0 (275), $+24.0$ (262), $+5.2$ sh (237), 0 (234), -5.1 (230), -8.0 sh (220), -16.9 (212); IR (KBr) ν_{max} 2945, 2930, 2853, 1717, 1655, 1616, 1447, 1373, 1314, 1236, 1161, 764 cm^{-1} ; ^1H NMR (CDCl_3) δ 7.74 (1H, d, $J = 16.1$ Hz, COCH=CH), 7.49 (1H, dd, $J = 7.8, 1.7$ Hz, H-6'), 7.39 (1H, dd, $J = 8.0, 1.3$ Hz, H-3'), 7.33 (1H, ddd, $J = 8.0, 7.4, 1.7$ Hz, H-4'), 7.29 (1H, ddd, $J = 7.8, 7.4, 1.3$ Hz, H-5'), 6.05 (1H, d, $J = 16.1$ Hz, COCH=CH), 4.96 (1H, dd, $J = 11.9, 3.2$ Hz, H-22b), 4.10 (1H, d, $J = 2.3$ Hz, H-21), 4.03 (3H, s, 7-OCH₃), 4.03 (1H, overlapped, H-1), 4.00 (1H, d, $J = 2.5$ Hz, H-11), 3.94 (1H, dd, $J = 11.9, 2.4$ Hz, H-22a), 3.74 (3H, s, 17-OCH₃), 3.38 (1H, ddd, $J = 8.0, 2.3, 1.5$ Hz, H-13), 3.10 (1H, ddd, $J = 11.5, 2.5, 2.5$ Hz, H-3), 2.93 (1H, dd, $J = 17.5, 2.5$ Hz, H-4 α), 2.70 (1H, dd, $J = 21.2, 8.0$ Hz, H-14 α), 2.40 (1H, d, $J = 21.2$ Hz, H-14 β), 2.25 (3H, s, NCH₃), 1.98 (3H, s, 6-CH₃), 1.58 (3H, s, 16-CH₃), 1.45 (1H, ddd, $J = 17.5, 11.5, 2.1$ Hz, H-4 β); ^{13}C NMR (CDCl_3 , 125 MHz) δ 185.9 (C, C-15), 185.5 (C, C-5), 182.4 (C, C-18), 181.2 (C, C-8), 165.0 (C, OCO), 155.5 (C, C-7), 154.7 (C, C-17), 142.10 (C, C-10), 142.06 (C, C-20), 140.8 (CH, COCH=CH), 135.4 (C, C-9), 135.1 (C, C-2'), 134.6 (C, C-19), 131.8 (C, C-1'), 131.5 (CH, C-4'), 130.2 (CH, C-3'), 128.9 (C, C-6), 127.7 (C, C-16), 127.4 (CH, C-6'), 127.2 (CH, C-5'), 119.4 (CH, COCH=CH), 117.0 (C, CN), 61.5 (CH₂, C-22), 61.2 (CH₃, 7-OCH₃), 60.6 (CH₃, 17-OCH₃), 58.2 (CH, C-21), 56.6 (CH, C-1), 54.5 (CH, C-13), 54.2 (CH, C-3), 54.0 (CH, C-11), 41.4 (CH₃, NCH₃), 25.6 (CH₂, C-4), 20.9 (CH₂, C-14), 8.8 (CH₃, 6-CH₃), 8.2 (CH₃, 16-CH₃); HRFABMS m/z 658.1968 $[\text{M}+\text{H}]^+$ (calcd for C₃₅H₃₃O₈N₃Cl, 658.1956).

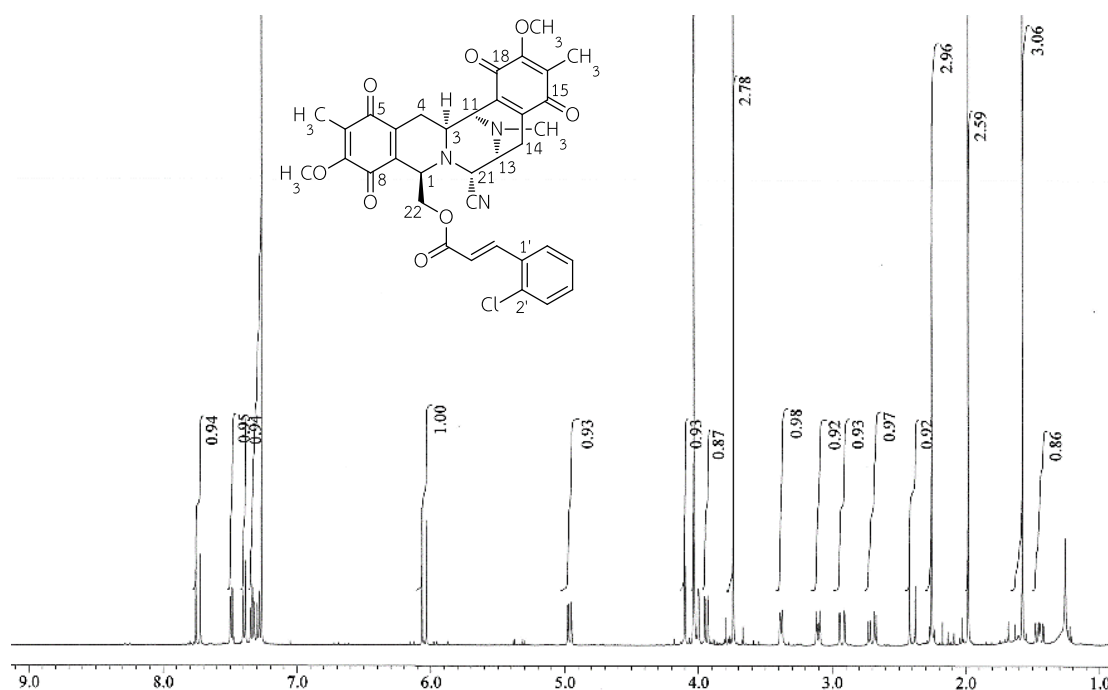


Figure C37 ^1H NMR spectrum (500 MHz) of 22-O-(2-chlorocinnamoyl) jorunnamycin A (R12) in CDCl_3

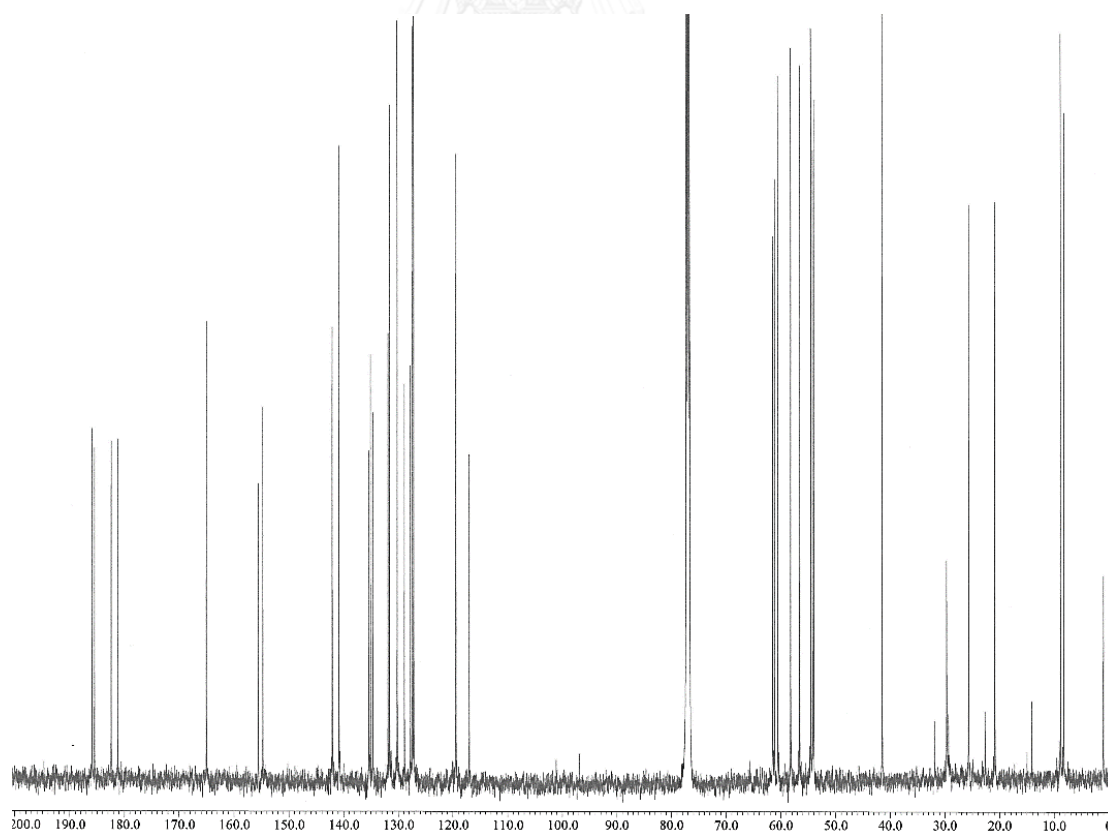
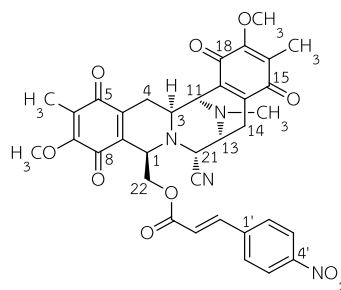


Figure C38 ^{13}C NMR spectrum (125 MHz) of 22-O-(2-chlorocinnamoyl) jorunnamycin A (R12) in CDCl_3



22-O-(4-Nitrocinnamoyl)jorunnamycin A (R13): yield 64.2%; yellow amorphous solid; $[\alpha]_D^{25}$ -189.1 (c 0.4, CHCl_3); CD $\Delta\epsilon$ nm (c 9.0 μM , MeOH, 24°C) 0 (395), -3.9 (365), -4.2 (345), -11.3 (301), 0 (274), $+12.9$ (262), 0 (239), -3.8 (228), -0.6 (211), -6.0 (204); IR (KBr) ν_{max} 2926, 2851, 1719, 1655, 1616, 1522, 1450, 1346, 1308, 1234, 1163, 847, 758 cm^{-1} ; ^1H NMR (CDCl_3 , 500 MHz) δ 8.25 (2H, d, $J = 9.1$ Hz, H-3' and H-5'), 7.60 (2H, d, $J = 9.1$ Hz, H-2' and H-6'), 7.45 (1H, d, $J = 16.2$ Hz, COCH=CH), 6.21 (1H, d, $J = 16.2$ Hz, COCH=CH), 4.83 (1H, dd, $J = 11.8, 3.2$ Hz, H-22b), 4.10 (1H, d, $J = 2.2$ Hz, H-21), 4.05 (1H, ddd, $J = 3.2, 2.9, 2.6$ Hz, H-1), 4.04 (3H, s, 7-OCH₃), 3.99 (1H, dd, $J = 11.8, 2.9$ Hz, H-22a), 3.98 (1H, d, $J = 2.9$ Hz, H-11), 3.84 (3H, s, 17-OCH₃), 3.40 (1H, ddd, $J = 7.8, 2.2, 1.7$ Hz, H-13), 3.12 (1H, ddd, $J = 11.6, 2.9, 2.6$ Hz, H-3), 2.94 (1H, dd, $J = 17.5, 2.6$ Hz, H-4 α), 2.72 (1H, dd, $J = 21.1, 7.8$ Hz, H-14 α), 2.39 (1H, d, $J = 21.1$ Hz, H-14 β), 2.27 (3H, s, NCH₃), 1.99 (3H, s, 6-CH₃), 1.60 (3H, s, 16-CH₃), 1.37 (1H, ddd, $J = 17.5, 11.6, 2.6$ Hz, H-4 β); ^{13}C NMR (CDCl_3 , 125 MHz) δ 186.0 (C, C-15), 185.6 (C, C-5), 182.4 (C, C-18), 181.1 (C, C-8), 165.0 (C, OCO), 155.6 (C, C-7), 154.9 (C, C-17), 148.7 (C, C-4'), 143.0 (CH, COCH=CH), 142.24 (C, C-10), 142.16 (C, C-20), 139.8 (C, C-1'), 135.2 (C, C-9), 134.7 (C, C-19), 128.8 (C, C-6 and CH, C-2' and C-6'), 128.1 (C, C-16), 124.2 (CH, C-3' and C-5'), 120.8 (CH, COCH=CH), 116.9 (C, CN), 62.6 (CH₂, C-22), 61.2 (CH₃, 7-OCH₃), 60.9 (CH₃, 17-OCH₃), 58.5 (CH, C-21), 56.3 (CH, C-1), 54.5 (CH, C-13), 54.3 (CH, C-3), 54.2 (CH, C-11), 41.5 (CH₃, NCH₃), 25.6 (CH₂, C-4), 21.0 (CH₂, C-14), 8.9 (CH₃, 6-CH₃), 8.5 (CH₃, 16-CH₃); HRFABMS m/z 669.2209 $[\text{M}+\text{H}]^+$ (calcd for $\text{C}_{35}\text{H}_{33}\text{O}_{10}\text{N}_4$, 669.2197).

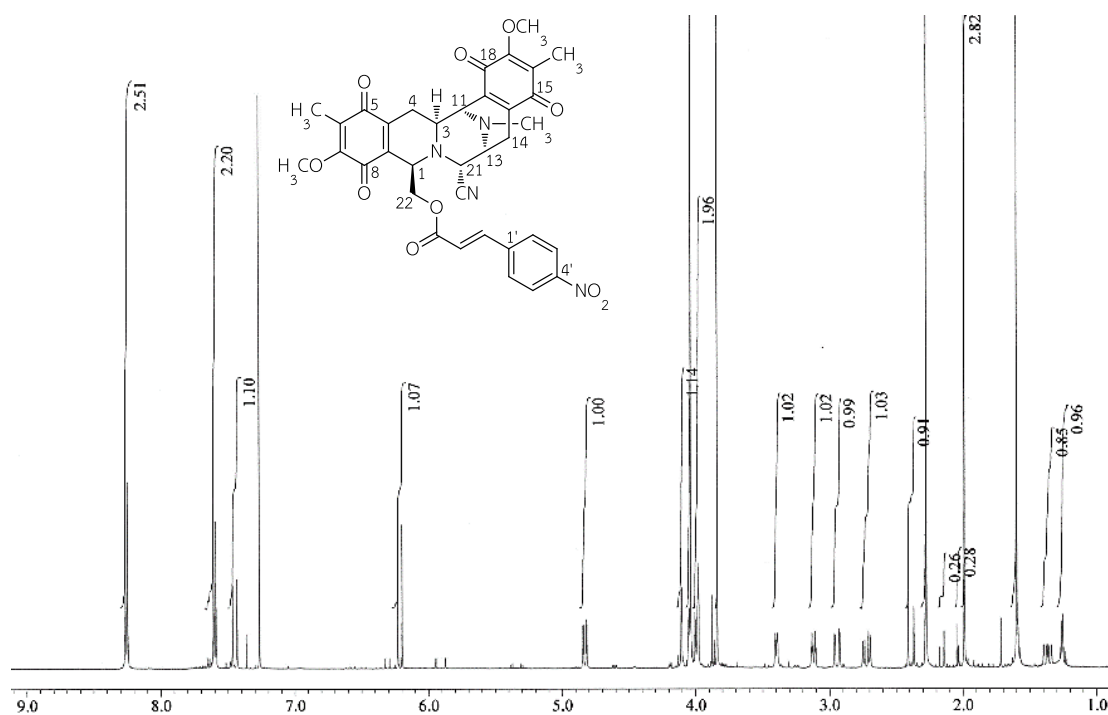


Figure C39 ¹H NMR spectrum (500 MHz) of 22-O-(4-nitrocinnamoyl) jorunnamycin A (R13) in CDCl₃

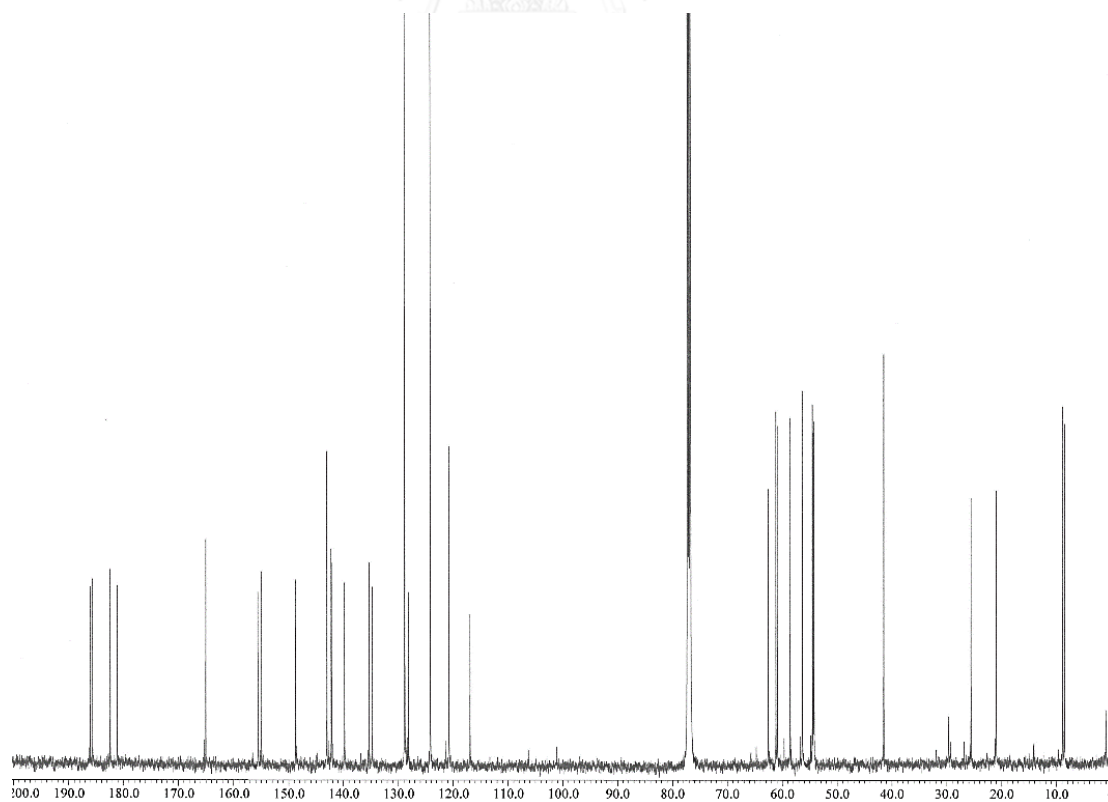
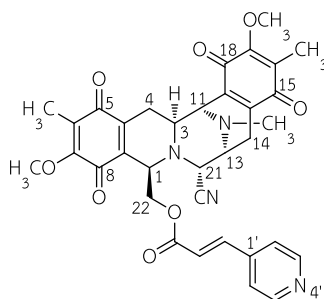


Figure C40 ¹³C NMR spectrum (125 MHz) of 22-O-(4-nitrocinnamoyl) jorunnamycin A (R13) in CDCl₃



22-O-[3-(4-Pyridyl)acryloyl]jorunnamycin A (R17): yield 35.3%; yellow amorphous solid; $[\alpha]_D^{29}$ -130.4 (c 0.3, CHCl_3); CD $\Delta\epsilon$ nm (c 12.8 μM , MeOH, 27°C) 0 (402), -24.8 (357), -17.2 (317), -75.2 (285), 0 (265), $+16.9$ (258), 0 (248), -21.7 (230), 0 (212); IR (KBr) ν_{max} 2961, 2928, 2854, 1721, 1655, 1616, 1450, 1414, 1373, 1310, 1300, 1261, 1234, 1163, 1098, 1082, 1028, 816, 801 cm^{-1} ; ^1H NMR (CDCl_3 , 500 MHz) δ 8.67 (2H, d, $J = 6.1$ Hz, H-3' and H-5'), 7.34 (1H, d, $J = 16.2$ Hz, $\text{COCH}=\text{CH}$), 7.30 (2H, d, $J = 6.1$ Hz, H-2' and H-6'), 6.26 (1H, d, $J = 16.2$ Hz, $\text{COCH}=\text{CH}$), 4.83 (1H, dd, $J = 11.8, 2.9$ Hz, H-22b), 4.09 (1H, d, $J = 2.4$ Hz, H-21), 4.04 (1H, ddd, $J = 2.9, 2.6, 2.6$ Hz, H-1), 4.03 (3H, s, 7-OCH₃), 3.99 (1H, dd, 11.8, 2.6 Hz, H-22a), 3.98 (1H, d, $J = 2.9$ Hz, H-11), 3.81 (3H, s, 17-OCH₃), 3.39 (1H, ddd, $J = 7.8, 2.4, 1.7$ Hz, H-13), 3.11 (1H, ddd, $J = 11.6, 2.9, 2.6$ Hz, H-3), 2.94 (1H, dd, $J = 17.5, 2.6$ Hz, H-4 α), 2.72 (1H, dd, $J = 21.2, 7.8$ Hz, H-14 α), 2.38 (1H, d, $J = 21.2$ Hz, H-14 β), 2.27 (3H, s, NCH₃), 1.99 (3H, s, 6-CH₃), 1.62 (3H, s, 16-CH₃), 1.35 (1H, ddd, $J = 17.5, 11.6, 2.6$ Hz, H-4 β); ^{13}C NMR (CDCl_3 , 125 MHz) δ 186.0 (C, C-15), 185.6 (C, C-5), 182.4 (C, C-18), 181.1 (C, C-8), 164.9 (C, OCO), 155.6 (C, C-7), 154.9 (C, C-17), 150.4 (CH, C-3' and C-5'), 142.9 (CH, $\text{COCH}=\text{CH}$), 142.23 (C, C-20), 142.16 (C, C-10), 141.1 (C, C-1'), 135.3 (C, C-9), 134.7 (C, C-19), 128.8 (C, C-6), 128.2 (C, C-16), 121.9 (CH, C-2' and C-6'), 121.4 (CH, $\text{COCH}=\text{CH}$), 116.9 (C, CN), 62.4 (CH₂, C-22), 61.2 (CH₃, 7-OCH₃), 60.9 (CH₃, 17-OCH₃), 58.5 (CH, C-21), 56.4 (CH, C-1), 54.5 (CH, C-13), 54.3 (CH, C-3), 54.2 (CH, C-11), 41.5 (CH₃, NCH₃), 25.6 (CH₂, C-4), 21.0 (CH₂, C-14), 8.9 (CH₃, 6-CH₃), 8.5 (CH₃, 16-CH₃); HRFABMS m/z 625.2304 [$\text{M}+\text{H}$]⁺ (calcd for C₃₄H₃₃O₈N₄, 625.2298).

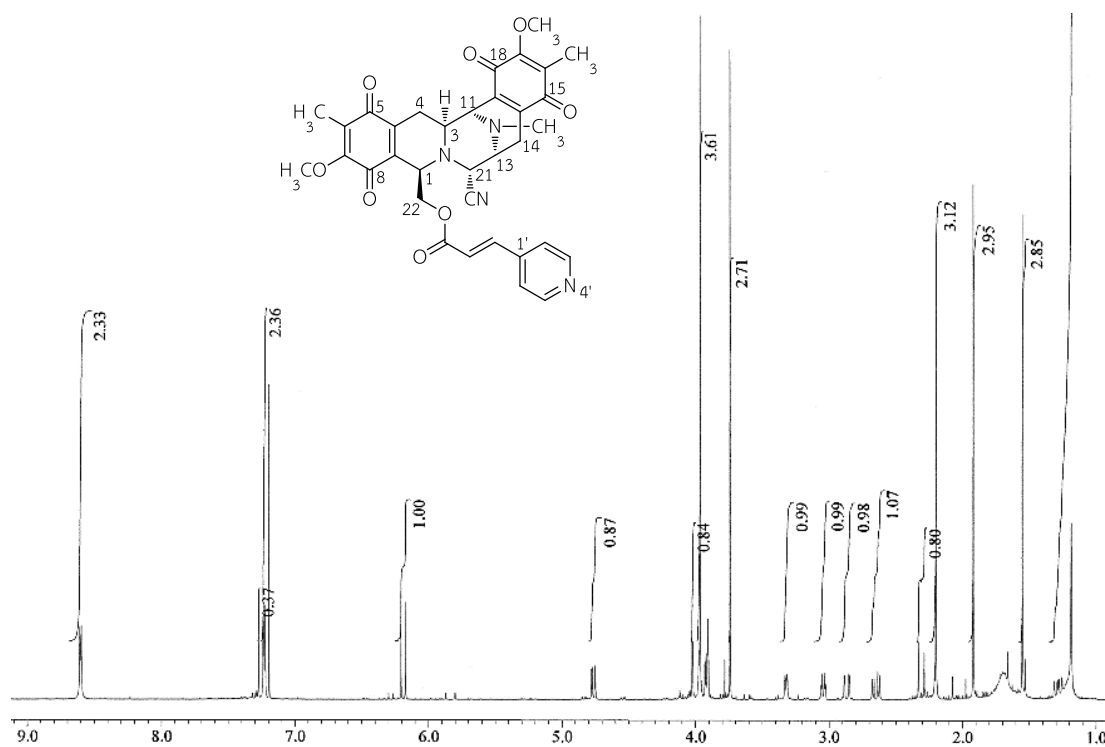


Figure C41 ^1H NMR spectrum (500 MHz) of 22-O-[3-(4-pyridyl)acryloyl] jorunnamycin A (R17) in CDCl_3

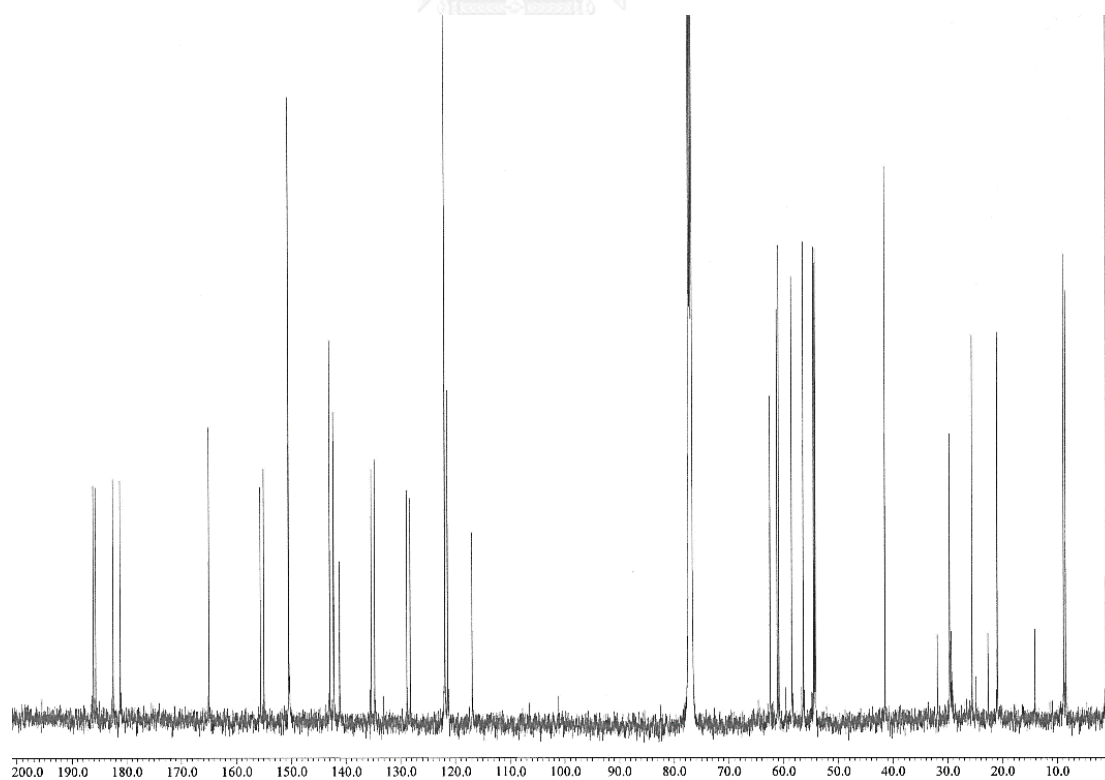
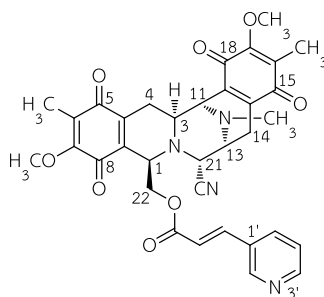


Figure C42 ^{13}C NMR spectrum (125 MHz) of 22-O-[3-(4-pyridyl)acryloyl] jorunnamycin A (R17) in CDCl_3



22-O-[3-(3-Pyridyl)acryloyl]jorunnamycin A (R18): yield 80.6%; yellow amorphous solid; $[\alpha]_D^{27}$ -180.2 (c 0.5, CHCl_3); CD $\Delta\epsilon$ nm (c 12.8 μM , MeOH, 25°C) 0 (402), -2.9 (360), -2.3 (323), -8.4 (285), 0 (270), $+5.0$ (259), 0 (241), -2.7 (223), 0 (212); IR (KBr) ν_{max} 2941, 2851, 1717, 1655, 1616, 1310, 1234, 1163 cm^{-1} ; ^1H NMR (CDCl_3 , 500 MHz) δ 8.67 (1H, d, $J = 2.2$ Hz, H-2'), 8.63 (1H, dd, $J = 5.0, 1.8$ Hz, H-4'), 7.75 (1H, ddd, $J = 8.1, 2.2, 1.8$ Hz, H-6'), 7.41 (1H, d, $J = 16.1$ Hz, $\text{COCH}=\text{CH}$), 7.34 (1H, dd, $J = 8.1, 5.0$ Hz, H-5'), 6.17 (1H, d, $J = 16.1$ Hz, $\text{COCH}=\text{CH}$), 4.84 (1H, dd, $J = 11.7, 2.9$ Hz, H-22b), 4.11 (1H, d, $J = 2.4$ Hz, H-21), 4.04 (1H, overlapped, H-1), 4.03 (3H, s, 7-OCH₃), 3.99 (1H, d, $J = 2.9$ Hz, H-11), 3.97 (1H, dd, $J = 11.7, 2.9$ Hz, H-22a), 3.83 (3H, s, 17-OCH₃), 3.39 (1H, ddd, $J = 7.7, 2.4, 1.7$ Hz, H-13), 3.11 (1H, ddd, $J = 11.6, 2.9, 2.6$ Hz, H-3), 2.93 (1H, dd, $J = 17.5, 2.6$ Hz, H-4 α), 2.72 (1H, dd, $J = 21.1, 7.7$ Hz, H-14 α), 2.40 (1H, d, $J = 21.1$ Hz, H-14 β), 2.27 (3H, s, NCH₃), 1.99 (3H, s, 6-CH₃), 1.62 (3H, s, 16-CH₃), 1.36 (1H, ddd, $J = 17.5, 11.6, 2.6$ Hz, H-4 β); ^{13}C NMR (CDCl_3 , 125 MHz) δ 186.0 (C, C-15), 185.6 (C, C-5), 182.4 (C, C-18), 181.1 (C, C-8), 165.2 (C, OCO), 155.6 (C, C-7), 155.0 (C, C-17), 151.4 (CH, C-4'), 149.7 (CH, C-2'), 142.3 (C, C-20 and CH, $\text{COCH}=\text{CH}$), 142.1 (C, C-10), 135.4 (C, C-9), 134.7 (C, C-19), 134.4 (CH, C-6'), 129.6 (C, C-1'), 128.8 (C, C-6), 128.2 (C, C-16), 123.7 (CH, C-5'), 118.7 (CH, $\text{COCH}=\text{CH}$), 116.9 (C, CN), 62.3 (CH₂, C-22), 61.2 (CH₃, 7-OCH₃), 60.8 (CH₃, 17-OCH₃), 58.5 (CH, C-21), 56.4 (CH, C-1), 54.5 (CH, C-13), 54.3 (CH, C-3), 54.2 (CH, C-11), 41.4 (CH₃, NCH₃), 25.5 (CH₂, C-4), 21.0 (CH₂, C-14), 8.8 (CH₃, 6-CH₃), 8.5 (CH₃, 16-CH₃); HRFABMS m/z 625.2295 [$\text{M}+\text{H}$]⁺ (calcd for C₃₄H₃₃O₈N₄, 625.2298).

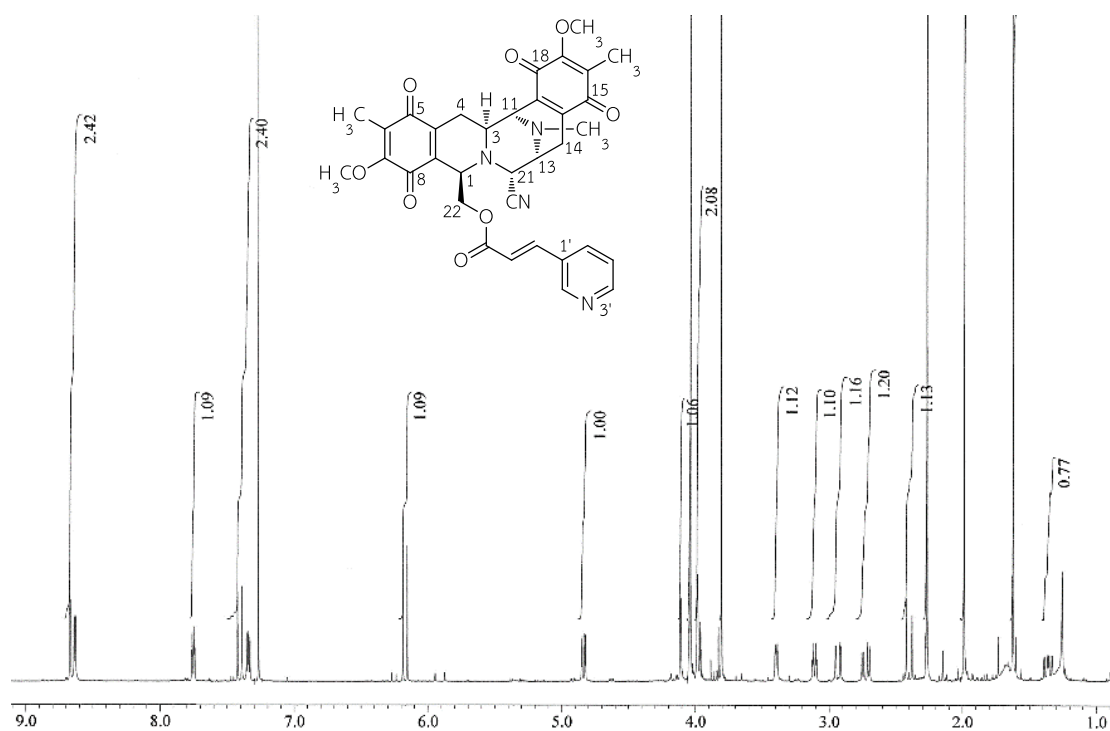


Figure C43 ^1H NMR spectrum (500 MHz) of 22-O-[3-(3-pyridyl)acryloyl]jorunnamycin A (R18) in CDCl_3

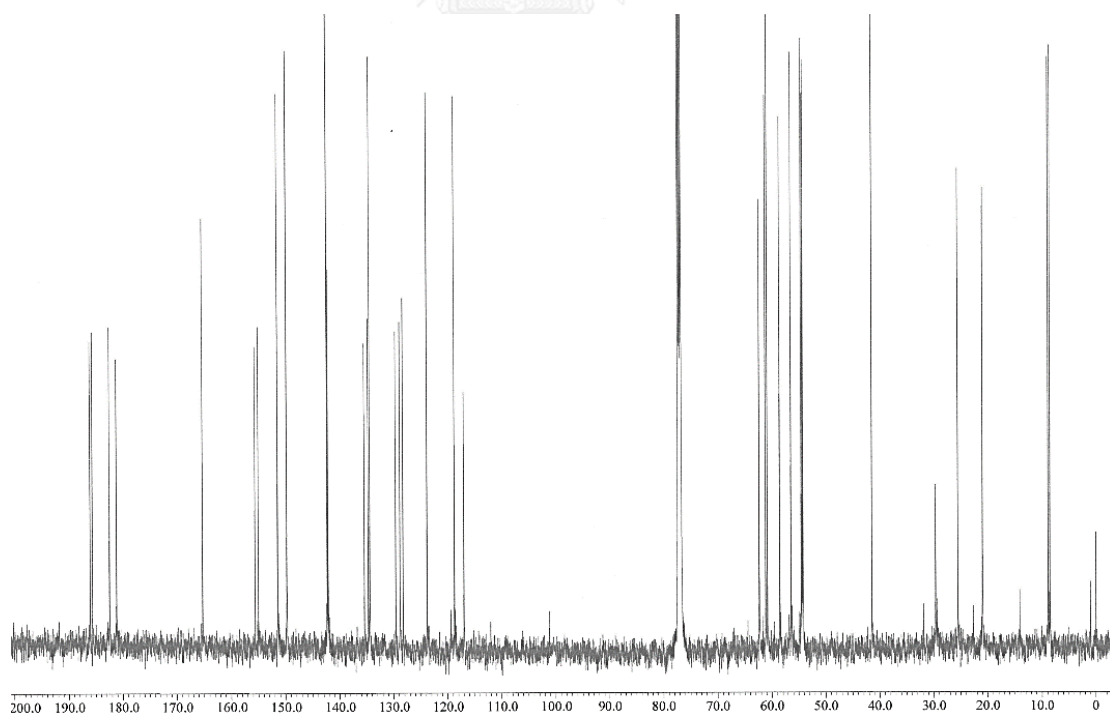


Figure C44 ^{13}C NMR spectrum (125 MHz) of 22-O-[3-(3-pyridyl)acryloyl]jorunnamycin A (R18) in CDCl_3

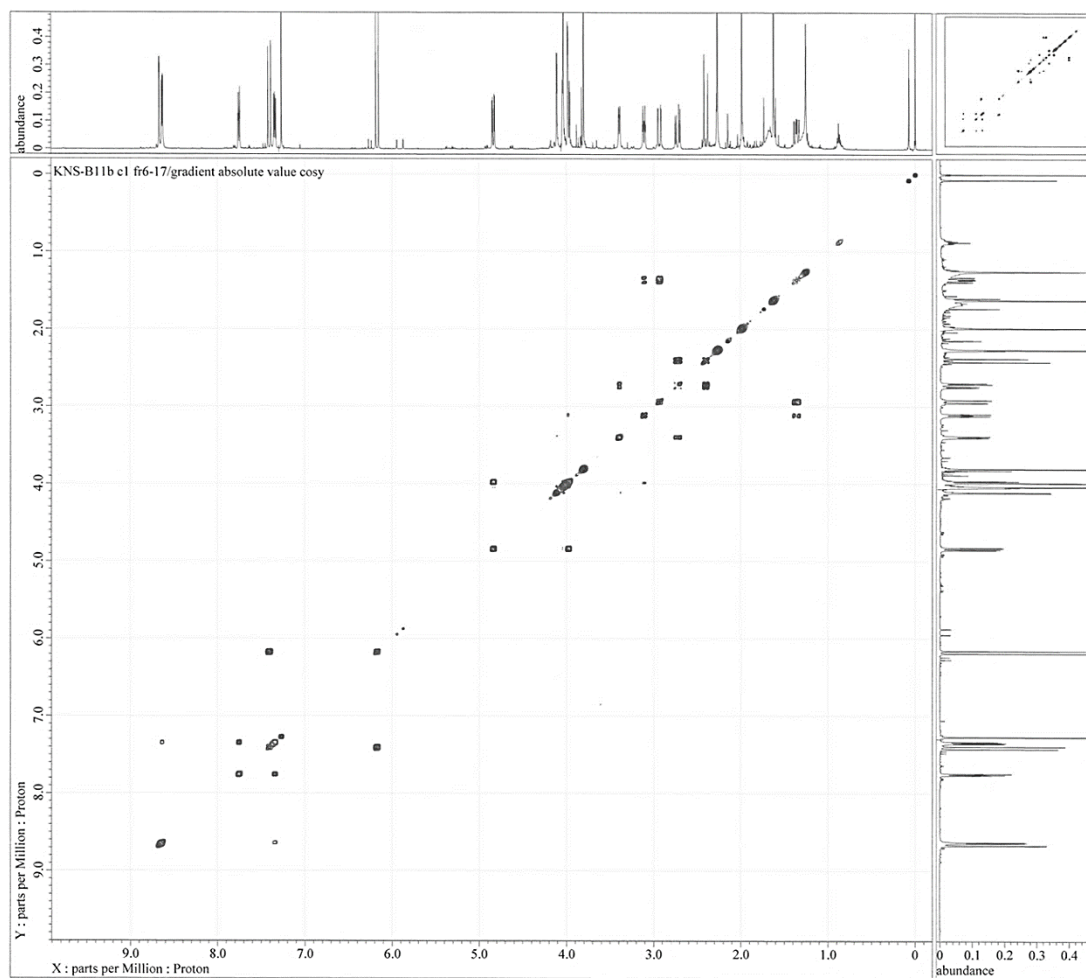


Figure C45 ^1H - ^1H COSY spectrum (500 MHz) of 22-O-[3-(3-pyridyl)acryloyl] jorunnamycin A (R18) in CDCl_3

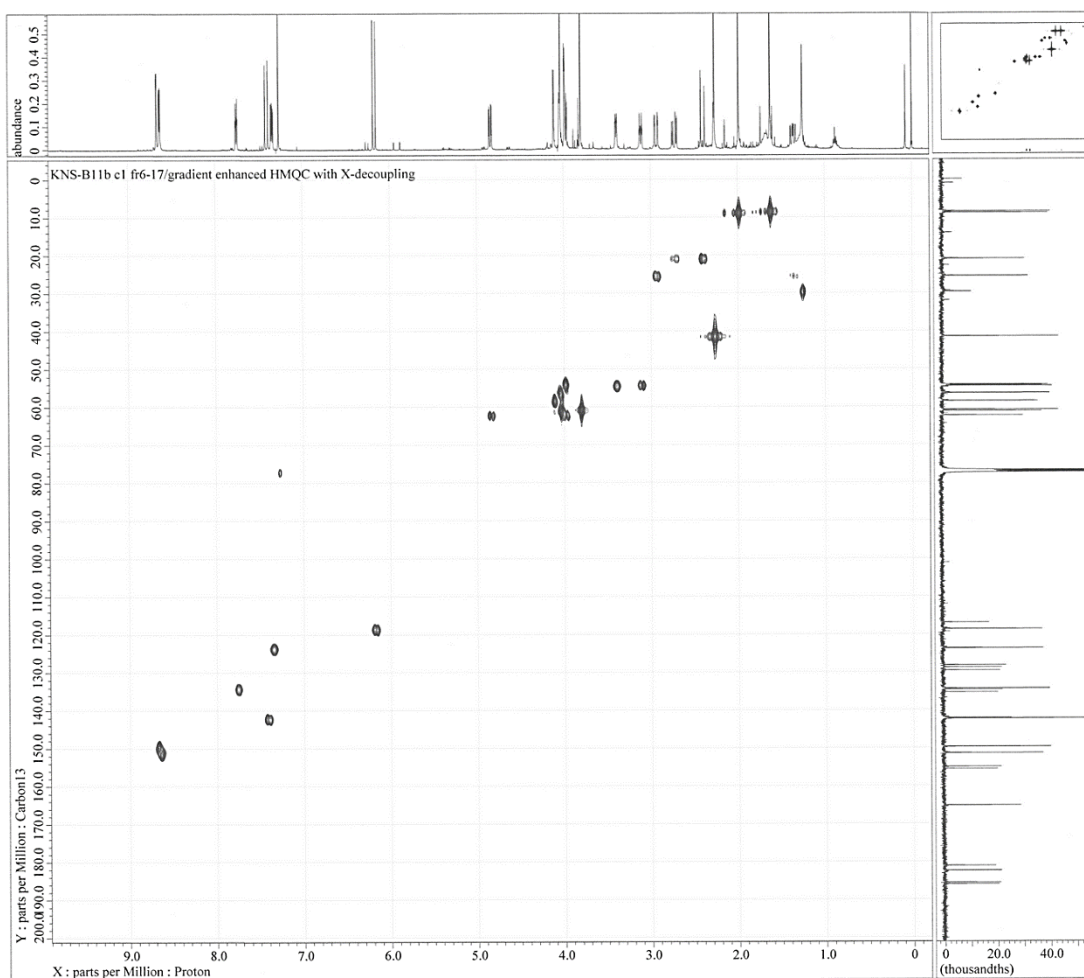


Figure C46 HMQC spectrum (500 MHz) of 22-O-[3-(3-pyridyl)acryloyl]

CHULA
jorunnamycin A (**R18**) in CDCl_3

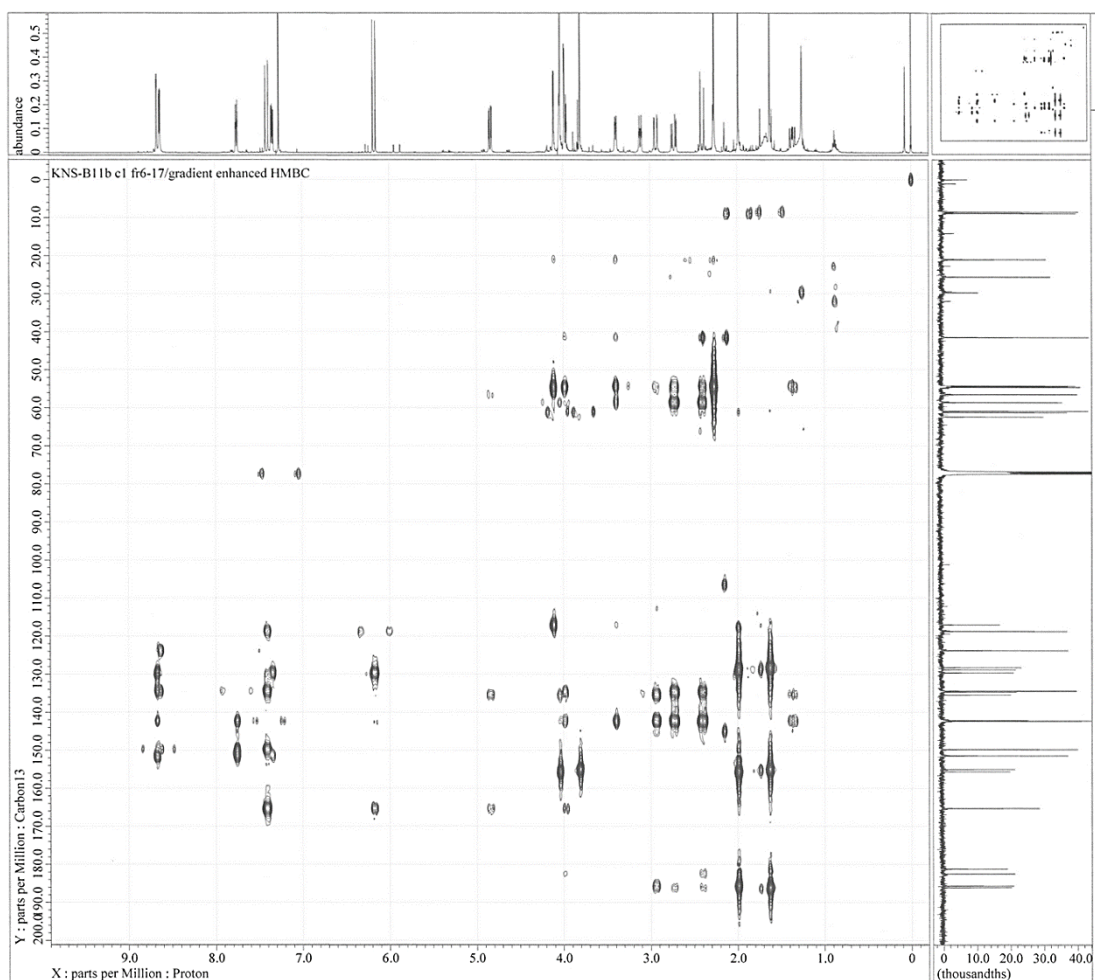


Figure C47 HMBC spectrum (500 MHz) of 22-O-[3-(3-pyridyl)acryloyl]jorunnamycin A (**R18**) in CDCl₃

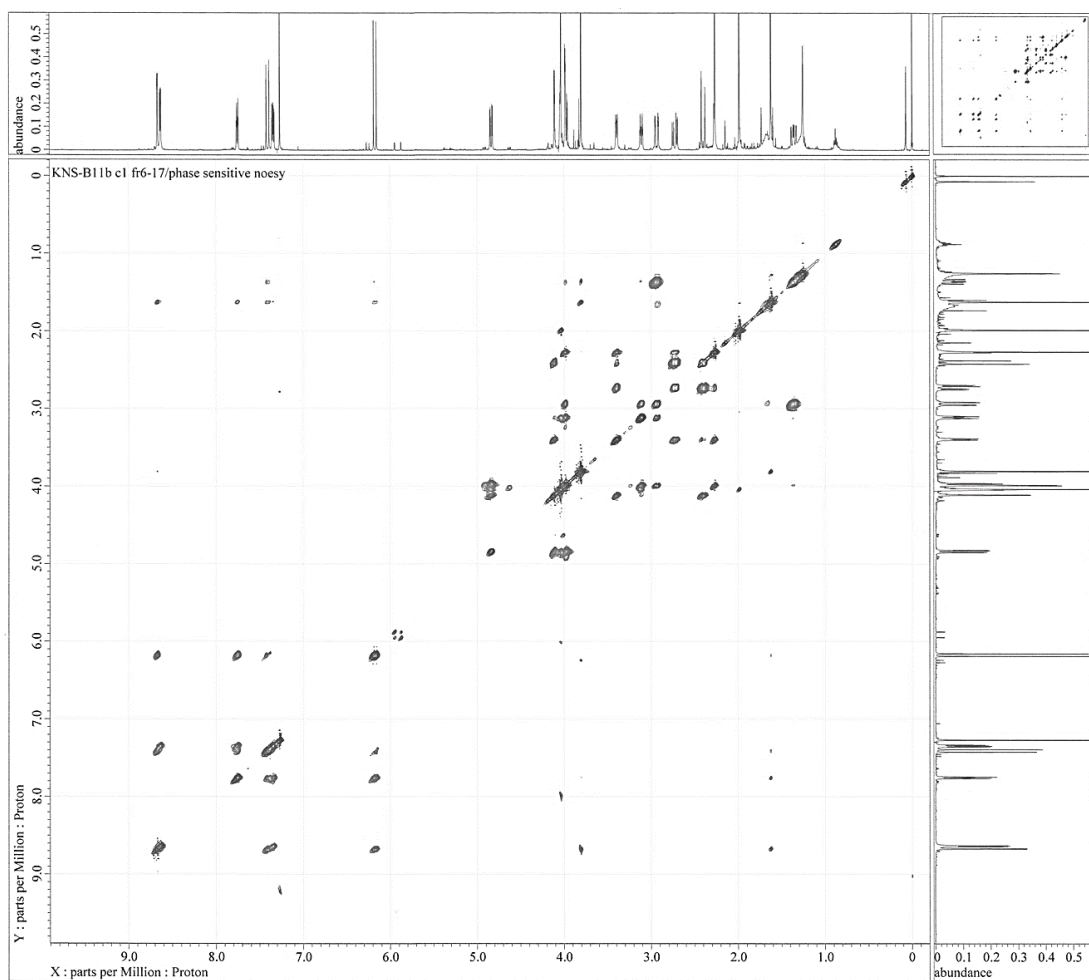


Figure C48 NOESY spectrum (500 MHz) of 22-O-[3-(3-pyridyl)acryloyl]
jorunnamycin A (R18) in CDCl₃

[Elemental Composition]

Data : 258FH001

Date : 21-Aug-2014 12:17

Sample: KNS-B11

Note : -

Inlet : Direct

Ion Mode : FAB+

RT : 3.67 min

Scan#: (17,21)

Elements : C 50/10, H 50/10, O 12/4, N 6/2

Mass Tolerance : 5mmu

Unsaturation (U.S.) : 17.0 - 24.0

Observed m/z	Int%	Err[ppm / mmu]	U.S.	Composition
625.2295	100.0	-0.6 / -0.3	20.5	C 34 H 33 O 8 N 4

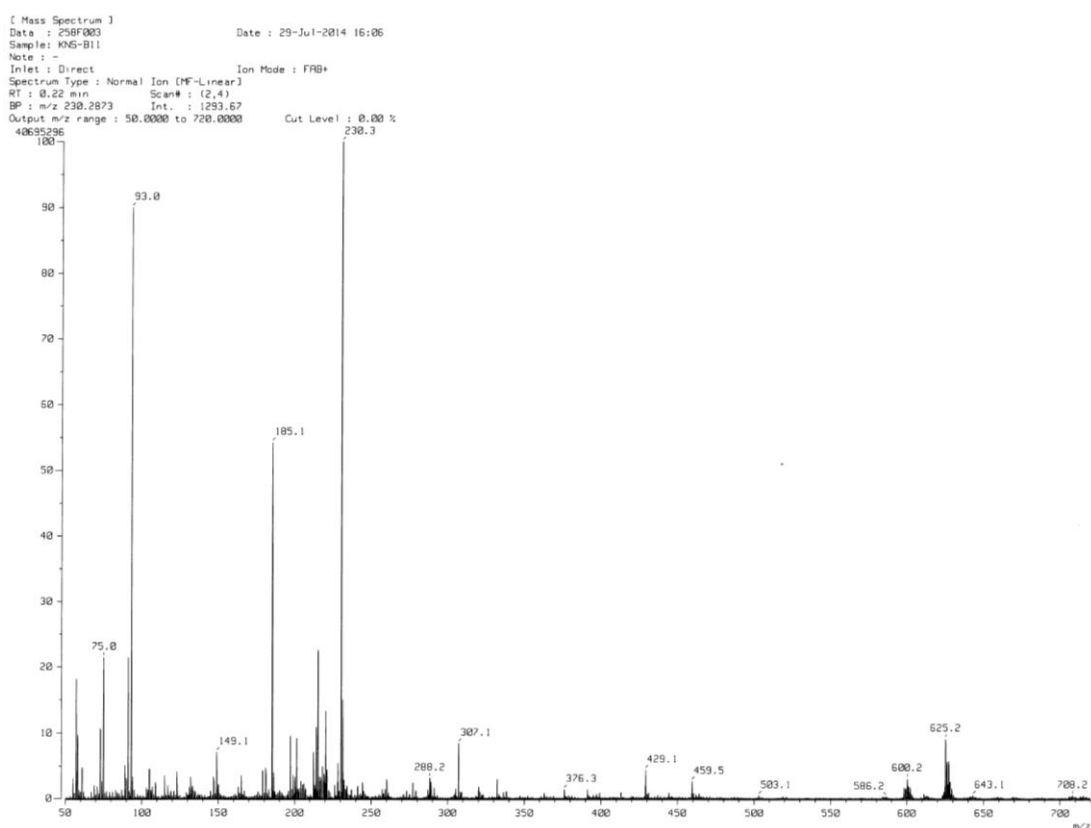


Figure C49 HRFABMS spectrum of 22-O-[3-(3-pyridyl)acryloyl]jorunnamycin A (R18)

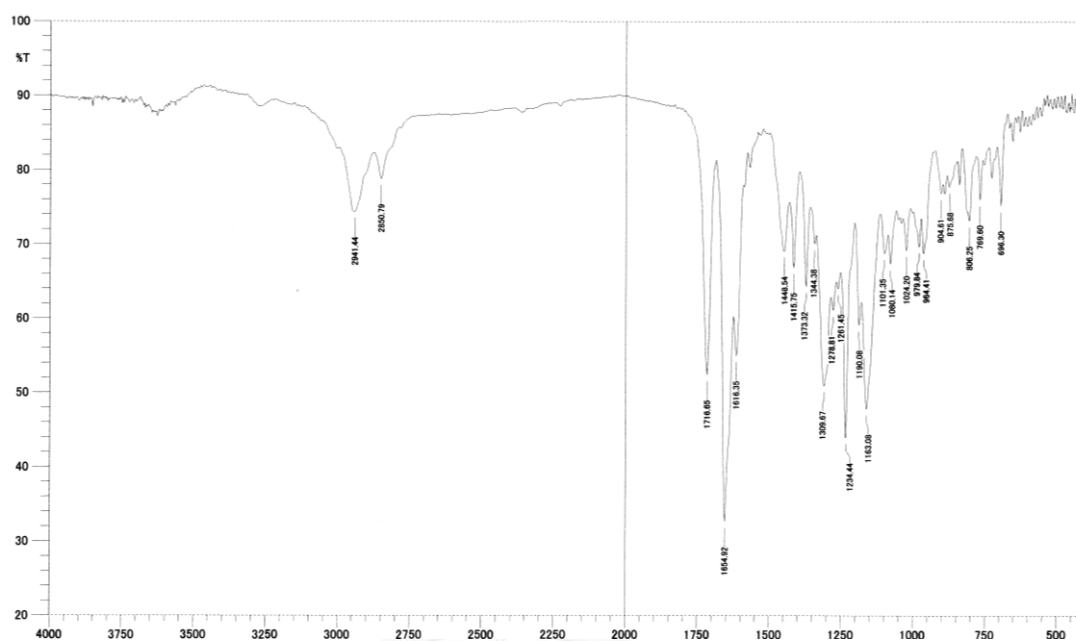


Figure C50 IR spectrum of 22-O-[3-(3-pyridyl)acryloyl]jorunnamycin A (R18)

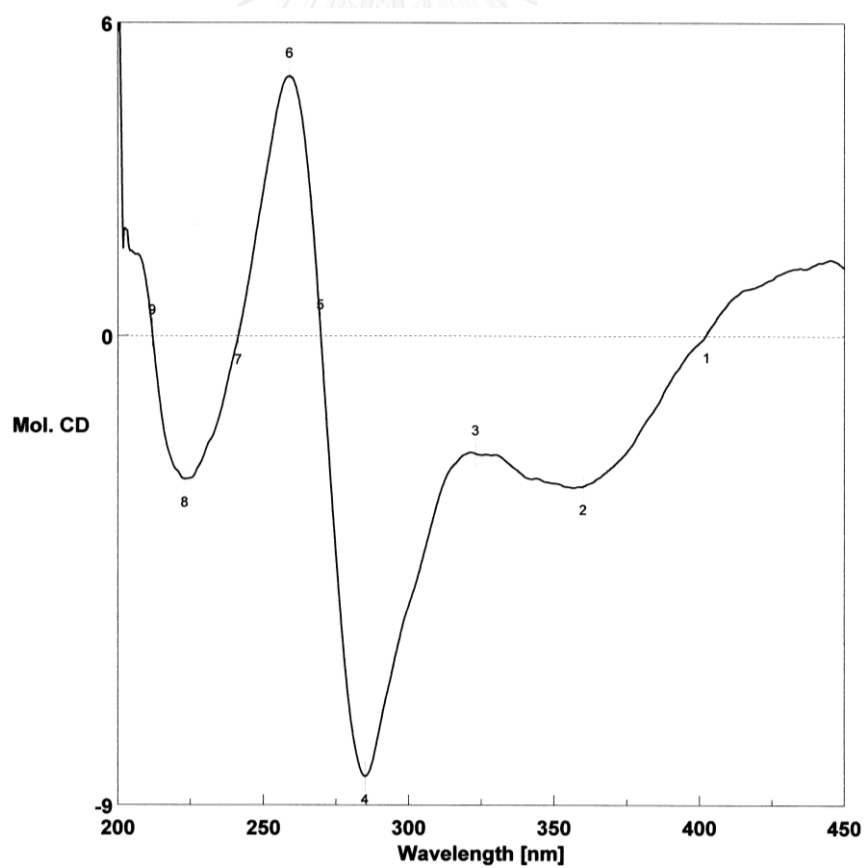
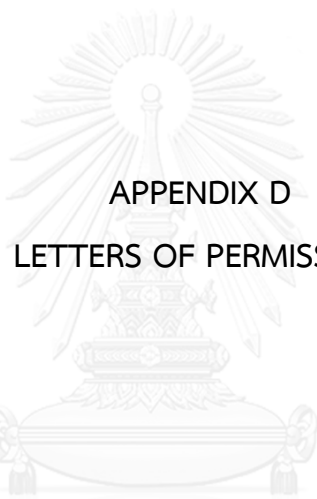


Figure C51 CD spectrum of 22-O-[3-(3-pyridyl)acryloyl]jorunnamycin A (R18) in MeOH



APPENDIX D
LETTERS OF PERMISSION

จุฬาลงกรณ์มหาวิทยาลัย
CHULALONGKORN UNIVERSITY

Permission of Natural Product Communications

INFORMATION FOR AUTHORS

Full details of how to submit a manuscript for publication in Natural Product Communications are given in Information for Authors on our Web site <http://www.naturalproduct.us>.

Authors may reproduce/republish portions of their published contribution without seeking permission from NPC, provided that any such republication is accompanied by an acknowledgment (original citation)-Reproduced by permission of Natural Product Communications. Any unauthorized reproduction, transmission or storage may result in either civil or criminal liability.

The publication of each of the articles contained herein is protected by copyright. Except as allowed under national "fair use" laws, copying is not permitted by any means or for any purpose, such as for distribution to any third party (whether by sale, loan, gift, or otherwise); as agent (express or implied) of any third party; for purposes of advertising or promotion; or to create collective or derivative works. Such permission requests, or other inquiries, should be addressed to the Natural Product Inc. (NPI). A photocopy license is available from the NPI for institutional subscribers that need to make multiple copies of single articles for internal study or research purposes.

To Subscribe: Natural Product Communications is a journal published monthly. 2015 subscription price: US\$2,595 (Print, ISSN# 1934-578X); US\$2,595 (Web edition, ISSN# 1555-9475); US\$2,995 (Print + single site online); US\$595 (Personal online). Orders should be addressed to Subscription Department, Natural Product Communications, Natural Product Inc., 7963 Anderson Park Lane, Westerville, Ohio 43081, USA. Subscriptions are renewed on an annual basis. Claims for nonreceipt of issues will be honored if made within three months of publication of the issue. All issues are dispatched by airmail throughout the world, excluding the USA and Canada.



Permission of Anticancer Research

Re: Request to reproduce copyrighted material in a dissertation

IIAR Subscriptions Department

Wed 4/27/2016 5:59 PM

To:kikns@hotmail.com <kikns@hotmail.com>;

Dear Miss Natchanun Sirimangkalakitti:

Following your request we are pleased to permit reproduction or use in other articles of any part of the paper entitled:

"Renieramycin M Sensitizes Anoikis-resistant H460 Lung Cancer Cells to Anoikis" by Sirimangkalakitti N et al

as published in Anticancer Res. 2016 Apr;36(4):1665-71,

provided that you mention the source of information.

With our best wishes,

John G. Delinasios

Managing Editor

Subject:Request to reproduce copyrighted material in a dissertation

Date:Wed, 27 Apr 2016 09:20:07 +0000

From:natchanun sirimungcalakitti <kikns@hotmail.com>

To:journals@iiar-anticancer.org <journals@iiar-anticancer.org>

Subject: Request to reproduce copyrighted material in a dissertation

Dear Editor-in-Chief of Anticancer Research,

Enclosed please find an attached file for the permission to reproduce copyrighted material.

Yours sincerely,

Miss Natchanun Sirimangkalakitti
 Department of Pharmacognosy and Pharmaceutical Botany,
 Faculty of Pharmaceutical Sciences, Chulalongkorn University,
 Pathumwan, Bangkok 10330, Thailand
 E-mail: kikns@hotmail.com

--

Dimitrios Palitskaris

Subscriptions Department

International Institute of Anticancer Research (IIAR)

ANTICANCER RESEARCH, IN VIVO and CANCER GENOMICS & PROTEOMICS

1st km Kapandritiou-Kalamou Road, P.O. Box 22, GR-19014 Kapandriti, Attiki, Greece

USA Branch: Anticancer Research USA, Inc., P.O.B. 280, Belmar, NJ 07719, USA

Tel: +30-22950-52945 ext. 1 Fax:+30-22950-52945 ext. 2

E-mail: subscriptions@iiar-anticancer.org

Web: <http://iiarjournals.org>

VITA

Miss Natchanun Sirimangkalakitti was born on August 21, 1987 in Bangkok, Thailand. She earned her Bachelor of Science in Pharmacy degree (2nd class honours) from the Faculty of Pharmaceutical Sciences, Chulalongkorn University, Thailand in 2010. Since then, she has been a Ph.D. student studying Pharmacognosy at Chulalongkorn University. She was awarded a scholarship in 2010 under the Royal Golden Jubilee Ph.D. Program Grant No. PHD/0276/2552 from the Thailand Research Fund. In 2013, she was supported to do a research in Japan for 10 months by the Meiji Pharmaceutical University Asia/Africa Center for Drug Discovery (MPU-AACDD) grant.

Publications

1. Cheun-Arom T, Chanvorachote P, Sirimangkalakitti N, Chuanasa T, Saito N, Abe I and Suwanborirux K. Replacement of a quinone by a 5-O-acetylhydroquinone abolishes the accidental necrosis inducing effect while preserving the apoptosis-inducing effect of renieramycin M on lung cancer cells. *Journal of Natural Products* 76: 1468-1474, 2013.

2. Sirimangkalakitti N, Olatunji O, Changwichit K, Saesong T, Chamni S, Chanvorachote P, Ingkaninan K, Plubrukarn A and Suwanborirux K. Bromotyrosine marine alkaloids with acetylcholinesterase inhibitory activity from the Thai sponge *Acanthodendrilla* sp. *Natural Product Communications* 10: 1945-1949, 2015.

3. Sirimangkalakitti N, Yokoya M, Chamni S, Chanvorachote P, Plubrukarn A, Saito N and Suwanborirux K. Synthesis and absolute configuration of acanthodendrilline, a new cytotoxic bromotyrosine alkaloid from the Thai marine sponge *Acanthodendrilla* sp. *Chemical and Pharmaceutical Bulletin* 64: 258-262, 2016.

4. Sirimangkalakitti N, Chamni S, Suwanborirux K and Chanvorachote P. Renieramycin M sensitizes anoikis-resistant H460 lung cancer cells to anoikis. *Anticancer Research* 36: 1665-1671, 2016.

5. Sirimangkalakitti N, Chamni S, Charupant K, Chanvorachote P, Mori N, Saito N and Suwanborirux K. Chemistry of renieramycins. Part 15: Synthesis of 22-O-ester derivatives of jorunnamycin A and their cytotoxicity against non-small cell lung cancer cells (Submitted to *Journal of Natural Products* as a Note, 12th May 2016).

Poster presentations

1. Sirimangkalakitti N, Saito N, Chanvorachote P and Suwanborirux K. Structure modification and cytotoxicity of 22-O-acyl analogs of renieramycin M, a marine bistetrahydroisoquinolinequinone alkaloid. RGJ-Ph.D. Congress XVI, 11-13 June 2015, Pattaya, Chonburi, Thailand.